



City Research Online

City, University of London Institutional Repository

Citation: Raoufi, N. (2014). Development of wavelength dependent pH optical sensor using Layer-by-Layer technique. (Unpublished Doctoral thesis, City University London)

This is the unspecified version of the paper.

This version of the publication may differ from the final published version.

Permanent repository link: <https://openaccess.city.ac.uk/id/eprint/3668/>

Link to published version:

Copyright: City Research Online aims to make research outputs of City, University of London available to a wider audience. Copyright and Moral Rights remain with the author(s) and/or copyright holders. URLs from City Research Online may be freely distributed and linked to.

Reuse: Copies of full items can be used for personal research or study, educational, or not-for-profit purposes without prior permission or charge. Provided that the authors, title and full bibliographic details are credited, a hyperlink and/or URL is given for the original metadata page and the content is not changed in any way.



**CITY UNIVERSITY
LONDON**

Development of wavelength dependent pH optical
sensor using Layer-by-Layer technique

By

Nahid Raoufi

Thesis submitted for the degree of

Doctor of Philosophy

April 30, 2014

**Instrumentation and Sensors Research Center (ISRC)
School of Engineering and Mathematical Sciences**

Northampton Square, London, EC1V 0HB

Table of Contents

Table of Figures	6
Table of Tables.....	16
Acknowledgement.....	17
List of Publication	19
Declaration	20
Abstract	21
Abbreviations	22
1. Introduction.....	24
1.1 Background	24
1.2 Aims and Objectives	25
1.3 Structure of the thesis.....	28
References	30
2. Overview of Thin Film Deposition Techniques.....	32
2.1 Introduction	32
2.2 Sol-Gel processing	35
2.2.1 Sol-gel chemistry.....	37
2.2.2 Surface sol-gel	41
2.2.3 Optical sensors based on sol-gel films	43
2.2.4 Advantages and disadvantages of the sol-gel process.....	45
2.3 Langmuir-Blodgett technique	46
2.3.1 Deposition of Langmuir-Blodgett films.....	51
2.3.2 Advantages and disadvantages of LB technique.....	60

2.4	Layer-by-layer self-assembly technique	62
2.4.1	Layer-by-layer deposition	64
2.4.2	Advantages of LbL technique	65
2.4.3	Disadvantages of LbL technique	67
2.5	Summary	68
	References	70
3.	Chemicals and Instrumentation	81
3.1	Introduction	81
3.2	Chemicals	83
3.2.1	pH indicator	83
3.2.2	Polymers	89
3.2.3	Types of chemicals	91
3.2.4	pH buffer solutions	91
3.3	Devices and components	92
3.3.1	Optical fibre	92
3.3.2	Connections and connectors	97
3.3.3	The light source	98
3.3.4	The detector	100
3.4	Preliminary operations of the sensor preparation	105
3.5	Experimental setup and data analysis	107
3.6	Summary	114
	References	115
4.	Principles of Layer-by-Layer Deposition Technique	118
4.1	Introduction	118
4.2	Important parameters	119

4.2.1	Substrate	120
4.2.2	Polyelectrolytes	121
4.2.3	Control of thickness.....	126
4.2.4	Dipping time (deposition time)	127
4.2.5	The concentration of the polyelectrolyte solution.....	128
4.2.6	Effect of pH of the polyelectrolyte solution.....	129
4.2.7	Effect of adding salt.....	131
4.2.8	Number of bilayers	136
4.2.9	Influence of drying	138
4.2.10	Stability	140
4.3	Materials and method.....	142
4.3.1	Dipping Time and Washing time	144
4.3.2	Rinsing method.....	144
4.3.3	Number of bilayers (n)	145
4.3.4	The concentration of the polyelectrolytes	145
4.3.5	Drying and method of drying	148
4.3.6	Adding salt to the solution.....	152
4.4	Summary	152
	References.....	154
5.	pH Indicator Selection.....	164
5.1	Introduction	164
5.2	Materials and method.....	166
5.2.1	Materials	166
5.2.2	Methodology.....	172
5.2.3	The performance of the selected indicators.....	176

5.3	Results and discussion.....	186
5.4	Summary	188
	References	190
6.	Enhanced Sensitivity of a Fibre Optic pH Sensor Coated with Brilliant Yellow	193
6.1	Introduction	193
6.2	Materials and methods	196
6.2.1	Materials	196
6.2.2	Fabrication of the sensors.....	197
6.2.3	Experiments.....	198
6.3	Results and discussion.....	201
6.3.1	Number of layers	203
6.3.2	Shape of the probe	214
6.3.3	Concentration of BY solution.....	217
6.3.4	Fibre core diameter.....	220
6.4	Summary	221
	References	224
7.	Stabilization and Reusability	228
7.1	Introduction	228
7.2	Materials and methods	232
7.2.1	Chemicals	232
7.2.2	Procedures	233
7.2.3	Experiments.....	235
7.2.4	Heat treatment	237
7.2.5	Using PAH and silica nanoparticle coatings	240

7.2.6	Use of APTMS and silica nanoparticles.....	246
7.2.7	Reusability and aging	251
7.3	Results and discussion.....	254
7.4	Summary	258
	References	260
8.	Conclusions and Future Work.....	264
8.1	Conclusion and overview of the work	264
8.2	Future work	269
	References	271

Table of Figures

Fig 2-1 Typical configurations of optical fibre chemical sensors. In A and B the fibre is used to direct light; in C and D the sensor phase modifies the transmission characteristics of the fibre. The indicator can be placed on the tip of the fibre (A and B) or on the side (C); part of the cladding can be removed and leave the fibre core exposed to the chemical interaction medium (D) [17].	34
Fig 2-2 Sol gel technologies and their products [36].	37
Fig 2-3 An example of sol-gel processing conditions on film formation [35].	39
Fig 2-4 Examples of deposition methods; (a) dip coating; (b) spin coating and (c) spray coating [42].	40
Fig 2-5 Schematic illustrations of three types of layer-by-layer adsorption based on the surface sol-gel process. Stepwise adsorption of metal alkoxides (a), alternate adsorption of metal alkoxides and polyhydroxyl compounds (b), and alternate adsorption of metal alkoxide and cationic compounds (c) [47].	42
Fig 2-6 The general chemical structure of an amphiphilic molecule.	47
Fig 2-7 Schematic diagram of a filter paper Wilhelmy plate. The water makes contact with the paper with contact angle = 0. The water exerts a force on the plate equal to σL , where σ is the surface tension and L is the length of the contact line of the water with paper [68].	48
Fig 2-8 Surfactant molecules at different phases during monolayer compression a) Spreading of an amphiphile solution at the air/water interface so-called gas phase; b) compressing of the monolayer after solvent evaporation to a desired surface pressure, so-called liquid phase; c) The monolayer undergoes different phase transitions, so-called solid phase and d) Transfer of the Langmuir monolayer at a solid substrate by vertical dipping – Langmuir-Blodgett film [33].	49
Fig 2-9 Typical π -A diagram of the Langmuir monolayer. (a) Gas phase; (b) liquid phase; (c) solid phase; and (d) monolayer collapse.	50

Fig 2-10 Schematic of Langmuir-Blodgett setup.	52
Fig 2-11 KSV NIMA Trough equipped with a Langmuir-Blodgett trough [77].	52
Fig 2-12 Principles of LB deposition on hydrophilic substrate: (a) Y- type deposition and (b) Z-type deposition [3].	55
Fig 2-13 Different types of LB film deposition: Y-type, alternative layers (ABAB...), X-type, and	56
Fig 2-14 Scheme of the LS technique.....	58
Fig 2-15 Schematic of the fibre optic sensor of Flannery et al. [87]......	58
Fig 3-1 The main components of a fibre optic chemical sensor. The transducer: is an indicator immobilised on the optical fibre. Measurand: H ⁺ concentration (supplied from pH buffer solutions). Light source is a tungsten halogen light. The detector: a spectrophotometer.....	82
Fig 3-2 Variation of the % formation of a monoprotic acid, AH, and its conjugate base, A ⁻ , with the difference between the pH and the pKa of the acid [1].	85
Fig 3-3 Chemical structure of some pH indicators e.g. Neutral Red (NR), Brilliant Yellow (BY), Litmus, Thiazol yellow G, Cyanidin and Thymol blue (TB).	90
Fig 3-4 The chemical structure of PAA (poly (acrylic acid)) and PAH (poly (allylamine hydrochloride)).	91
Fig 3-5 Types of optical fibres (a) step-index multimode, (b) graded- index multimode and (c) single-mode optical fibre [23]......	93
Fig 3-6 The full acceptance angle and θ_{\max} in an optical fibre.	95
Fig 3-7 Transmission profile of the multimode fibres used [25]......	96
Fig 3-8 The cross section of the bundle of 6 fibres grouped together.	97
Fig 3-9 The structure of the connections of a sensor device.	97
Fig 3-10 Emission spectra of light sources used in sensors. (a) white light sources and (b) LEDs/lasers light sources [21]......	100
Fig 3-11 Absorption of light by dyes.....	101
Fig 3-12 Illustration of a single beam UV-vis (a), double beam UV- vis (b) and simultaneous UV-vis (c) instruments	102

Fig 3-13 The photograph of the prepared optical sensor probe compared to 1 pence coin.	107
Fig 3-14 The experimental setup for a fibre optic chemical sensor (The photo was taken by Jie Cao).	108
Fig 3-15 Comparison between spectroscopy of deposited glass slide and the optical fibre in presence of buffer solution.	110
Fig 3-16 Dose-Response curve fitting model sample.	113
Fig 3-17 Degree of ionization versus pH for two kinds of indicators. The slope is positive for the indicator with negative functional group and is negative for the indicator with positive functional group.	113
Fig 4-1 The sequence of layer-by-layer electrostatic deposition.	119
Fig 4-2 Some standard polyions frequently used for multilayer fabrication by LbL deposition technique.	124
Fig 4-3 Schematic of globular conformation of a polymer chain with low charge density (right) is shown in comparison with a polymer chain with high charge density (left). Polymer chains with lower charge density form globular conformations and so thicker layers [58].	127
Fig 4-4 Complete pH matrix showing the average incremental thickness contributed by a PAH/PAA bilayer as a function of dipping solution pH [55].	130
Fig 4-5 The effect of salt in polyelectrolyte multilayers structure [9].	131
Fig 4-6 The effect of salt on a polyelectrolyte molecule in solution in high and low concentration of salt [89].	133
Fig 4-7 Thickness of (PDADMA/PSS) ₁₀ built from 10 mM PDADMA and PSS solutions at various salt concentration on Si wafers [81].	134
Fig 4-8 The root-mean-square roughness of (PDDA/PSS) ₁₀ deposited from different NaCl concentrations. The error bars represent standard deviations [91].	134
Fig 4-9 The film thickness versus number of layers for three sets of experiments of (PSS/PAH) _n deposition in different salt solution [9].	135

Fig 4-10 Thickness as a function of the number of layers for a (PSS/PDADMAC) _n multilayer deposited on silicon wafer from 1.0 M NaCl(aq). polymer concentration 1 mM [52].	137
Fig 4-11 Film thickness with increasing numbers of bilayers for single anion/ cation in deposited films [66].	137
Fig 4-12 Wet sample versus dried sample [100].	139
Fig 4-13 The heat treatment effect on the layers coated on the surface i.e the chemical reaction in PAH/PAA multilayer assemblies after heat treatment [112].	141
Fig 4-14 Neutral red chemical structure.	142
Fig 4-15 The absorbance spectra (up) and the peak wavelength (down) versus number of bilayers of (NR/PAA) _n coated on the glass slide while the concentration of the dye solution was 2 mM.	146
Fig 4-16 The effect of concentration of the solutions on the peak wavelength (up) and the absorbance (down) for (NR/PAA) _n in the various number of bilayers.	147
Fig 4-17 The effect of concentration of the solutions on the absorbance spectra for (NR/PAA) _n	148
Fig 4-18 Comparison the maximum absorbance (up) and the peak wavelength changes (down) for the glass slides coated by (NR/PAA) _n at three different drying conditions by N ₂ gas: without drying, drying after washing and drying after each stage.	150
Fig 4-19 Comparison the glass slides coated by (NR/PAA) ₂₀ at three different drying conditions: without drying, drying after washing, drying after each stage.....	151
Fig 4-20 The effect of salt concentration on the appearance of the coated glass.	152
Fig 4-21 Different drying methods have different effect on the deposited glass slide.	152
Fig 5-1 Neutral Red's chemical structure.	167
Fig 5-2 Absorbance Spectra for NR at different pH buffer solutions	167
Fig 5-3 Chemical Structure of Brilliant Yellow.	168

Fig 5-4 Absorbance spectra for Brilliant Yellow in different pH buffer solutions.	168
Fig 5-5 Chemical structure of Alizarin Red S.	169
Fig 5-6 Absorbance spectra for ARS in different pH buffer solutions.....	169
Fig 5-7 Suggested chemical structure for Litmus. The repeating unit consists of a substituted phenoxazone and two orcinol residues [21].....	170
Fig 5-8 Orcinol(left) and Phenoxizone (right) chemical structures.....	170
Fig 5-9 Chemical structure of Poly (aniline).	171
Fig 5-10 Absorbance spectra for Poly (aniline) in different pH buffer solutions [22].	171
Fig 5-11 Chemical structure of Congo Red.....	172
Fig 5-12 Absorbance spectra for Congo Red at different pH buffer solutions [23].	172
Fig 5-13 The sensor part is a coated core which ended by a silver mirror.	175
Fig 5-14 The peak wavelength value and absorbance changes when adding bilayers on the surface for (PAH/BY) _n deposited on the glass slide.	177
Fig 5-15 The absorbance spectra for a probe coated with (PAH/BY) ₂₀ . The concentration of BY and PAH solutions was 0.25 mM and 2.5 mM respectively. (Probe code: OFBY)	177
Fig 5-16 The peak wavelength as a function of the pH value of the buffer solution for a probe coated with (PAH/BY) ₂₀ (Probe code: OFBY).....	178
Fig 5-17 The peak wavelength value and absorbance changes when adding bilayers on the surface for (NR/PAA) _n deposited on the glass slide.....	179
Fig 5-18 The optical fibre coated with NR in different pH buffer solutions from pH 3 to pH 10. The concentration of NR and PAA solutions was 0.25 mM and 2.5 mM respectively. (Probe code: OFNR)	179
Fig 5-19 The peak wavelength for each spectrum in respect to pH for Fibre OFNR.	180

Fig 5-20 The peak wavelength value and absorbance changes when adding bilayers on the surface for (PAH/ARS) _n deposited on the glass slide.....	181
Fig 5-21 The optical fibre coated with ARS in different pH buffer solutions from pH 3.0 to pH 9.0. The concentration of ARS and PAH solutions was 0.5 mM and 2.5 mM respectively. (Probe code: OFARS).....	181
Fig 5-22 The peak wavelength for each spectrum in respect to pH for Fibre OFARS. (a) for range of pH from 3.0 to 9.0 (b) for low pHs (c) for high pHs.	182
Fig 5-23 The wavelength value and absorbance changes when adding bilayers on the surface for (PAH/(ARS+BY)) _n deposited on the glass slide.	182
Fig 5-24 Absorbance spectra for the optical fibre coated with (PAH/(ARS+BY)) ₂₀ in different pH buffer solutions from pH 6.0 to pH 9.0 (Probe code: OFABY).	183
Fig 5-25 The optical fibre coated with (PAH/(ARS+BY)) ₂₀ in different pH buffer solutions from pH 6.0 to pH 9.0. (Probe code: OFABY).....	184
Fig 5-26 The absorbance spectra for the optical fibre coated with ((PAA+NR)/ARS) ₂₀ in different pH buffer solutions from pH 6.0 to pH 9.0. The concentration of ARS, NR and PAH solutions was 0.5 mM, 0.5 mM and 2.5 mM respectively. (Probe code: OFANR)	185
Fig 5-27 The optical fibre coated with ((PAA+NR)/ARS) ₂₀ in different pH buffer solutions from pH 6.0 to pH 9.0. (Probe code: OFANR).....	185
Fig 5-28 Dark and fine spots on the surface of the coated glass slide with (NR/PAA) ₁₅ while the surface coated with (PAH/BY) ₁₆ is totally homogenous.	187
Fig 6-1 Schematic of the U-bend and straight probes.	199
Fig 6-2 The experimental set up for straight probes (up) and U-bend probes (down).	200
Fig 6-3 Absorbance spectra for the straight optical fibre coated using 4 bilayers of (PAH/BY) in different pH buffer solutions.....	204

Fig 6-4 Absorbance spectra for the straight optical fibre coated using 5.5 bilayers of (PAH/BY) in different pH buffer solutions.....	205
Fig 6-5 Absorbance spectra for the straight optical fibre coated using 6 bilayers of (PAH/BY) in different pH buffer solutions.....	205
Fig 6-6 Absorbance spectra for the straight optical fibre coated using 7.5 bilayers of (PAH/BY) in different pH buffer solutions.....	206
Fig 6-7 Absorbance spectra for the straight optical fibre coated using 8 bilayers of (PAH/BY) in different pH buffer solutions.....	206
Fig 6-8 Absorbance spectra for the straight optical fibre coated using 9.5 bilayers of (PAH/BY) in different pH buffer solutions.....	207
Fig 6-9 The peak wavelength for each spectrum with respect to pH for probes with different number of bilayers.....	207
Fig 6-10 The peak wavelength for each spectrum with respect to pH for probes with different number of bilayers.....	208
Fig 6-11 The peak wavelength for each spectrum with respect to pH for probes with different number of bilayers.....	208
Fig 6-12 The peak wavelength for each spectrum with respect to pH for probes with different number of bilayers.....	209
Fig 6-13 The average wavelength shift for a sample of 0.2 pH units at each measurement from pH 7 to pH 9 for the probes with 600 micron core diameter and 0.25mM of BY solution and different number of bilayers.	209
Fig 6-14 The value of pKa for each probe versus number of layers.	212
Fig 6-15 The peak wavelength for each spectrum with respect to pH for probes with different shapes when concentration of BY solution is 0.5 mM.	213
Fig 6-16 The peak wavelength for each spectrum with respect to pH for probes with different shapes when concentration of BY solution is 0.25 mM.	214
Fig 6-17 The average wavelength shift for a sample of 0.2 pH units at each measurement from pH 7 to pH 9 for the probes coated with (PAH/BY) ₆ and variable properties.	215
Fig 6-18 The value of pKa for each probe versus shape of the probes at different core diameter and concentration of BY.	216

Fig 6-19 The peak wavelength for each spectrum with respect to pH in different concentrations of brilliant yellow solutions for big U-bend sensors.	218
Fig 6-20 The peak wavelength for each spectrum with respect to pH in different concentrations of brilliant yellow solutions for small U-bend sensors.	219
Fig 6-21 The peak wavelength for each spectrum with respect to pH in different concentrations of brilliant yellow solutions for straight sensors.	219
Fig 6-22 The peak wavelength for each spectrum with respect to pH for probes with different core diameter. The wide fibre (P12) and the narrow one (P05).	221
Fig 7-1 Chemical structure of (a) APTMS, (b) Poly (allylamine) hydrochloride [PAH] and (c) brilliant yellow.	233
Fig 7-2 The maximum value of the relative absorbance (up) and the peak wavelength (down) versus pH for the consecutive measurements of the pH solutions for (PAH/BY) ₈ on the glass slide. No heat treatment or drying was used in the process. (The sample is designated GS01)	236
Fig 7-3 The maximum value of the relative absorbance (up) and the peak wavelength (down) versus pH for the consecutive measurements of the pH solutions for (PAH/BY) ₁₆ on the glass slide. The sample was cured at 120°C for 4 hours. (The sample is designated GS02).	238
Fig 7-4 The maximum value of the relative absorbance (up) and the peak wavelength (down) versus pH for the consecutive measurements of the pH solutions for (PAH/BY) ₆ on the glass slide. The sample was cured at 120°C for 4 hours. (The sample is designated GS03).	239
Fig 7-5 The maximum value of the relative absorbance (up) and the peak wavelength (down) versus pH for the consecutive measurements of the pH solutions for (PAH/BY) ₆ (PAH/SiO ₂) ₂ on the glass slide. (The sample designated as GS04)	241
Fig 7-6 The maximum value of the relative absorbance (up) and the peak wavelength (down) versus pH for the consecutive measurements of the pH solutions for	

(PAH/BY) ₆ (PAH/SiO ₂) ₂ on the glass slide. The sample was cured at 130°C for 7 hours. (The sample designated as GS05).....	242
Fig 7-7 The maximum value of the relative absorbance (up) and the peak wavelength (down) versus pH for the consecutive measurements of the pH solutions for (PAH/BY) ₆ (PAH/SiO ₂) ₂ on the glass slide. The sample was cured at 130°C for 7 hours and exposed to UV light for 20 minutes. (The sample designated as GS06).....	243
Fig 7-8 The maximum value of the relative absorbance (up) and the peak wavelength (down) versus pH for the consecutive measurements of the pH solutions for (PAH/(BY+SiO ₂)) ₆ on the glass slide. The sample was cured at 120°C for 4 hours. (The sample designated GS07).....	245
Fig 7-9 APTMS is polymerized in aqueous solution after hydrolysis.	247
Fig 7-10 Two possibilities reaction between molecules of APTMS and silica nanoparticles.....	247
Fig 7-11 The maximum value of the relative absorbance (up) and the peak wavelength (down) versus pH for the consecutive measurements of the pH solutions for (PAH/BY) ₆ (APTMS/SiO ₂) ₂ on the glass slide. The sample was cured at 120°C for 4 hours. (The sample designated GS08).....	248
Fig 7-12 The maximum value of the relative absorbance (up) and the peak wavelength (down) versus pH for the consecutive measurements of the pH solutions for (PAH/BY) ₆ (APTMS/SiO ₂) ₂ on the glass slide. The sample was cured at 120°C for 4 hours and examined after a week. (The sample designated GS09).....	249
Fig 7-13 The maximum value of the relative absorbance (up) and the peak wavelength (down) versus pH for the consecutive measurements of the pH solutions for (PAH/BY) ₆ APTMS on the glass slide. The sample was cured at 120°C for 4 hours. (The sample designated GS10).....	250
Fig 7-14 The spectra for the coated glass slides with (PAH/BY) ₆ dipped into the fresh buffer solution for three times and each time for 60 minutes. Up: pH 6 (The sample designated	

GS11), Down: pH 8 (The sample is designated GS12). The samples were cured at 120°C for 4 hours.252

Fig 7-15 The spectra for the coated glass slides with (PAH/BY)₆(APTMS/SiO₂)₂ dipped into the fresh buffer solution for three times and each time for 60 minutes. Up: pH 6 (The sample is designated GS13), Down: pH 8 (The sample is designated GS14). The samples were cured at 120°C for 4 hours.253

Table of Tables

Table 3-1 pH indicators and their colour with respect to pH range [166, 167].	88
Table 4-1 The effect of dipping time on the absorbance for the glass slide coated with (NR/PAA) ₅ .	144
Table 4-2 The effect of rinsing method on the absorbance for the glass slide coated with (NR/PAA) ₆ .	144
Table 4-3 The effect of presence of NaCl in the polyelectrolyte solutions on the absorbance for (NR/PAA) ₆ .	151
Table 4-4 The effect of drying method (gas and oven) on the absorbance and wavelength for (NR/PAA) ₆ .	151
Table 5-1 The parameters for curve fitting based on Dose-Response model for the created probe. A1 and A2 are lowest and highest values of peak wavelength respectively, p is the slope factor, pK _a is the acid dissociation constant and Y is curve gradient in the inflection point.	186
Table 5-2 Cross comparison of the prepared sensors.	186
Table 6-1 Dose-Response curve properties for the prepared probes.	202
Table 7-1 The peak wavelength for two times consecutive measurements for the glass slides, designated GS04, GS08 and GS09 in pH solutions from 6 to 9 and then from 9 to 6.	258

Acknowledgement

I would like to express my sincere and deep gratitude to my advisor, Professor Muttukrishnan Rajarajan for his thoughtful guidance, steady encouragement and support. His style of supervising also allowed me to pursue a number of interesting subjects, which were quite beneficial to me. Additionally, I appreciate that he allowed me to support my daughter during my research.

I am also deeply indebted to Professor Tong Sun for letting me work in her laboratory. I greatly benefited from her comments on my presentations and her advice academically and personally. Working with her has been the most rewarding experience of my professional life.

Special thanks to Professor Kenneth Grattan for his advice, suggestions and support about my experiments as well as his important comments on my papers.

I would like to say my utmost gratitude to Dr Frederic Surre. It was he who introduced the Layer-by-Layer technique to me. I owe him a great deal for his constructive suggestions and ideas. I appreciate his invaluable help and encouragement throughout the completion of this research.

I would also like to thank Dr Ahad Bagherzadeh, Vice-Chancellor of Azad University in Oxford for his unlimited support.

I would also like to thank Dr. Hien Nguyen who aided me in this project. Her expertise in the area of chemistry has greatly aided my work.

I wish to thank all the researchers and students at Instrumentation and Sensors Research Center (ISRC) who have kindly assisted me through out this research through helpful comments and technical discussions, including Dr Jie Cao, Dr Shanika Lourdes Alwis, Mr Hieu Tu, Dr Thillainathan Venugopalan, Dr Ewan Galbraith, Dr Matthias Fabian, Dr Mohammad Uthman, Mr Fei Li, Ms Afrouz Farshad Mehr and Ms Labiba Gilani for their cheerful assistance and friendship.

Very especial thanks to my parents, for their endless encouragement, love and support both emotionally and financially.

I also wish to thank my husband Nasser and my daughter Alieyeh for their boundless love, hope and for always standing with me through all the ups and downs.

The staff of City University London and Azad University in Oxford especially Jim Hooker, Nathalie Chateline, Shekoufeh Tahmasebi and Mr Arfaei for being accommodating to my queries.

Finally, I gratefully acknowledge the financial support provided by Azad University- South Tehran Branch and City University London.

List of Publication

1. Raoufi, N.; Surre, F.; Sun, T.; Grattan, K.T.V. and Rajarajan, M.; Selection of optimized pH indicator for coating on optical fibre using the layer-by-layer technique, under preparation for *Sensors and Actuators B: Chemical*
2. N. Raoufi, F. Surre, M. Rajarajan, T. Sun and K.T.V. Grattan, Optical sensor for pH monitoring using a layer-by-layer deposition technique emphasizing enhanced stability and re-usability, *Sensors and Actuators B: Chemical*, Volume 195, May 2014, Pages 692–701
3. N. Raoufi, F. Surre, M. Rajarajan, T. Sun and K.T.V. Grattan, Fibre Optic pH Sensor Using Optimized Layer-by-Layer Coating Approach, *Sensors Journal, IEEE*, 14 (2014) 47 – 54, DOI: 10.1109/JSEN.2013.2280283.
4. N. Raoufi, F. Surre, T. Sun, M. Rajarajan and K.T.V. Grattan, Wavelength dependent pH optical sensor using the layer-by-layer technique, *Sensors and Actuators B: Chemical*, 169 (2012) 374-381, DOI: 10.1016/j.snb.2012.05.024.
5. Raoufi, N.; Surre, F.; Sun, T.; Grattan, K.T.V. and Rajarajan, M.; Improvement of Optical Properties of pH- sensitive Nanolayers Coating Deposited using Layer-by-Layer Technique, *IEEE Sensors 2012*, DOI: 10.1109/ICSENS.2012.6411515
6. Nahid Raoufi , Frederic Surre, Tong Sun, Rajarajan Muttukrishnan, Kenneth T. V. Grattan, Optimisation of the design of fibre optic pH sensor based on layer-by-layer coating, *SPIE Photonics Europe 2012* , [8439-93]
7. Raoufi, N.; Surre, F.; Sun, T.; Grattan, K.T.V.; Rajarajan, M.; Fibre Optic pH sensor using optimized Layer-by-Layer coating, *Europtrode XI 2012: Optical, Chemical Sensors and Biosensors*, p-178

Declaration

I grant powers of discretion to the University Librarian to allow the thesis to be copied in whole or in part without further reference to the author. This permission covers only single copies made for study purposes, subject to normal conditions of acknowledgement.

Abstract

Stable and reliable operation of an optical sensor for pH monitoring is important for many industrial applications. This dissertation reports a series of studies on the development of novel and highly sensitive fibre optic sensors which are based on wavelength, instead of intensity changes and the development of thin film optical fibre working combinations for effectively enhancing the durability and value of the sensor probe.

Several novel optical fibre sensors were fabricated and evaluated in this work. In order to measure the pH of a solution using optical methods, the sensor probes were prepared using layer-by-layer deposition techniques, a simple and versatile method to deposit a sensitive thin film i.e. active pH indicators on such optical fibre-based devices.

In further work, the selection of a charged and water-soluble pH indicator which introduces the highest wavelength shift, while varying the pH of the media, was investigated since the wavelength shift was considered as the basis of the sensitivity index. Brilliant yellow (BY) was applied as an indicator because of its greater wavelength shift with pH change compared to the use of other indicators. Poly (allylamine hydrochloride) (PAH) was also used as a cross-linker. To this end, the layers of BY/PAH were deposited on the bare silica core optical fibre using the layer-by-layer technique.

The research was then developed to optimize the design factors that have an important effect on the sensitivity of the device. Utilizing U-shaped fibre with small radius which coated six bilayers of (BY/PAH) prepared from a polyion solution of low concentration was seen to provide a sensor with wider range of sensitivity which presents a highly sensitive device working over a smaller pH range offering higher resolution.

In a further study, covering the sensitive thin film with two layers of silica nanoparticles was seen to improve the wavelength stability and enhance the device shelf life. The particular result is that the peak wavelength continued to remain constant for a pH; however, the layers were destroyed during the course of several measurement events.

Consequently, the optimal sensor configuration which was designed, created and evaluated in this work was a novel wavelength-dependent measurement device which is capable of being utilized as a high resolution pH sensor (obtaining ± 0.2 pH unit). It shows a wider range of sensitivity (pH 6.8 to pH 9.4) and the highest sensitivity achieved so far (~ 5.5 nm average wavelength shift for 0.2 pH units). It is a re-usable sensor which can be stored without any apparent aging effects. In addition to this it is a device which is easy and economical to prepare.

Abbreviations

A_1	Lowest value of peak wavelength in Dose-Response model
A_2	Highest value of peak wavelength in Dose-Response model
APTMS	Aminopropyl-trimethoxy silane
ARS	Alizarin red S
BY	Brilliant yellow
c_i	Molar concentration of ion i
CVD	Chemical vapour deposition
ESA	Electrostatic Self-Assembly
I	Ionic strength
K_a	Acid dissociation constant
LB	Langmuir - Blodgett
LbL	Layer-by-Layer
LD	Laser diodes
LED	Light emitted diode
LS	Langmuir-Schaefer
NA	Numerical aperture
n_{air}	Refractive index of air
n_{clad}	Refractive index of the cladding
n_{core}	Refractive index of the core
NR	Neutral red
p	Slope factor
PAA	Poly (acrylic acid)

PAH	Poly (allylamine hydrochloride)
PSS	Poly (sodium styrenesulfonate)
SPR	Surface Plasmon Resonance
UV	Ultra violet
z_i	Charge number of ion i
$\theta_{\text{acceptance}}$	Acceptance angle
π	Surface pressure
σ	Surface tensions of water covered by LB monolayer
σ_0	Surface tensions of pure water

1. Introduction

1.1 Background

Nowadays there is a significant need to detect and analyse a wide variety of chemical and biochemical substances. In addition to this, the measurement of parameters such as pH, humidity, volatile gas concentration, soluble gases, alcohol, heavy metals, soluble ions, glucose and pathogenic bacteria proteins have played an important role in many important areas of life, including environmental monitoring, health and safety measurement, biotechnology, medicine, drug discovery and food monitoring. The sensing of critical chemical and biochemical compounds is very important for crisis-mitigation and monitoring of materials used in chemical and bio-terrorism. As a result, a range of chemical/biological sensors have been developed by the scientific community to meet a wide range of industrial needs. pH is one of the most common analytical measurements in both industrial processing and laboratory research in which real time measurement is needed. For instance, pH is important in industry for process control in bioreactors [1, 2] and precipitation of heavy metal ions in industrial waste waters. It is widely used in quality control in the medical field for clinical analysis of blood [3] and body fluids [4-6], or in food industries, for example in the control of freshness of meat [7] and drinking

water [8]. It also has an important role in environmental monitoring [9]. However, optical pH sensors have been considered more widely than other types of pH sensors in recent times, due to the demand for fast, reliable and high resolution sensors. Fibre optic techniques present many advantages that made such a technology a suitable candidate for real time pH point-sensing.

1.2 Aims and Objectives

New thin-film materials and devices with specific optical, chemical, electronic, mechanical and other properties are required for applications as sensors and measurement tools, in areas such as solar and photovoltaic cells, biocompatibility systems, microelectronic devices, communication systems, information storage, display systems, environmental treatment/purification systems and in many other fields.

The sensitivity of a pH sensor is, a measure of the degree of change in the sensor output with change in the solution pH. For example in optical sensors this transduction effect (that can then be related to the measurand) can be absorbance [10-12], reflected optical power [13, 14], transmitted power [15], or the wavelength at maximum absorbance [16]. Therefore, the sensitivity of the device will depend in part on the optimum choice of this transduction mechanism.

However, in this work, the design and characterization of a wavelength dependent pH optical sensor has been studied. This mechanism allows a sensor

reading independent of source variation or any perturbation other than pH change.

In order to achieve optical recognition in the sensor device, active indicators must be used as sensitive films. Hence active indicators like azo dyes (for colourimetric purposes) should be immobilized on the optical fibres in the sensor device. Changing the optical properties of sensitive films by changing the analyte concentration is the basis of the recognition technique used. In this work the H^+ concentration is the main parameter that has been measured through a pH monitoring. To date, reports of a limited number of pH indicators, such as neutral red, methylene blue and prussian blue which have been deposited onto optical fibres to create pH sensors have been published [11, 17-21]. In the present study, in order to identify a very suitable pH indicator which shows better performance based on wavelength change with narrow intervals based on colourimetric measurements, several indicators would be examined and their characteristics monitored and compared with each other and the indicator with the highest wavelength shift would be seen as very promising.

The focus of this research has been to investigate several different techniques to improve the optical properties of pH-sensitive nanolayer coatings deposited using the layer-by-layer (LbL) technique. The LbL is a versatile self-assembly method, relying on electrostatic attraction between molecules, positively and negatively charged, that has demonstrated its potential to create tailor-made nanocoatings for sensing applications.

This thesis aims to develop a suite of pH optical sensors which work based on the wavelength shift principle and show high accuracy and stability.

The major objectives of the work reported in this thesis are:

- To review critically the key literature associated with thin film deposition and self-assembly techniques as well as to create a comparison between these techniques and the layer-by-layer technique and thus to use the information developed in the design of devices.
- To carry out a series of experiments to identify the most important parameters and the best process conditions for the preparation of the multilayer thin films to be used to coat the optical fibres used and thus create these novel optical fibre sensors.
- To identify and select the most appropriate pH indicators which demonstrate stable and reproducible wavelength shifts with pH change.
- To create and optimize fibre optic pH sensor designs based on the results of a series of experiments, thus leading to the most suitable values of different parameters for optimum sensor devices.
- To monitor and optimize the stability of the films deposited on the optical fibres in order to enhance the stability of the sensors for use in continuous measurement and to create re-usable sensors with stable performance in terms of wavelength change.

The sensor designed and evaluated in the work was designed to be a reliable, portable, easy-to use and inexpensive sensor system which will work, being

based on the wavelength shift with a narrow pH change that will be a highly effective device in the field of fibre optic sensors.

1.3 Structure of the thesis

This thesis has aimed to pioneer better pH optical fibre sensor design, operating through as a precise function of wavelength, with high resolution. The layer-by-layer process was employed as a method for creation of reliable optical thin films. The thesis consists of eight Chapters reporting on work undertaken to achieve the objectives set out above.

Chapter 1 begins with a brief overview of the necessity for pH sensing and the use of self-assembly multilayers, comprising a short introduction to the aims, objectives and structure of the work.

Chapter 2 describes a review of the literature showing published techniques to create a self-assembly multilayer coatings covering different techniques and their pros and cons and thus providing a basis for the design of a new optical sensor system.

Chapter 3 reviews the key details of the materials and components, utilized to prepare and apply to creating a fibre optic chemical sensor using the layer-by-layer deposition technique.

Chapter 4 is structured as two main sections: a review of the principles of the layer-by-layer technique as well as the most important parameters in this process and secondly preliminary experiments on coated glass slides prepared

based on the layer-by-layer technique to optimize the fabrication process for use in optical fibre devices for recognizing purposes.

Chapter 5 reports on an investigation of the functions of a number of pH indicators, to identify the most suitable pH indicator, which shows the optimum wavelength shift whilst the pH changes over very narrow pH intervals and based on colourimetric measurements, making comparison with the use of other indicators.

Chapter 6 is structured to report a detailed study carried out on the effects of different parameters on fibre optic pH sensors prepared as discussed above. This chapter investigates influential factors in the key sensing properties i.e. number of bilayers, thickness of the layers and number of molecules constituted the layers resulting from changing the concentration of the polyelectrolyte solution and also the shape of the probe; straight and/or U-bend with a view to optimizing the performance of the device.

Chapter 7 presents an overview of the variety of techniques studied to improve the stability of the films and to obtain a sensor with stable wavelength, independent on the length of usage and thus with optimized performance.

Chapter 8 concludes the thesis with a report of the results obtained from the range of sensors developed and studied in this work. This chapter also describes the scope of further developments and future applications of the sensors designed, towards the overall objective of achieving the optimum sensor design.

References

- [1] A. S. Jeevarajan, S. Vani, T. D. Taylor, and M. M. Anderson, "Continuous pH monitoring in a perfused bioreactor system using an optical pH sensor," *Biotechnology and Bioengineering*, vol. 78, pp. 467-472, May 2002.
- [2] P. Harms, Y. Kostov, and G. Rao, "Bioprocess monitoring," *Current Opinion in Biotechnology*, vol. 13, pp. 124-127, Apr 2002.
- [3] S. A. Grant and R. S. Glass, "A sol-gel based fiber optic sensor for local blood pH measurements," *Sensors and Actuators B: Chemical*, vol. 45, pp. 35-42, 1997.
- [4] S. A. Grant, K. Bettencourt, P. Krulevitch, J. Hamilton, and R. Glass, "In vitro and in vivo measurements of fiber optic and electrochemical sensors to monitor brain tissue pH," *Sensors and Actuators B: Chemical*, vol. 72, pp. 174-179, 2001.
- [5] E. J. Netto, J. I. Peterson, M. McShane, and V. Hampshire, "A fiber-optic broad-range pH sensor system for gastric measurements," *Sensors and Actuators B: Chemical*, vol. 29, pp. 157-163, 1995.
- [6] F. Baldini, P. Bechi, S. Bracci, F. Cosi, and F. Pucciani, "In vivo optical-fibre pH sensor for gastro-oesophageal measurements," *Sensors and Actuators B: Chemical*, vol. 29, pp. 164-168, 1995.
- [7] O. A. Young, R. D. Thomson, V. G. Merhtens, and M. P. F. Loeffen, "Industrial application to cattle of a method for the early determination of meat ultimate pH," *Meat Science*, vol. 67, pp. 107-112, 2004.
- [8] A. Dybko, W. Wroblewski, J. Maciejewski, R. Romaniuk, and Z. Brzozka, *Fiber optic probe for monitoring of drinking water* vol. 3105. Bellingham: SPIE - Int Soc Optical Engineering, 1997.
- [9] G. Marinenko and W. F. Koch, "A critical review of measurement practices for the determination of pH and acidity of atmospheric precipitation," *Environment International*, vol. 10, pp. 315-319, 1984.
- [10] J. Lin, "Recent development and applications of optical and fiber-optic pH sensors," *Trends in Analytical Chemistry*, vol. 19, pp. 541-552, 2000.
- [11] J. Goicoechea, C. R. Zamarreño, I. R. Matías, and F. J. Arregui, "Optical fiber pH sensors based on layer-by-layer electrostatic self-assembled Neutral Red," *Sensors and Actuators B: Chemical* vol. 132, pp. 305-311, 2008.
- [12] S. Kodaira, S. Korposh, S.-W. Lee, W. J. Batty, S. W. James, and R. P. Tatam, "Fabrication of highly efficient fibre-optic gas sensors using SiO₂/polymer nanoporous thin films," in *3rd International Conference on Sensing Technology*, Tainan, Taiwan, 2008.

-
- [13] I. D. Villar, I. R. Matias, and F. J. Arregui, "Fiber-optic chemical nanosensors by electrostatic molecular self-assembly," *Current Analytical Chemistry*, vol. 4, pp. 341-355, 2008.
- [14] I. D. Villar, I. R. Matías, F. J. Arregui, and R. O. Claus, "ESA-based in fiber nanocavity for hydrogen peroxide detection," *IEEE Transactions On Nanotechnology*, vol. 4, pp. 187-193, 2005.
- [15] I. R. Matias, F. J. Arregui, J. M. Corres, and J. Bravo, "Evanescent field fiber-optic sensors for humidity monitoring based on nanocoatings," *IEEE Sensors Journal* vol. 7, pp. 89-95, 2007.
- [16] C. R. Zamarreño, M. Hernáez, I. D. Villar, I. R. Matías, and F. J. Arregui, "Optical fiber pH sensor based on lossy-mode resonances by means of thin polymeric coatings," *Sensors Actuat B-Chem* vol. 155, pp. 290-297, 2011.
- [17] J. Goicoechea, C. R. Zamarreño, I. R. Matias, and F. J. Arregui, "Utilization of white light interferometry in pH sensing applications by mean of the fabrication of nanostructured cavities," *Sensors and Actuators B: Chemical* vol. 138, pp. 613-618, 2009.
- [18] J. Goicoechea, C. R. Zamarreño, I. R. Matías, and F. J. Arregui, "Study on White Light Optical Fiber Interferometry for pH Sensor Applications," in *IEEE Sensors Conference*, 2007.
- [19] F. J. Arregui, I. L. I. R. Matias, and R. Claus, "An optical fiber pH sensor based on the electrostatic self-assembly method," *IEEE Sensors Journals*, pp. 107-110, 2003.
- [20] Y. Egawa, R. Hayashida, and J.-i. Anzai, "Multilayered assemblies composed of brilliant yellow and poly(allylamine) for an optical pH sensor," *Analytical Sciences* vol. 22, pp. 1117-1119, 2006.
- [21] J. M. Corres, I. R. Matias, I. D. Villar, and Francisco J. Arregui, "Design of pH sensors in long-period fiber gratings using polymeric nanocoatings," *IEEE Sensors Journal*, vol. 7, pp. 455-463 2007.

2. Overview of Thin Film Deposition Techniques

2.1 Introduction

Thin film materials are the key elements in the continued technological advances made in the fields of optoelectronics, photonics and magnetic devices. The incorporation of molecules into a thin film can be achieved by molecular self-assembly processing, without external intervention which produces thermodynamically stable molecular structures. The driving forces between the molecules are intermolecular attractions, typically modelled as ionic, hydrogen, van der Waals and covalent bonds. Thin films are formed mostly by deposition, either physical or chemical methods. As far as the diversity of compounds especially organic compounds is concerned, several million compounds exhibit a wide variety of molecular properties and hence it is not surprising that there are different routes for the preparation of thin films. For example spin coating is a very popular preparation method for polymeric thin films [1]. For fatty acids and the molecules which have the structure similar to the lipids, the most common methods are Langmuir-Blodgett (LB) and Langmuir-Schaefer (LS) [2-4] and covalently self-assembled monolayer processing is commonly used for deposition of bio-chemical materials such as protein, DNA and enzymes [5-8].

One of the important applications of thin film deposition is its use to functionalize an optical fibre for optical recognition purposes [9]. Optical sensors, sometimes called optrodes, represent a group of chemical sensors in which electromagnetic radiation in the optical part of the spectrum is used to generate the analytical signal in a transduction element. These sensors can be based on various optical principles (absorbance, reflectance, luminescence and fluorescence), covering different regions of the spectra (UV, visible, IR, NIR) and allowing the measurement of the degree of change in the sensor output which can be absorbance [10-12], reflected optical power [13, 14], transmitted power [15] and the wavelength at maximum absorbance [16], for instance. Optical fibres are commonly employed in this type of sensors to transmit the electromagnetic radiation to and from a sensing region that is in direct contact with the sample. The most common are distal-type sensors, in which the indicator chemistry is immobilized at the tip of a single or bifurcated optical fibre. Alternatively, the sensing chemical reagent can be immobilized along a section of the core of the optical fibre to make an evanescent field sensor as illustrated in Fig 2-1.

In a pH optical fibre sensor a thin film of a pH indicator is deposited onto the tip or distal end of the fibre. To immobilize the pH indicator many deposition techniques have been used so far such as the sol-gel, Langmuir-Blodgett and layer-by-layer approaches.

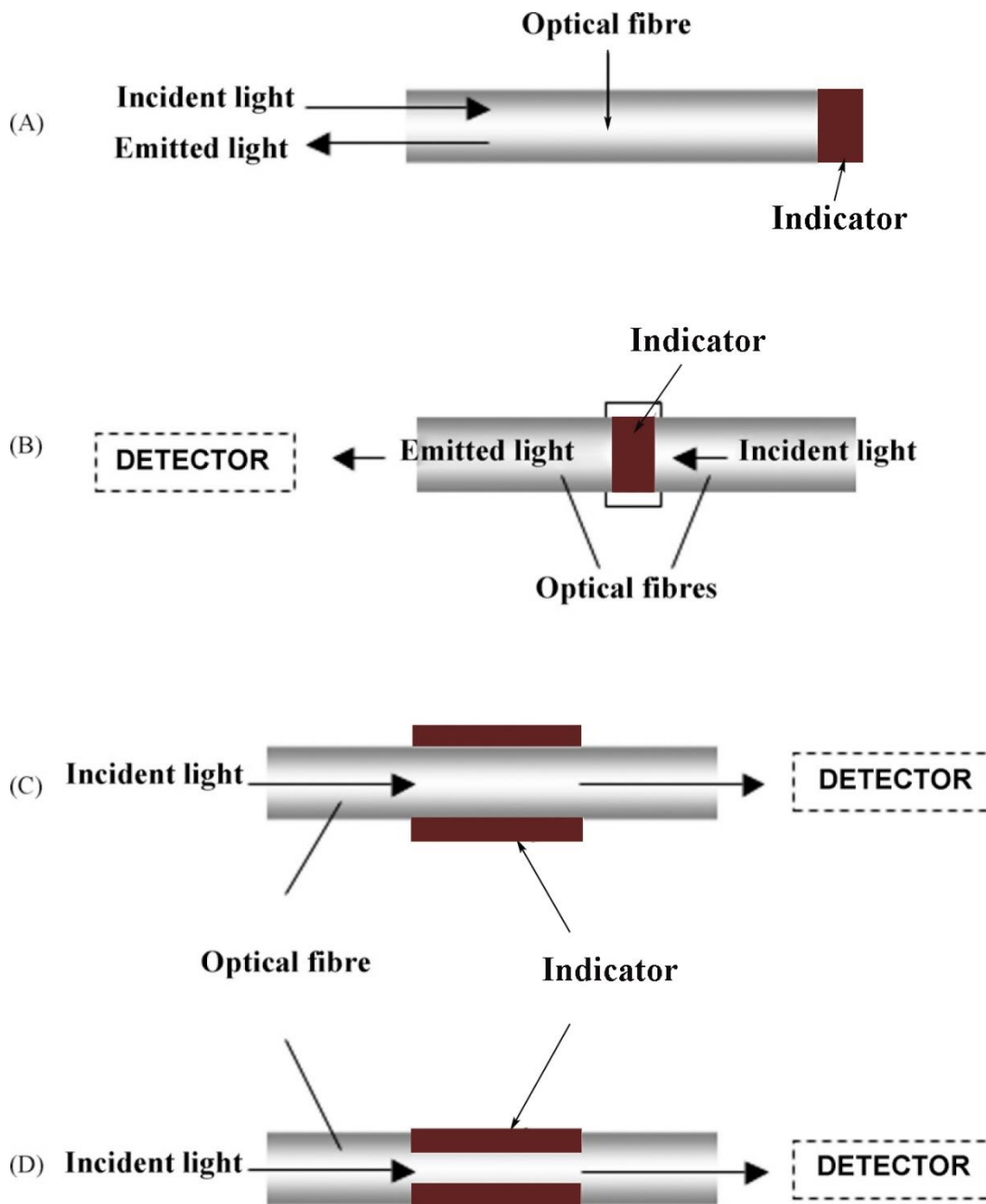


Fig 2-1 Typical configurations of optical fibre chemical sensors. In A and B the fibre is used to direct light; in C and D the sensor phase modifies the transmission characteristics of the fibre. The indicator can be placed on the tip of the fibre (A and B) or on the side (C); part of the cladding can be removed and leave the fibre core exposed to the chemical interaction medium (D) [17].

The properties of thin films can be controlled individually by varying the thickness parameter of the film used. The nanometer scale coatings deposited on optical fibres are achieved using three main techniques, namely, Langmuir-

Blodgett, sol-gel and layer-by-layer approaches. This section explores these techniques and their characteristic and has provided an overview of the literature on thin film deposition techniques and recommendation for future designs, taking advantage of the gaps identified in current activity in the field.

2.2 Sol-Gel processing

The *sol-gel* technique is a deposition method widely used in materials science to prepare nanomaterials, especially composites [18-20]. The sol-gel method initially applied for ceramic fabrication. Later this method was successfully adopted for the processing of a wide variety of materials, from monolithic ceramic and glasses, to fine powders, thin films, ceramic fibres, microporous inorganic membranes, and extremely porous aerogel materials [18, 21-28]. The most widespread use of sol-gel is in coatings devices such as in antireflective coatings, optical or infra-red absorbing coatings, electrically conductive coatings and coating that protects against scratch, oxidation and erosion on all types of materials [18, 29-32].

The first step of any sol-gel process always consists of selecting the precursors (the preparatory materials) of the desired materials. It is the precursor that, by its chemistry, lead the reaction towards the formation of either colloidal particles (e.g. metal alkoxides) or polymeric gels (e.g. metals). The use of a combination of different precursors and procedures enhances different chemical synthesis

and hence different products such as organic-inorganic hybrid materials [20, 22].

In the typical procedure, the precursor is mixed with water and a co-solvent (usually ethanol or methanol), yielding a homogeneous *sol*. Hydrolysis and polycondensation can be accelerated by employing an appropriate acid or base catalyst. As the reactions proceed, gradual increase of the solution's viscosity occurs and a rigid, porous, interconnected *gel* is formed. This gel is a bi-phasic system containing both a liquid phase (solvent) and a solid phase (integrated network, typically polymer network). After aging and drying at room temperature, a xerogel is obtained, which may be further densified at high temperatures if a non-porous material is intended. Thin xerogel films (in the range of 100 nm) can be formed on the solid substrates by dip coating, spin coating, or spraying of the solution. Heating of the xerogel completely removes solvent molecules which lead to further aggregation of inorganic clusters and the formation of solid materials, either bulk or in the form of thin films. Subsequent repeating of the routine allows the formation of thicker multilayered film [2, 20, 33, 34]. Sol-gel technologies and their products that are available at present are illustrated in Fig 2-2.

A quick, supercritical drying carried out at high temperature leads to the formation of the aerogel, a highly porous and extremely low density (greater than 75% porosity) material. On the other extreme, a very slow evaporation of the solvent at ambient conditions causes the precipitation of solid phase, and eventually yields fine, uniform particles [2, 35].

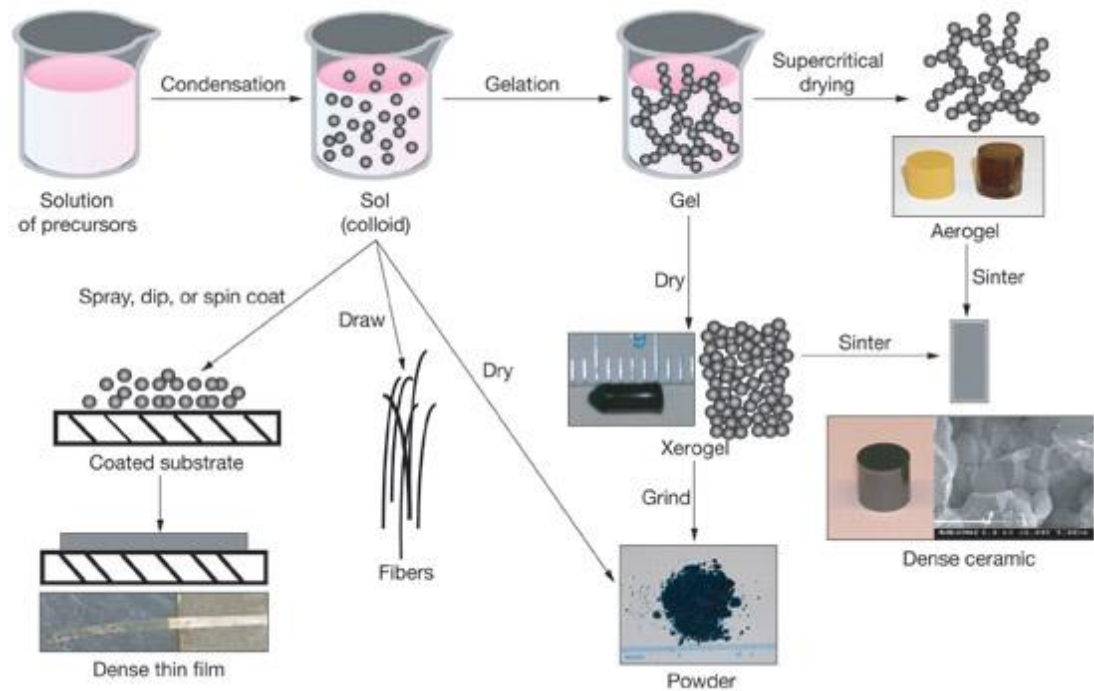


Fig 2-2 Sol gel technologies and their products [36].

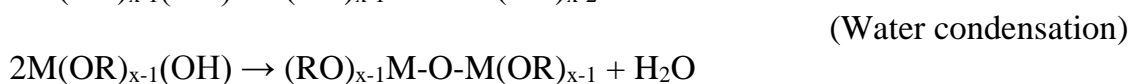
2.2.1 Sol-gel chemistry

There are two distinct reactions in the sol-gel process: hydrolysis of the alcohol groups and condensation of the resulting hydroxyl groups. The chemistry of the sol-gel process is largely based on an alkoxide solution route [2]. Metal alkoxides are members of the family of *metalorganic* compounds, which have the general formula $M(OR)_x$ where R is an alkyl group and M can be silicon, aluminum, titanium, zirconium and other metals and an alkoxide ion is the conjugate base of an alcohol [24, 35, 37-39]. Typical alkoxides are: tetraethyl orthosilicate ($Si(OC_2H_5)_4$ or TEOS), tetramethyl orthosilicate ($Si(OCH_3)_4$ or TMOS), zirconium propoxide ($Zr(OC_3H_7)_4$) and titanium butoxide ($(Ti(OC_4H_9)_4)$).

The sol-gel reaction, initiated by a catalyst, starts with the hydrolysis of alkoxides in the water-alcohol mixed solution, in which an alkoxide ligand replaces with a hydroxyl ligand as shown in the scheme below [20, 38]:



Once hydrolysis has occurred the sol can react further and condensation (polymerisation) occurs.



It is these condensation reactions that lead to gel formation. In condensation two hydrolyzed fragments join together and either an alcohol or water is released. Condensation occurs by either nucleophilic¹ substitution or nucleophilic addition.

The hydrolysis can be triggered by changes in pH of the solution. Acidic solutions are typically transparent, but become opaque at alkaline pH. This critical pH value indicates a transition point, when the reaction of hydrolysis becomes irreversible, and the sol-gel process begins. Fig 2-3 shows the effect of pH on the structure of produced thin films [35, 40].

¹ A molecule or group having a tendency to donate electrons or react at electron-poor sites such as protons.

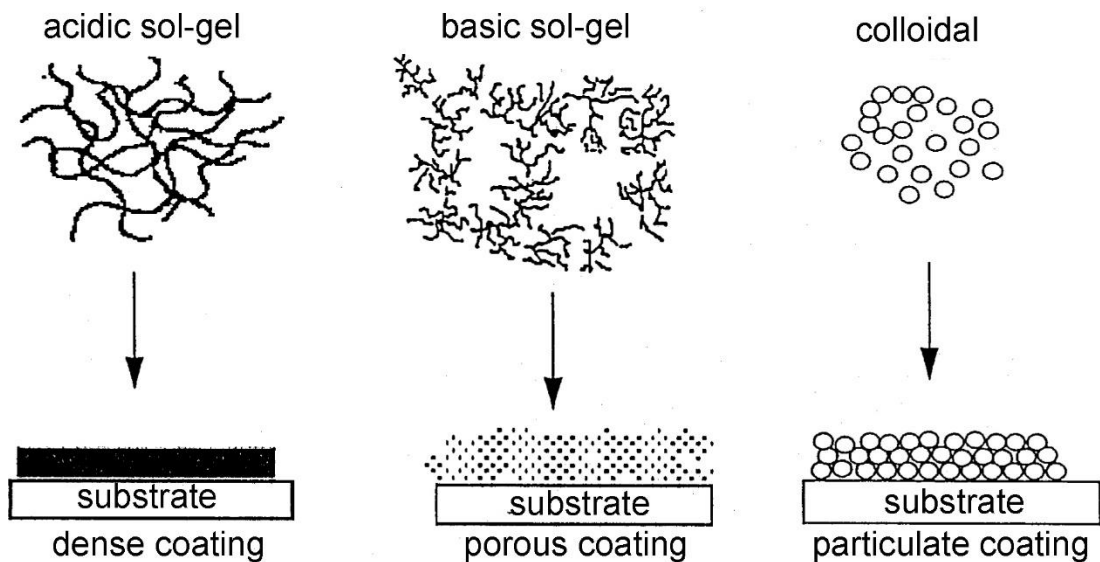


Fig 2-3 An example of sol-gel processing conditions on film formation [35].

Sol-gel films can be deposited by spraying, dip coating or spin coating [35]. This process is very often performed in the dip-coating regime, in which the solid substrate is slowly pulled out from the solution containing the required chemicals. The reaction known as gelation (i.e. sol-gel transition of the solution in contact with the atmosphere) takes place in a thin liquid layer wetting the substrate. The xerogel coating obtained requires additional annealing to remove the residual solvent. The thickness of the resulting inorganic layer depends on the viscosity of the solution, the withdrawal speed, and the wetting conditions of the substrate (i.e., the contact wetting angle between the solution and the substrate) [2].

Another common method of performing the sol-gel reaction is spin coating, in which the solution is dispensed onto the substrate rotating at high speed. In this method a small drop of coating material is placed on the centre of a disc, which

is then spun rapidly about its axis. The drop is then driven by two competing forces: centrifugal forces cause the material to be thrown radially outwards, whereas surface tension and viscous forces will work against this spreading. Larger centrifugal forces creates thinner coating film. As the film thins, the solvent evaporates and the solution viscosity increases, reducing the radial flow. Eventually, the viscosity becomes so large that relative motion virtually ceases and the process is completed by evaporating the residual solvent [41]. Spin coating is commonly used in manufacturing microelectronic devices or magnetic storage discs.

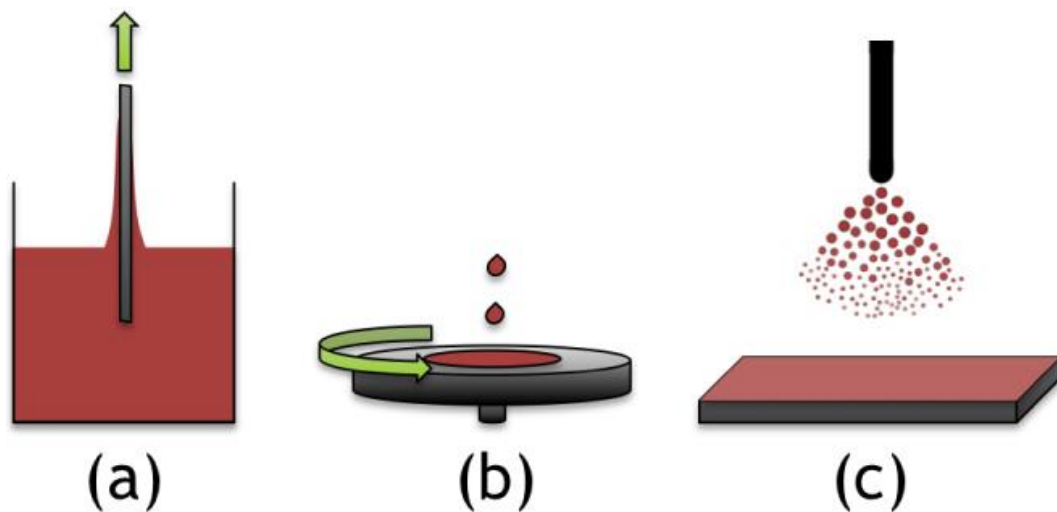


Fig 2-4 Examples of deposition methods; (a) dip coating; (b) spin coating and (c) spray coating [42].

In the spray coating the coating solution is directly sprayed onto the hot substrate at the glass manufacturer, mainly for the use as low-E (low emissivity) glasses in architecture [43]. However, these technologies are rather costly and

optical quality coatings can only be deposited on flat or weakly bent substrates [44].

For sol–gel coatings, the most popular deposition technique is the dip coating process, as it is easy to perform and results in high quality thin films.

The final stage of the formation of thin solid films prepared by the sol-gel route is annealing. Two processes occur during annealing: (1) final evaporation of solvent from the film matrix, and (2) further aggregation and sintering of nanoclusters. The resulting films are typically polycrystalline, with the grain size ranging from 10 to 20 nm [2].

The physico-chemical properties of the obtained gel and consequently the product depend on the parameters of the process. Factors such as the type of precursor, the pH, the nature and concentration of the catalyst, H₂O:Si molar ratio (R), the type of additives, mechanical agitation, temperature, method and extension of drying, the presence of doping substances, or even the chemical nature of the gelation vessel may have a strong influence on the kinetics, growth reactions, hydrolysis, and condensation reactions as well as on the product characteristics such as porosity, surface area, refractive index, thickness and mechanical properties.

2.2.2 Surface sol-gel

Ultrathin metal oxide gel films with molecular thickness can be formed on the substrate surface, too. To do so, the functionalised solid substrate with hydroxyl

groups is immersed in the alkoxide solution, rinsed with adequate organic solvent and the chemisorbed alkoxides are hydrolysed, as shown in Fig 2-5 (a). At this stage, hydroxyl groups are regenerated on the film surface, which can be employed for further chemisorption of metal alkoxides. This process, which is named the surface sol-gel process, is applicable to various alkoxides of titanium, zirconium, aluminium, silica, indium, tin, and vanadium metals [45].

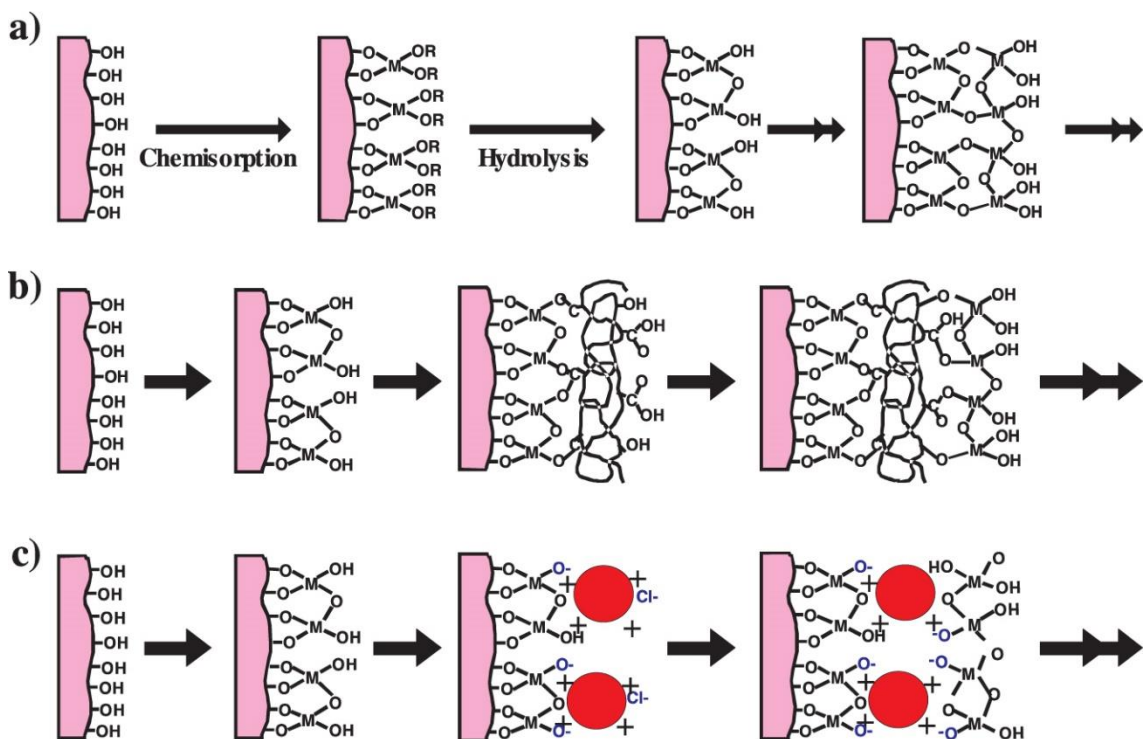


Fig 2-5 Schematic illustrations of three types of layer-by-layer adsorption based on the surface sol-gel process. Stepwise adsorption of metal alkoxides (a), alternate adsorption of metal alkoxides and polyhydroxyl compounds (b), and alternate adsorption of metal alkoxide and cationic compounds (c) [47].

The increase in thickness in one adsorption cycle is adjusted to a precision of less than 1 nm. Generation of the surface hydroxyl group is achieved by hydrolysis of chemisorbed alkoxides as well as by chemisorption of

polyhydroxyl compounds as illustrated in Fig 2-5 (b) [46]. For example, by repeating chemisorption of titanium butoxide ($\text{Ti}(\text{O}_n\text{Bu})_4$) and poly(acrylic acid) (PAA), alternating layers of 1 nm thick TiO_2 -gel and PAA have been formed on the substrate by Ichinose et al. [46]. Similar multilayer assemblies are obtainable from various combinations of metal alkoxides and polyhydroxy compounds. This methodology has been utilized to incorporate organic dyes, protected amino acids, and sugar compounds into metal oxide gel films to conduct molecular imprinting techniques [47-49].

2.2.3 Optical sensors based on sol-gel films

The sol-gel deposition of thin films of a large number of materials for various sensor applications has been reported so far. The use of the sol-gel process to produce materials for optical chemical sensors and biosensors is continuing to attract considerable interest. In most optical sensors, the chemical transducer (analyte¹-sensitive) consists of immobilized chemical reagents e.g. organic and inorganic dyes, enzymes, proteins and so on, placed in the sensing region of the optical fibre either by direct deposition or by encapsulation in a polymeric matrix. The choice of the polymer support may influence the performance of the sensor, namely its selectivity and response time, and is governed by parameters like mechanical stability, permeability to the analyte and suitability for reagent immobilization [17, 50, 51]. Porous glass-like materials obtained by the sol-gel

¹ An *analyte* is a substance whose chemical constituents are being identified and measured.

method present several properties that make them attractive for use in optical chemical sensing applications [52-54].

Paula et al. in literature [17] have presented a comprehensive overview of the sol-gel thin films-based optical sensors. Applications reviewed include numerous sensors for determination of pH, gases, ionic species and solvents, as well as biosensors. Their survey clearly illustrates the growing interest on the sol-gel process to develop optical sensors.

As mentioned earlier, in order to obtain effective sensor devices, the chemical or biological transducer can be added to the sol during different steps of the process. The nature of the sol-gel process and the chemical inertia of sol-gel glass make the system ideal for the immobilization of numerous organic, organometallic and biological molecules. These combinations yield advanced materials that exhibit the flexibility and functionality of organics and many of the useful properties of inorganics, including stability, hardness and chemical resistance. For example, the fabrication of integrated optics devices¹ using sol-gel precursors and photo-curable polymers coatings [55-57] allows the fabrication of a range of sensor configurations on planar substrates with higher sensitivity and photo-stability than dispersed dye molecules in a matrix which carries the problem of leaching [17, 51].

¹ An integrated optics device is a device that integrates multiple (at least two) photonic functions.

2.2.4 Advantages and disadvantages of the sol-gel process

Although potential applications of sol-gel processing are numerous, the actual number of successful applications is rather few. There are many advantages and disadvantages in sol-gel processing in creating coatings for sensors. Thin films benefit from most of following advantages [2, 17, 20, 50, 58, 59]

- High purity
- High chemical homogeneity with multicomponent systems.
- Relatively low temperature of preparation (usually 200-600°C).
- Preparation of ceramics and glasses with novel compositions.
- Ease of fabrication for special products such as films, powder and fibres.
- Straightforward chemistry.
- Smaller particle size and morphological control in powder synthesis.
- Leading to inorganic-organic hybrid materials.
- The adjustment of appropriate viscosities for coating.
- The composition can be highly controllable.

Despite its advantages, the sol-gel technique rarely arrives at its full industrial potential due to several critical issues that need to be considered [17, 20, 26, 28, 35, 51, 59] such as those shown below:

- Weak bonding
- Expensive and hazardous raw materials.
- Large shrinkage during fabrication.

- High permeability.
- Difficult controlling of porosity.
- The trapped organics with the thick coating often result in failure during thermal process.
- The present sol-gel technique is very substrate-dependent.
- The coating suffers from contraction and cracking.
- Leaching of reagent materials in sensing devices.
- Diffusion-limited response time in sensors.
- Limited life time usage as a sensor.
- Instable sensitivity.
- Unable repeatability of measurement in sensing devices.

2.3 Langmuir-Blodgett technique

A *Langmuir* film can be defined as an amphiphilic spread monolayer of atoms or molecules floating at the liquid-gas interface (or liquid-liquid) [42, 60, 61]. Amphiphilic molecules such as fatty acids contain a hydrophilic head group and a hydrophobic tail [62] as shown in Fig 2-6. These molecules, having the general chemical formula $(\text{CH}_3-(\text{CH}_2)_n-\text{COOH})$, contain a highly polar COOH head group and a nonpolar $(\text{CH}_2)_n-\text{CH}_3$ hydrocarbon chain. The nonpolar part which is a hydrophobic group can also consist of fluorocarbon chains and hydrophilic part can contain a polar group such as $-\text{OH}$, $-\text{NH}_3^+$, $-\text{PO}_4^-$, $(\text{CH}_2)_2\text{NH}_3^+$, etc. [63-65]. These amphiphilic molecules sometimes called surface-active-agent compounds or *surfactants* and the majority of them tend to

orient themselves on the water surface with the polar “head” of each molecule in contact with the water and the chain tilted at a more or less steep angle with the plane of the water surface [2, 66].

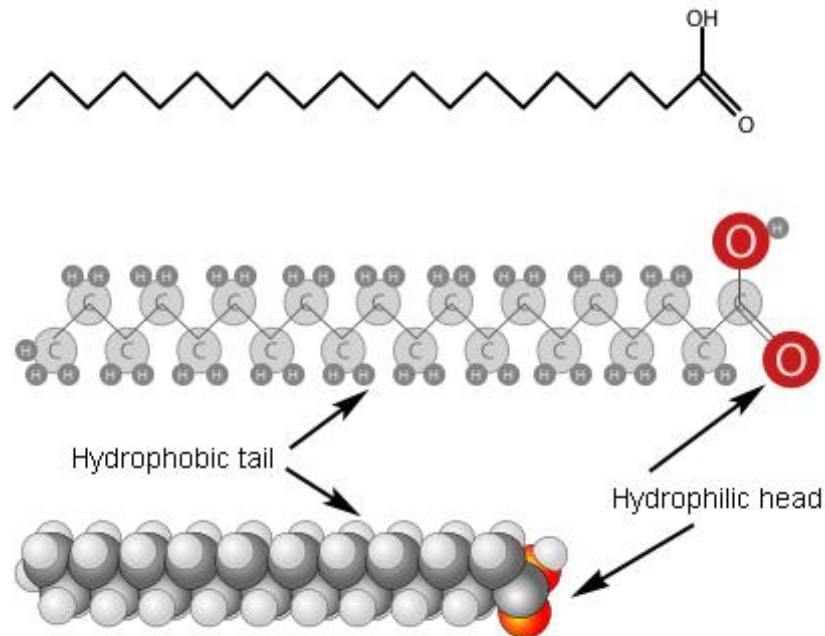


Fig 2-6 The general chemical structure of an amphiphilic molecule.

Monolayer formation is made by the forces of self-assembly on insoluble molecules at the surface of the liquid and can be characterized by the parameter of the surface pressure (π), defined as the difference between the surface tensions of pure water (σ_0) (i.e. 72-73 mN/m at room temperature [67]) and of water covered by the monolayer (σ) :

$$\pi = \sigma_0 - \sigma \quad (\text{Eq. 2.1})$$

There is a variety of methods for measuring surface pressure. Wilhelmy plate, shown in Fig 2-7, is the most common method to measure the surface pressure which is based upon the measurement of the weight of a hydrophilic plate

partially submerged in the water. If the contact angle of the water with the plate is θ , then the force exerted on the plate by the water is

$$F = \sigma L \cos(\theta) \quad (\text{Eq. 2.2})$$

where L is the perimeter of the cross section of the plate. The Wilhelmy plates used can be a filter paper, for which the contact angle is zero, leaving $F = \sigma L$.

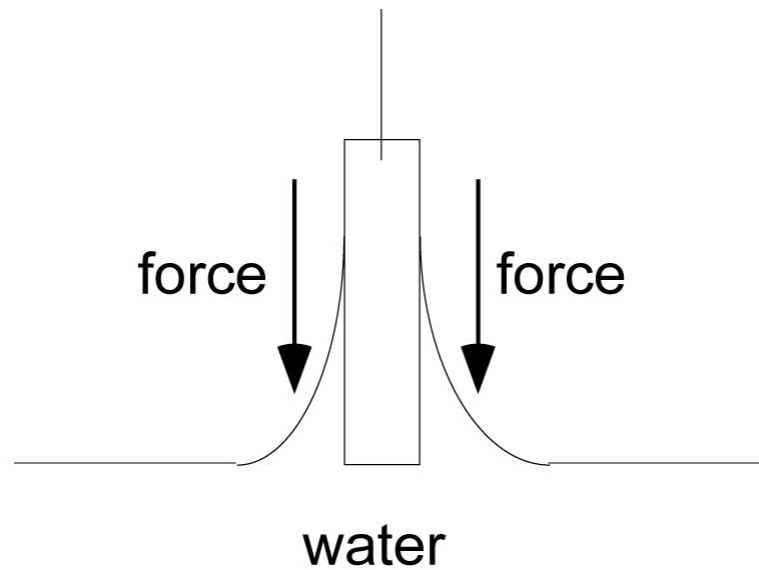


Fig 2-7 Schematic diagram of a filter paper Wilhelmy plate. The water makes contact with the paper with contact angle = 0. The water exerts a force on the plate equal to σL , where σ is the surface tension and L is the length of the contact line of the water with paper [68].

In *Langmuir-Blodgett film* (or LB film) method one or more Langmuir films is deposited onto a solid surface by vertical dipping of the solid substrate into the water subphase (or vice versa) [69]. As can be seen in Fig 2-8, the molecular density at the air-water interface is controlled using moveable barriers. By moving the barriers the film could be made to undergo compression or expansion, which changes the surface tension of the air-water interface enabling

interaction between the molecules [70]. This process takes several phases as can be seen from Fig 2-8 (a-d).

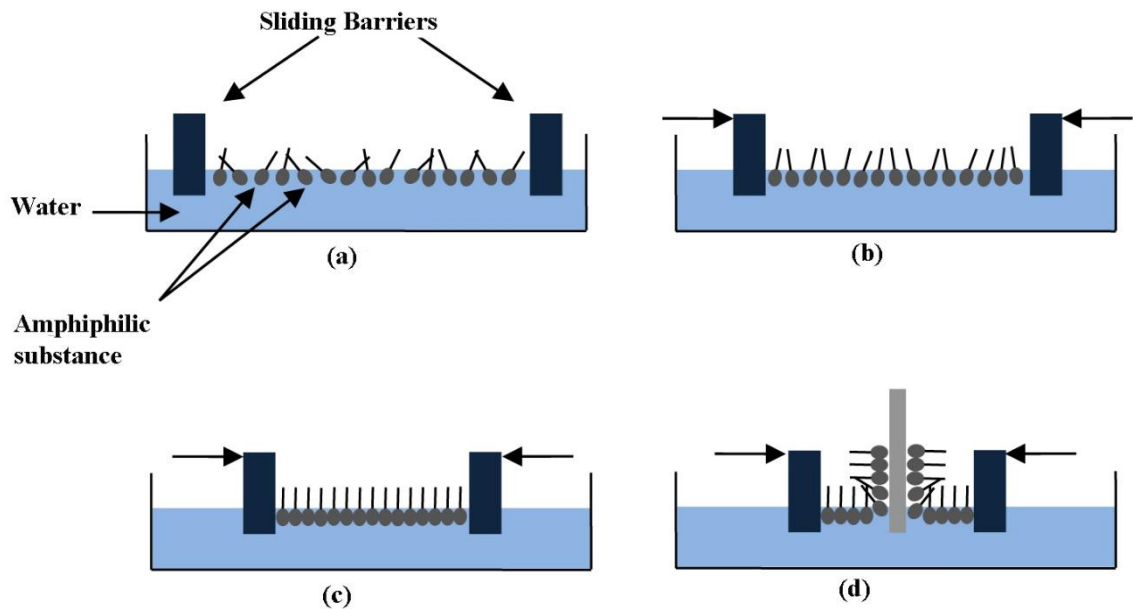


Fig 2-8 Surfactant molecules at different phases during monolayer compression a) Spreading of an amphiphile solution at the air/water interface so-called gas phase; b) compressing of the monolayer after solvent evaporation to a desired surface pressure, so-called liquid phase; c) The monolayer undergoes different phase transitions, so-called solid phase and d) Transfer of the Langmuir monolayer at a solid substrate by vertical dipping – Langmuir-Blodgett film [33].

Initially the surface pressure is zero, thus no interactions occur between the molecules which are randomly oriented. The molecules behaviour similar to a two-dimensional gas which is termed as the “gas phase”. Upon further compression, when the surface pressure is increased by moving the barriers inwards, the molecules begin to interact with each other and the hydrophobic tails of the molecules arise to lift from the surface. The molecules are pushed closer together which is termed the “liquid phase”. At the “solid phase”, the molecules are further compressed and would be in contact which reduces the surface area occupied by each molecule close to its cross-sectional area. In this

state the molecules are densely packed and in which the molecules form an ordered array. The deposition of the film on a substrate is then performed by dipping the substrate through the thus formed monolayer [3, 33, 62, 70, 71]. This can be seen schematically in Fig 2-8 (d).

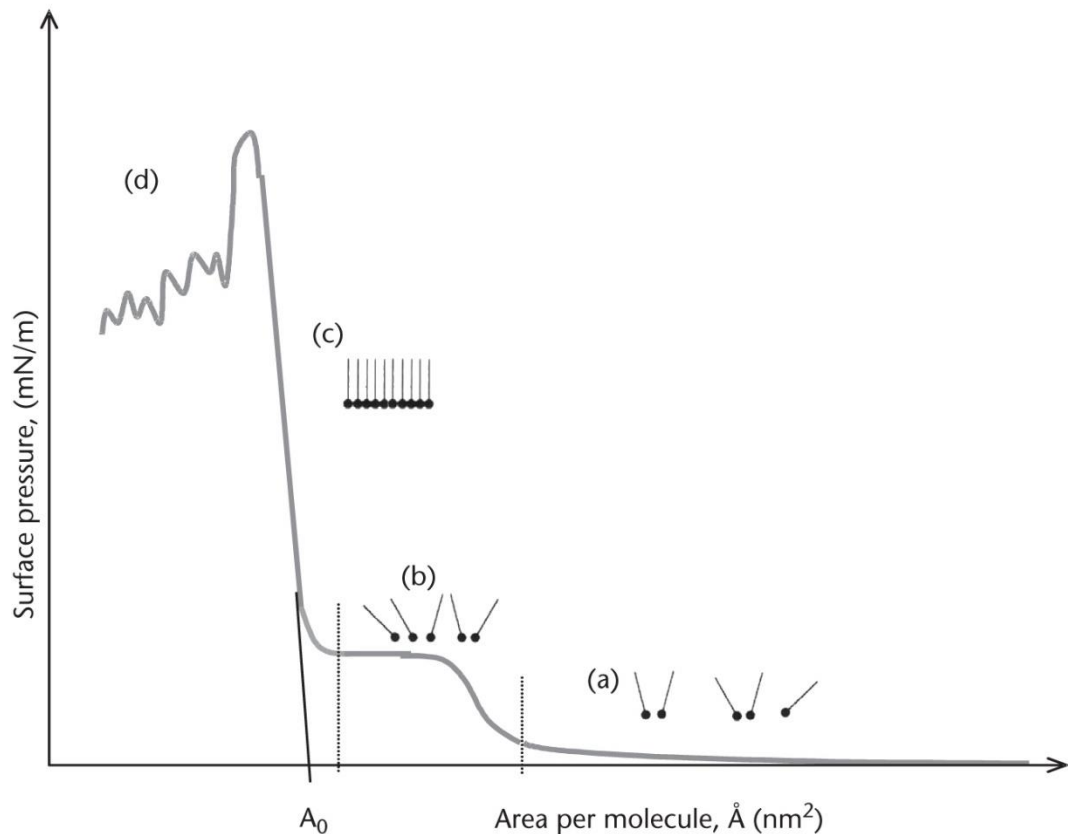


Fig 2-9 Typical π -A diagram of the Langmuir monolayer. (a) Gas phase; (b) liquid phase; (c) solid phase; and (d) monolayer collapse.

The most important index of monolayer properties of an amphiphilic material is given by measuring the surface pressure as a function of the area of water surface available to each molecule such as that shown in Fig 2-9. This is carried out at constant temperature and is known as a surface pressure - area isotherm or simply “isotherm”. Usually an isotherm is recorded by compressing the film

(reducing the surface area by means of a moving barrier) at a constant rate while continuously monitoring the surface pressure. Depending on the material being studied, repeated compressions and expansions may be necessary to achieve a reproducible trace [65, 71-74]. The water subphase is temperature-controlled throughout the entire process [75].

2.3.1 Deposition of Langmuir-Blodgett films

A Langmuir film can be used for building up a highly organised monolayer of amphiphilic molecules [76]. The multilayer structures of Langmuir films are commonly called Langmuir-Blodgett or simply LB films. In classical LB technique, it is fulfilled by the sequential dipping and withdrawing of a solid substrate into the water subphase. The LB deposition is carried out in the “solid” phase. The surface pressure is then high enough to ensure sufficient cohesion in the monolayer, e.g. the attraction between the molecules in the monolayer is high enough so that the monolayer does not fall apart during transfer to the solid substrate. Repeated deposition can be achieved to obtain well-organised multilayers on the solid substrate. The deposition setup is schematically shown in Fig 2-10. Fig 2-11 shows Langmuir-Blodgett trough structured by KSV NIMA Company.

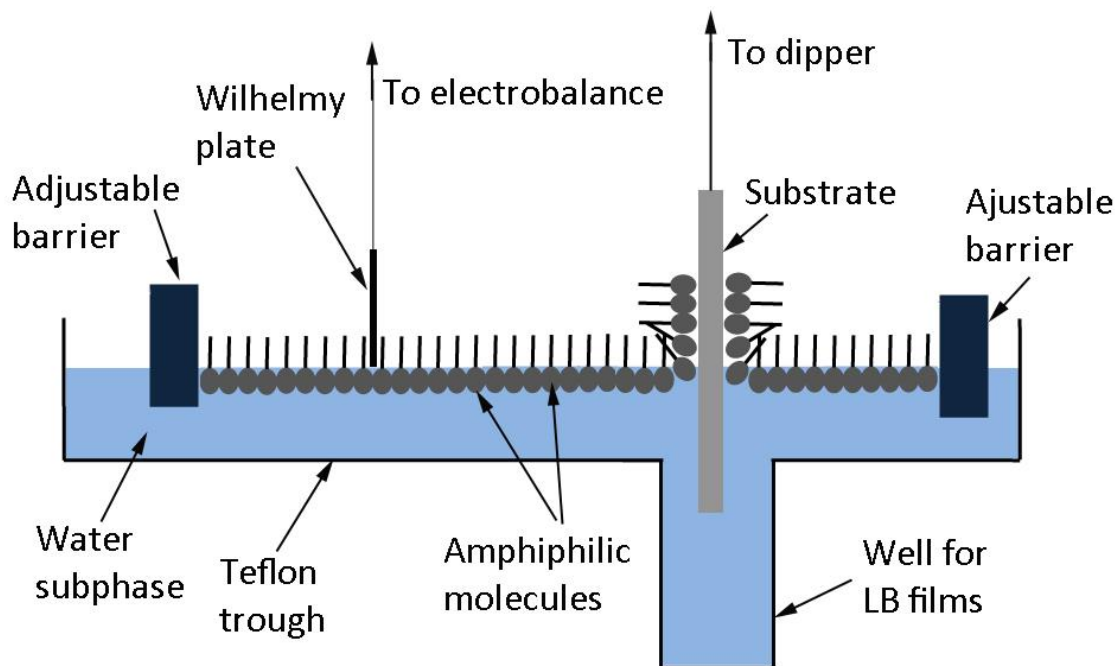


Fig 2-10 Schematic of Langmuir-Blodgett setup.

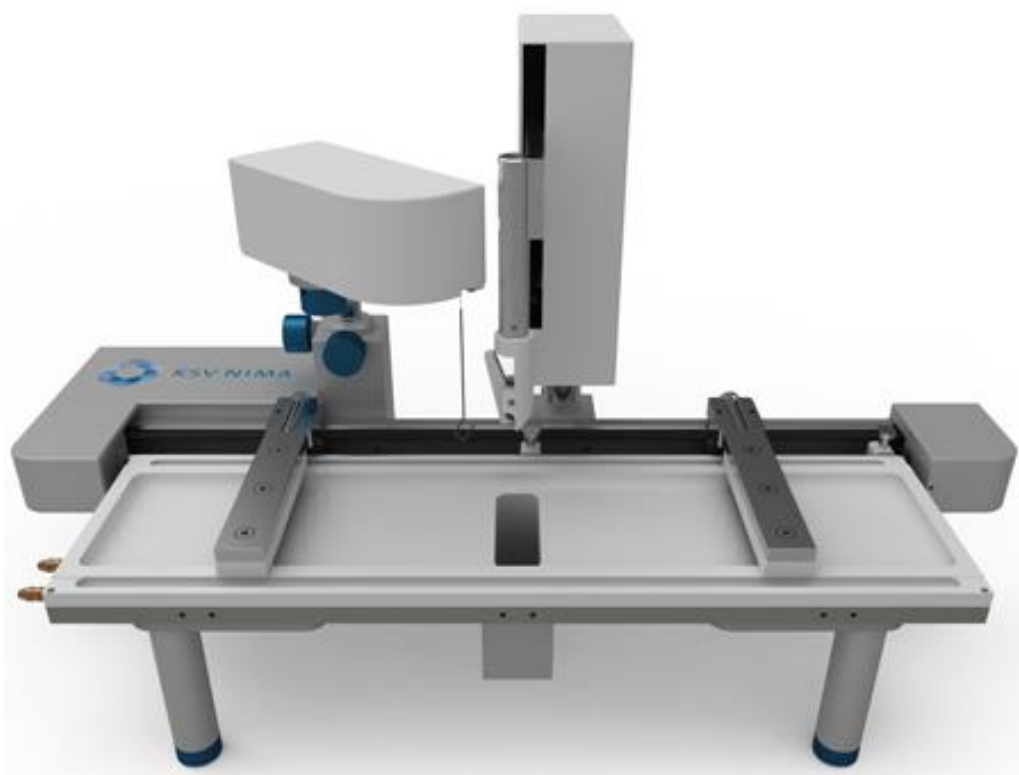
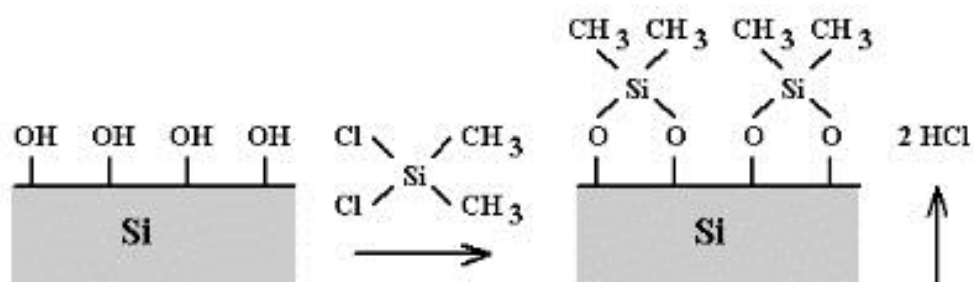


Fig 2-11 KSV NIMA Trough equipped with a Langmuir-Blodgett trough [77].

In the case of hydrophobic substrate, the deposition process starts from dipping. Some materials such as glass, quartz, silicon, etc. can be made hydrophobic by surface silanization [78]. Silicon becomes hydrophobic after treatment by hydrofluoric acid (HF) (but for few minutes). For silanization of the surface the substrate is dipped into solution of dimethyldichlorosilane ($(\text{CH}_3)_2\text{SiCl}_2$) in hexane (5%) for 15 to 20 minutes and then into hexane, acetone and again hexane for 3- 5 minutes for each. Finally, washing with soap (mechanically) and with distilled water [3, 78]. The following reaction happens during the silanization of the surface:



Highly hydrophilic substrate can be prepared by surface treatment with acids, alkalines or solution of hydrogen peroxide [3, 78].

It should be noted that only selected compounds from the fatty acids family, having a number of carbon atoms between 14 and 24, are suitable for LB film deposition [71].

Successful, repeatable deposition of LB films requires careful cleaning of the LB deposition trough, and also of the substrate. The vertical motion of the substrate can be either down into the water (downstroke) or up out of the water (upstroke). If the surface of the substrate is prepared such that it is hydrophilic,

the first layer is deposited by raising the solid substrate from the subphase through the monolayer. On the downstroke, the hydrophobic tail groups of the floating monolayer are attracted to those of the deposited LB film, thus depositing a second layer. Repeated dipping allows the film to be built one layer at a time, using these nanoscale building blocks. Fig 2-12(a) represents an illustration of this process with the adjacent layers packing head-to-head and tail-to-tail, and the overall film is termed Y-type which is the most common configuration [3, 70, 74]. If the solid substrate is hydrophobic the first layer is deposited by lowering the substrate into the subphase through the monolayer. Depending on the behaviour of the molecule the solid substrate can be dipped through the film until the desired thickness of the film is achieved. Different kinds of LB multilayers can be produced and/or obtained by successive deposition of monolayers on the same substrate. When the monolayer deposits only in the up or down direction, the multilayer structure is called either Z-type or X-type. Intermediate structures are sometimes observed for some LB multilayers and they are often referred to be XY-type multilayers. The production of so called alternating layers which consist of two different kind of amphiphiles is also possible by using specific instruments. In such an instrument there is a trough with two separate compartments both possessing a floating monolayer of a different amphiphile. These monolayers can then be alternately deposited on one solid substrate. Such a film is illustrated in Fig 2-13.

There are several parameters that affect on the type of LB film which can be produced. These are the nature of the spread film, the subphase composition and temperature, the surface pressure during the deposition and the deposition speed, the type and nature of the solid substrate and the time the solid substrate is stored in air or in the subphase between the deposition cycles [4, 63, 74, 79, 80]. Moreover, there are many external factors affecting the successful film transfer, and thus the quality of LB films, relating to issues such as water contamination, surface contamination, dust contamination and vibration [2, 3].

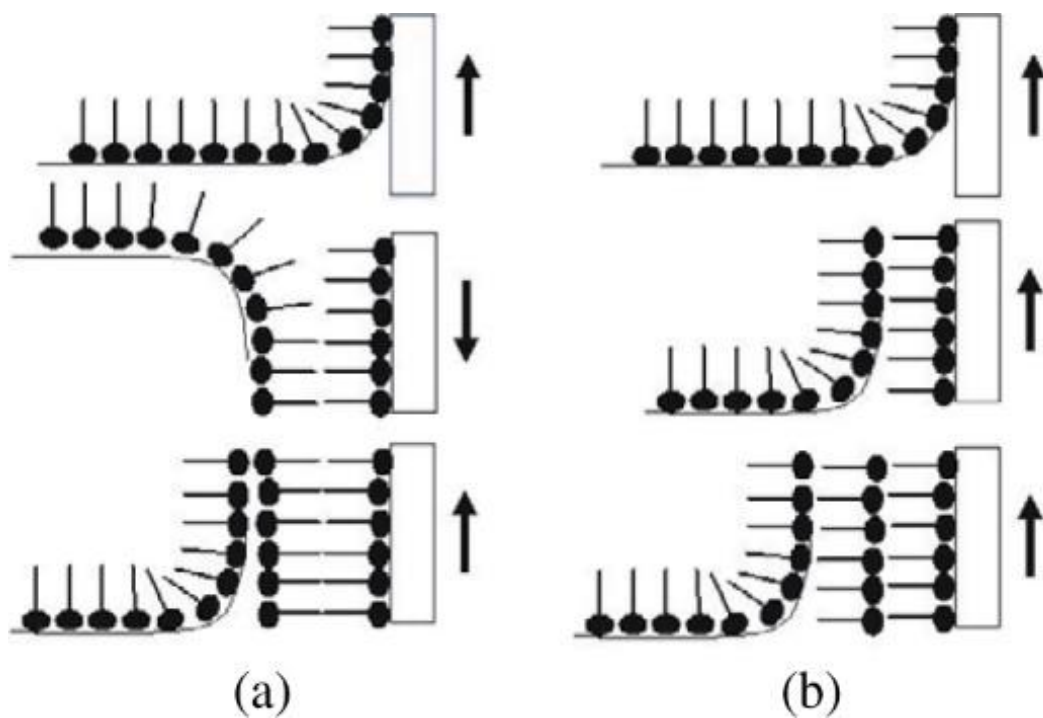


Fig 2-12 Principles of LB deposition on hydrophilic substrate: (a) Y-type deposition and (b) Z-type deposition [3].

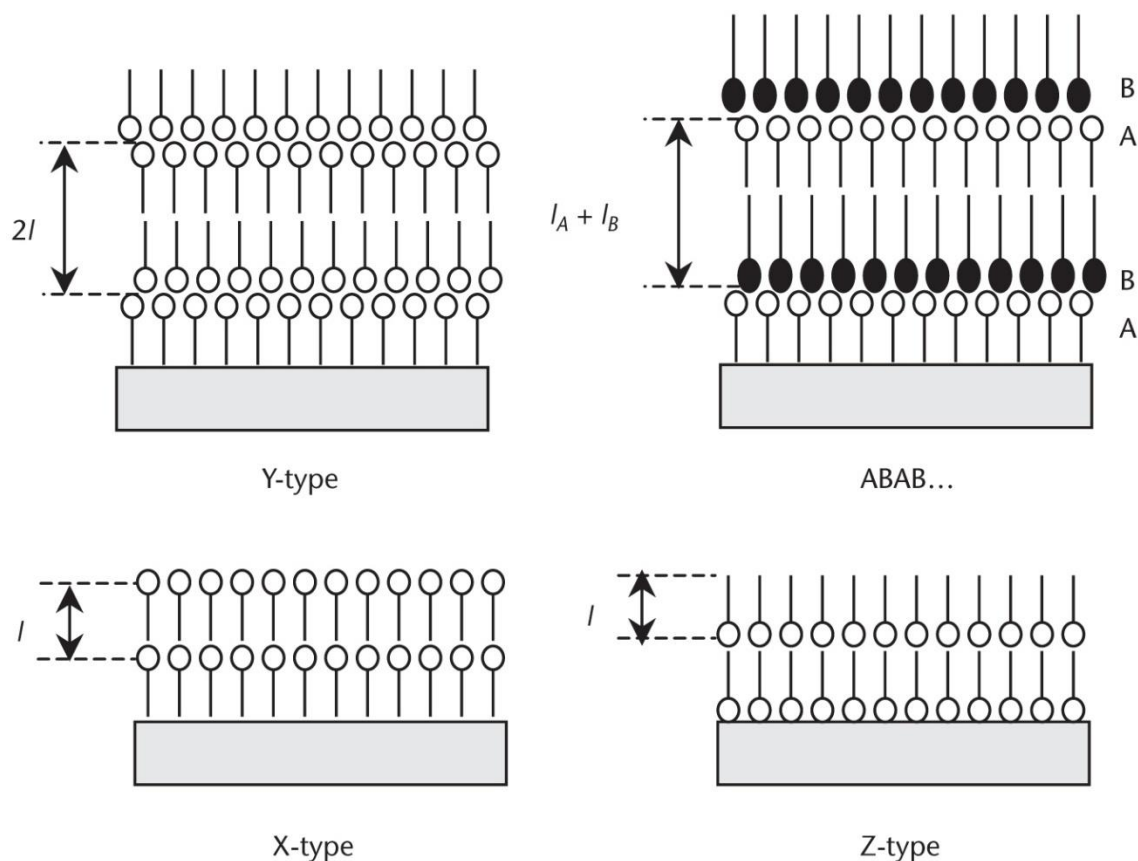


Fig 2-13 Different types of LB film deposition: Y-type, alternative layers (ABAB...), X-type, and Z-type [2].

The Langmuir-Blodgett films may be produced from fatty acid bivalent metal salts, which can be formed on the water surface according to the following reaction:



To perform such reactions in the monolayer, respective salts of bivalent metals, such as Cd^{2+} , Pb^{2+} , Cu^{2+} and Fe^{2+} typically with the concentration in the range of 10^{-4} M, have to be added to the water subphase [2, 81, 82]. Such monolayers are much more stable as compared to those formed from pure fatty acid

molecules, and thus yield much better quality LB films [62, 63]. The speed with which a film attaches itself to the solid substrate is governed by three factors, pH, salt concentration, and temperature of the water subphase [60, 83].

A *Langmuir-Schaefer* film is an alternative way to deposit the monolayer on a solid substrate and is very similar to Langmuir-Blodgett film. It is a film formed by one or several Langmuir films deposited onto a solid surface by horizontal dipping the solid substrate from the air towards water or from water through to the air as illustrated in Fig 2-14.

The immobilization of globular protein molecules onto different solid substrates by LB technique practically is often problematic. Because the majority of proteins are not amphiphilic, but soluble in water, they cannot form stable monolayers on the water surface. Therefore, proteins dissolved in the aqueous subphase can be electrostatically attached to the phospholipid monolayer on the air-water interface. The transfer of such phospholipid/protein complexes onto the solid substrate can be done by Langmuir-Schaeffer (LS) method [84].

Nanoparticles, with high electron density, can be polarized and form stable monolayers on the water surface, and can be transferred onto solid substrates with either the Langmuir-Schaeffer or the Langmuir-Blodgett methods. An alternative method is to sandwich nanoparticles between amphiphile bilayers constructed using the Langmuir-Blodgett technique [81].

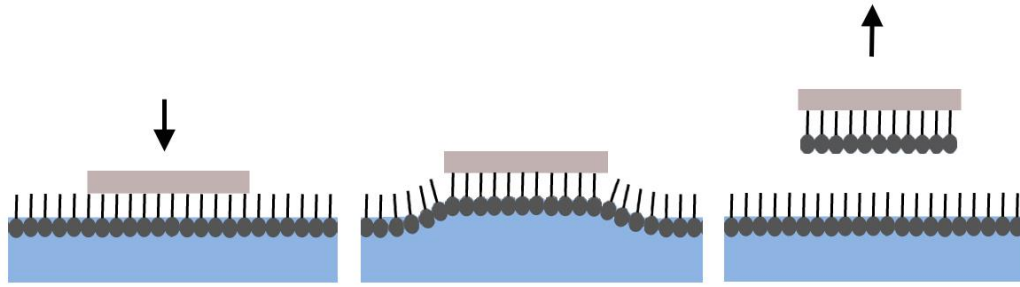


Fig 2-14 Scheme of the LS technique.

The LB technique has been used for a number of fibre optic sensor applications [85-87]. For example, Flannery et al. [87] used Langmuir-Blodgett (LB) films deposited directly onto the polished region of an optical fibre to form a single-mode planar waveguide, evanescently coupled to a side-polished single-mode fibre for pH sensing. They could control the film thickness to 3 nm as shown in Fig 2-15.

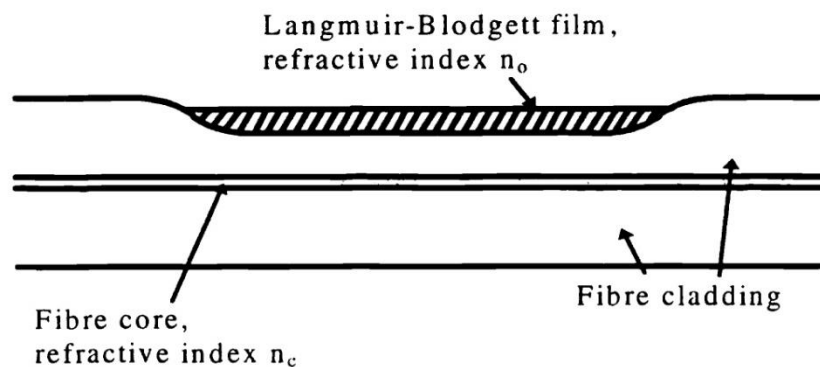


Fig 2-15 Schematic of the fibre optic sensor of Flannery et al. [87].

Another example is the work of Rees et al [85] who utilized the LB film deposition technique to investigate the effects of coating a thin film of tricosenoic acid on the transmission spectra of an optical fibre. This has been

achieved by spreading the acid from dilute chloroform solutions onto the pure water subphase of one compartment of a Nima Technology Model 2410A LB trough, leaving for 10 min at $\sim 20^{\circ}\text{C}$, and then being compressed at $0.5\text{ cm}^2\text{s}^{-1}$ ($\sim 0.1\%$ of total surface area). Deposition was then done at a surface pressure of 30 mN/m and a transfer rate of 10 mm/min . The fibre was oriented such that the dipping direction was aligned with the long axis of the fibre and it was alternately dipped and withdrawn through the floating monolayer at the air-water interface. Multiple layers had produced a Y-type structure. The film thickness was then determined by the product of the number of layers and the thickness of each molecular layer (2.6 nm). Choi et al. [88] developed a fibre optic biosensor using alcohol dehydrogenase (ADH)-immobilized Langmuir-Blodgett (LB) films for the measurement of ethanol concentration. The enzyme was immobilized on the lipid monolayers by adsorption from the aqueous subphase solution. From the measurement of the surface pressure-area isotherm and retained enzyme activity for the four types of lipids, they determined that negatively charged arachidic¹ acid (its molecular structure shown in Fig 2-6) was the most suitable for adsorption of ADH, based on its electrostatic force as well as hydrophobicity, compared to other lipids they applied (the full-text of this literature was not accessible). Caseli et al. reported in their work [89] on the construction of a new phytic² acid biosensor on the basis of the Langmuir-Blodgett (LB) technique. Phytase was inserted in the subphase solution of

¹ Arachidic acid, also called eicosanoic acid, is the saturated fatty acid with a 20-carbon chain. It is a minor constituent of peanut oil and corn oil.

² A saturated cyclic acid, is the principal storage form of phosphorus in many plant tissues, especially bran and seeds.

dipalmitoylphosphatidylglycerol (DPPG) Langmuir monolayers, and its incorporation to the air-water interface was monitored with surface pressure measurements. Phytase was able to be incorporated into DPPG monolayers even at high surface pressures, of 30 mN/m, under controlled ionic strength, pH, and temperature conditions. Tao et al. [90] used the Langmuir–Blodgett technique to assemble monolayers (with areas over 20 cm²) of aligned parallel silver nanowires which could be used as substrates for deposition of sensitive layers for sensing devices.

2.3.2 Advantages and disadvantages of LB technique

Although the LB technique is one of the oldest methods for deposition of thin films, it offers several advantages over other techniques. The most important advantages of multilayers created by means of LB technique are as follows [67, 68, 91-94]:

- High uniformity of the film combined with mutual orientation of the molecules and functional groups composing the film.
- The possibility of precise controlling of film thickness to an accuracy of a single molecule.
- A useful tool to fabricate monolayer and/or multilayer films with controllable structure in the molecular level.
- High ratio of the active surface area of the molecular layers to the film volume.

- The possibility of varying the chemical nature of the film by varying the nature of the amphiphile or by creating mixed monolayers.
- It has a high potential to use in a variety of industrial applications.
- The deposition process can be carried out in low temperature and normal pressure.

There are several disadvantages of the LB film technique which are as follow [62, 65, 70, 79, 95-98]

- Poor mechanical and thermal stability of LB films because the resultant films formed are held together by Van der Waals forces.
- LB films are poorly adhesive, too soft and fragile, and therefore can be easily damaged during preparation and exploitation.
- Lack of flexibility in shape and size of the substrate. It enables to align layers for only flat panels.
- In addition to the poor thermostability of films built from aliphatic compounds, there have been reports of changes in film properties with time.
- Lack of flexibility in choosing molecules of different structures and functions. It can only be used for molecules that are water-insoluble and have surfactant-like properties.
- Any change in the pressure can change the packing of the molecules and hence alter the orientation of them. Excess pressure can break the monolayers.

- In some cases, X and Z type films, both of which can re-orient and form thermodynamically stable Y-films.
- It is very difficult to form films several hundred Angstroms thick with good optical behaviour.

Due to these disadvantages of LB films, this method is not very feasible for use in commercial optoelectronic device applications. The layer-by-layer technique described below can be used to offset many of these disadvantages of LB films.

2.4 Layer-by-layer self-assembly technique

To date, several familiar techniques have been widely used to create a sensitive thin film in both liquid and gas phases. However, each of these techniques presents some advantages and disadvantages.

The layer-by-layer (LbL) self-assembly technique offers a number of advantages over the methods highlighted above. It can both control the thickness of the film in nanometer scale and allows for efficient deposition of thin films with well-defined properties. The LbL deposition technique is frequently used for preparing nanostructured multilayered thin films to design highly tailored surfaces on different substrates e.g. glass, ceramics, metals, wood, plastics and so on [99-102] with different shapes and sizes [103-105]. Due to the nature of the layer-by-layer technique, a variety of reagents can be used such as polymers [106, 107], nanoparticles [12, 108, 109], metals [106,

110], dyes [11, 111, 112], quantum dots [113, 114], nanotubes [115], biomolecules like enzymes [116], proteins [117] and so forth.

This technique allows the incorporation of a wide variety of molecules to provide multiple functions and properties to indicate a variety of chemical/biochemical components [118-121] for detecting a single measurand or a number of analytes at the same time [122-124]. For example a sensor designed with the deposition of pH indicator molecules performs for pH measurement and with the deposition of palladium is able to recognize hydrogen. Also using gold nanoparticles in layers encourages Surface Plasmon Resonance¹ (SPR) effect while the incorporation of hydrophilic/hydrophobic molecules could change the sensor for humidity measurement. A sensor based on the LbL technique is also able to have the ability to sense more than one analyte simultaneously. For example a carbon nanotube–polyelectrolyte composite multilayer thin film fabricated by a layer-by-layer (LbL) method has been applied to develop a multifunctional material to measure strain and corrosion processes [124]. The simultaneous detection of proteins i.e. tumor necrosis factor (TNF- α), P24 and follicle stimulating hormone (FSH) [125] is another example. In the work presented by Kirsch in [126] multi-analyte detection has been realized through the layer-by-layer assembly process by using multiple enzymes within the layers such as Glucose Oxidase and Acetylcholinesterase (AChE). This sensor showed the capability to distinguish

¹ *Surface plasmon resonance* (SPR) is the collective oscillation of electrons in a solid or liquid stimulated by incident light. The resonance condition is established when the frequency of light photons matches the natural frequency of surface electrons oscillating against the restoring force of positive nuclei.

between organophosphate neurotoxins (e.g. pesticides and chemical warfare agents¹) and non-organophosphate compounds.

2.4.1 Layer-by-layer deposition

The so-called *layer-by-layer* (LbL) deposition technique which is also called the multilayer electrostatic self-assembly (ESA) technique is based on the construction of molecular multilayers by electrostatic attraction between oppositely charged polyelectrolytes in each monolayer deposited [127]. The technique involves the construction of complex composite materials with nanoscale precision in film thickness, one layer at a time [128].

This technique is a simple and relatively cheap method to deposit alternate layers of materials. Thin films are created by depositing alternate layers of opposite charges with wash steps in between, providing a high degree of control of the film thickness with a few nanometer resolution especially for biomaterials which require precise control of film thickness [129]. The layer-by-layer technique was developed by Decher and co-workers in the early 1990s [130]. Decher describes this technique as “an enabling technology for the nanoconstruction of multifunctional films on solvent accessible surfaces”.

In this approach, a charged substrate (assumed as negative charge) is dipped into a polycation solution where a monolayer of polycation molecules is deposited by adsorption, due to the strong electrostatic attraction between the

¹ A *chemical warfare agent* (CWA) is a chemical substance whose toxic properties are used to kill, injure or incapacitate human beings.

charged surface and the oppositely charged molecules in the solution leading to an oppositely charged surface (now positively charged). Usually, the substrate is rinsed in pure water upon the formation of the polycation monolayer in order to remove any excess surface-attached molecules that are not ionically bonded to the monolayer structure. The substrate is then dipped into a polyanion solution, and rinsed again with pure water to form an anionic molecular monolayer on top of the cationic layer. These two steps are repeated for a coating that needs multiple layers. A noticeable consequence of this process is that the polycations and polyanions overlap each other at the molecular level, so adjacent layers interpenetrate to some degree [33, 129]. Building up the monolayers at the molecular level which is typically within nanometer scale, and the interpenetration of the consecutive monolayers together with the overlapping effect, lead to a material that is optically homogeneous [2]. The detailed and comprehensive description of this technique is given in Chapter 4.

2.4.2 Advantages of LbL technique

In summary, the major advantages demonstrated by using the LbL technique over conventional methods of making optical thin films is summarised below:

- ***Mechanically high stability film;*** owing to much stronger Coulomb interaction, both between the polymer layers, and between the first layer and substrate, as compared to weak van der Waals forces in LB films [2].

- ***High degree of control over thickness;*** due to the linear growth of the films with the number of deposition cycles, this method provides an extremely uniform film and the thickness can be precisely controlled with even 1 nm resolution.
- ***Synthesis at room temperature and pressure;*** as a result of this factor, the deposition process is flexible for a wide range of substrates without neither damaging the substrate nor providing the specific instrument.
- ***Wide range of reagent molecules;*** as the basis of this process is the electrostatic attraction of opposite charges, it can be used for varied reagents such as polymers , nanoparticles , metals , dyes , quantum dots , nanotubes , biomolecules like enzymes , proteins and etc.
- ***Broad range of layer functionality;*** because a variety of reagents can be used, the secondary properties such as optical, electronic and mechanical properties can be easily incorporated in the film.
- ***Inexpensive process through large scale automation;*** there are no complex reaction mechanisms. The process simply comprises of dipping a charged substrate with oppositely charged polyelectrolyte solutions and rinsing it afterwards. Thus the process is extremely cost effective and can be easily automated.
- ***Long term shelf-life;*** since the molecular layers are arranged by electrostatic forces to gain a thermodynamic stability, the resulting films are highly stable and their structural ordering does not decay over the stored-time.

- ***Environment friendly***; since it is water based process, it does not need any volatile organic compounds and the power consumption is also negligible.
- ***Independent of substrate size and topology***; unlike Langmuir-Blodgett, sputtering and evaporation processes, substrates of any size or shape maybe coated uniformly on all sides.
- ***Independent of substrate materials***; this process can be applied for preparing multilayered thin films on different solid substrates e.g. glass, ceramics, metals, wood, plastics, organic films semiconductors, and so on. [[102, 128, 132, 133]
- ***Compatibility with conventional photolithographic processes***; the meeting of lithography and LbL technique overcomes the resolution limit of photolithography and also assists self-assembly to form complex patterns to create integrated devices [[134, 135].
- ***Molecular level uniformity***; due to the growth of thin films at the molecular level the technique presents a uniform film.

2.4.3 Disadvantages of LbL technique

These can be summarized as:

- ***Time consuming***; long time is required to assemble a single film (up to 20 minutes). The low speed deposition limits the use of this method to relatively thin film formation.

- ***Some factors make it hard to control;*** a variety of factors such as charge transfer interactions and hydrogen bonding impact the process and make it difficult to control [136].
- ***Instability in high polarity solution;*** as a result of electrostatic interactions, high polar solutions such as the solution with extreme pH values may cause an ionic strength problem and devastation of the layers.
- ***Difficulty in application of multilayers to large surface areas;*** alternative methods to overwhelm this problem is to use spraying or spinning approach instead of dip coating [137].
- ***Less ordered thin film;*** the prepared films are less ordered, as compared to LB films [2].

2.5 Summary

The coating deposition methods discussed, i.e. Langmuir Blodgett and sol-gel approaches were introduced in detail, with their advantages and disadvantages considered and the LbL technique (used in this work for the deposition of sensitive thin films on fibre) was explained. The sol-gel is a chemical synthesis technique for preparing gels, glasses, ceramic powders and thin films. The sol-gel process generally involves the use of metal alkoxides, which undergo hydrolysis and condensation polymerization reactions to give gels. The sol-gel process comprises solution, gelation, drying, and densification. The development of sol-gel-based optical materials has also been quite successful,

and applications include monoliths (lenses, prisms and lasers), fibers (waveguides), and a wide variety of optical films.

A Langmuir–Blodgett film contains one or more monolayers of an organic material, deposited from the surface of a liquid onto a solid by immersing the solid substrate into (or from) the liquid. A monolayer is adsorbed homogeneously with each immersion or emersion step, thus films with very accurate thickness can be formed.

Both sol-gel and Langmuir-Blodgett approaches are satisfactory for the deposition of sensitive layers onto a fibre optic. However, the LbL technique addresses the disadvantages of these two techniques and demonstrates better results.

A more detailed characterization of the coating of a substrate deposited using LbL technique is discussed in Chapter 4.

References

- [1] D. W. Schubert, "Spin coating as a method for polymer molecular weight determination," *Polymer Bulletin*, vol. 38, pp. 177-184, 1997/02/01 1997.
- [2] A. Nabok, *Organic and inorganic nanostructures*: Artech House, 2005.
- [3] W. J. Stephen and P. T. Ralph, "Fibre optic sensors with nano-structured coatings," *Journal of Optics A: Pure and Applied Optics*, vol. 8, pp. S430-S435, 2006.
- [4] J. A. zaszczinski, R. Viswanathan, L. Madsen, J. Garnæs, and D. K. Schwartz, "Langmuir-Blodgett Films," *Science*, vol. 263, pp. 1726-1733, 1994.
- [5] L. A. Chrisey, G. U. Lee, and C. E. O'Ferrall, "Covalent attachment of synthetic DNA to self-assembled monolayer films," *Nucleic Acids Research*, vol. 24, pp. 3031-3039, 1996.
- [6] S. M. Amador, J. M. Pachence, R. Fischetti, J. P. McCauley, A. B. Smith, and J. K. Blasie, "Use of self-assembled monolayers to covalently tether protein monolayers to the surface of solid substrates," *Langmuir*, vol. 9, pp. 812-817, 1993/03/01 1993.
- [7] M. Zohreh, S. M. Ghoreishi, M. Behpour, and M. Mohammadhassan, "Applied electrochemical biosensor based on covalently self assembled monolayer at gold surface for determination of epinephrine in the presence of Ascorbic acid," *Arabian Journal of Chemistry*.
- [8] J. Cao, E. K. Galbraith, T. Sun, and K. T. V. Grattan, "Cross-Comparison of Surface Plasmon Resonance-Based Optical Fiber Sensors With Different Coating Structures," *IEEE Sensors Journal*, vol. 12, pp. 2355-2361, Jul 2012.
- [9] J. B. S. G. Decher, *Multilayer Thin Films*: Wiley-VCH Verlag GmbH & Co., 2002.
- [10] J. Lin, "Recent development and applications of optical and fiber-optic pH sensors," *Trends in Analytical Chemistry*, vol. 19, pp. 541-552, 2000.
- [11] C. R. Z. n. J. Goicoechea, I.R. Mat'ias, F.J. Arregui, "Optical fiber pH sensors based on layer-by-layer electrostatic self-assembled Neutral Red," *Sensors and Actuators B* vol. 132, pp. 305-311, 2008.
- [12] S. K. Suguru Kodaira, Seung-Woo Lee, William J. Batty, Stephen W. James, Ralph P. and Tatam, "Fabrication of Highly Efficient Fibre-Optic Gas Sensors Using SiO₂/Polymer Nanoporous Thin Films," in *3rd International Conference on Sensing Technology*, Tainan, Taiwan, 2008.
- [13] I. R. M. Ignacio Del Villar, Francisco J. Arregui, "Fiber-Optic Chemical Nanosensors by Electrostatic Molecular Self-Assembly," *Current Analytical Chemistry*, vol. 4, pp. 341-355, 2008.

- [14] I. R. M. Ignacio Del Villar, Francisco J. Arregui and Richard O. Claus, "ESA-Based In-Fiber Nanocavity for Hydrogen–Peroxide Detection," *IEEE Transactions on Nanotechnology*, vol. 4, pp. 187-193, 2005.
- [15] F. J. A. Ignacio R. Matias, Jesus M. Corres and Javier Bravo, "Evanescent Field Fiber-Optic Sensors for Humidity Monitoring Based on Nanocoatings," *IEEE Sensors Journal*, vol. 7, pp. 89-95, 2007.
- [16] M. H. C.R. Zamarreño, I. Del Villar, I.R. Matías and F.J. Arregui, "Optical fiber pH sensor based on lossy-mode resonances by means of thin polymeric coatings," *Sensors and Actuators B* vol. 155, pp. 290-297, 2011.
- [17] P. C. A. Jerónimo, A. N. Araújo, and M. Conceição B.S.M. Montenegro, "Optical sensors and biosensors based on sol–gel films," *Talanta*, vol. 72, pp. 13-27, 4/15/ 2007.
- [18] A. C. Pierre, *Introduction to Sol-Gel Processing*: Springer US, 1998.
- [19] G. Mattei, C. de Julián Fernández, P. Mazzoldi, C. Sada, G. De, G. Battaglin, *et al.*, "Synthesis, Structure, and Magnetic Properties of Co, Ni, and Co–Ni Alloy Nanocluster-Doped SiO₂ Films by Sol–Gel Processing," *Chemistry of Materials*, vol. 14, pp. 3440-3447, 2002/08/01 2002.
- [20] C. J. Brinker and G. W. Scherer, *Sol-Gel Science: The Physics and Chemistry of Sol-Gel Processing*: Academic Press, 1990.
- [21] S. Zhu and A. B. Bocarsly, "Cyanogels: Processing by Spin Coating," in *Dekker Encyclopedia of Nanoscience and Nanotechnology* vol. 5, ed: Taylor & Francis Group, 2009.
- [22] J. Wen and G. L. Wilkes, "Organic/inorganic hybrid network materials by the sol-gel approach," *Chem. Mater.*, vol. 8, pp. 1667-1681, 1996.
- [23] A. Lobnik, I. Oehme, I. Murkovic, and O. S. Wolfbeis, "pH optical sensors based on sol-gels: chemical doping versus covalent immobilization," *Analytica Chimica Acta*, vol. 367, pp. 159-165, 1998.
- [24] G. Li and M. Nogami, "Preparation and optical properties of sol-gel derived ZnSe crystallites doped in glass films," *Journal of Applied Physics* vol. 75, pp. 4276-4278, 1994.
- [25] I. A. Rahman and V. Padavettan, "Synthesis of Silica Nanoparticles by Sol-Gel: Size-Dependent Properties, Surface Modification, and Applications in Silica-Polymer Nanocomposites—A Review," *Journal of Nanomaterials*, vol. 2012, pp. 1-15, 2012.
- [26] T. Olding, S. M., and D. Barrow, "Ceramic Sol-Gel Composite Coatings for Electrical Insulation," *Thin Solid Films*, vol. 398-399, pp. 581-586, 2001.

- [27] K. M. Kulinowski, P. Jiang, H. Vaswani, and V. L. Colvin, "Porous metals from colloidal templates," *Advanced Materials*, vol. 12, pp. 833-838, 2000.
- [28] G. Kordas, "Sol-gel preparation of MgO fibers," *Journal of Materials Chemistry*, vol. 10, pp. 1157-1160, 2000.
- [29] L. L. Hench and J. K. West, "The sol-gel process," *Chemical Reviews*, vol. 90, pp. 33-72, 1990/01/01 1990.
- [30] L. C. Klein, *Sol-Gel Optics: Processing and Applications*: Springer US, 1994.
- [31] J. J. Perez-Bueno, L. L. Diaz-Florez, J. F. Perez-Robles, F. J. Espinoza-Beltran, A. Manzano-Ramirez, R. Ramirez-Bon, *et al.*, "Optical processes in SiO₂ sol-gel glass colored with organic dyes," *Inorganic Materials*, vol. 36, pp. 1060-1069, Oct 2000.
- [32] J. S. Yin and Z. L. Wang, "Template-assisted self-assembly and cobalt doping of ordered mesoporous titania nanostructures," *Advanced Materials*, vol. 11, pp. 469-472, 1999.
- [33] L. S. M. Alwis, "Optimization of Polymer Coated Long Period Grating-based Sensors," PhD, School of Engineering and Mathematical Sciences, City University London, 2013.
- [34] P. Yang, *The Chemistry of Nanostructured Materials*: World Scientific, 2003.
- [35] C. C. Koch, *Nanostructured Materials: Processing, Properties and Applications*: Elsevier Science, 2006.
- [36] K. Rath. (2005). *Novel Materials from Solgel Chemistry*.
- [37] A. S. Edelstein and R. C. Cammaratra, *Nanomaterials: Synthesis, Properties and Applications, Second Edition*: Taylor & Francis, 1998.
- [38] H. S. Nalwa, *Nanostructured Materials and Nanotechnology*: Academic Press, 2002.
- [39] R. A. Fischer, *Precursor Chemistry of Advanced Materials: CVD, ALD and Nanoparticles*: Springer, 2010.
- [40] C. J. Brinker, R. Sehgal, S. L. Hietala, R. Deshpande, D. M. Smith, D. Lop, *et al.*, "Sol-gel strategies for controlled porosity inorganic materials," *Journal of Membrane Science*, vol. 94, pp. 85-102, 1994.
- [41] R. Denk, M. Geissert, M. Hieber, J. Saal, and O. Sawada, "The Spin-Coating Process: Analysis of the Free Boundary Value Problem," *Communications in Partial Differential Equations*, vol. 36, pp. 1145-1192, 2011/07/01 2011.
- [42] C. D. Bain and G. M. Whitesides, *Modelling Organic Surfaces with Self-Assembled Monolayers*. Harvard University Cambridge MA, Department of Chemistry: Defense Technical Information Center, 1989.

- [43] L. Pawlowski, *The Science and Engineering of Thermal Spray Coatings*: Wiley, 2008.
- [44] J. Puetz, G. Gasparro, and M. A. Aegerter, "Liquid film spray deposition of transparent conducting oxide coatings," *Thin Solid Films*, vol. 442, pp. 40-43, 2003.
- [45] I. Ichinose, H. Senzu, and T. Kunitake, "A Surface Sol-Gel Process of TiO₂ and Other Metal Oxide Films with Molecular Precision," *Chem. Mater.*, vol. 9, pp. 1296-1298, 1997.
- [46] I. Ichinose, T. Kawakami, and T. Kunitake, "Alternate Molecular Layers of Metal Oxides and Hydroxyl Polymers Prepared by the Surface Sol-Gel Process," *Advanced Materials*, vol. 10, pp. 535-539, 1998.
- [47] G. Decher and J. B. Schlenoff, *Multilayer Thin Films*: Wiley-VCH Verlag GmbH & Co., 2002.
- [48] S.-W. Lee, I. Ichinose, and T. Kunitake, "Molecular Imprinting of Azobenzene Carboxylic Acid on a TiO₂ Ultrathin Film by the Surface Sol-Gel Process," *Langmuir*, vol. 14, pp. 2857-2863, 1998.
- [49] I. Ichinose, H. Senzu, and T. Kunitake, "Stepwise Adsorption of Metal Alkoxides on Hydrolyzed Surfaces: A Surface Sol-Gel Process," *Chem. Lett.*, pp. 831-832, 1996.
- [50] P. R. Ohodnicki Jr, S. Natesakhawat, J. P. Baltrus, B. Howard, and T. D. Brown, "Characterization of optical, chemical, and structural changes upon reduction of sol-gel deposited SnO₂ thin films for optical gas sensing at high temperatures," *Thin Solid Films*, vol. 520, pp. 6243-6249, 7/31/ 2012.
- [51] B. D. McCraith, C. McDonagh, A. K. McEvoy, T. Butler, G. O'Keeffe, and V. Murphy, "Optical chemical sensors based on Sol-Gel materials: recent advances and critical issues," *Journal of Sol-Gel Science and Technology*, vol. 8, pp. 1053-1061, 1997/01/01 1997.
- [52] J. Lin and C. W. Brown, "Sol-gel glass as a matrix for chemical and biochemical sensing," *TrAC Trends in Analytical Chemistry*, vol. 16, pp. 200-211, 4// 1997.
- [53] O. Lev, M. Tsionsky, L. Rabinovich, V. Glezer, S. Sampath, I. Pankratov, *et al.*, "Organically modified sol-gel sensors," *Analytical Chemistry*, vol. 67, pp. 22A-30A, 1995/01/01 1995.
- [54] C.-Y. Li, X.-B. Zhang, Z.-X. Han, B. Akermark, L. Sun, G.-L. Shen, *et al.*, "A wide pH range optical sensing system based on a sol-gel encapsulated amino-functionalised corrole," *Analyst*, vol. 131, pp. 388-393, 2006.
- [55] P. Etienne, P. Coudray, Y. Moreau, and J. Porque, "Photocurable Sol-Gel Coatings: Channel Waveguides for Use at 1.55 μm ," *Journal of Sol-Gel Science and Technology*, vol. 13, pp. 523-527, 1998/01/01 1998.

- [56] S. Aubonnet, H. F. Barry, C. von Bultzingslowen, J. M. Sabattie, and B. D. MacCraith, "Photo-patternable optical chemical sensors based on hybrid sol-gel materials," *Electronics Letters*, vol. 39, pp. 913-914, 2003.
- [57] J. R. Askim, M. Mahmoudi, and K. S. Suslick, "Optical sensor arrays for chemical sensing: the optoelectronic nose," *Chemical Society Reviews*, vol. 42, pp. 8649-8682, 2013.
- [58] J. Zarzycki, "Past and Present of Sol-Gel Science and Technology," *Journal of Sol-Gel Science and Technology*, vol. 8, pp. 17-22, 1997/01/01 1997.
- [59] M. N. Rahaman, *Ceramic Processing and Sintering*: Taylor & Francis, 2003.
- [60] K. B. Blodgett, "Films Built by Depositing Successive Monomolecular Layers on a Solid Surface," *Journal of the American Chemical Society*, vol. 57, pp. 1007-1022, 1935/06/01 1935.
- [61] P. G. de Gennes, "Wetting: statics and dynamics," *Reviews of Modern Physics*, vol. 57, pp. 827-863, 1985.
- [62] I. R. Peterson, "Langmuir-Blodgett films," *Journal of Physics D: Applied Physics*, vol. 23, p. 379, 1990.
- [63] S. A. Hussain, *Langmuir-Blodgett Films*: GRIN Verlag, 2011.
- [64] V. M. Kaganer, H. Möhwald, and P. Dutta, "Structure and phase transitions in Langmuir monolayers," *Reviews of Modern Physics*, vol. 71, pp. 779-819, 04/01/ 1999.
- [65] G. L. Gaines, *Insoluble monolayers at liquid-gas interfaces*: Interscience Publishers, 1966.
- [66] L. Komitov, B. Stebler, G. Gabrielli, M. Puggelli, A. Sparavigna, and A. Strigazzi, "Amphiphilic Langmuir-Blodgett Films as a New Tool for Inducing Alignment Transition in Nematics," *Molecular Crystals and Liquid Crystals Science and Technology. Section A. Molecular Crystals and Liquid Crystals*, vol. 243, pp. 107-124, 1994/03/01 1994.
- [67] S. Raleva. (2013). *Langmuir-Blodgett Technology*.
- [68] A. Feder, "Optical Studies of Monolayers at the Air/Water Interface," PhD, Department of Physics, Harvard University Cambridge, Massachusetts, 1997.
- [69] G. Decher, "An Introduction to Ultrathin Organic Films from Langmuir-Blodgett to Self-Assembly. Von A. Ulman. Academic Press, New York, 1991," *Angewandte Chemie*, vol. 104, pp. 498-499, 1992.
- [70] N. Osvaldo and J. Oliveira, "Langmuir-Blodgett Films - Properties and Possible Applications," *Brazilian Journal of Physics*, vol. 22, pp. 60-69, 1992.

- [71] M. C. Petty, *Langmuir-Blodgett Films: An Introduction*: Cambridge University Press, 1996.
- [72] D. O. Shah, *Micelles: Microemulsions, and Monolayers: Science and Technology*: Taylor & Francis, 1998.
- [73] D. K. Chattoraj and K. S. Birdi, *Adsorption and the Gibbs surface excess*: Plenum Press, 1984.
- [74] (2013). *Langmuir and Langmuir-Blodgett Films, WHAT and HOW ?*
- [75] R. G. Laughlin, *The aqueous phase behaviour of surfactants*: Academic Press INC, 1996.
- [76] F. Schreiber, "Structure and growth of self-assembling monolayers," *Progress in Surface Science* vol. 65, pp. 151-256, 2000.
- [77] (2012). *Langmuir, Langmuir-Blodgett, Langmuir-Schaefer Technique*.
- [78] V. I. Troitsky. (2012). *Methods of deposition of molecular organized thin films*.
- [79] A. Ulman, *Characterization of Organic Thin Films*: Momentum Press, 2010.
- [80] D. K. Schwartz, "Langmuir–Blodgett Films, Formation and Structure of," in *Encyclopedia of Materials: Science and Technology (Second Edition)*, K. H. J. B. Editors-in-Chief: , W. C. Robert, C. F. Merton, I. Bernard, J. K. Edward, M. Subhash, *et al.*, Eds., ed Oxford: Elsevier, 2001, pp. 4392-4399.
- [81] G. A. Ozin, "Nanochemistry: Synthesis in Diminishing Dimensions," *Advanced Materials*, vol. 4, pp. 612-649, Oct 1992.
- [82] P. Yang and F. Kim, "Langmuir–Blodgett Assembly of One-Dimensional Nanostructures," *ChemPhysChem*, vol. 3, pp. 503-506, 2002.
- [83] K. B. Blodgett and I. Langmuir, "Built-Up Films of Barium Stearate and Their Optical Properties," *Physical Review*, vol. 51, pp. 964-982, 06/01/1937.
- [84] F. Hide, B. J. Schwartz, M. A. Diaz-Garcia, and A. J. Heeger, "Laser Emission from Solutions and Films Containing Semiconducting Polymer and Titanium Dioxide Nanocrystals," *Chemical Physics Letters* vol. 256, pp. 424-430, 1996.
- [85] N. D. Rees, S. W. James, R. P. Tatam, and G. J. Ashwell, "Optical fiber long-period gratings with Langmuir—Blodgett thin-film overlays," *Optics Letters*, vol. 27, pp. 686-688, 2002.
- [86] D. Flannery, S. W. James, R. P. Tatam, and G. J. Ashwell, "pH sensor using Langmuir-Blodgett overlays on polished optical fibers," *Optics Letters*, vol. 22, pp. 567-569, 1997.

- [87] D. Flannery, S. W. James, R. P. Tatam, and G. J. Ashwell, "Fiber optic pH sensors using thin-film Langmuir-Blodgett overlay waveguides on single-mode optical fibers," 1997, pp. 264-272.
- [88] J. W. Choi, J. Y. Bae, J. H. Min, K. S. Cho, and W. H. Lee, "Fiber-optic ethanol sensor using alcohol dehydrogenase-immobilized Langmuir-Blodgett film," *Sensors and Materials*, vol. 8, pp. 493-504, 1996.
- [89] L. Caseli, M. L. Moraes, V. Zucolotto, M. Ferreira, T. M. Nobre, M. E. D. Zaniquelli, *et al.*, "Fabrication of phytic acid sensor based on mixed phytase-lipid Langmuir-Blodgett films," *Langmuir*, vol. 22, pp. 8501-8508, Sep 2006.
- [90] A. Tao, F. Kim, C. Hess, J. Goldberger, R. He, Y. Sun, *et al.*, "Langmuir-Blodgett Silver Nanowire Monolayers for Molecular Sensing Using Surface-Enhanced Raman Spectroscopy," *Nano Letters*, vol. 3, pp. 1229-1233, 2003/09/01 2003.
- [91] S. N. Shtykov, T. Y. Rusanova, A. V. Kalach, and K. E. Pankin, "Application of Langmuir-Blodgett films as modifiers of piezoresonance sensors," *Sensors and Actuators B: Chemical*, vol. 114, pp. 497-499, 3/30/ 2006.
- [92] D. K. Schwartz, "Langmuir-Blodgett film structure," *Surface Science Reports*, vol. 27, pp. 241-334, 1997.
- [93] Y. Chen, Y. Kong, Y. Wang, P. Ma, M. Bao, and X. Li, "Supramolecular self-assembly study of a flexible perylenetetracarboxylic diimide dimer in Langmuir and Langmuir-Blodgett films," *Journal of Colloid and Interface Science*, vol. 330, pp. 421-427, 2009.
- [94] T. Moriizumi, "Langmuir-Blodgett films as chemical sensors," *Thin Solid Films*, vol. 160, pp. 413-429, 6// 1988.
- [95] D. M. Nguyen, T. M. Mayer, S. F. Hubbard, K. D. Singer, J. A. Mann, and J. B. Lando, "Polar Polymeric Langmuir-Blodgett Films for Optical Applications," *Macromolecules*, vol. 30, pp. 6150-6157, 1997/10/01 1997.
- [96] A. Ulman, *An Introduction to Ultrathin Organic Films: From Langmuir-Blodgett to Self-Assembly: Academic Press Inc*, 1991.
- [97] M. A. Baldo, V. G. Kozlov, and P. E. Burrows, "Low pressure organic vapor phase deposition of small molecular weight organic light emitting device structures," *Applied Physics Letters*, vol. 71, pp. 3033-3035, 1997.
- [98] G. G. Roberts, "An applied science perspective of Langmuir-Blodgett films," *Advances in Physics*, vol. 34, pp. 475-512, 1985.
- [99] G. Decher, "Fuzzy Nanoassemblies: Toward Layered Polymeric Multicomposites," *Science*, vol. 277, pp. 1232-1237, 1997.

- [100] Y. L. Aprillya Rosidian, and Richard O. Claus, "Ionic Self-Assembly of Ultrahard ZrO₂/Polymer Nanocomposite Thin Films," *Advanced Materials*, vol. 10, pp. 1087-1091, 1998.
- [101] F. J. Arregui, Ignacio R. Matias, Richard O. Claus and Kristie L. Cooper, "Molecularly Self-Assembled Optical Fiber Sensors," *IEEE Sensors Conference*, pp. 198-202, 2002.
- [102] O. Mermut and C. J. Barrett, "Stable sensor layers self-assembled onto surfaces using azobenzene-containing polyelectrolytes," *Analyst*, vol. 126, pp. 1861-1865, 2001.
- [103] G. Decher, J.D. Hong and J. Schmitt, "Buildup of ultrathin multilayer films by a self-assembly process: III. Consecutively alternating adsorption of anionic and cationic polyelectrolytes on charged surfaces," *Thin Solid Films*, vol. 210/21 I, pp. 831-835, 1992.
- [104] F. Surre, W. B. Lyons, T. Sun, K.T.V. Grattan, S.O'Keeffe, E. Lewis. C. Elosua and C. B. M. Hernaez, "U-bend fibre optic pH sensors using layer-by-layer electrostatic self-assembly technique," *Journal of Physics: Conference Series, Sensors & their Applications XV*, vol. 178, pp. 1-4, 2009.
- [105] K. A. Soichi Otsuki, Takahisa Taguchi, "A novel fiber-optic gas-sensing configuration using extremely curved optical fibers and an attempt for optical humidity detection," *Sensors and Actuators B* vol. 53, pp. 91-96, 1998.
- [106] S. Kaul, S. Chinnayelka, and M. J. McShane, "Self-Assembly of Polymer/Nanoparticle Films for Fabrication of Fiber-Optic Sensors Based On SPR," in *Optical Fibers and Sensors for Medical Applications IV*, Bellingham, WA, 2004.
- [107] I. R. Matias, Jesus M. Corres, Ignacio del Villar, Francisco J. Arregui, , "Design of pH Sensors in Long-Period Fiber Gratings Using Polymeric Nanocoatings," *IEEE Sensors Journal*, vol. 7, pp. 455-463 2007.
- [108] N. A. Kotov, I. Dekany and J. H. Fendler, "Layer-by-layer self-assembly of polyelectrolyte-semiconductor nanoparticles composite films," *J. Phys. Chem.*, vol. 99, pp. 13065-13069, 1995.
- [109] I. R. Matias, Jesus M. Corres, Miguel Hernaez, Javier Bravo and Francisco J. Arregui, "Optical Fiber Humidity Sensors Using Nanostructured Coatings of SiO₂ Nanoparticles," *IEEE Sensors Journal*, vol. 8, pp. 281-285, 2008.
- [110] Yi Liu and Tianhong Cui, "Ion-sensitive field-effect transistor based pH sensors using nano self-assembled polyelectrolyte/nanoparticle multilayer films," *Sensors and Actuators B* vol. 123, pp. 148-152, 2007.

- [111] R. H. Yuya EGAWA, Jun-ichi ANZAI, "Multilayered Assemblies Composed of Brilliant Yellow and Poly(allylamine) for an Optical pH Sensor," *Analytical Sciences*, vol. 22, pp. 1117-1119, 2006.
- [112] P. S. Grant and M. J. McShane, "Development of Multilayer Fluorescent Thin Film Chemical Sensors Using Electrostatic Self-Assembly," *IEEE Sensors Journal*, vol. 3, pp. 139-146, 2003.
- [113] Francisco J. Arregui, Gonzaga de Bastida, Javier Goicoechea, Ignacio R. Matias, "Quantum Dots-Based Optical Fiber Temperature Sensors Fabricated by Layer-by-Layer," *IEEE Sensor Journal*, vol. 6, pp. 1378-1379, 2006.
- [114] P. Jorge, M. A. Martins, T. Trindade, J. L. Santos, and F. Farahi, "Optical fiber sensing using quantum dots," *Sensors* vol. 7, pp. 3489-3534, 2007.
- [115] K. J. Loh, J. P. Lynch, and N. A. Kotov, "Passive wireless strain and pH sensing using carbon nanotube-gold nanocomposite thin films," in *Sensors and smart structures, technologies for civil, mechanical, and aerospace systems* San Diego, California, USA 19-22 March 2007, pp. 652919.1-652919.
- [116] A. S. Jesús M. Corres , Francisco J. Arregui , Ignacio R. Matías , Joaquín Roca, "Fiber optic glucose sensor based on bionanofilms," *Sensors and Actuators B* vol. 131, pp. 633-639, 2008.
- [117] I. R. Matias, Ignacio Del Villar , Francisco J. Arregui and Jesus M. Corres, "Fiber optic glucose biosensor," *Optical Engineering*, vol. 45, pp. 104401-1-104401-6, 2006.
- [118] M. Zhang, Y. Yan, K. Gong, L. Mao, Z. Guo, and Y. Chen, "Electrostatic layer-by-layer assembled carbon nanotube multilayer film and its electrocatalytic activity for O₂ reduction," *Langmuir*, vol. 20, pp. 8781-8785, 2004.
- [119] U. Jan and Q. Husain, "Preparation of a highly stable, very active and highyield multilayered assembly of glucose oxidase using carbohydrate-specific polyclonal antibodies," *Biotechnology Applied Biochemistry*, vol. 39, pp. 233-239, 2004.
- [120] I. D. Villar, I. R. Matías, F. J. Arregui, and R. O. Claus, "ESA-based in fiber nanocavity for hydrogen peroxide detection," *IEEE Transactions On Nanotechnology*, vol. 4, pp. 187-193, 2005.
- [121] G. de Bastida, F. J. Arregui, J. Goicoechea, and I. R. Matías, "Quantum dots-based optical fiber temperature sensors fabricated by layer-by-layer," *IEEE Sensors*, vol. 6, pp. 1378-1379, 2006.
- [122] F. J. Arregui, I. R. Matías, K. L. Cooper, and R. O. Claus, "Simultaneous Measurement of Humidity and Temperature by Combining a Reflective Intensity-Based Optical Fiber Sensor and a Fiber Bragg Grating," *IEEE Sensors Journal*, vol. 2, pp. 482-487, 2002.

- [123] C. Malins, M. Niggemann, and B. D. MacCraith, "Multi-analyte optical chemical sensor employing a plastic substrate," *Meas. Sci. Technol.*, vol. 11, pp. 1105-1110, 2000.
- [124] R. Narayanaswamy, "Optical chemical sensors and biosensors for food safety and security applications," *Acta Biologica Szegediensis*, vol. 50, pp. 105-108 2006.
- [125] K. J. Loh, J. Kim, J. P. Lynch, N. W. Shi Kam, and N. A. Kotov, "Multifunctional layer-by-layer carbon nanotube–polyelectrolyte thin films for strain and corrosion sensing," *Smart Materials and Structures* vol. 16, pp. 429-438, 2007.
- [126] S. Derveaux, B. G. Stubbe, C. Roelant, M. Leblans, B. G. De Geest, J. Demeester, *et al.*, "Layer-by-Layer Coated Digitally Encoded Microcarriers for Quantification of Proteins in Serum and Plasma," *Analytical Chemistry*, vol. 80, pp. 85-94, 2008/01/01 2007.
- [127] J. S. Kirsch, "Layer-by-Layer Assembly of Bio-functionalized Carbon Nanotubes for Rapid and Discriminate Detection of Organophosphate Neurotoxins," 2013.
- [128] G. Decher, "Fuzzy Nanoassemblies: Toward layered polymeric multicomposites," *Science*, vol. 277, pp. 1232-1237, 1997.
- [129] G. Decher, M. Eckle, J. Schmitt, and B. Struth, "Layer-by-layer assembled multicomposite films," *Current Opinion in Colloid & Interface Science*, vol. 3, pp. 32-39, 1998.
- [130] G. S. Grant, D. Koktysh, B. Yun, R. Matts, and N. Kotov, "Layer-By-Layer Assembly of Collagen Thin Films: Controlled Thickness and Biocompatibility," *Biomedical Microdevices*, vol. 3, pp. 301-306, 2001/12/01 2001.
- [131] G. Decher, J. D. Hong, and J. Schmitt, "Buildup of ultrathin multilayer films by a self-assembly process: III. Consecutively alternating adsorption of anionic and cationic polyelectrolytes on charged surfaces," *Thin Solid Films*, vol. 210/21 I, pp. 831-835, 1992.
- [132] A. Rosidian, Y. Liu, and R. O. Claus, "Ionic self-assembly of ultrahard ZrO₂/polymer nanocomposite thin films," *Advanced Materials*, vol. 10, pp. 1087-1091, 1998.
- [133] I. R. Matias, F. J. Arregui, R. O. Claus, and K. L. Cooper, "Molecularly self-assembled optical fiber sensors," *IEEE Sensors: Conference proceedings*, vol. 1, pp. 198-202, 2002.
- [134] A. F. Lasagni, D. Yuan, and S. Das, "Layer-by-Layer Interference Lithography of Three-dimensional Microstructures in SU-8," *Advanced Engineering Materials*, vol. 11, pp. 408-411, 2009.
- [135] J. H. Hah, S. Mayya, M. Hata, Y.-K. Jang, H.-W. Kim, M. Ryoo, *et al.*, "Converging lithography by combination of electrostatic layer-by-layer self-assembly and 193 nm photolithography: Top-down meets bottom-

up," *Journal of Vacuum Science & Technology B: Microelectronics and Nanometer Structures*, vol. 24, pp. 2209-2213, 2006.

- [136] A. Delcorte, P. Bertrand, X. Arys, A. Jonas, E. Wischerhoff, B. Mayer, *et al.*, "ToF-SIMS study of alternate polyelectrolyte thin films: chemical surface characterization and molecular secondary ions sampling depth," *Surface Science*, vol. 366, pp. 149-165, 1996.
- [137] M. J. McShane and Y. M. Lvov, "Layer-by-Layer electrostatic self-assembly," in *Dekker Encyclopedia of Nanoscience and Nanotechnology*, ed: Marcel Dekker, 2004.

3. Chemicals and Instrumentation

3.1 Introduction

This section looks in details at the materials and components utilized to prepare and create a fibre optic chemical sensor using layer-by-layer deposition technique. The deposition of sensitive layers was carried out on two different substrates; glass slides and optical fibres. Glass slides were applied for an initial study prior to using optical fibres for further and complementary experiments. The overview of the setup of a fibre optic chemical sensor is shown in Fig 3-1. In this scheme shown, the transducer is a chemical substance (reagent) immobilised on the optical fibre converts a parameter of the optical signal from a light source as a function of the concentration of the measurand. The detector measures the changes of the optical properties being measured. The main reagent in this work is a pH indicator and a polymer is used as a cross-linker. A series of pH buffer solutions is applied to provide the measurand (H^+). A white tungsten halogen light is used as a light source which covers the whole visible range starting from 360 nm up to 2000 nm. The detector is an UV-visible spectrophotometer to measure the properties of light passing through the glass slide and the optical fibre. Software is used to visualize the light properties

(PerkinElmer UV Winlab for the glass slide and SpectraSuite for the optical fibre). The materials and elements which have been utilized in this study are sorted in two parts, chemicals and devices.

Chemicals:

- A transducer which is a pH indicator.
- The measurand which is hydrogen ion supplied from pH buffer solutions.

Devices and components:

- A waveguide which is a pieces of optical fibre.
- The connectors to connect pieces of the optical fibres together and to instruments.
- The light source.
- The detector which is a spectrophotometer.

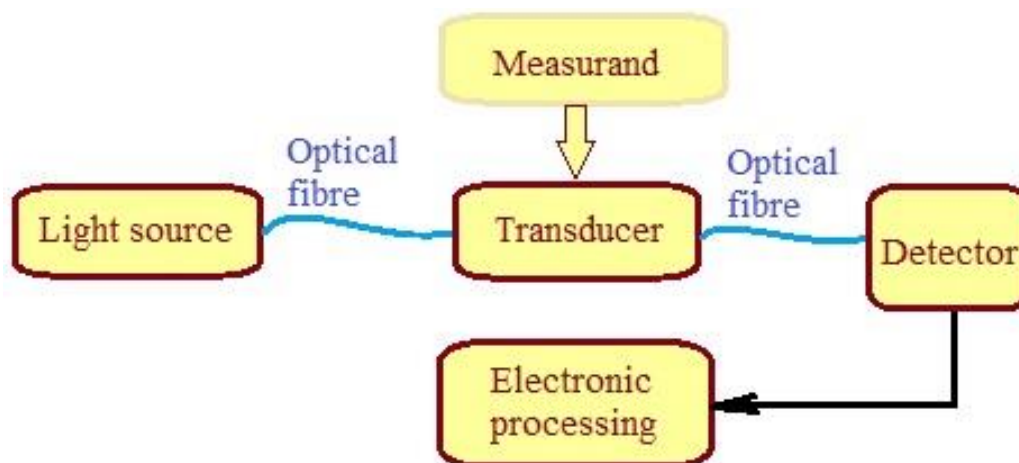


Fig 3-1 The main components of a fibre optic chemical sensor. The transducer: is an indicator immobilised on the optical fibre. Measurand: H^+ concentration (supplied from pH buffer solutions). Light source is a tungsten halogen light. The detector: a spectrophotometer.

3.2 Chemicals

3.2.1 pH indicator

A **pH indicator** is a chemical which changes colour when it is placed in acids or bases. In fact, a pH indicator is a chemical detector which introduces hydrogen ion (H^+) or hydroxyl ion (OH^-) concentration in a solution.

pH itself is an abbreviation for "power of hydrogen" and is the negative logarithm of hydrogen ion concentration in an aqueous solution which usually runs from 0 to 14. A strong acid may have a pH of 0-2, while a strong base may have a pH of 13-14. A pH around 7 is considered to be neutral. Pure water has a pH very close to 7. Each whole pH value below 7 is ten times more acidic than the higher value and each whole pH value above 7 is ten times less acidic than the one below it. For example, a pH of 2 is ten times more acidic than a pH of 3 and 100 more acidic than a pH value of 4. When the pH changes 0.2 units the concentration of hydrogen ion becomes 1.6 times.

pH indicator's molecule can be protonated (gain H^+) or deprotonated (lose H^+) depending on the pH of the solution. As the pH indicator is itself frequently a weak acid or a base, which when dissolved in water dissociates slightly and forms ions with different colours. If AH is an acidic indicator molecule that is undissociated acid the following reaction will take place:



Where A^- is known as the conjugate base of the acid.

In a specific pH of the solution HA, A⁻ and H⁺ are in equilibrium and their concentrations maintain constant with the passing of time. The equilibrium constant can be called the “acid dissociation constant” and is defined as:

$$K_a = \frac{[H^+][A^-]}{[HA]}$$

where brackets represent the concentration of the AH, H⁺ and A⁻.

If the terms pK_a and pH are defined as shown below:

$$pK_a = -\log_{10}K_a$$

$$pH = -\log_{10}[H^+]$$

then the above equation after rearranging will change to the “Henderson-Hasselbalch equation” as shown below:

$$pH = pK_a + \log_{10} \frac{[A^-]}{[HA]}$$

or

$$pH - pK_a = \log_{10} \frac{[A^-]}{[HA]}$$

At half-ionization [A⁻] = [HA] then pH is numerically equal to pK_a as shown in Fig 3-2.

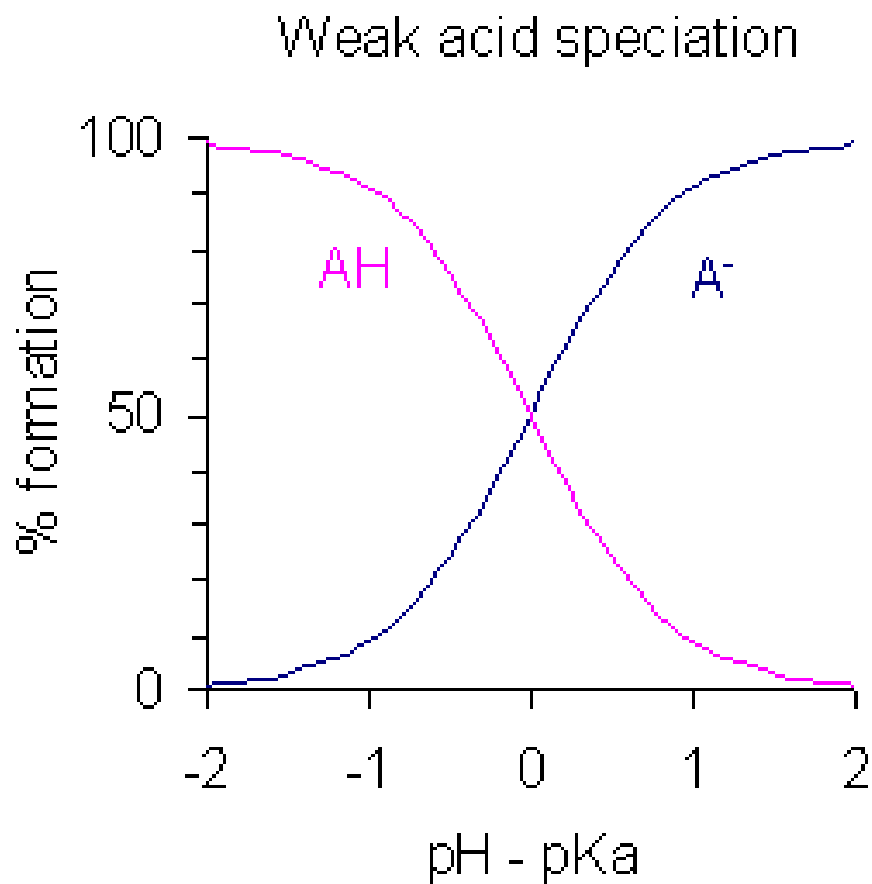


Fig 3-2 Variation of the % formation of a monoprotic acid, AH, and its conjugate base, A⁻, with the difference between the pH and the pK_a of the acid [1].

Some indicators have two or more functional acidic or basic groups and have more than one pK_a and pH range. In terms of acidic indicators, there is separate dissociation equilibrium for each proton they are able to lose. Then for a diprotic acid like H₂A that has two acidic protons, two different levels of dissociation equilibrium are defined as below:



For each step it can be written:

$$K_{a1} = \frac{[H^+][HA^-]}{[H_2A]}$$

$$K_{a2} = \frac{[H^+][A^{2-}]}{[HA]}$$

and overall:



and

$$K = \frac{[H^+]^2[A^{2-}]}{[H_2A]} = K_{a1}K_{a2}$$

The term pK_a depends on the concentration of individual ionic chemical species and the charge of ion [2, 3] which influence on ionic strength of a solution. The ionic strength (I) is defined as

$$I = \frac{1}{2} \sum_{i=1}^n c_i z_i^2$$

where c_i is the molar concentration of ion i (M, mol/L), z_i is the charge number of that ion, and the sum is taken over all ions in the solution.

When the ionic strength rises larger concentrations of ions are required to reach equilibrium, so pK_a will decrease as a function of the ionic strength.

Choi *et.al.* has illustrated [4] that in the layer-by-layer technique the effective pK_a of a polyelectrolyte substantially differs from solution state value when

incorporated into a multilayer film. On the other hand, the degree of ionization affects the thickness of the deposited layers [4], likewise adding a copolymer such as sodium chloride to the polyelectrolyte solution increases the ionic strength and degree of ionization [5]. Furthermore, the pH of the polyelectrolyte solution is an important parameter that can change the ionic strength and the degree of ionization and it can then create a thicker or thinner multilayer film [6]. Therefore, every thin film has its own pK_a which depends on several factors such as the utilization of a copolymer, the pH of the polyelectrolyte solution and the degree of ionization of the deposited material.

Table 3-1 shows some pH indicators and their change of colour depending on the pH. Fig 3-3 shows the chemical structures of some of the most interesting and relevant indicators.

A suitable indicator for layer-by-layer deposition must be positively or negatively charged and water soluble, with significant colour change. For example litmus, although has a significant change from red to blue via a changing pH from acidic to alkaline, it is not adequately water soluble. Furthermore, a phenolic hydroxyl group is dissociable at high pH region and structurally is not strong enough to attract positive charged molecules easily. Thymol blue is another example, it is an anionic agent having one phenolic hydroxyl group and one sulphonate group, and its colour changes, as shown in Table 3-1, makes it suitable for a high range of pH measurement. However it is not water soluble and is dissolved in ethanol and propanol easily. As the table shows, neutral red and brilliant yellow present good performances in neutral

zone (6.0 – 8.0) and both of them are charged molecules. Brilliant yellow contains two negative charges derived from sulphonate groups and two phenolic hydroxyl groups are ionized negatively at high pH. In contrast, neutral red is a positive charged molecule because of the presence of amine functional groups. As neutral red has been used for both pH sensing and layer-by-layer deposition purposes in many published works [7-11], experiments were initiated with neutral red to recognize the optimum conditions of the deposition thin film using layer-by-layer technique.

Table 3-1 pH indicators and their colour with respect to pH range [166, 167].

Indicator	Transition range	pH	Low pH colour	High pH colour
Gentian violet (Methyl violet)	0.0–2.0		yellow	blue-violet
Leucomalachite green (first transition)	0.0–2.0		yellow	green
Leucomalachite green (second transition)	11.6–14		green	colourless
Thymol blue (first transition)	1.2–2.8		red	yellow
Thymol blue (second transition)	8.0–9.6		yellow	blue
Methyl yellow	2.9–4.0		red	yellow
Bromophenol blue	3.0–4.6		yellow	purple
Congo red	3.0–5.0		blue-violet	red
Methyl orange	3.1–4.4		red	orange
Bromocresol green	3.8–5.4		yellow	blue-green
Methyl red	4.4–6.2		red	yellow
Methyl red / Bromocresol green	4.5–5.2		red	green
Azolitmin	4.5–8.3		red	blue

Bromocresol purple	5.2–6.8	yellow	purple
Bromothymol blue	6.0–7.6	yellow	blue
Phenol red	6.8–8.4	yellow	red
Neutral red	6.8–8.0	red	yellow
Brilliant yellow	6.6- 8.0	yellow	orange
Thiazol yellow	11.0-13.0	yellow	red
Naphtholphthalein	7.3–8.7	colourless to reddish	greenish to blue
Cresol Red	7.2–8.8	yellow	reddish-purple
Phenolphthalein	8.3–10.0	colourless	fuchsia
Thymolphthalein	9.3–10.5	colourless	blue
Alizarine Yellow R	10.2–12.0	yellow	red
Litmus	4.5-8.3	red	blue
Cyanidin (first transition)	0-3.0	red	cerise
Cyanidin (second transition)	3.0-4.0	cerise	purple
Cyanidin (third transition)	4.0-5.0	purple	blue
Cyanidin (fourth transition)	5.0-8.0	blue	aquamarine
Cyanidin (fifth transition)	8.0-9.0	aquamarine	emerald green
Cyanidin (sixth transition)	9.0-11.0	emerald green	lime
Cyanidin (seventh transition)	11.0-14.0	lime	yellow

3.2.2 Polymers

It is generally accepted that macromolecule materials are more suitable for building up layers through Electrostatic Self-Assembly (ESA) [14]. Hence, larger molecular weight chains simply spread out and occupy more surface area without increasing the thickness of the adsorbed layer [6]. It is common for both negative and positive charged layers to be selected as polymers; moreover,

using the polymers as either positive or negative layers has been reported [5, 15, 16]. In the present work, two kinds of polymers were used: PAH as a polycation and PAA as a polyanion. Fig 3-4 shows their chemical structures. The amine group in PAH provides a positive charge while the hydroxyl group in PAA presents a negative charge.

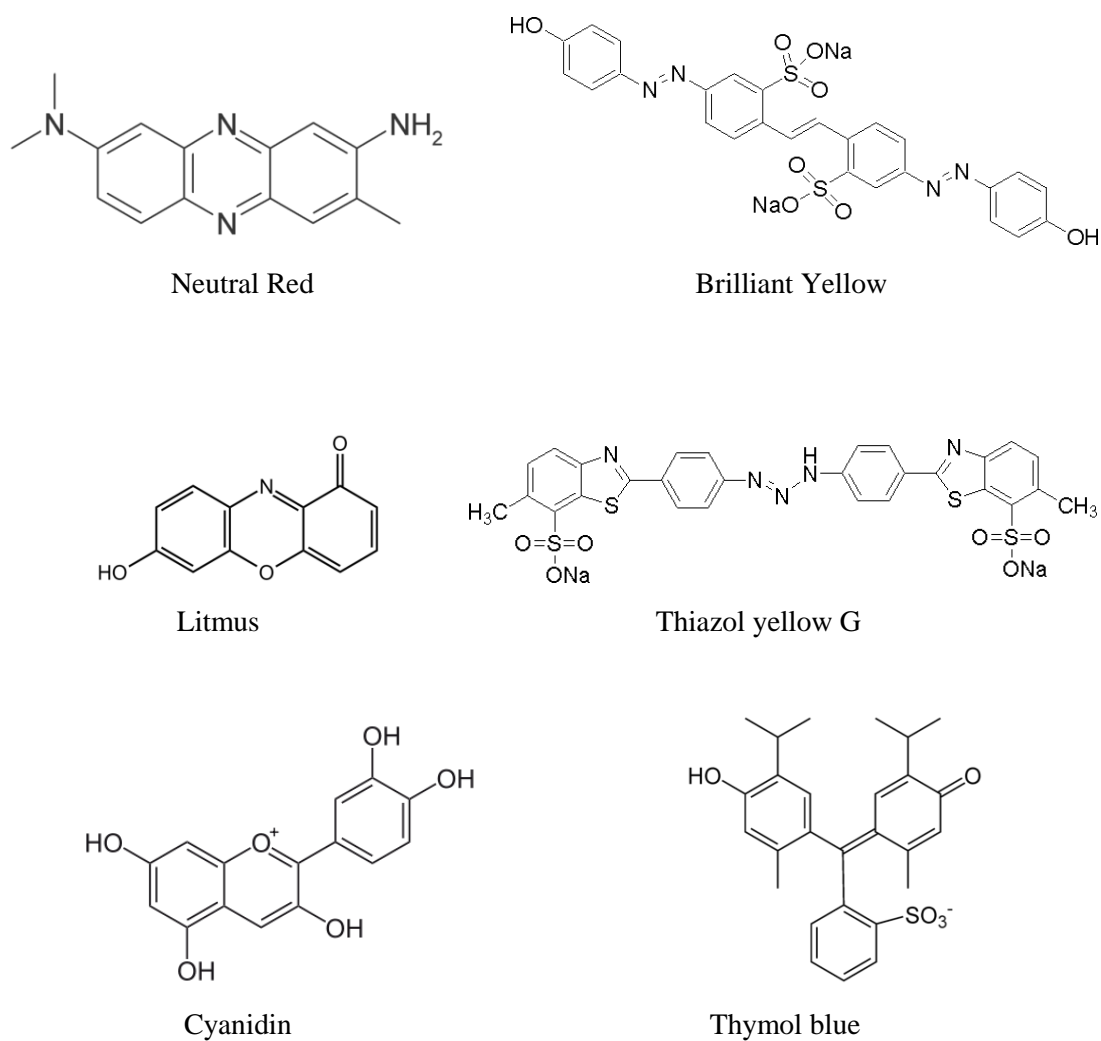


Fig 3-3 Chemical structure of some pH indicators e.g. Neutral Red (NR), Brilliant Yellow (BY), Litmus, Thiazol yellow G, Cyanidin and Thymol blue (TB).

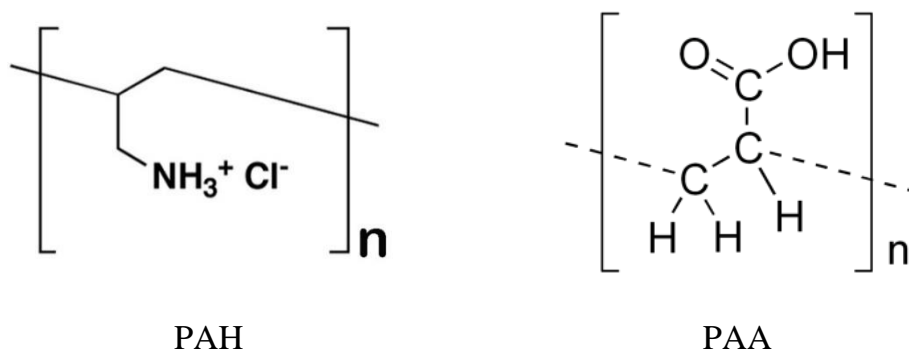


Fig 3-4 The chemical structure of PAA (poly (acrylic acid)) and PAH (poly (allylamine hydrochloride)).

3.2.3 Types of chemicals

The indicators and chemicals applied to develop the optical sensors reported in this work were brilliant yellow (BY) (dye content 70%), alizarin red S (ARS), neutral red, polyaniline (emeraldine salt), average Molecular weight (MW) >15,000, Poly(allylamine hydrochloride) (PAH) average MW ~15,000 and Poly (acrylic Acid) (PAA) solution with average MW ~100,000, 35 wt. % in H₂O, 3-Aminopropyl-trimethoxy silane (APTMS) 99%, SM-30 contents 30 wt. % in H₂O, and H₂SO₄.

3.2.4 pH buffer solutions

Changing the optical properties of sensitive films by changing the analyte concentration is based on a recognition measurement. In the case of pH sensing, the concentration of the H⁺ is the primary measurand of pH monitoring. In order to prepare the pH buffer solutions in pH range of 6.60 to 9.0 the instructions from Robinson *et al.* [17] were used. For wide range of pH from acidic to alkaline, 95 mL of mixture of 2.5 mM NaH₂PO₄ and 2.5 mM citric

acid monohydrate in distilled water was placed in a conical flask. The buffer was adjusted to the desired pH with aqueous NaOH. The solution was then transferred to 100 mL volumetric flask and made up to 100 mL with distilled water.

3.3 Devices and components

3.3.1 Optical fibre

It is about four decades since optical fibre has been applied in sensing due to its many advantages such as highly sensitive, quick response, small size, remote sensing capability, immunity to electromagnetic interference (EMI), nonconductive, electrically passive, low loss, high bandwidth, lightweight, relatively low cost and so on.

Fibre optic sensors have been proposed for sensing a wide variety of parameters, both physical such as temperature, strain, pressure, magnetic and electric fields, rotation rate, acceleration, acoustic waves, liquid level and refractive index [18, 19] and chemical such as pH, environmental monitoring and recognition of chemicals e.g. hydrogen, ammonia, CO₂, hydrogen peroxide and so forth [20, 21]. Optical fibre sensors can be designed to work as either extrinsic, if the modulation is performed by some external transducer or intrinsic, if the modulation takes place directly in the fibre. Optical modulation mechanisms can be based on intensity, phase, wavelength and polarization. There are three basic types of optical fibre, single-mode, graded-index multimode and step-index multimode. A mode in an optical fibre is a set of

electromagnetic waves that participates in the propagation of light along an optical fibre [22].

Fibres that carry more than one mode at a specific light wavelength are called multimode fibres. However, single mode fibres have very small diameter core that they can carry only one mode which travels as a straight line at the centre of the core.

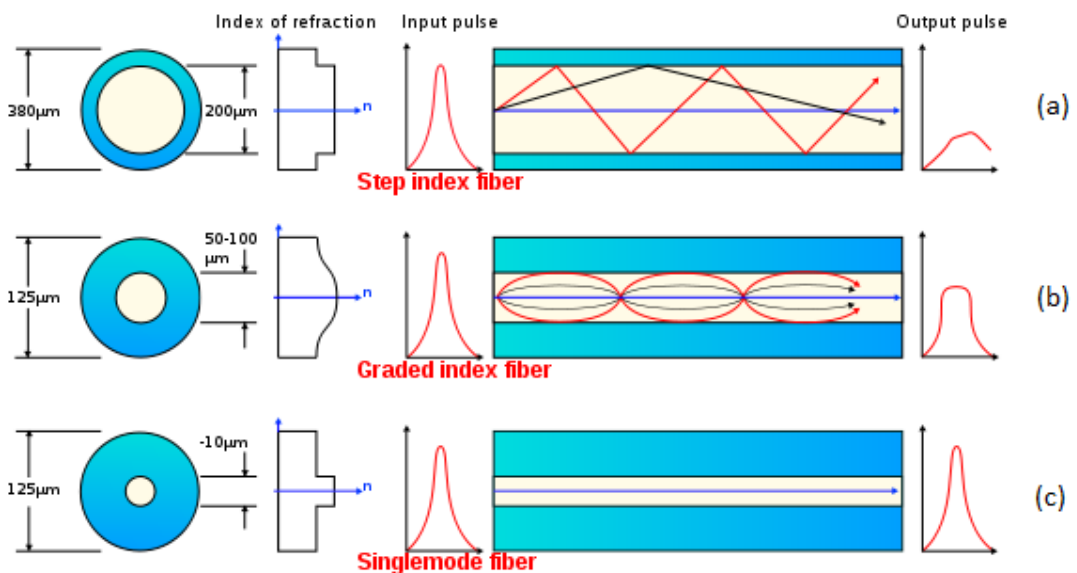


Fig 3-5 Types of optical fibres (a) step-index multimode, (b) graded-index multimode and (c) single-mode optical fibre [23].

In a stepped-index multimode fibre, Fig 3-5 (a), the number of rays or modes of light which are guided is determined by the core size and the core-cladding refractive index difference. In a graded-index multimode fibre, Fig 3-5 (b) the core refractive index varies across the core diameter. Since light travels more slowly in the high-index region of the fibre relative to the low-index region. An

optical fibre with a core diameter of less than 10 microns can be a single-mode fibre, Fig 3-5 (c), if only one fundamental mode is guided.

The main requirement of the fibre used in an optrode (an optical sensor device) is to guide the light to and from the sensing part. Multimode fibres are the most frequently used in chemical sensors (according to [24] around 70 %). Single-mode fibres are used only in 5% of sensors whereas planar waveguides are applied in 25 % of constructions. Because of the advantages of multimode fibres over other types of fibres for this purpose such as (1) they are relatively easy to work with; (2) because of the larger core size, light is easily coupled into and from them; (3) they can be used with both lasers and LEDs as light sources; and (4) coupling losses are less than those of single-mode fibres.

Multimode fibres are capable of transmitting light over short and medium distances with low loss. In chemical sensors, fibres with 50 μm to 1.5 mm glass core diameter are widely used. The diameters of plastic fibres vary from 0.25 to 1.5 mm [21].

Other property of optical fibres is numerical aperture which is a dimensionless number that characterizes the range of angles over which the system can accept or emit light and is defined by following equation generally:

$$NA = n_{air} \sin \theta_{acceptance}$$

where NA is abbreviation for numerical aperture, n_{air} is the index of refraction of the media (commonly air) and $\theta_{acceptance}$ is the angle made with the axis by the most oblique ray entering the instrument.

In optical fibres, it describes the range of angles within which light that is incident on the fibre will be transmitted along it. A multi-mode optical fibre only propagates light that enters the fibre within a certain cone, known as the acceptance cone of the fibre. The half-angle of this cone is called the acceptance angle, θ_{max} as shown in Fig 3-6. For step-index multimode fibre, the acceptance angle is determined only by the indexes of refraction of the core and the cladding, n_{core} and n_{clad} :

$$NA = n_{air} \sin \theta_{max} = \sqrt{n_{core}^2 - n_{clad}^2}$$

To maximize the amount of light that can be launched in a fibre, a large core with a large numerical aperture is preferable.

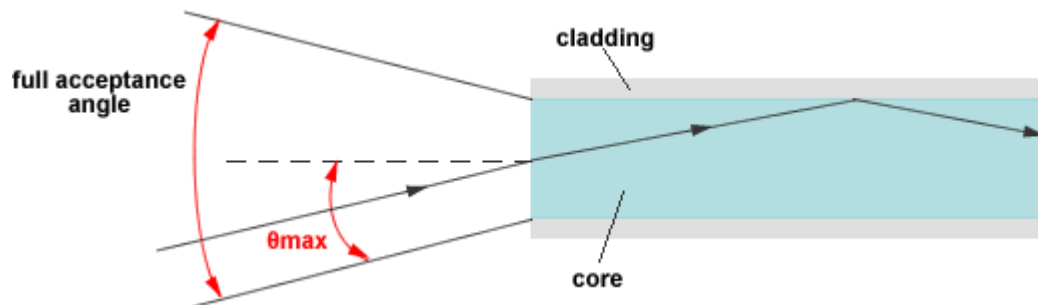


Fig 3-6 The full acceptance angle and θ_{max} in an optical fibre.

All fibres used in this work were step-index multimode with a numerical aperture (NA) of 0.37 and consisting of a silica core and a hard polymer cladding. A typical transmission profile is shown in Fig 3-7.

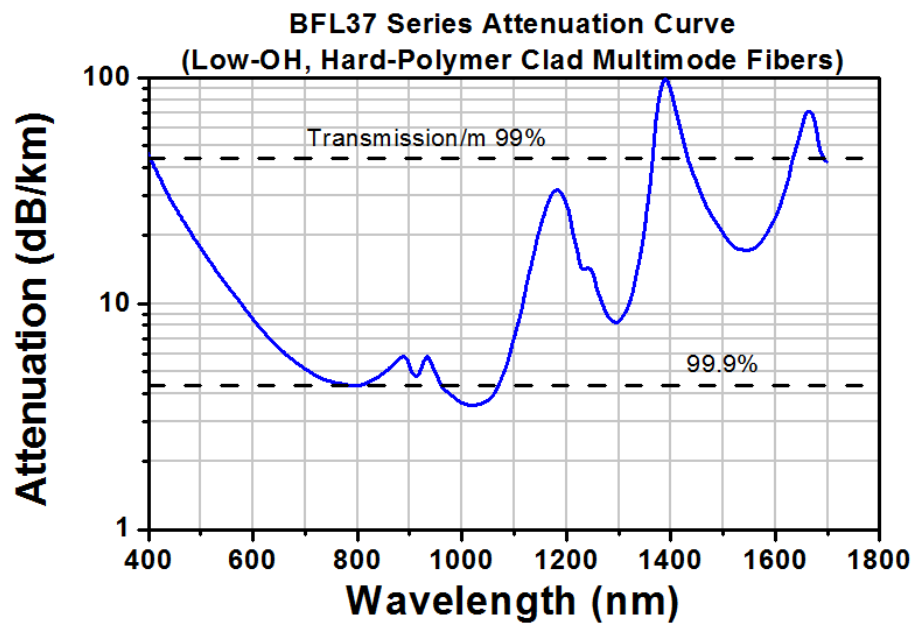


Fig 3-7 Transmission profile of the multimode fibres used [25].

The fibre bundle which is attached to the light source and the fibre bundle couples the reflected light to the spectrometer, of which cross section shown in Fig 3-8, and consisting of 6 fibres of 200 μ m core diameter. These two bundles are joined together with a 2 \times 1 (Y shape) fibre coupler, made using two multimode UV/Visible fibres with hard polymer cladding, 600 μ m silica core and 0.37 NA, which is connected to the sensor probe with the active sensing region being located at the distal end of the fibre. This structure is shown in Fig 3-9. Since the light from the analyte is usually a limiting factor, the six surrounding fibres are used for the collection of a known level of light while the central fibre is used to guide the interrogating light. The sensor probe consists of a short length of 600 μ m core diameter fibre (will be changed to study the effect of the diameter on the sensitivity), of which distal ends are polished. The

diameter of the fibre probe is approximately equal to the diameter of the fibre bundle, which consists of three 200 μ m fibres side by side.

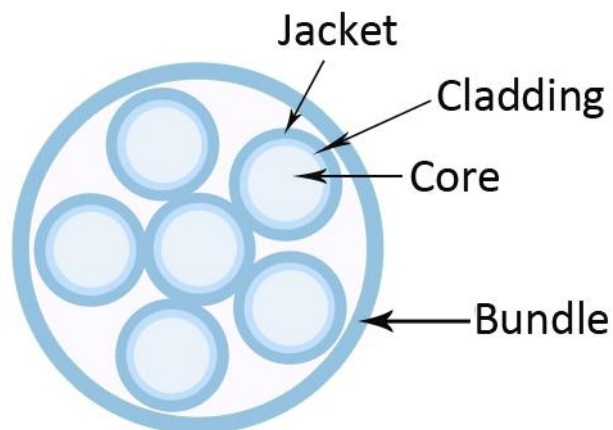


Fig 3-8 The cross section of the bundle of 6 fibres grouped together.

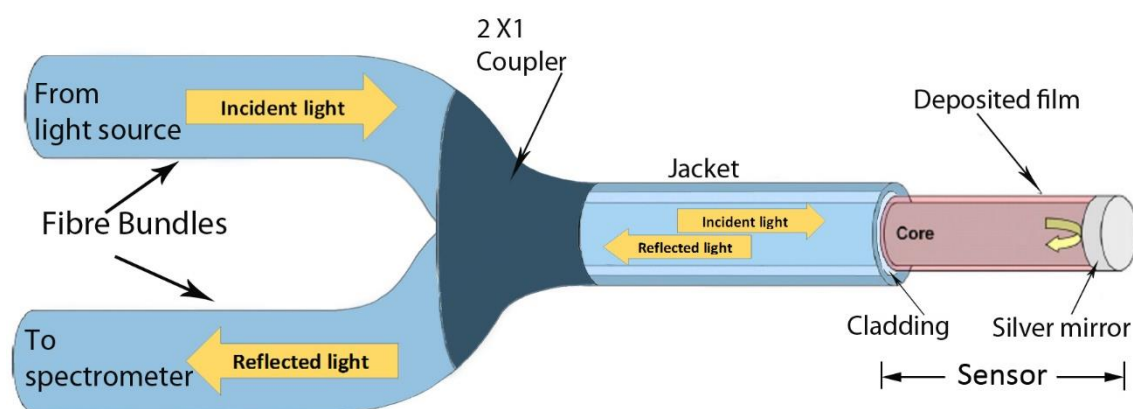


Fig 3-9 The structure of the connections of a sensor device.

3.3.2 Connections and connectors

The effective interconnection of the components is as important as the fibre itself in the device. The main requirement of the connectors is to connect light source to fibre, fibre to fibre and fibre to optodetector e.g. spectrophotometer.

Depending on specific applications, the different forms and shapes of the connectors can be utilized. They can be classified into three types:

(a) Demountable connectors: fibre to fibre, fibre to light source, fibre to photodetector.

(b) Splices – permanent joints between two fibres.

(c) Couplers for distribution of the light between fibres.

It is important to minimize the optical power that may be lost in any connection, thus to ensure that fibre optic connections have adequate power for correct operation especially in communication links, where good optical power budgeting, reflecting the maximum amount of power it can transmit, is required.

An optical power loss can be caused by a number of factors that are categorized into intrinsic and extrinsic losses. The mismatching of the core area, the numerical aperture and the fibre profile can cause intrinsic losses. Moreover, some factors like interface inhomogeneity, poor cleavage and mechanical misalignment can bring about the extrinsic losses.

Using stone-paper to polish the surface of the core a smooth cross section can be created which can be effective in reduction of the light losses.

3.3.3 The light source

The light source is an integral part of a fibre optic sensor. Its main role is to deliver the appropriate light to interact with an analyte or an indicator. It should possess a wavelength well-matched to the spectral properties of the sensors in order to obtain the highest sensitivity. There are many various light sources

utilized in the fibre optic chemical sensors. They differ in spectral properties, generated optical power and coherence. Considering the spectral bandwidth of the light sources, they can be classified into three main groups:

- a) Monochromatic (lasers, laser diodes)
- b) Pseudomonochromatic (light emitting diodes)
- c) Continuous (incandescent lamps, arc lamps)

A comparison of spectral properties of typical continuous light sources is presented in Fig 3-10. Incandescent and gas discharge lamps are called white light sources because they emit light in a very broad spectral range. Fig 3-10 shows three of them, which are the most frequently used in chemical sensors. A xenon arc lamp seems to be the most widely used light source. It emits radiation from the UV to infrared but it is expensive and the optical power is not very stable. If a sensor needs to be excited only in the UV range, a deuterium lamp can give better results. This is a relatively short-lived lamp (1000-2000 hours of use) and usually quite expensive. Tungsten halogen lamps are much cheaper than the previously mentioned types. Powered by a relatively simple power supply, they emit stable optical signal and have long lifetime (10,000 hours) [21, 26].

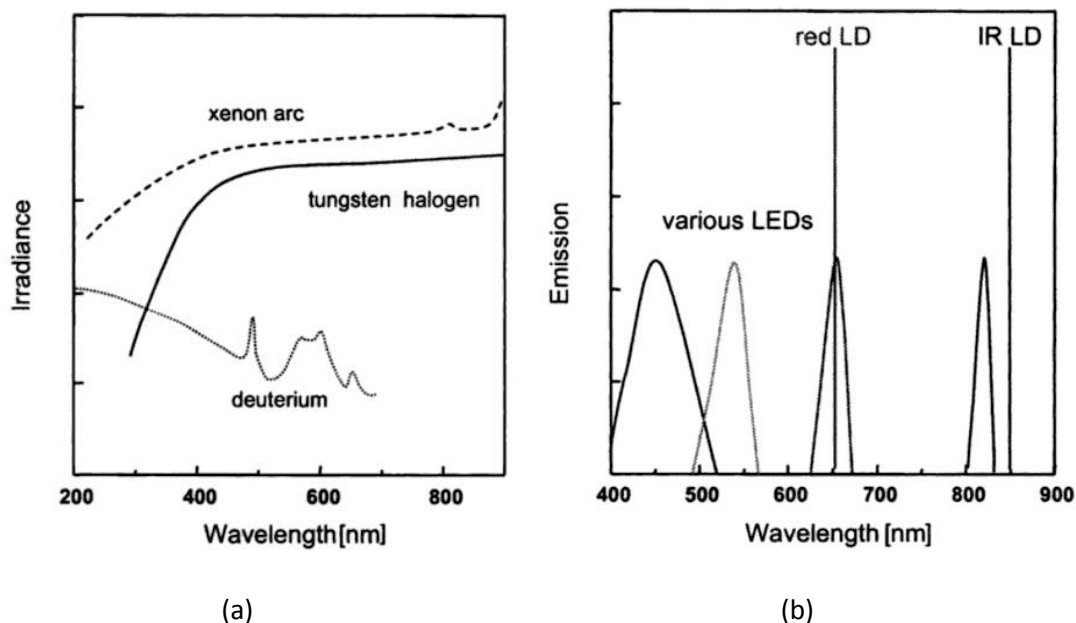


Fig 3-10 Emission spectra of light sources used in sensors. (a) white light sources and (b) LEDs/lasers light sources [21].

Light emitted by an LED is usually nearly monochromatic (pseudomonochromatic). LEDs are robust and their lifetimes are more than 100000 hours. The spectral characteristics of several typical LEDs, in comparison with laser diodes (LD), are shown in Fig 3-10. The light source applied in this work is a tungsten halogen lamp supplied from Ocean Optics to have a stable irradiation in the wavelength range of 400 nm to 700 nm (visible zone). Thus the selected indicators have spectra in this wavelength range in addition to stability of optical signal and its longer lifetime.

3.3.4 The detector

Visible light absorption is what causes objects to be coloured. For example, a blue dye appears blue because the light at the red end of the spectrum is absorbed, leaving the blue light to be transmitted as shown in Fig 3-11.

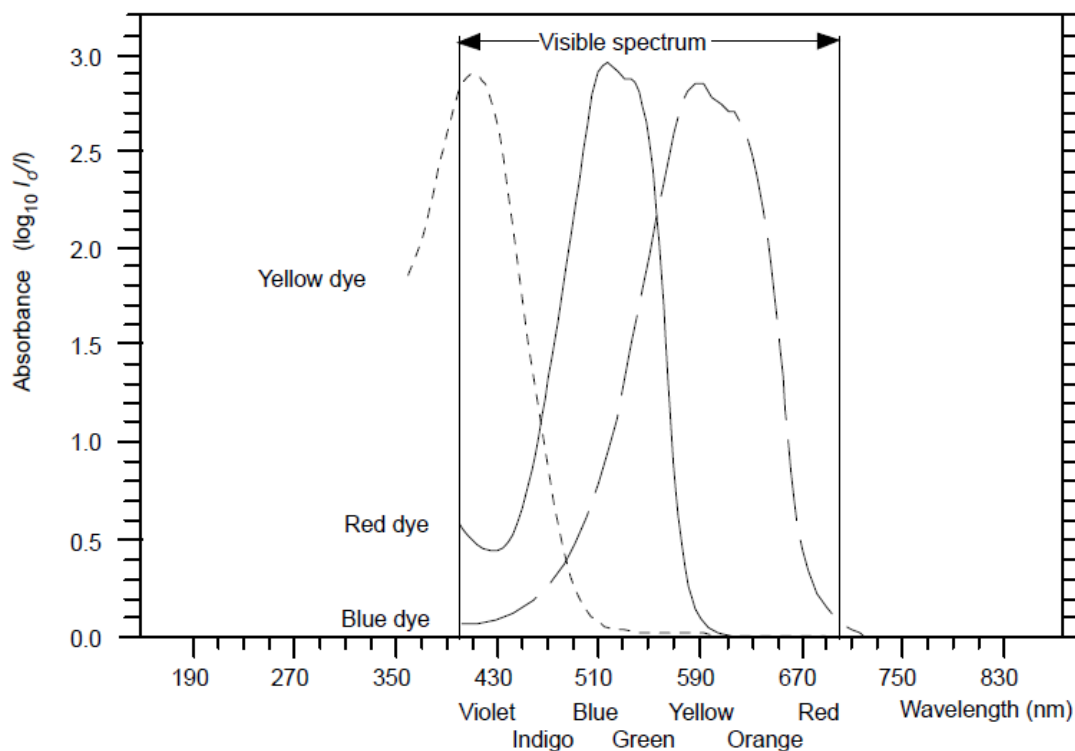


Fig 3-11 Absorption of light by dyes.

Visible light lies in the wavelength range 400–700 nm. When light is absorbed by a material, the valence (outer) electrons in the detector are typically promoted from their normal (ground) states to higher energy (excited) states. The energy of visible light depends on its frequency, and is approximately equivalent to 170,000 J mol⁻¹ (mole of photons) for red light and 300 kJ mol⁻¹ for blue light. The promotion of electrons to different energy levels is not restricted to electromagnetic radiation in the visible part of the spectrum and it can also occur in the ultraviolet region.

If the measurement is made at a specific colour (i.e. wavelength), the process is called photometry. If the measurement is made across a range of colours (i.e.

wavelengths), it is called spectrometry. Thus spectrophotometry is a collective term for both spectrometry and photometry.

The spectrophotometer is a device to measure the intensity at the wavelength. It essentially breaks down the light into wavelength constituent and measures the intensity at particular wavelength values.

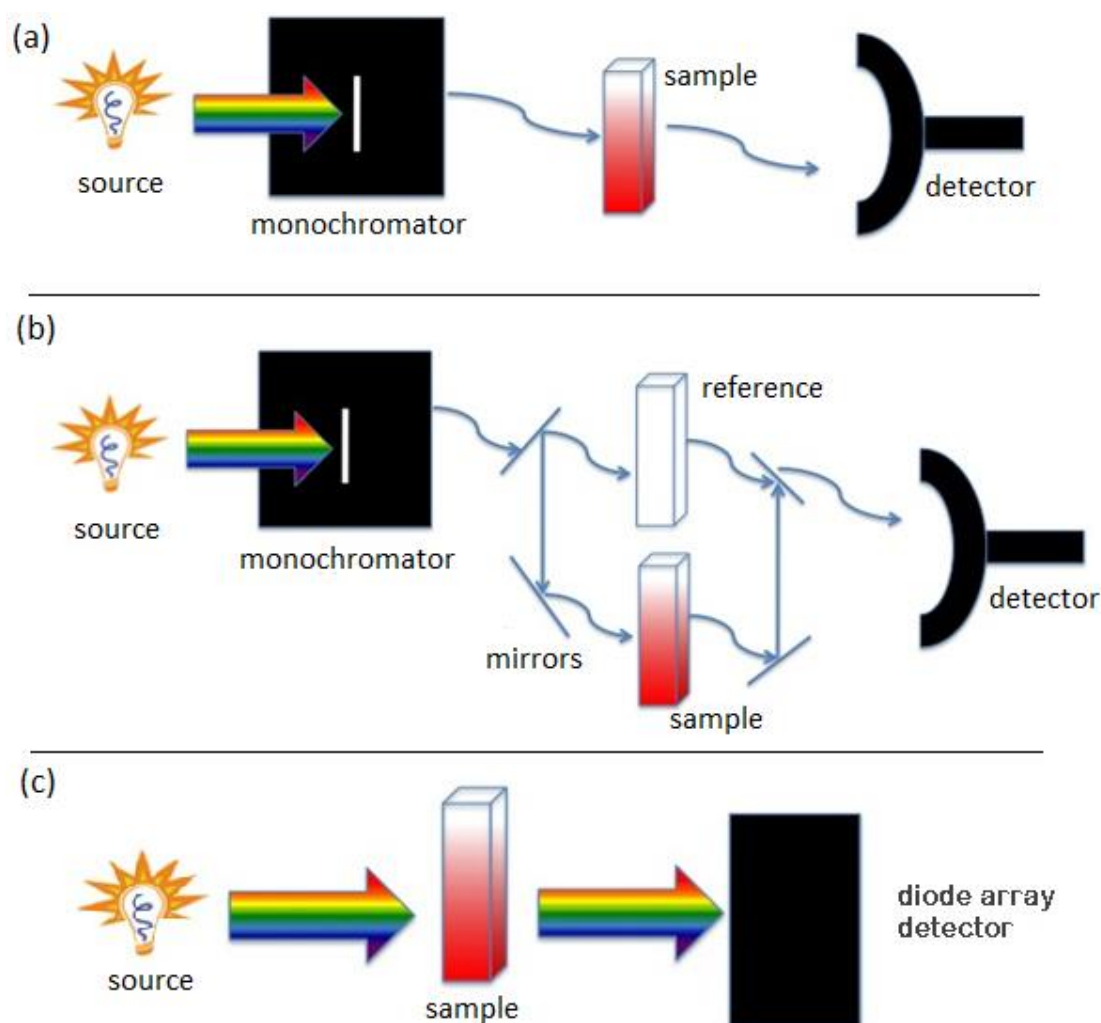


Fig 3-12 Illustration of a single beam UV-vis (a), double beam UV-vis (b) and simultaneous UV-vis (c) instruments .

There are three types of spectrometer instruments typically used to collect UV-vis spectra:

- 1) Single beam spectrometer.
- 2) Double beam spectrometer.
- 3) Simultaneous spectrometer.

All of these instruments have a light, a sample holder and a detector, but some have a filter for selecting one wavelength at a time. The single beam instrument (Fig 3-12 (a)) has a filter or a monochromator between the source and the sample to analyse one wavelength at a time. The double beam instrument (Fig 3-12 (b)) has a single source and a monochromator and then there is a splitter and a series of mirrors to get the beam to a reference sample and the sample to be analysed, this allows for more accurate readings. In contrast, the simultaneous instrument (Fig 3-12 (c)) does not have a monochromator between the sample and the source; instead, it has a diode array detector that allows the instrument to simultaneously detect the absorbance at all wavelengths. The simultaneous instrument is usually much faster and more efficient, but all of these types of spectrometers work well.

Single and double beam spectrometer show an absorption spectrum in the ultraviolet or visible region. A UV detector employs a deuterium discharge lamp (D2 lamp) as a light source, with the wavelength of its light ranging from 190 to 380 nm. While a UV-VIS detector employs an additional tungsten lamp (W lamp) with longer wavelength. In this type of spectrometer, light from the lamp is shone onto the diffraction grating¹, and dispersed according to wavelength. In diode array detector the absorption is detected in UV to VIS region. It has

¹ A **diffraction grating** is an optical component with a periodic structure, which splits and diffracts light into several beams travelling in different directions.

multiple photodiode arrays to obtain information over a wide range of wavelengths at one time.

In recent years, several attempts have been made to make these spectrophotometers to a size comparable to mobile phone. This specific version of spectrophotometer is called miniature spectrophotometer (or mini-spectrophotometer) and are designed to be used with optical fibres. In a mini-spectrometer light coming through a fibre hits a mirror and reflects toward the grating which spreads light to a rainbow-like spectrum. An array of charge-couple devices (CCD) catches this spectrum, delivering the whole spectrum instantaneously to a computer. This CCD is essentially the same thing as used in digital cameras. A CCD is an integrated circuit etched onto a silicon surface forming light sensitive elements called pixels. Photons incident on this surface generate charge that can be read by electronics and turned into a digital copy of the light patterns falling on the device. Each pixel in a CCD can hold a maximum number of electrons, called 'Full Well Capacity.' This number can vary widely (10ke⁻ to 500ke⁻) and depends mostly on the physical dimensions of the pixel (the bigger, the more electrons it can hold). All CCDs generate photoelectrons at different rates depending on the wavelength of light incident on the surface. Many factors contribute to the conversion of photons into electric signal called quantum efficiency (QE). The dynamic range of a CCD is typically specified as the maximum achievable signal divided by the total noise, where the signal strength is determined by the full-well capacity, and noise is the sum of dark and read noises. As the dynamic range of a device is increased,

the ability to quantitatively measure the dimmest intensities in an image (intrascene performance) is improved.

The spectrophotometer used in this work is the Maya2000 pro from Ocean Optics that is a spectrometer with high sensitivity (optical resolution to ~ 0.035 nm) and deep UV measurement (200 – 1050 nm). The optical bench is designed to improve stray light and low noise characteristics. Compared to similar models it offers greater than 75% quantum efficiency, high dynamic range and excellent UV response.

Another photodetector used in measuring intensity versus wavelength for the light pass through liquids and glass slides is UV/Visible spectrophotometer model Lambda 35 supplied by PerkinElmer. It works in the wavelength range of 190-1100 nm with variable bandwidth 0.5, 1, 2 and 4 nm. This optical bench which utilized deuterium and tungsten halogen lamps is designed to offer true double-beam operation, sealed and quartz-coated high-throughput optics and fast scanning.

3.4 Preliminary operations of the sensor

preparation

To develop the sensor probe a silica multimode fibre with a core diameter of 600 μm was used. To create an evanescent sensor the jacket (the cover of the fibre) was removed from a given length of the distal end of the fibre (the length considered for sensor) and the tip of the fibre was polished with 5 μm , 3 μm , 1 μm and 0.3 μm stone-papers respectively. As the cladding is acetone soluble, it

was removed easily. The distal end of the fibre was treated by Piranha solution (30:70 (v/v) mixture of Hydrogen peroxide (H_2O_2) (30%) and concentrated sulfuric acid (H_2SO_4)) for 60 minutes to produce the negatively charged surface and was then rinsed in distilled water followed by drying with compressed nitrogen. To reflect the radiated light back and guide it to the other end of the fibre a mirror was placed at the tip of the fibre.

In order to prepare a mirror at the distal end of the fibre 2 ml of 0.1M AgNO_3 is placed in a vial and NH_3 solution is then added drop by drop until the brown sediment dissolves. 1.4 ml of 0.8 M KOH is added to the vial, if brown precipitate reforms NH_3 drop-wisely is used to have a clear solution. This solution is called Tollen's reagent. The cleaned fibre core is rinsed with 0.2% tin chloride (SnCl_2) solution and followed with distilled water and is then dipped into the vial containing the Tollen's reagent. By adding 0.4ml of 0.25M dextrose to the vial silver starts to cover the surface and the mirror would be ready in approximately 1 minute.

The fibre is now ready to be coated with positively charged molecules. The layer-by-layer technique is based on the successive deposition of oppositely charged molecules onto solid surface. The process of the coating details will be described in the following chapters. The performance of the prepared sensor will be examined with the evaluation of the peak wavelength changes when the sensor is dipped into different pH buffer solutions.

3.5 Experimental setup and data analysis

The multilayer coating deposited by self-assembly layer-by-layer technique are initially done on glass microscope slides of dimensions 76×26 mm with thickness of 1.0/1.2 mm and then on a standard hard cladding multimode fibre with low OH, silica core of 600 μm and numerical aperture (NA) of 0.37 purchased from Thorlabs.

In the case of using glass slides, Perkin-Elmer spectrophotometer is employed to record the absorbance spectra. To study the behavior of deposited indicator on glass slides in different pH buffer solutions, the glass slide is placed into the beaker which contained the buffer solution of a specific pH and the beaker is located in the spectrometer in front of light irradiation. The output absorbance spectrum is recorded by using the Perkin-Elmer UV Winlab software [27].

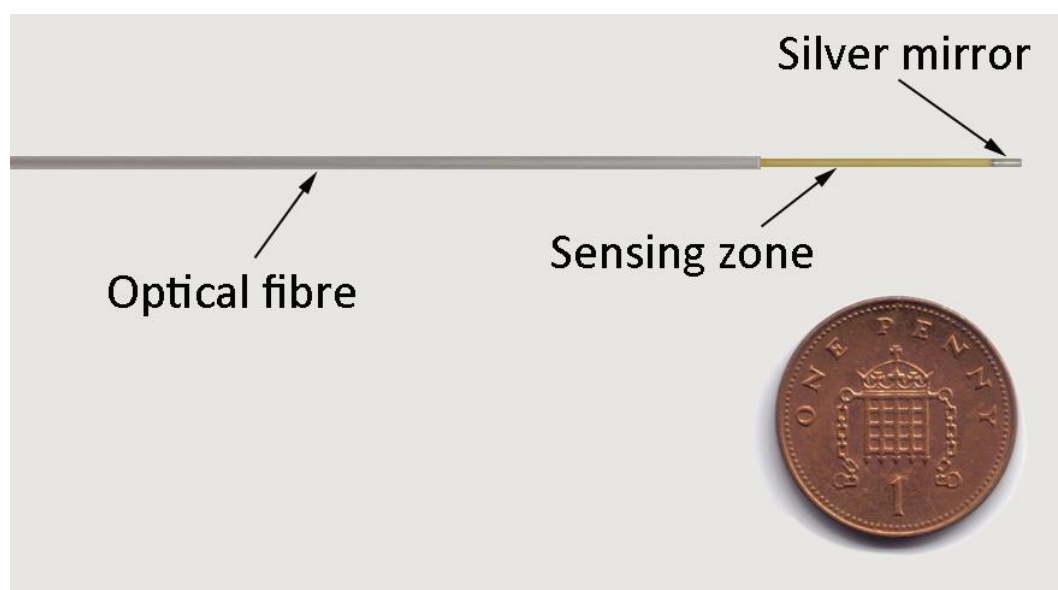


Fig 3-13 The photograph of the prepared optical sensor probe compared to 1 pence coin.

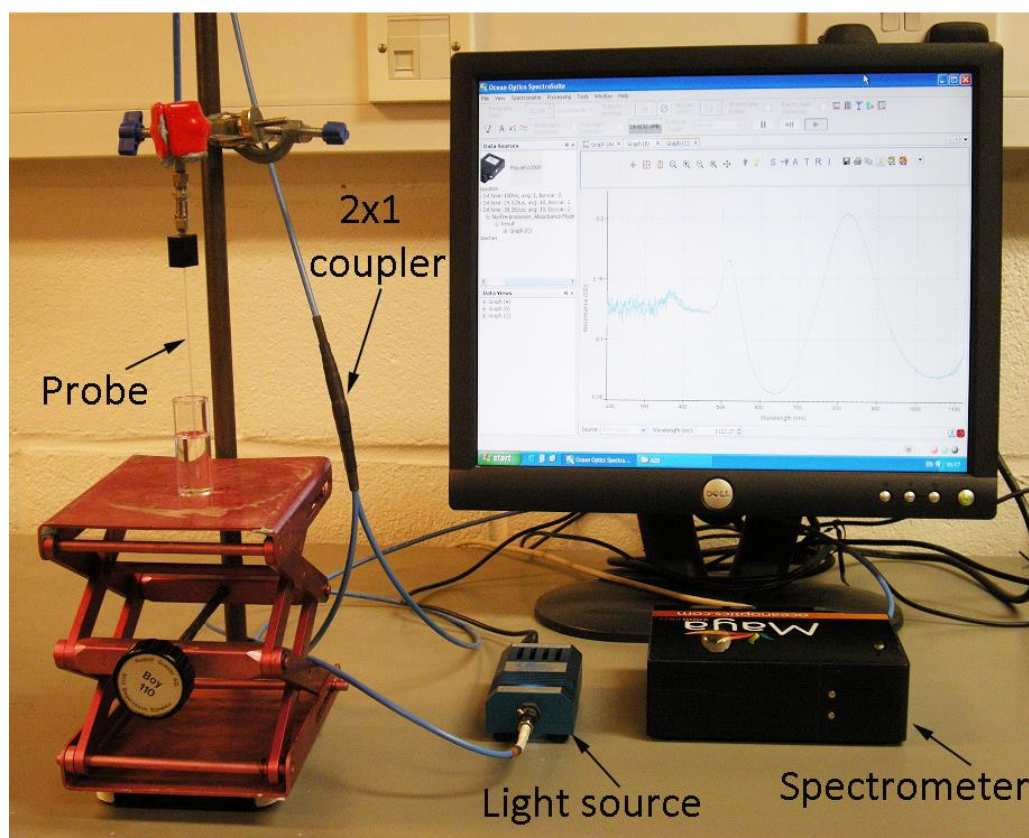


Fig 3-14 The experimental setup for a fibre optic chemical sensor (The photo was taken by Jie Cao).

To measure the absorbance spectra of the coated optical fibre the Ocean Optics Maya2000 pro spectrometer is used. The prepared sensor (shown in Fig 3-13) is connected to the light source and spectrometer as the setup shown in Fig 3-14. In this setup the output light from a white light source passes through a multimode UV/Visible fibre which is connected to the fabricated sensor probe. The distal end of the fibre which is coated with a pH indicator is dipped into a buffer solution at a specific pH. Due to interaction with pH solution, the indicator changes its colour and as a result a portion of the total light is absorbed at a specific wavelength by the sensing layer and the remaining light is emitted through the other end of the fibre coupler and is guided to the mini

spectrometer. The output from spectrometer is then displayed by the spectroscopy application software “SpectraSuite” [28]. The absorbance is calculated with respect to the reference spectrum of the dry sensor, i.e. not in a pH solution.

The probe is designed using coated optical fibre (polycation/polyanion)_n and is applied as follows:

1. Dipping into a pH buffer solution
2. Recording the absorbance spectrum
3. Taking out from the pH buffer solution
4. Dipping into another pH buffer solution
5. Recording the absorbance spectrum
6. Continuing the above steps (1-5) with all pH buffer solutions from low to high pH.

All measurements took place in stable conditions and each spectrum was recorded after observing stable results (about 50- 60 second). No cleaning steps between measurements was done.

The spectra produced from the coated glass slide are different from the spectra of the deposited fibre. Fig 3-15 compares the spectrometric properties of an incident ray radiating onto both the fibre and the glass slide. In the case of using glass slide, the incident ray passes through two films and the glass medium to be characterized.

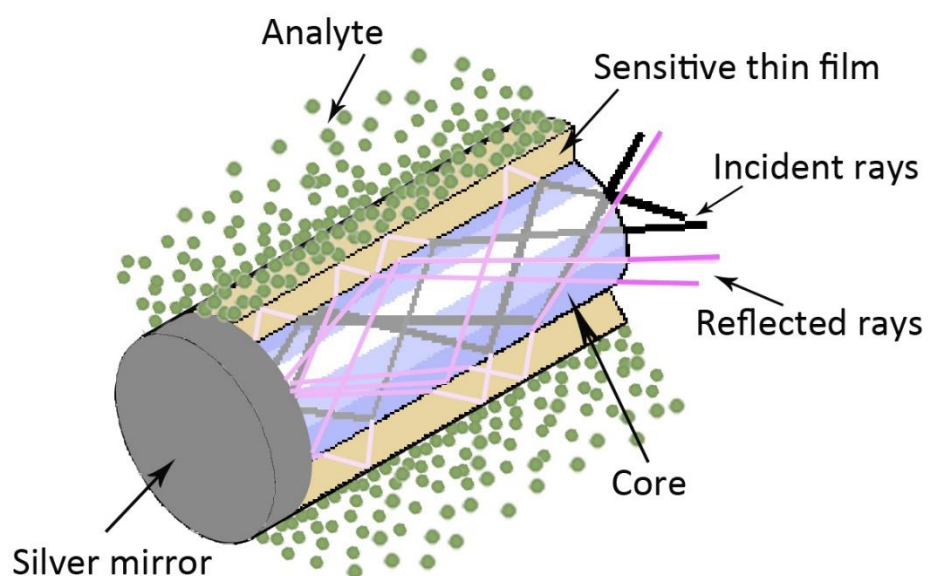
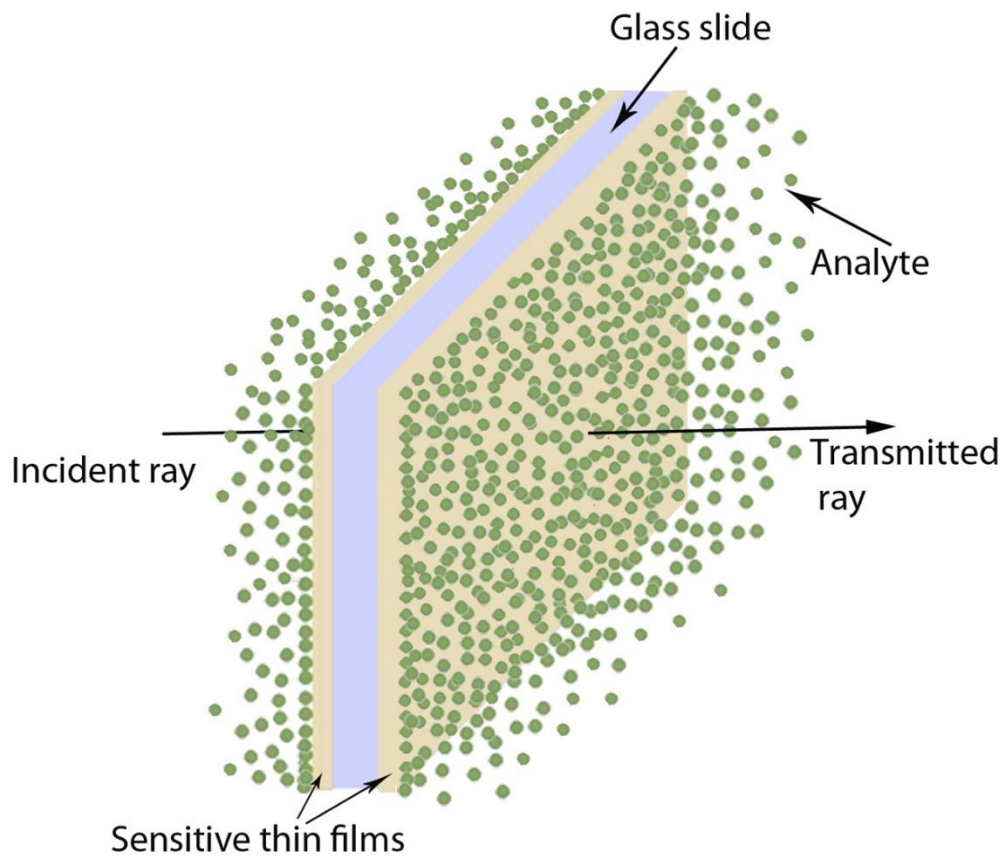


Fig 3-15 Comparison between spectroscopy of deposited glass slide and the optical fibre in presence of buffer solution.

For fibre optic, the incident light would not enter into thin film media if the refractive index of the thin film is lower than the index of the core. Some rays which are the evanescent wave may still enter the coating. This will depend on the Numerical Aperture (NA) of the coated fibre. However, if thin film has a higher refractive index than the core then the coming incident ray inside the core would transfer to the film after hitting the core-film interface while the path angle changes because of the refractive index difference. This light could be then totally reflected back to the medium or transmitted to the solution or reflected back to the medium whereas a part of it being transmitted to the solution that it depends on the refractive index of both thin film and solution. As a result, whatever is characterized by the spectrometer has a different intensity and consequently different property is achieved from similar light in the glass slide. Therefore, it is expected to have different absorbance spectra for the coated optical fibre.

Measuring the absorbed light at different wavelengths in different pH buffer solutions using a spectrophotometer will give a group of spectra. The wavelength of maximum point of each graph was plotted with respect to pH so the generated graph which is an S-shaped curve mainly obey nonlinear fitting method, Dose-Response model, according to the following equation [29, 30] and as shown in Fig 3-16:

$$\lambda(pH) = A_1 + \frac{A_2 - A_1}{1 + 10^{(pK_a - pH)p}} \quad (\text{Eq. 3-1})$$

Where λ is the peak wavelength value in each solution with given pH value and is a function of pH, A_1 and A_2 are the lowest and the highest values of peak wavelength respectively, p is the slope factor and pK_a is the acid dissociation constant. The more sensitive sensor shows dramatic wavelength shift from A_1 to A_2 while the steeper area introduces the range of pH (from pH_1 to pH_2 as shown in Fig 3-16) in which the sensor has a good performance in comparison with other pHs. The inflection point in this graph demonstrates “ pK_a ” of the thin film which is a function of the degree of ionization, revealing the pH at which 50% of the thin film’s functional groups are ionized [4]. The first derivative of Equation (3-1) in inflection point which shows the average curve slope in steeper area can be written as:

$$\left. \frac{d\lambda}{dpH} \right|_{pH=pK_a} = p \cdot \ln(10) \cdot (A_2 - A_1) = 2.3p(A_2 - A_1) \quad (\text{Eq. 3-2})$$

The wavelength varies with the colour of indicator which depends on the degree of ionization. The highest ionization for positive molecules happens in low pHs and for negative molecules happens in high pHs as shown in Fig 3-17. Then Dose-Response graph demonstrates a negative slope for the indicator with positive functional group and a positive slope for the indicator with a negative functional group.

There are many software programs today that can be used to plot the graphs, fit the curves and carry out simulation. The software programs that are used in this work are SigmaPlot, MatLab and OriginPro.

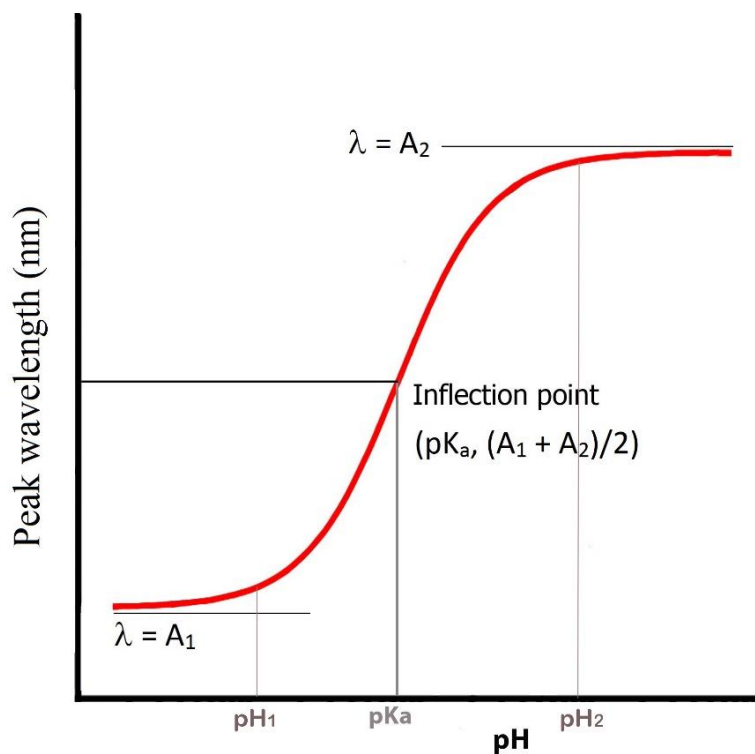


Fig 3-16 Dose-Response curve fitting model sample.

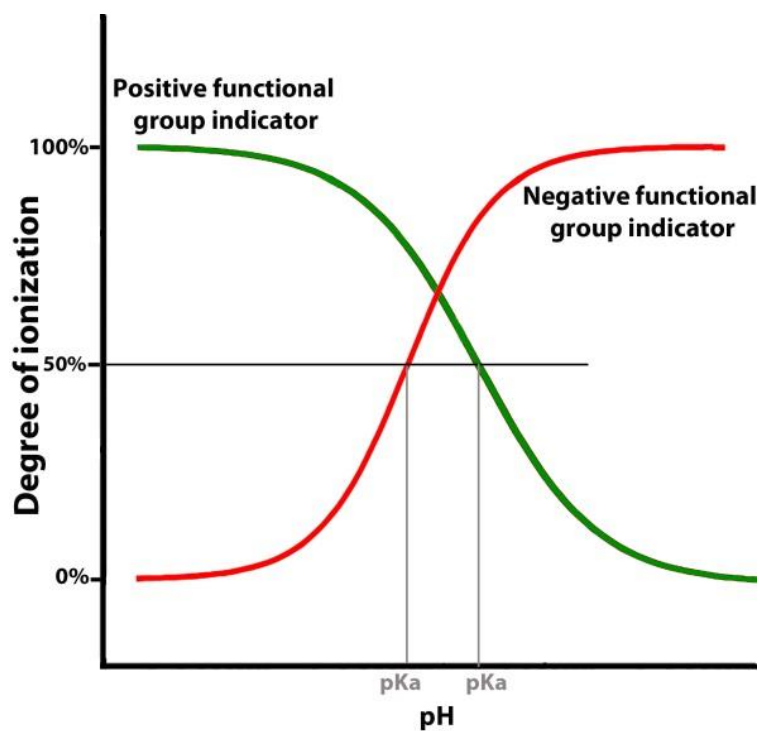


Fig 3-17 Degree of ionization versus pH for two kinds of indicators. The slope is positive for the indicator with negative functional group and is negative for the indicator with positive functional group.

3.6 Summary

The major components making up a fibre optic chemical sensor system have been discussed in this chapter, namely the transducer i.e. pH indicators and components and devices i.e. the optical fibre, the connectors, the light source and the detector.

A pH indicator which is a weak acid is a chemical detector for hydrogen ions in a solution via colour change that is considered to be the basis for colourimetry recognition. A variety of chemical reagents and their colour variation were introduced.

Optical fibres must be able to capture and guide the optical signal at a given wavelength with minimal loss. The choice of light source depends on the optical power and the wavelength that transducer is active in. The detector must match the spectral range of the transducer; in addition the sensitivity of the detector must be taken into consideration.

The preliminary operations for the sensor preparation, the experimental setup used in the practical studies and the method of data processing was brought in last part of this chapter.

References

- [1] K. A. Hunter, *Acid-base chemistry of aquatic systems*. Dunedin, New Zealand: University of Otago, 1998.
- [2] C. D. Kennedy, "Ionic Strength and the Dissociation of Acids " *Biochemical education* vol. 18, 1990.
- [3] J. L. Bada, "The pKa of a weak acid as a function of temperature and ionic strength: An experiment using a pH meter," *Journal of Chemical Education*, vol. 46, p. 689, 1969/10/01 1969.
- [4] M. F. R. Jeeyoung Choi, "Influence of the Degree of Ionization on Weak Polyelectrolyte Multilayer Assembly," *Macromolecules*, vol. 38, pp. 116-124, 2005.
- [5] E. Poptoshev, B. Schoeler, and F. Caruso, "Influence of solvent quality on the growth of polyelectrolyte multilayers," *Langmuir*, vol. 20, pp. 829-835, 2004.
- [6] S. S. Shiratori and M. F. Rubner, "pH-Dependent thickness behavior of sequentially adsorbed layers of weak polyelectrolytes," *Macromolecules*, vol. 33, pp. 4213-4219, 2000.
- [7] F. J. Arregui, I. Latasa, I. R. Matias, and R. Claus, "An optical fiber pH sensor based on the electrostatic self-assembly method," *IEEE Sensors: Conference proceedings*, pp. 107-110, 2003.
- [8] J. Goicoechea, C. R. Zamarreño, I. R. Matías, and F. J. Arregui, "Optical fiber pH sensors based on layer-by-layer electrostatic self-assembled Neutral Red," *Sensors and Actuators B: Chemical* vol. 132, pp. 305-311, 2008.
- [9] J. Goicoechea, F. J. Arregui, J. Corres, and I. R. Matias, "Study and Optimization of Self-Assembled Polymeric Multilayer Structures with Neutral Red for pH Sensing Applications," *Journal of Sensors*, vol. 2008, pp. 1-7, 2008.
- [10] F. Surre, W. B. Lyons, T. Sun, K. T. V. Grattan, S. O'Keeffe, E. Lewis, *et al.*, "U-bend fibre optic pH sensors using layer-by-layer electrostatic self-assembly technique," *Journal of Physics: Conference Series, Sensors & their Applications XV*, vol. 178, pp. 1-4, 2009.
- [11] P. Hashemi and R. A. Zarjani, "A wide range pH optical sensor with mixture of Neutral Red and Thionin immobilized on an agarose film coated glass slide," *Sensors and Actuators B-Chemical*, vol. 135, pp. 112-115, 2008.
- [12] A. K. Covington, "ACID-BASE INDICATORS," in *CRC Handbook of Chemistry and Physics*, W. M. Haynes, Ed., 91st ed: CRC Press (Taylor and Francis Group), 2010.

- [13] R. W. Sabnis, *Handbook of acid-base indicators*: Taylor & Francis Group, 2008.
- [14] G. Decher, "Fuzzy Nanoassemblies: Toward layered polymeric multicomposites," *Science*, vol. 277, pp. 1232-1237, 1997.
- [15] G. Decher, J. D. Hong, and J. Schmitt, "Buildup of ultrathin multilayer films by a self-assembly process: III. Consecutively alternating adsorption of anionic and cationic polyelectrolytes on charged surfaces," *Thin Solid Films*, vol. 210/21 I, pp. 831-835, 1992.
- [16] I. R. Matias, F. J. Arregui, R. O. Claus, and K. L. Cooper, "Molecularly self-assembled optical fiber sensors," *IEEE Sensors: Conference proceedings*, vol. 1, pp. 198-202, 2002.
- [17] R. A. Robinson and R. H. Stokes, *Electrolyte solutions*. London: Butterworths, 1968.
- [18] K. T. V. Grattan and B. T. Meggitt, *Optical Fiber Sensor Technology: Volume 2: Devices and Technology*: Springer-Verlag GmbH, 1998.
- [19] J. Dakin and B. Culshaw, *Optical Fiber Sensors: Applications, analysis, and future trends*: Artech House, 1997.
- [20] L. S. Grattan and B. T. Meggitt, *Optical Fiber Sensor Technology: Volume 4: Chemical and Environmental Sensing*: Springer, 1999.
- [21] F. Baldini, A. N. Chester, J. Homola, and S. Martellucci, *Optical Chemical Sensors*: Springer, 2006.
- [22] G. Keiser, *Optical Fiber Communications*: McGraw-Hill Education, 2010.
- [23] <https://learningnetwork.cisco.com/thread/4414>, (2011) *The Cisco learning network*,
- [24] G. Boisdé and A. Harmer, *Chemical and biochemical sensing with optical fibers and waveguides*: Artech House, 1996.
- [25] Dgardner,
http://www.thorlabs.com/newgrouppage9.cfm?objectgroup_id=1988,
(Oct 23, 2012). *0.37 NA and 0.39 NA Step-Index Multimode Fibers*.
- [26] OceanOptics, <http://www.oceanoptics.com/products/hl2000.asp>, (2012). *HL-2000 Tungsten Halogen Light Sources*.
- [27] PerkinElmer,
<http://www.perkinelmer.com/Catalog/Product/ID/UVWINLAB>, (2012)
UV WinLab Software,
- [28] OceanOptics, <http://www.oceanoptics.com/Products/spectrasuite.asp>,
(2012). *SpectraSuite*.
- [29] M. Szabelski, K. Guzow, A. Rzeska, J. Malicka, M. Przyborowska, and W. Wiczak, "Acidity of carboxyl group of tyrosine and its analogues and derivatives studied by steady-state fluorescence spectroscopy," *Journal*

of Photochemistry and Photobiology A: Chemistry, vol. 152, pp. 73-78, 2002.

- [30] Y. Mendelson, "Optical Sensors," in *The Biomedical Engineering Handbook*, E. Joseph and D. Bronzino, Eds., Second Edition ed: CRC Press LLC, 2000.

4. Principles of Layer-by-Layer Deposition Technique

4.1 Introduction

The concept of alternate attraction of oppositely charged polyions began with Iler's demonstration of successive deposition of negative silica colloids and positive alumina fibrils in 1966 [1]. But it was Decher and his group at the Gutenberg University in Germany who developed this method and fabricated optically transparent multilayer films at the beginning of the 1990s [2- 6].

The layer-by-layer technique is based on the successive deposition of oppositely charged molecules on a charged substrate; the negatively charged surface is simply dipped into the polycation solution for a few minutes. As a result, a thin layer of the positive molecules is formed onto the surface. The substrate is then dipped into the pure distilled water for minutes to remove unbounded molecules from its surface. The substrate is alternatively placed into the polyanion solution to form the next molecular monolayer. Unbounded molecules are again washed out using pure distilled water. Therefore, one bilayer (polycation/polyanion) is synthesized. This procedure is repeated to build up a multilayer coating. The steps in Fig 4-1 illustrate the multilayer coating procedure. Each pair of negatively and positively charged layers is called a bilayer. The composition

and structure of each layer can be controlled by appropriately choosing molecules and adjusting the deposition parameters. The thickness of each bilayer depends on the components used. For example, the thickness of a PAA/PSS layer is about 1 nm [7]. However, adding sodium chloride to the polyion solutions causes an increase in thickness.

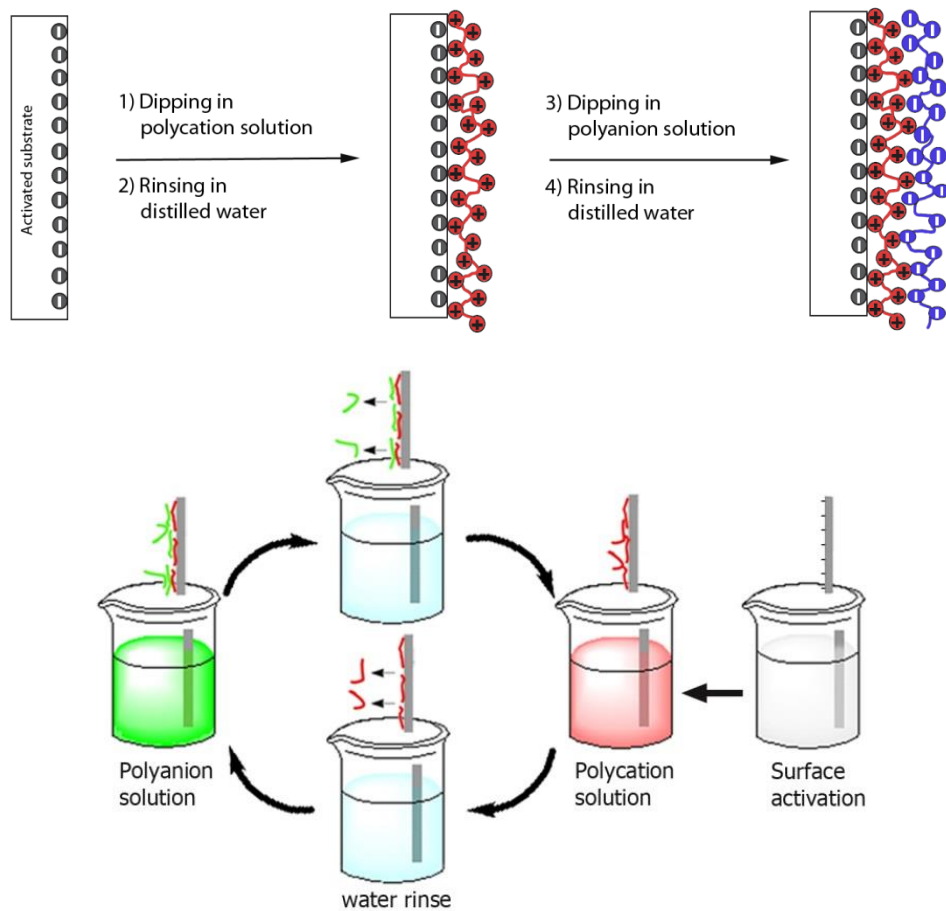


Fig 4-1 The sequence of layer-by-layer electrostatic deposition.

4.2 Important parameters

The deposition process on a surface using layer-by-layer technique is a self-organized thin film. The production of which can be controlled by many

parameters such as adsorption time, ionic strength¹, solvent composition, polyelectrolyte concentration, heat treatment and pH of the polyelectrolytes solution. The structure and properties of each layer depends on these mentioned parameters. The deposition is highly reproducible as long as the deposition conditions are maintained strictly constant. Some of these parameters are investigated in the next sections.

4.2.1 Substrate

Nanolayer thin films have been deposited using the LbL technique on a number of different substrates including glass, quartz, mica, silicone, plastic, wood and textile [8-13]. Gold and silver have also been used as base substrates [14-17]. Meanwhile, nanolayer thin films have been successfully built on both hydrophilic (fluorine, glass, and silicon) and hydrophobic (silanized glass) substrates by this technique [18]. In case of using UV-visible spectroscopy and optical microscopy glass and quartz are the most suitable substrates owing to their transparency [8].

Each of the different types of substrates has different physical property in regards to their topology, smoothness and roughness. However, due to the characteristics of the layer-by-layer deposition technique, the adsorption mostly depends on the surface charge distribution of the substrate [19, 20].

Suitable substrate must carry a minimal surface charge which, if not inherent, can be created by surface treatment. Basically, surface modification may

¹ A quantity representing the strength of the electric field in a solution, equal to the sum of the molalities of each type of ion present multiplied by the square of their charges.

provide charges to any substrate. The common substrates such as quartz, glass and single crystal silicon are first cleaned with a 30:70 mixture of 30% hydrogen peroxide (H_2O_2) and concentrated sulfuric acid (H_2SO_4), called the “piranha solution”, at room temperature for one hour.

The deposition of a film depends on the polyelectrolytes used and the adsorption conditions. Therefore, the amount of polyelectrolyte adsorbed during the first few deposition steps depend on the substrate and that substrate’s surface charge [9, 20-22]. The influence of the substrate is typically lost after a few layer-by-layer deposition cycles.

4.2.2 Polyelectrolytes

According to IUPAC (International Union of Pure and Applied Chemistry) definition a polyelectrolyte molecule is a macromolecule in which a substantial portion of the constitutional units have ionizable or ionic groups, or both [23]. Decher modified the definition based on layer-by-layer deposition i.e. polymers with ionizable surface groups to form polyions that were successively layered onto a substrate by electrostatic interaction [24]. Polyelectrolytes aqueous solutions, depending on the charges they carry (being negative or positive) turn into either polyanions or polycations.

Polyelectrolytes can be utilized in the formation of multilayer thin film known as polyelectrolyte multilayers (PEMs). During layer-by-layer deposition, the multilayer can be constructed by alternative dipping of the charged substrate into the dilute solutions of polycation and polyanion. The thin film is built up

due to electrostatically cross-linked films of polycation-polyanion layers while the thickness of the layers is controlled down to single-nanometer scale.

Polyelectrolyte multilayers is originally assembled based on electrostatic interaction between charged polymers. However, the LbL technique has been developed to build up the layers based on incorporation of hydrogen bonding and electrostatic force from the late 1990s [25-28].

Charged polymers used for PEM assembly are classified as strong or weak polyelectrolytes based on their charged groups. Those polymers that maintain a fixed charge over a broad range of pH conditions are termed “strong polyelectrolytes.” Polymers that exhibit pH-dependent ionization are called “weak polyelectrolytes” [29]. Process of formation of multilayers from weak polyelectrolytes can be controlled by pH of the solution as it is clear that pH influences charge density of the polyelectrolyte chains and thus their conformation and mutual interactions [30].

In general, a substance with a negatively charged functional group such as sulfonic acid, sulfuric acid, or carboxylic acid is used as a polyanion. For example, conductive polymers such as polystyrene sulfonate (PSS), polyvinyl sulfate (PVS), polyacrylic acid (PAA), polymethacrylic acid (PMA), poly (1-(4-(3-carboxy-4-hydroxyphenylazo) benzenesulfonamido)-1,2-ethanediyl) (PAZO), poly(anilinepropanesulfonic acid) (PAPSA), sulfonated polyaniline (SPAN), poly(thiophene-3-acetic acid) (PTAA), poly(2-acrylamido-2-methyl-1-propanesulfonic acid) (PAMPSA) and biopolymers such as DNA are used. However, polystyrene sulfonate (PSS), polyacrylic acid (PAA) are more

popular. Furthermore, a substance having a positively chargeable functional group such as a quaternary ammonium or amino group can be used as a polycation. For example, polyethyleneimine (PEI), polyallylamine hydrochloride (PAH), polydiallyldimethylammonium chloride (PDDA), polyvinylpyridine (PVP), polystylenemethylenediethylmethylamine (PSMDEMA), a precursor of poly(phenylene vinylene) (Pre-PPV), polymethylpyridylvinyl (PMPyV), or protonated poly(p-pyridyl vinylene) (R-PHPyV) and poly((2-(methacryloyloxy)ethyl) trimethylammonium chloride) (PCM) can be used. Although, polyethyleneimine (PEI) and polyallylamine hydrochloride (PAH) are the most popular. Some of these polyions are shown in Fig 4-2. Combinations of polyelectrolytes with other materials, including nucleic acids [31], DNA and proteins [32-34], viruses and micro-organisms [35, 36], enzymes [37, 38], gold colloid [15, 16], quantum dots [39-41], silica [42, 43], clay mineral [44], carbon nanomaterials [45], nanoparticles [46], fluorescent materials [47], dyes [48, 49] and other inorganics [50, 51] have rapidly grown. As all these mentioned materials can be easily deposited on the substrate.

The thickness of the thin film made from polyelectrolytes depends on the type of polyelectrolytes. For example, the average thickness of each bilayer of PSS/PDADMA [270 Å/bilayer in 1 M NaCl] is 7 times higher than the average thickness of each bilayer for PSS/PAH under the same conditions [52]. This demonstrates the importance of polyelectrolyte type in determining the ultimate film thickness.

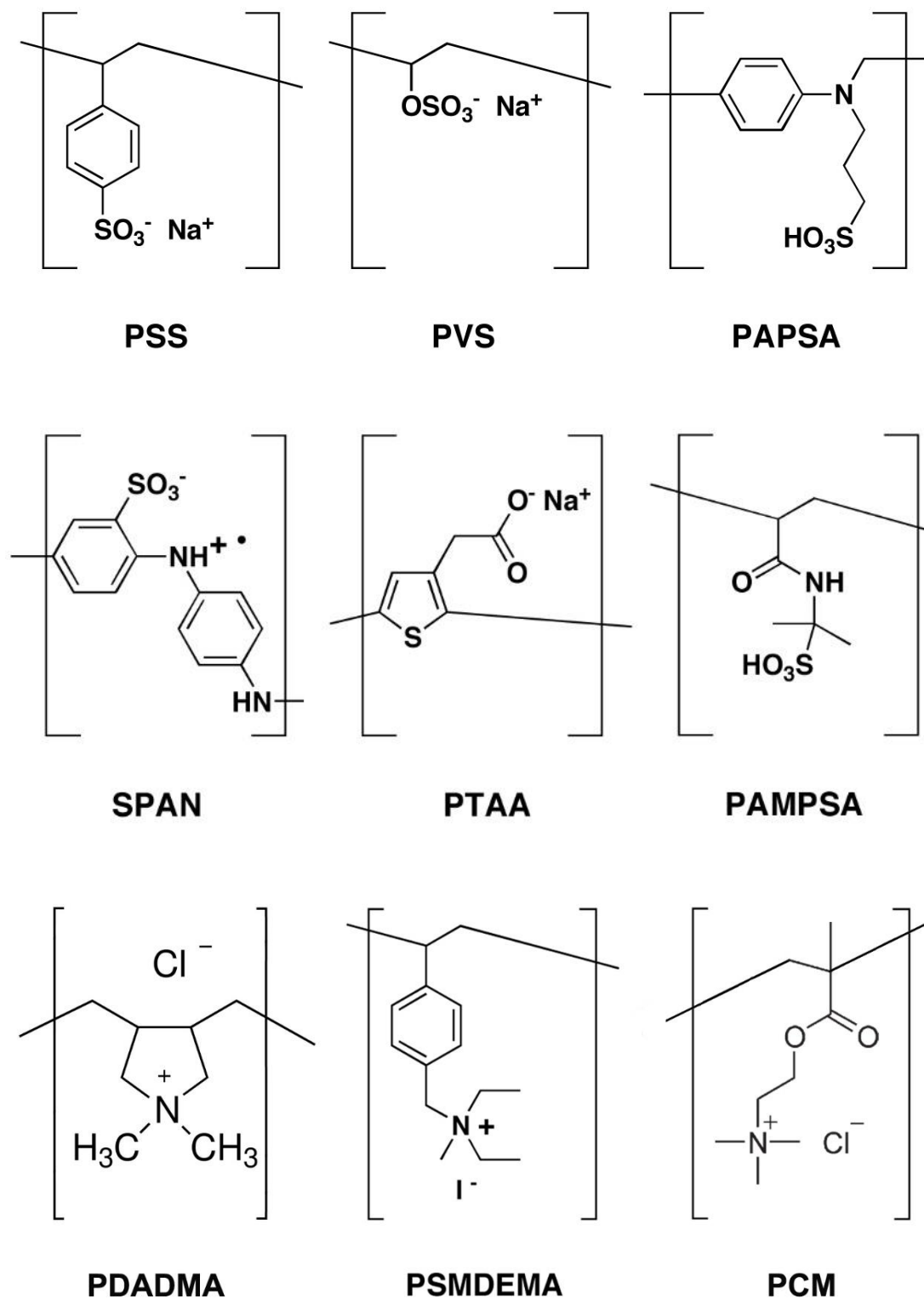


Fig 4-2 Some standard polyions frequently used for multilayer fabrication by LbL deposition technique

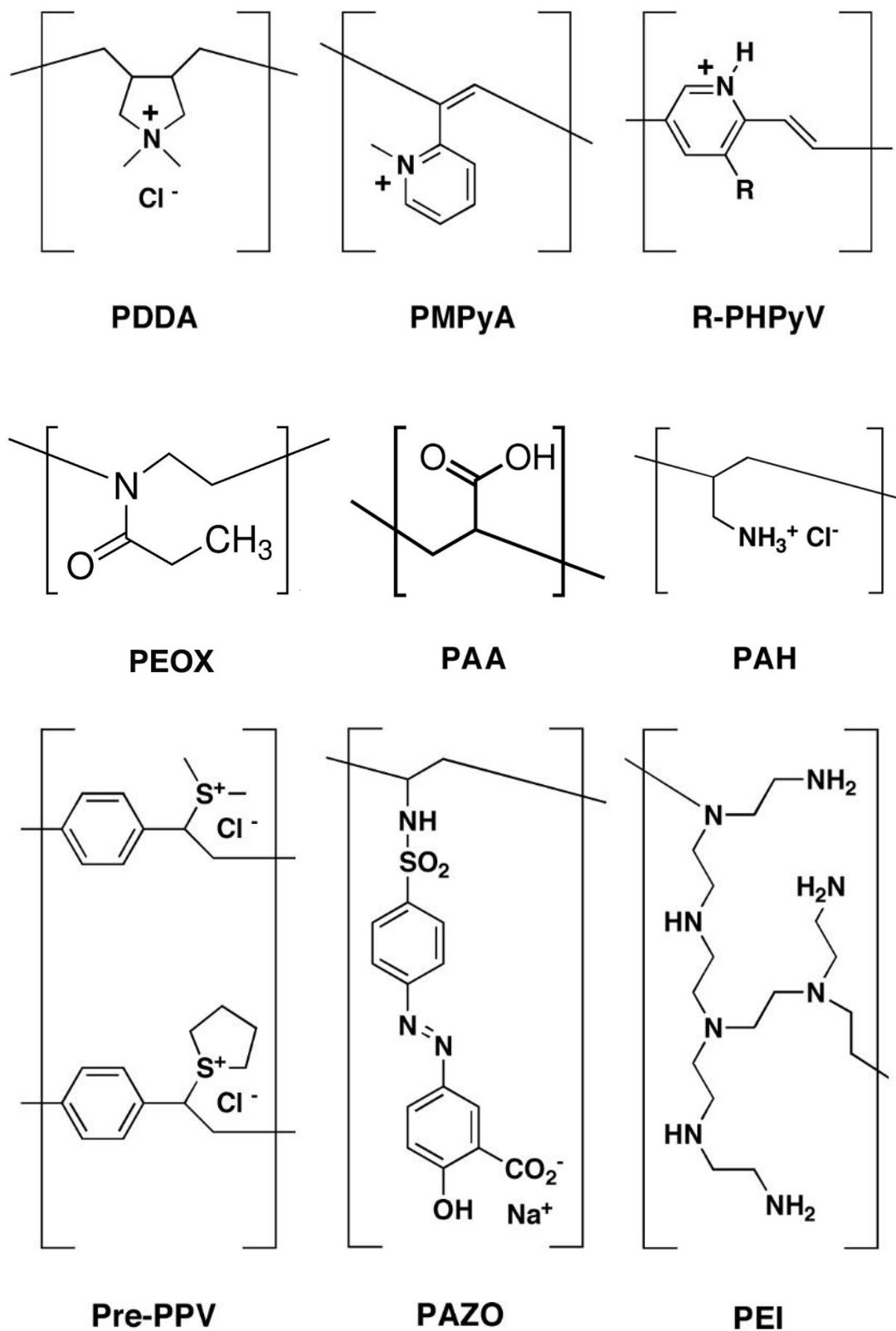


Fig 4-2 (continue) Some standard polyions frequently used for multilayer fabrication by LbL deposition technique.

4.2.3 Control of thickness

when a surface is exposed alternately to polyelectrolytes of opposite charge, a polymer composite film of uniform thickness is obtained [20].

The thickness of the thin film is affected by the substrate surface properties and the deposition conditions. Parameters like density of surface charge and surface roughness related to the substrate are important. Meanwhile, the thickness of each layer also depends on operational factors such as polyelectrolyte concentration, dipping time, ionic strength and pH of the polyelectrolyte solution, temperature, rinsing time and drying time [8, 30]. The deposition is highly reproducible if these parameters are maintained strictly constant [52, 53].

The ionic strength is an essential parameter to control the thickness of the layers. The layer fabricated with a strong polyelectrolyte is always thinner than a weak polyelectrolyte. The thickness of the deposited layers of strong polyelectrolytes (which are highly charged) is often down to thickness of a molecule; while weak polyelectrolyte solutions give thicker layers of which thickness are sometimes as much as 16 times greater than the strong one [54, 55]. Because varying the charge density of the polyelectrolyte influences the morphology and the thickness of the thin films. Normally, the polymer molecules are in the form of long chains and the ionic charge is homogeneously distributed among them. Addition of salts (generally NaCl) as counter ions, neutralizes some fraction of the charges and reduces the repulsion force along the polymer chain. Following the lack of available repulsion force, the polymer chains curl and form cluster conformations [56-58].

As shown in Fig 4-3, layers deposited from such solutions are generally thicker due to circular arrangement of the polymer molecules. According to Shiratori & Rubner [55] there is no dependency between thickness of the fully-charged deposited polymer layer and the molecular weight of the polymer over a range of at least $3000-10^6$ g/mol.

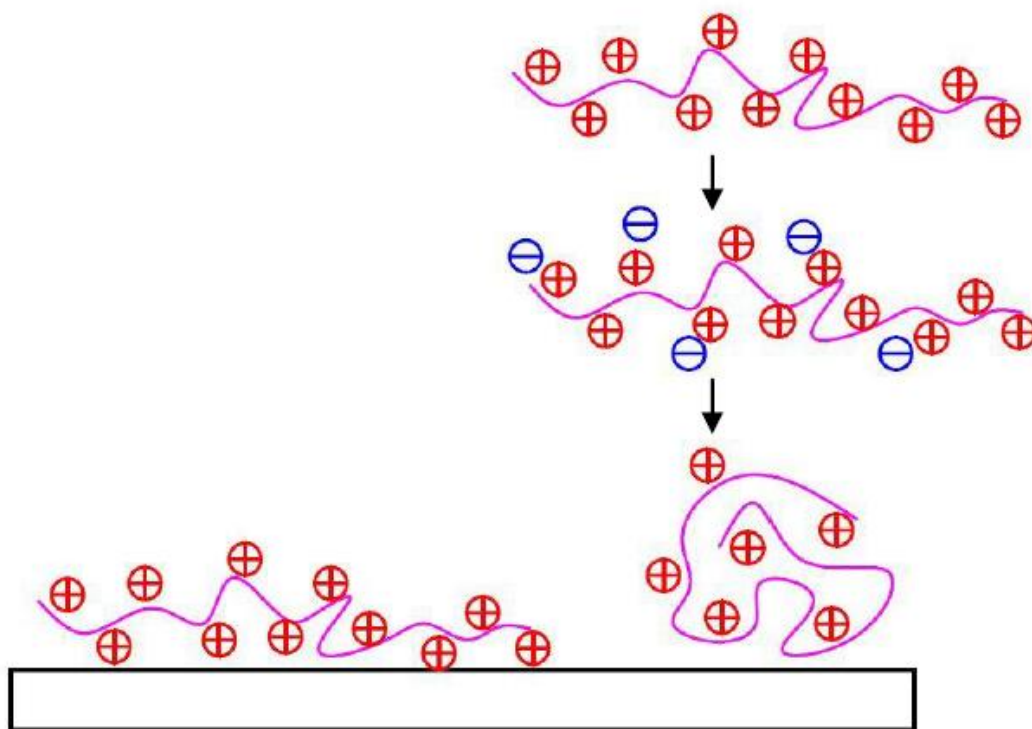


Fig 4-3 Schematic of globular conformation of a polymer chain with low charge density (right) is shown in comparison with a polymer chain with high charge density (left). Polymer chains with lower charge density form globular conformations and so thicker layers [58].

4.2.4 Dipping time (deposition time)

The deposition of each polyion takes place within two stages. Firstly, the polyion chains attract electrostatically to the charged adsorption sites by a small number of ions that lasts a few second. Then, the remaining adsorption sites

should be filled after adjustment and penetration of the polyion chains between the sites already filled. This stage takes from few minutes up to 20 minutes. In practice, 97% of polyions are adsorbed within a few minutes [7, 16, 41, 52, 59-65]. As illustrated in literature [8] adsorption mainly occurs during the first 2 minutes after exposure of the substrate to the polyelectrolyte solution. Changing the dipping time changes the time available for the ions to arrange themselves and ionically bond to the surface. Due to an increase in the number of the molecules on the surface and an increase of the dipping time, a thicker layer will be formed. However, the growth of the thickness of the layer is not proportional to the time. For example, a 20 minute increase in dipping time, from two to twenty two minutes results in a 20% increase in the layer thickness. Here the dipping time is increased over 10 times. However, the change in thickness is only 20%. Typically, 1 to 5 minutes dipping is used for the layers, depending on the type of polyions used [66].

Removing of extra molecules from the surface is observed when the washing time is increased. This in return reduces the layer thickness. It has been shown that 2 to 3 minutes of rinsing in pure water immediately after adsorption removed approximately 10 to 20% of the weakly attached molecules [19].

4.2.5 The concentration of the polyelectrolyte solution

An increase on the concentration of the polyion solutions increases the chance of sticking the molecules on the substrate. It subsequently forms a thicker layer.

In most studies reported to date, polyelectrolyte concentrations have been set to about 10^{-2} mol/L (based on the constitutional repeat unit) [8, 37, 49, 52, 67]. At low electrolyte concentrations the adsorbed layers are thin and the adsorbed amount hardly depends on the molecular weight [56].

4.2.6 Effect of pH of the polyelectrolyte solution

The properties of polyelectrolyte films can be controlled by changing the characteristics of the solution such as the pH level. The greatness of electrostatic force in polyelectrolyte multilayer films can be altered through variation of the polyelectrolyte charge densities by adjusting the pH values of the solutions [54, 55, 68-70]. This method is especially useful for cases in which the polyelectrolyte is weak, which means that it can be neutralized near the neutral pH. Polyanions commonly comprising carboxyl or sulfonate groups are fully charged at high pH and polycations commonly including amine groups are fully charged at low pH [8, 70, 71]. In other words, pH of the polyions solution controls the degree of ionization of weak polyelectrolytes, and it therefore directs their conformation and interactions and consequently the layer thickness [9, 29].

Adjusting pH of the polyelectrolyte solution at a given value by adding a few drops of acid or base raises the ionic strength and then leads to form thicker adsorbed layers; while, the adjusted pH will modify the charge density of the polyelectrolytes. An increasing charge density on the polyions will create thinner deposited layers. As a result, changing pH may increase or decrease film

thickness, in dependence of the polyelectrolyte system chosen. Extreme pH values may completely prevent film growth or destroy the constructed film [8, 55, 72, 73]. Shiratori et al. investigated in literature [55] the role of pH of the weak polyions solutions in the layer thickness. Their findings are summarized in Fig 4-4 displaying the average incremental thickness contributed to each multilayer thin film of PAA/PAH. As shown in this figure by simply controlling pH, it is possible to deposit unusually thick bilayers ($>120 \text{ \AA}$) or very thin bilayers ($<10 \text{ \AA}$) or, in some cases, completely prevent the multilayer deposition process (for example, when the pH of the PAH solution is 3.5 and the pH of the PAA solution is 7.5).

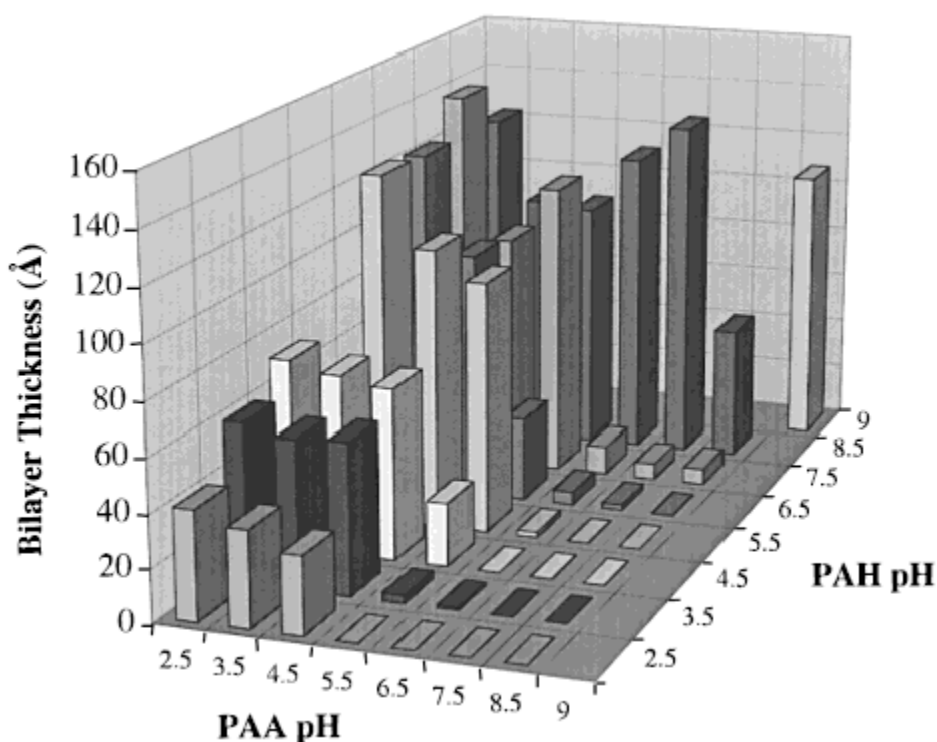


Fig 4-4 Complete pH matrix showing the average incremental thickness contributed by a PAH/PAA bilayer as a function of dipping solution pH [55].

4.2.7 Effect of adding salt

It has been recommended [9, 22, 29, 52, 56, 74] to add salt in the polyelectrolyte solutions. Presence of salt causes the film thickness slightly, but very precisely, to increase with increasing salt concentrations. Polyion concentration, molecular weight, and deposition time are known to be less important variables than the salt in multilayer thickness [52]. Addition of salt can also change the polymer chain conformation [29]. Fig 4-5 shows how the presence of salt effects the thickness of the film. Polymer positive charge is balanced by a polymer negative charge in the absence of salt (intrinsic). However, in the case, when salt is present, polymer charge is balanced by salt counterions.

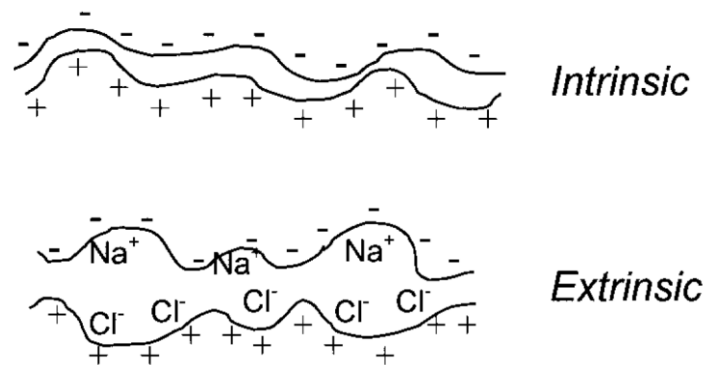


Fig 4-5 The effect of salt in polyelectrolyte multilayers structure [9].

Addition of salts to the polyion solutions increases the ionic strength of the polymers which in turn increases the film thickness [2, 20, 52, 60-63, 75, 76] and decreases the charge density [77-79]. While small amounts of salt can speed up the adsorption process somewhat [76, 79-81], adsorption is slowed down at

high ionic strengths [82, 83]. Nevertheless, it should be remembered that very high ionic strengths can induce desorption of the polymers, in particular when using weak polyelectrolytes [8, 84].

LiCl, NaCl, NaBr, NaI, KCl, CsCl, MgCl₂, Na₂SO₄ [52, 77, 85-88] have been added to the polyelectrolyte solutions to increase the ionic strength. However, NaCl is the most common. Obviously, the salt concentration is a significant variable in the film thickness and its photonic absorbance.

Dubas *et.al.* showed in literature [78] that the thickness of the thin film levels out in salt (NaCl) concentration of less than 10⁻² M and more than 10⁻¹ M for (PSS/PAH)₆. They also presented in work [52] there is an almost linear relationship between NaCl concentration and the thickness of thin film for (PSS/PDADMAC)₁₀ when the concentration changes from 10⁻² M to 2 M. This is in contrast to the recent findings of Gang and Gao [86] who reported that the thickness of multilayers was significantly influenced by the salts type i.e. the thickness increased along with the increase of NaCl concentration used during the assembly, whereas it kept constant when NaBr was used in growth of the PSSMA/PDADMAC multilayers. As a result, the thickness of a bilayer is influenced by both type of salt and type of polyelectrolyte in addition to the concentration of the salt solution. Nonetheless, for a given pair of polycations and polyanions, the concentration of salt in the deposition solution appears to exert the strongest influence on the adsorption process and the thickness of each polymer layer [74].

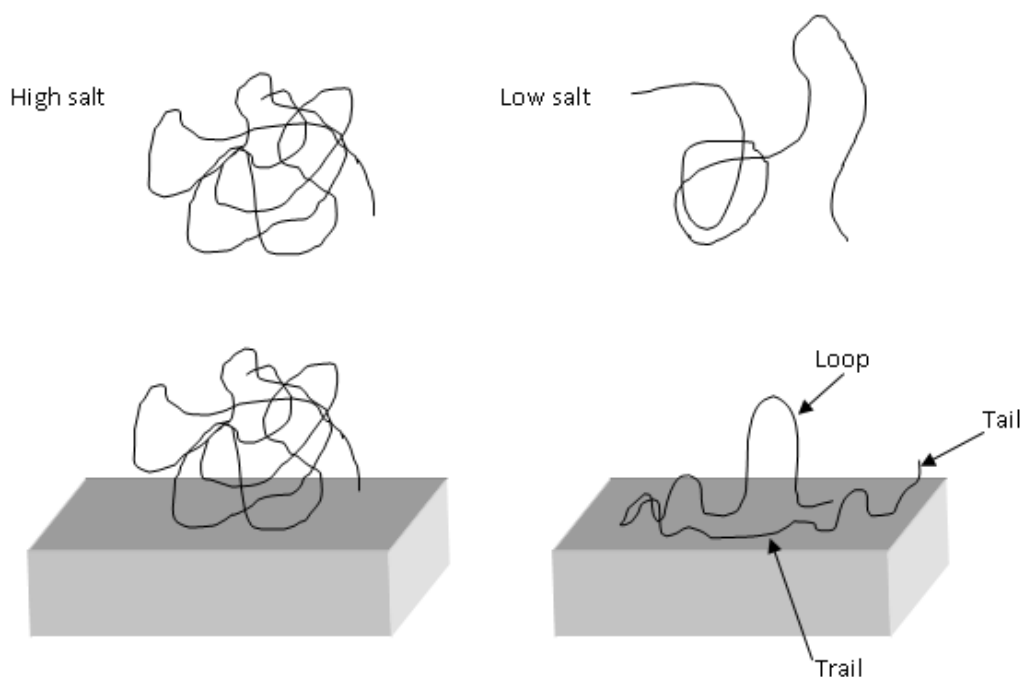


Fig 4-6 The effect of salt on a polyelectrolyte molecule in solution in high and low concentration of salt [89].

In exploring growth conditions, it is generally observed that at low salt concentration, polyelectrolytes tend to be extended in the bulk and interact strongly with the surface and are formed thin layers. The molecules of polyelectrolytes are assumed conformations with loops, trails and tails. At intermediate salt, the polymers become more coiled due to charge screening, and the adsorbed layer mass and thickness increase. At high salt concentration the repulsion is screened; hence the polyelectrolytes behave more like uncharged polymers. They can adopt conformations with loops and tails, and the adsorbed amount increases but the layer is not so uniform as the intermediate and low concentration of salt are. [52, 56, 83, 90]. Fig 4-6 illustrates the effect of salt on a polyelectrolyte molecule in solutions of high and low salt concentrations.

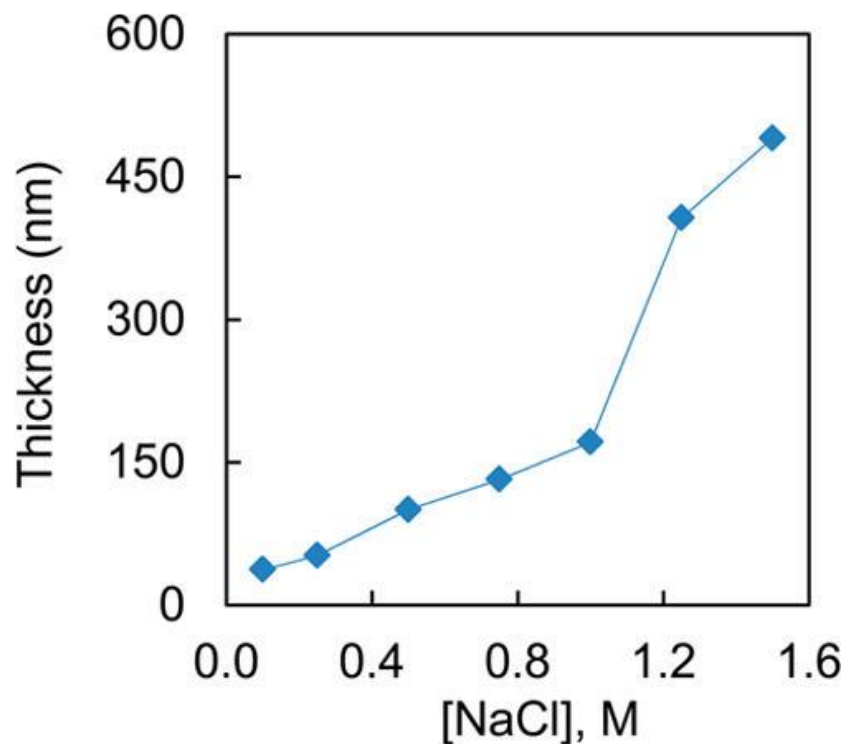


Fig 4-7 Thickness of (PDADMA/PSS)₁₀ built from 10 mM PDADMA and PSS solutions at various salt concentration on Si wafers [81].

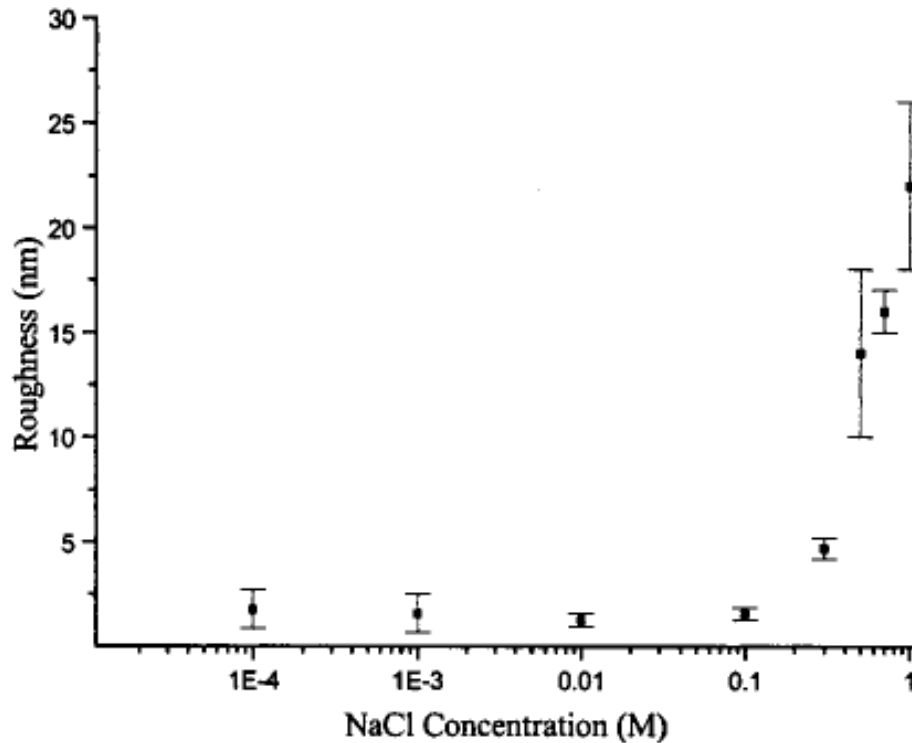


Fig 4-8 The root-mean-square roughness of (PDDA/PSS)₁₀ deposited from different NaCl concentrations. The error bars represent standard deviations [91].

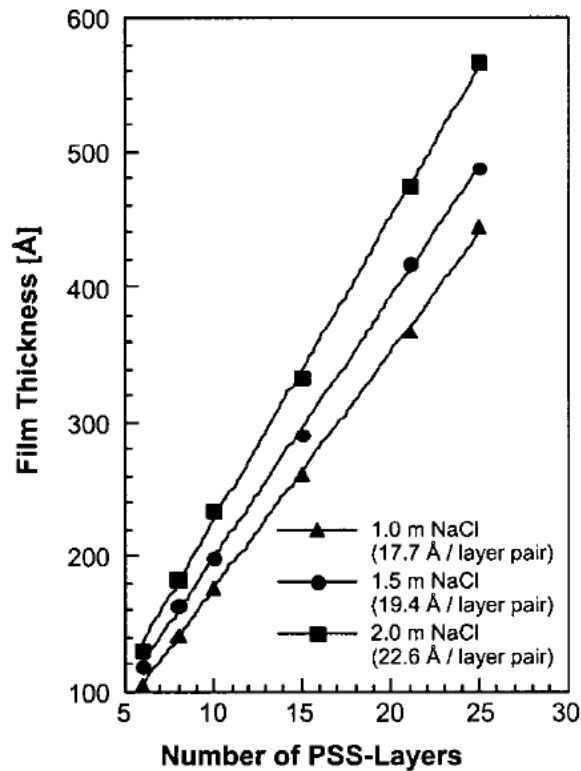


Fig 4-9 The film thickness versus number of layers for three sets of experiments of $(\text{PSS}/\text{PAH})_n$ deposition in different salt solution [9].

Fig 4-7 shows that how the thickness of the film varies with salt concentration for $(\text{PDADMA}/\text{PSS})_{10}$ and Fig 4-8 illustrates the roughness of 10-bilayer films of PDDA/PSS deposited from different NaCl concentrations. For low salt concentrations, the roughness remained constant at a small value. Films prepared from higher salt (NaCl) solutions are noticeably rougher [89, 91] as shown in Fig 4-8. The film thickness versus number of layers for three sets of experiments of $(\text{PSS}/\text{PAH})_n$ deposition in different salt solution are shown in Fig 4-9.

4.2.8 Number of bilayers

Total film thickness can be adjusted by controlling the number of bilayers. The amount of polyelectrolyte deposited in each adsorption step gradually increases with increasing layer number [92].

At the first layers; which varies from two to six (one to three bilayers) in previous work [33, 70, 93, 94], smaller amounts of polyion are adsorbed as compared with next layers [37, 52]. In this step the amount of adsorbed polymer normally increases before reaching a more constant level [52, 60]. The multilayer growth also follows an exponential-like pattern rather than the usually observed linear dependence of thickness on the number of deposited layers [70, 95]. The surface charge of the substrate determines how long it takes to reach a constant level [92]. However, as long as the polyelectrolytes create an electrostatic equilibrium, constant growth is eventually reached despite the substrate characteristics [96-98] as shown in Fig 4-10.

Numerous studies have shown experimental evidence of a linear increase of film thickness with the number of deposited layers independent of the nature of the initial substrate, after reaching the electrostatic equilibrium [61, 66, 70, 95], as shown in Fig 4-11.

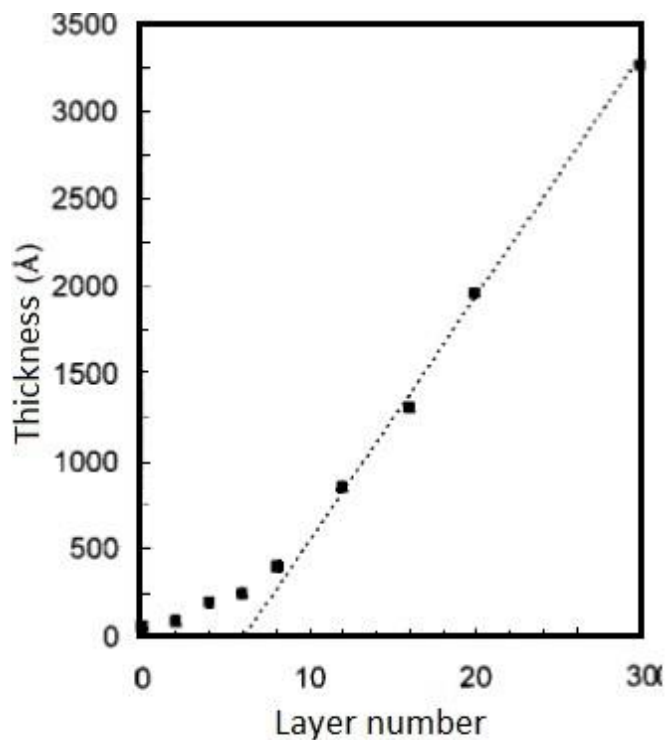


Fig 4-10 Thickness as a function of the number of layers for a $(\text{PSS}/\text{PDADMAC})_n$ multilayer deposited on silicon wafer from 1.0 M $\text{NaCl}_{(\text{aq})}$, polymer concentration 1 mM [52].

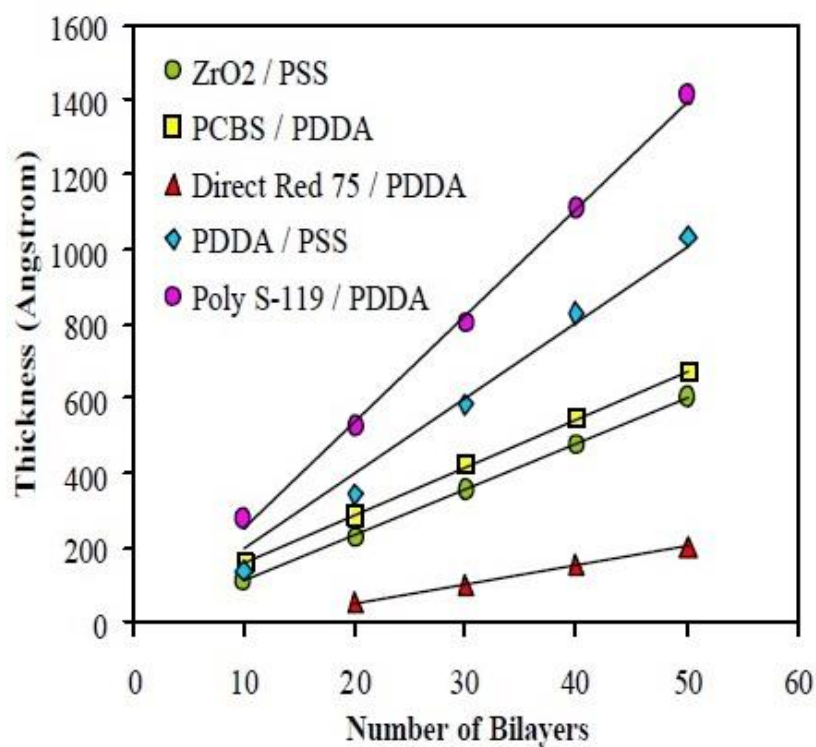


Fig 4-11 Film thickness with increasing numbers of bilayers for single anion/ cation in deposited films [66].

4.2.9 Influence of drying

The applied drying procedure is another parameter which influences film growth. Drying the film to remove the water layer from the film surface affects film characteristics comprising the thickness and optical absorbance of the films. In the standard LbL process, the film is not dried and remains wet at all stages.

There are many evidence reported [99-102] that the samples dried after adsorption of each layer had higher adsorbed amounts than samples prepared without drying and it was shown that drying makes the films flatter and rather hydrophobic. It was also reported that drying at every step of adsorption increased the thickness of adsorbed films due to enhanced surface roughness of each bilayer [52, 66, 103, 104]. De Souza et al. [105] noted that drying affects the film build-up and morphology, with LbL films dried under room conditions displaying a more homogeneous surface (lower roughness) and higher adsorbed amounts when compared with films dried under vacuum or by nitrogen flow. The lower roughness was attributed to lower solvent evaporation rates for samples dried in air. An increased ionic strength was also shown to lead to rougher surfaces [106]. From studies already conducted [10, 11] on Poly R-478/PDDA films, dried films (where the film was dried after each monolayer was deposited) showed 20% greater thickness and 15% greater optical absorbance than the un-dried films. Though, the conflicting evidence for the role of drying reported by Patel et al. [107] that the net growth of an enzyme layer increases when the drying step is omitted. Drying of enzymes layers

reduces the activity of the assembly to some extent. However, Dubas showed in literature [52] that the layer thickness for deposition of PSS/PADMA thin film does not depend on whether the multilayer has been dried between layers.

Muthukumar [108] theoretically predicted that the drying can affect the contents of counterions in films prepared by LbL from solutions having different ionic strengths. Lourenco [100] showed that the amount of counterions in PAH/PSS LbL films decreased by almost one order of magnitude when the film was dried under room conditions after adsorption of each layer and explained that this was due to water removal during the drying process which allows the formation of NaCl nanocrystals, that subsequently dissolve into the solution in the adsorption of the next layer. For wet samples the increase in salt concentration leads to a decrease in the number of NH^{+3} ionized groups. He summarized the effect of drying in Fig 4-12.

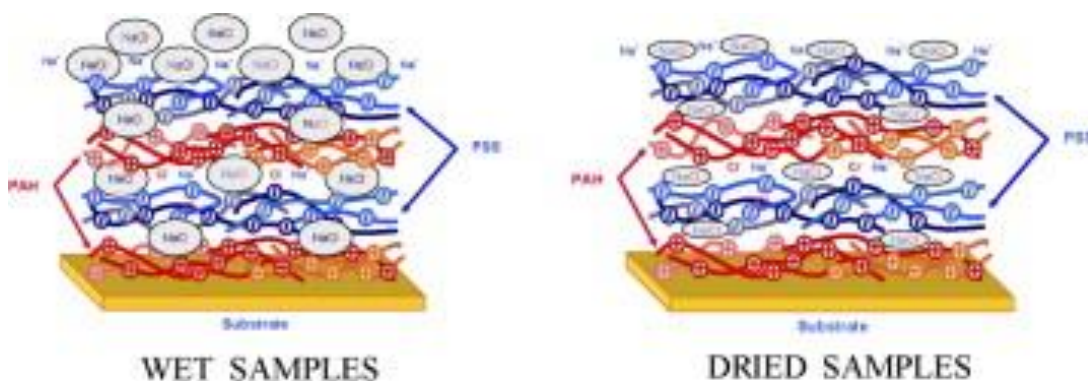


Fig 4-12 Wet sample versus dried sample [100].

4.2.10 Stability

The stability of the multilayer is largely determined by the electrostatic interactions of the anionic-cationic polymer pair and, hence, depends on type and concentration of the salt, strength of ions and polyelectrolytes, polymer's molecular weight, pH of the solutions and the thermal energy.

In order to form a stable multilayer thin film, a minimum charge density in each layer is needed. This minimum charge density depends on the salt concentration and salt type, and also very strongly on the chemical identity of the charged units being relied on to form the thin film [8, 29, 109]. Stronger ion pairing will also yield more stable multilayers [9]. Moreover, high molecular weight polymers promote the stability of the layers [44, 110, 111]. High and low pH solutions can potentially discharge the ions and destruct the layers, while heat treatment causes the chemical reaction between the molecules of two adjacent layers and makes the stronger bonds and more stable multilayer film, in other words, the multilayer structure could be stabilized by crosslinks formed during the curing of the deposited film under heating as shown in Fig 4-13. Although, upon heating, the film thickness decreases.

Generally, chemical, thermal or UV crosslinking can significantly alter the stability of a given polyelectrolyte multilayer too [99, 113, 114].

Highly charged polyelectrolytes form very stable multilayers [115]. While multilayers of weak polyelectrolytes are potentially unstable, since a variation in the pH can influence the polymer charges [61].

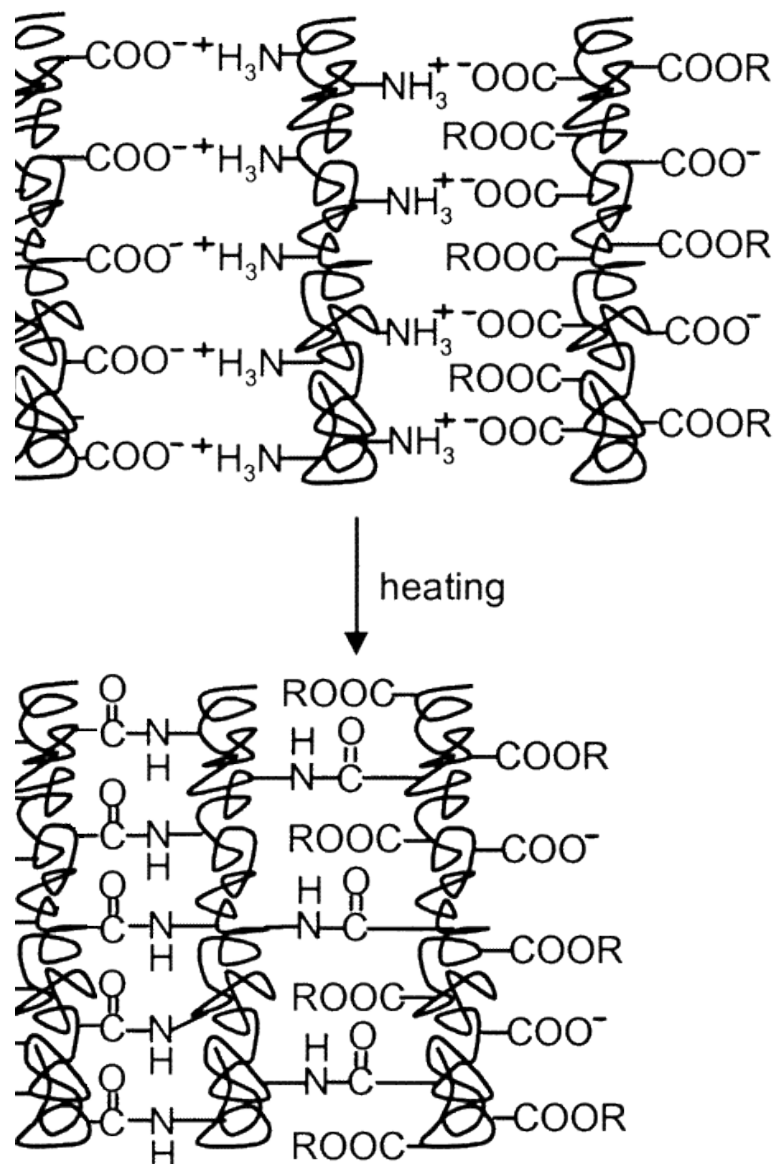


Fig 4-13 The heat treatment effect on the layers coated on the surface i.e the chemical reaction in PAH/PAA multilayer assemblies after heat treatment [112].

Unstable multilayers could be stabilized by rinsing unbounded molecules before switching to the other polymer solution. For weak polyelectrolytes, which have a pH dependent charge, also the pH of the solution was shown to be an important variable for stability [61].

4.3 Materials and method

Neutral Red (NR) was widely applied as a pH indicator in majority of the published work using LbL method. Hence NR was initially selected to study the LbL technique and find out the best conditions for the coating. The molecule of neutral red carries an amine group with positive charge and applied as a polycation. Poly (acrylic acid) (PAA) with negatively charged functional group was also applied as a cross-linker. The deposition was initially carried out on the glass microscope slides of dimensions 76×26 mm with thickness of 1.0 mm.

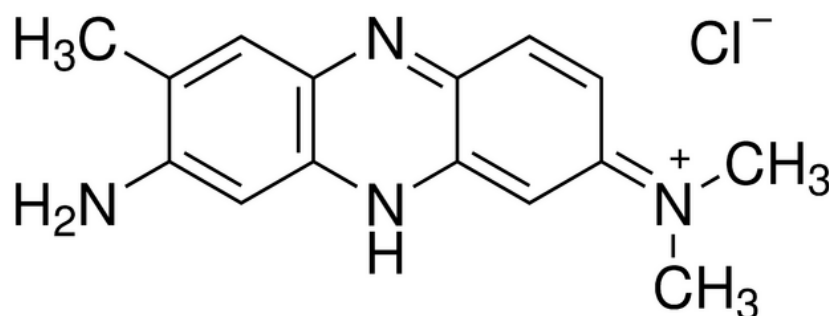


Fig 4-14 Neutral red chemical structure.

To build up the layers onto the glass slide or fibre surface, cleaning and modifying of the surface is necessary. The first step is to clean the surface ultrasonically in normal water for 15 minutes to remove dust and some impurities and then to immerse it into piranha solution (70% concentrated sulfuric acid, 30% oxygen peroxide) for about an hour to treat and functionalize the surface. The substrate is then washed with distilled water and dried by N₂ gas flush. The negatively charged surface is ready to attract the positively

charged molecules. Therefore, the substrate is immersed into a polycation solution for a specific time period (2- 5 minutes). After forming the monolayer and dipping out, the substrate is extensively rinsed with fresh distilled water for a specific time period (2- 5 minutes) to remove the un-bonded molecules. To assemble the second monolayer a similar procedure is followed for the polyanion solution. Subsequently, the substrate is alternately immersed into polycation and polyanion solutions to create a multilayer deposition.

The polyelectrolyte solutions were prepared by dissolving a certain amount of polyanion or polycation in pure distilled water or saline water.

In a different set of experimental work, the following parameters were changed and the glass slide optical behaviour was investigated by spectroscopy of the samples to determine the characteristics of the film.

Dipping time (t_{Polyion})

Washing time (t_{Rinsing})

Rinsing method

Number of bilayers (n)

The concentration of the solutions

Adding salt to the solutions

Drying and method of drying

It should be taken into consideration in all experiments that thicker film gives greater absorbance spectra.

4.3.1 Dipping Time and Washing time

Due to an increase in the number of molecules on the surface because of an increase in the dipping time, the absorbance spectra measured with the spectrometer showed an increase in absorbance. Removing of extra molecules from the surface happened when the washing time is increased and caused the decrease of the thickness and consequently the absorbance. In conclusion, changing the time directly changes the absorbance. Table 4-1 shows the effect of dipping time on the absorbance for (NR/PAA)₅ with 10mM concentration in the presence of 0.2M salt in the solutions without drying.

Table 4-1 The effect of dipping time on the absorbance for the glass slide coated with (NR/PAA)₅.

Dipping time	Absorbance	Wavelength (nm)
2 min	0.17	523
3 min	0.20	522
5 min	0.26	522

Table 4-2 The effect of rinsing method on the absorbance for the glass slide coated with (NR/PAA)₆.

Rinsing method	Absorbance
Ultrasonic	0.20
Magnetic Stirrer	0.57
Without stirring	0.74

4.3.2 Rinsing method

Washing out the un-bonded molecules of each built up layer should be done thoroughly. Cleaning ultrasonically in distilled water, using the magnetic stirrer during the cleaning or dipping in the distilled water has been examined. The result showed ultrasonic cleaner removed higher molecules and made thinner film with lower absorbance, while immersing the coated substrate in pure water

with no further action caused only the loose molecules to be removed producing a thicker film. Table 4-2 compares the absorbance for the samples that are cleaned by these three different methods for (NR/PAA)₆ with 10 mM concentration in the presence of 10⁻³ M salt in the solutions without drying.

4.3.3 Number of bilayers (n)

Increasing the number of bilayers increases the thickness of the thin film and accordingly increases the absorbance. Fig 4-15 shows the change in the absorbance and the peak wavelength with the increase in the number of bilayers for (NR/PAA)_n when the concentration of the solutions were 2 mM and the dipping time was the same as the rinsing time. Building up more bilayers affects the amount of absorbance directly as adding the number of bilayers increases the absorbance whilst reducing the wavelength.

4.3.4 The concentration of the polyelectrolytes

An increase in the concentration of the polyion solutions increases the number of molecules depositing on the film. It subsequently causes a higher absorbance. Three different concentration of the solution were tested. The enhancement is seen in absorbance with regards to both concentration of the solution and number of bilayers as shown in Fig 4-17 and Fig 4-16 (down). In spite of this fact that the peak wavelength decreases with number of bilayers for concentration of 10 mM, it roughly remains constant for concentration of 2 mM as shown in Fig 4-16 (up).

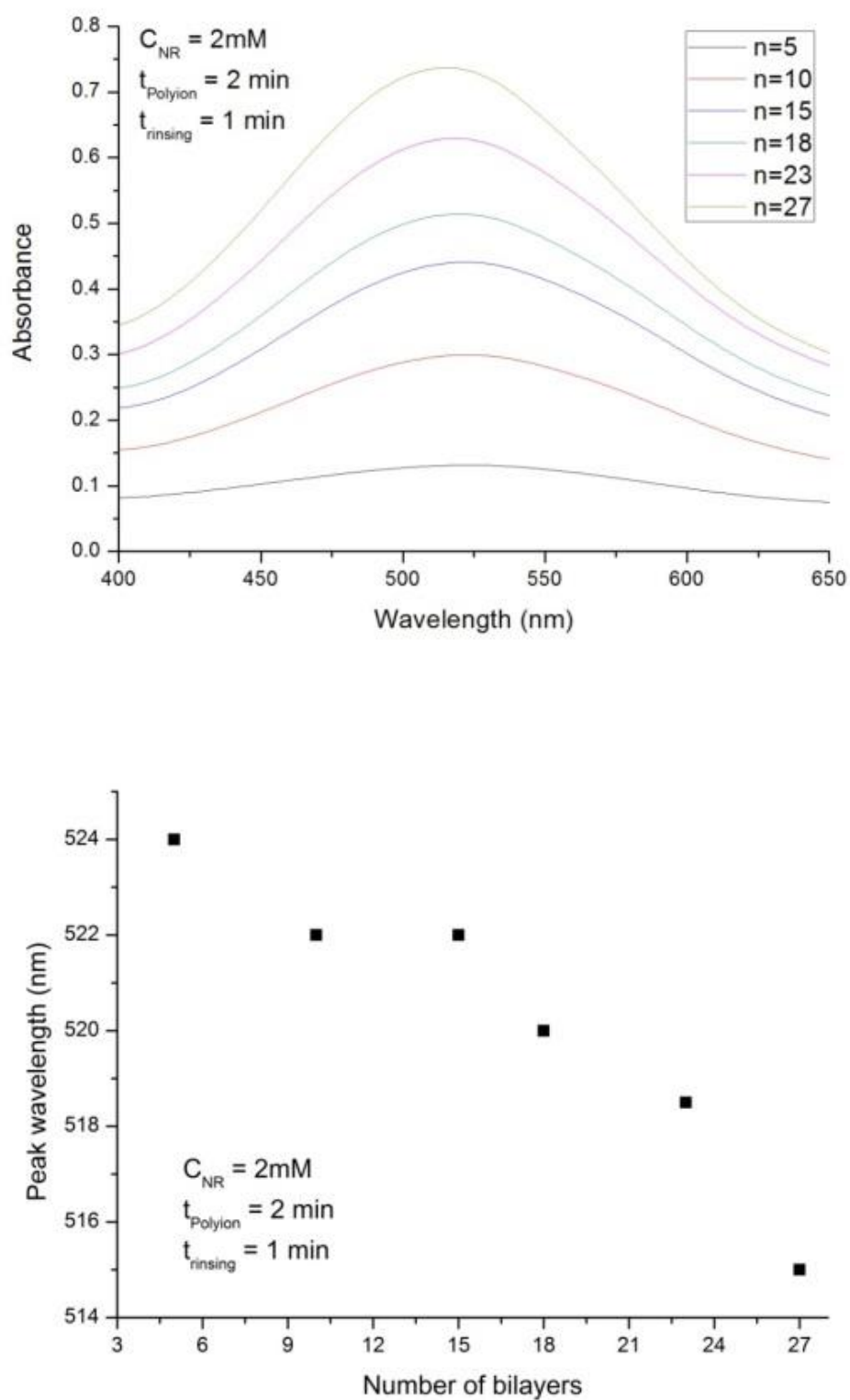


Fig 4-15 The absorbance spectra (up) and the peak wavelength (down) versus number of bilayers of $(\text{NR}/\text{PAA})_n$ coated on the glass slide while the concentration of the dye solution was 2 mM.

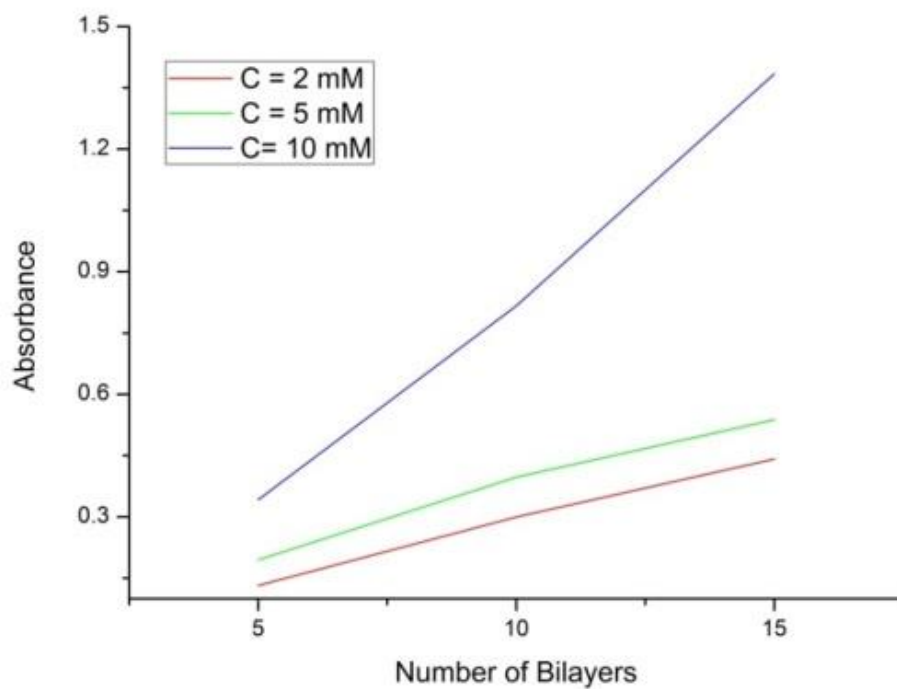
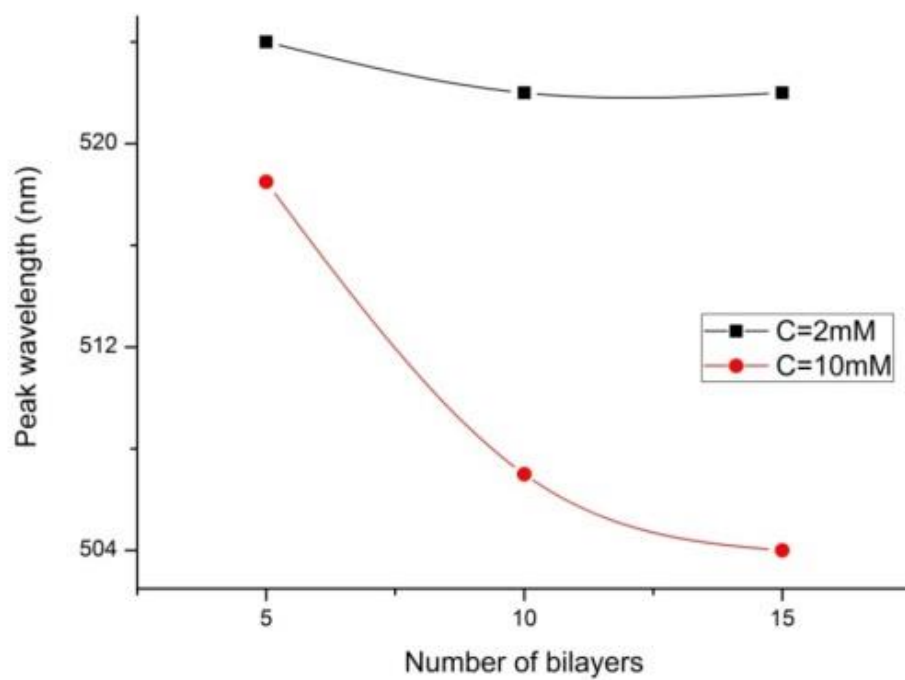


Fig 4-16 The effect of concentration of the solutions on the peak wavelength (up) and the absorbance (down) for $(NR/PAA)_n$ in the various number of bilayers.

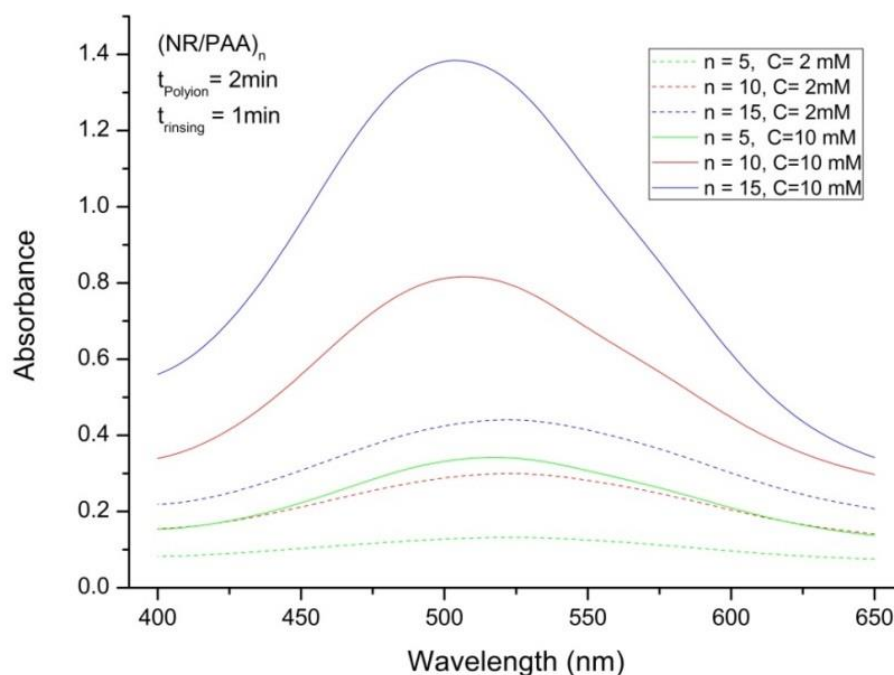


Fig 4-17 The effect of concentration of the solutions on the absorbance spectra for (NR/PAA)_n.

4.3.5 Drying and method of drying

The drying procedure affects the thickness, the absorbance and the peak wavelength of the films. Drying the polymer film on the coated surface before rinsing increased the stickiness of the molecules and consequently increased the absorbance. The thickest film with the highest absorbance while a decrease seen in the peak wavelength produced when the gas applied for drying as shown in Fig 4-21 and Table 4-4. Whereas the layers built up without drying had the lower absorbance in respect to dried samples. This result can be seen in Table 4-4 where it shows the absorbance for (NR/PAA)₆ at 2 mM solution concentration. Moreover, it was observed that drying after each step created a

thicker film than drying after rinsing at each step. The dried glass slide after each step shows different behaviours in both absorbance and wavelength. As can be seen in Fig 4-18 the highest absorbance took place in the case of drying after each step whereas the peak wavelength is the lowest for this sample. When the sample dries after each step, changing the absorbance as well as changing the peak wavelength took place faster than two other cases. It means that drying the glass slide after building up each layer causes the immobilization of extra molecules. While rinsing the sample immediately after coating causes washing out of many molecules from the surface of the coated layer and thereupon thinness of the layer. Fig 4-19 shows the coated glass slides at these three cases. The darker colour is seen in the glass slide that was dried after each stage of coating. In summary, the deposition in wet film creates the thinner film but more stable at dried film. Because washing the sample after each step without drying causes onto the strong bonded molecules to remain.

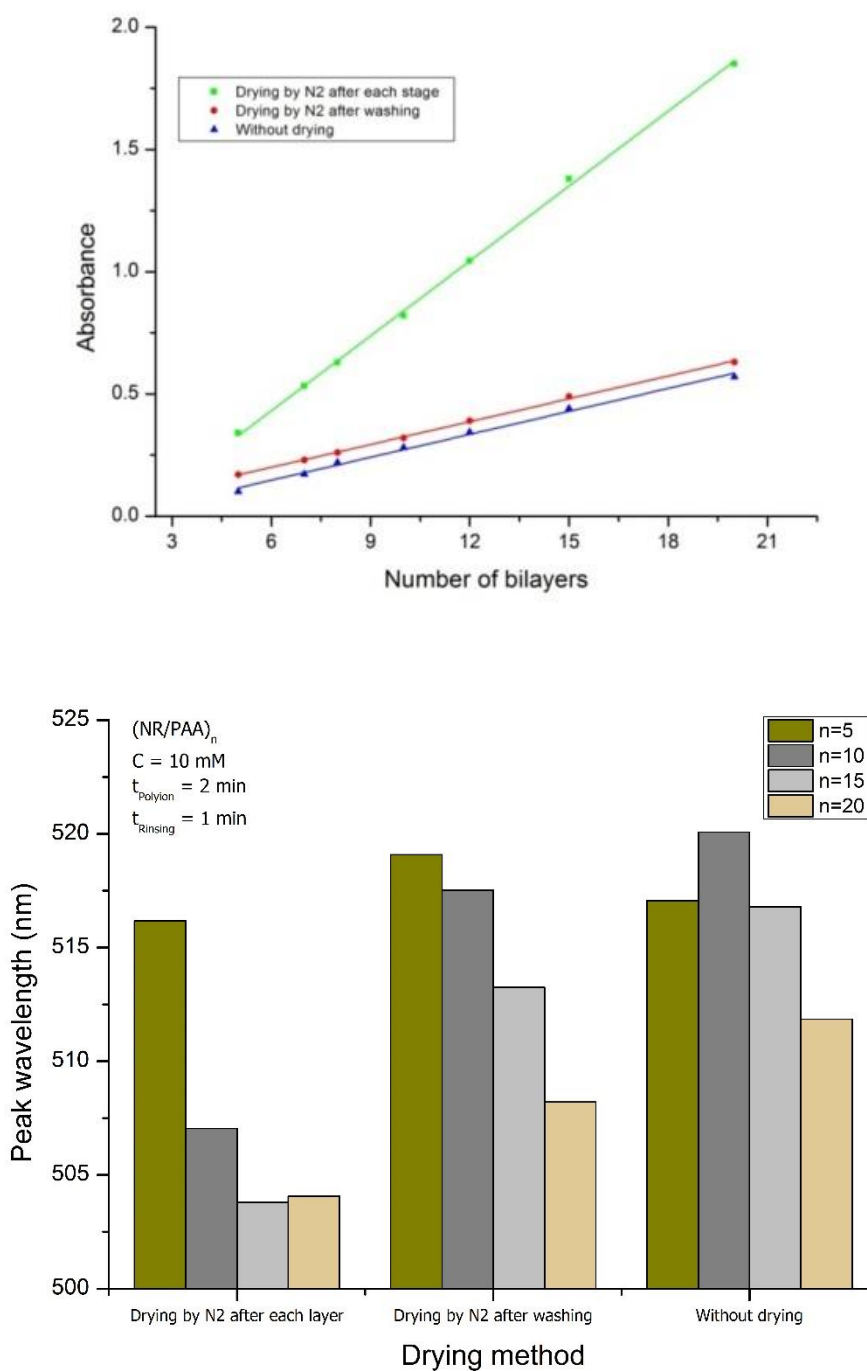


Fig 4-18 Comparison the maximum absorbance (up) and the peak wavelength changes (down) for the glass slides coated by (NR/PAA)_n at three different drying conditions by N₂ gas: without drying, drying after washing and drying after each stage.



Fig 4-19 Comparison the glass slides coated by (NR/PAA)₂₀ at three different drying conditions: without drying, drying after washing, drying after each stage.

Table 4-3 The effect of presence of NaCl in the polyelectrolyte solutions on the absorbance for (NR/PAA)₆.

Salt concentration	Absorbance
1 M	0.047
0.2 M	0.20
10 ⁻² M	0.35
10 ⁻³ M	0.15
0 M (without salt)	0.10

Table 4-4 The effect of drying method (gas and oven) on the absorbance and wavelength for (NR/PAA)₆.

Drying method	Absorbance	Wavelength (nm)
Drying by gas	0.68	513.0
Drying by oven	0.54	521.81
Without drying	0.22	522.08

4.3.6 Adding salt to the solution

The role of salt was studied in a series of experiments on (NR/PAA)_n and its effect on the absorbance is shown in Table 4-3. The presence of salt to 10⁻² M raises the absorbance, while it has inverse effect when its concentration becomes more than 10⁻² M. Fig 4-20 compares the appearance of the coated glass slides in two different salt concentrations; 0.2 M and 10⁻² M. The very low and very high concentration of salt in the polyions solution shows undesirable effect on the uniformity of the layers.



Fig 4-20 The effect of salt concentration on the appearance of the coated glass.



Fig 4-21 Different drying methods have different effect on the deposited glass slide.

4.4 Summary

This chapter investigated the principles of layer-by-layer deposition technique and its important parameters. There are many evidence reported in literatures

that confirm the effect of each of these factors on thin film characterization. While substrate should be functionalized for taking of coating, parameters such as dipping time, pH and concentration of the polyelectrolyte solutions, salt addition to the polyelectrolyte and drying of thin film also need to be controlled to control the process of formation of multilayer and to obtain a multilayered thin film with a specified thickness.

References

- [1] R. K. Iler, "The adhesion of submicron silica particles on glass," *Journal of Colloid and Interface Science*, vol. 38, pp. 496-501, 1972.
- [2] Y. Lvov, G. Decher, and H. Möhwald, "Assembly, Structural Characterization, and Thermal-Behavior of Layer-by-Layer Deposited Ultrathin Films of Poly(vinyl sulfate) and Poly(allylamine)," *Langmuir*, vol. 9, pp. 481- 486, 1993.
- [3] Y. Lvov, G. Decher, and G. Sukhorukov, "Assembly of thin-films by means of successive deposition of alternate layers of DNA and Poly(allylamine)," *Macromolecules*, vol. 26, pp. 5396-5399, 1993.
- [4] Y. Lvov, H. Haas, G. Decher, H. Moehwald , and A. Kalachev, "Assembly of polyelectrolyte molecular films onto plasma-treated glass," *J. Phys. Chem*, vol. 97, pp. 12835-12841, 1993.
- [5] G. Decher, Y. Lvov, and J. Schmitt, "Proof of multilayer structural organization in self-assembled polycation polyanion molecular films," *Thin Solid Films*, vol. 244, pp. 772-777, 1994.
- [6] Y. Lvov, H. Haas, G. Decher, H. Moehwald, A. Mikhailov, B. Mtchedlishvily, *et al.*, "Successive deposition of alternate layers of polyelectrolytes and a charged virus," *Langmuir*, vol. 10, pp. 4232-4236, 1994.
- [7] A. Nabok, *Organic and inorganic nanostructures*: Artech House, 2005.
- [8] P. Bertrand, A. Jonas, A. Laschewsky, and R. Legras, "Ultrathin polymer coatings by complexation of polyelectrolytes at interfaces: suitable materials, structure and properties," *Macromolecular Rapid Communications*, vol. 21, pp. 319-348, 2000.
- [9] G. Decher and J. B. Schlenoff, *Multilayer Thin Films*: Wiley-VCH Verlag GmbH & Co., 2002.
- [10] W. Chen and T. J. McCarthy, "Layer-by-Layer Deposition: A Tool for Polymer Surface Modification," *Macromolecules*, vol. 30, pp. 78-86, 1997/01/01 1997.
- [11] T. M. Cooper, A. L. Campbell, and R. L. Crane, "Formation of polypeptide-dye multilayers by electrostatic self-assembly technique," *Langmuir*, vol. 11, pp. 2713-2718, 1995/07/01 1995.
- [12] S. T. Dubas, P. Kumlangdudsana, and P. Potiyaraj, "Layer-by-layer deposition of antimicrobial silver nanoparticles on textile fibers," *Colloids and Surfaces A: Physicochemical and Engineering Aspects*, vol. 289, pp. 105-109, 2006.
- [13] A. Armin, M. Soltanolkotabi, and P. Feizollah, "On the pH and concentration response of an evanescent field absorption sensor using a

- coiled-shape plastic optical fiber," *Sensors and Actuators a-Physical*, vol. 165, pp. 181-184, Feb 2011.
- [14] A. B. Artyukhin, O. Bakajin, P. Stroeve, and A. Noy, "Layer-by-layer electrostatic self-assembly of polyelectrolyte nanoshells on individual carbon nanotube templates," *Langmuir*, vol. 20, pp. 1442-1448, Feb 17 2004.
- [15] Y.-I. Su and C. Li, "Stable multilayer thin films composed of gold nanoparticles and lysozyme," *Applied Surface Science*, vol. 254, pp. 2003-2008, 2008.
- [16] Y. J. Liu, Y. X. Wang, and R. O. Claus, "Layer-by-layer ionic self-assembly of Au colloids into multilayer thin-films with bulk metal conductivity," *Chemical Physics Letters*, vol. 298, pp. 315-319, Dec 18 1998.
- [17] C. H. Lu, F. Wei, N. Z. Wu, L. Huang, X. S. Zhao, X. M. Jiao, *et al.*, "Au nanoparticle micropatterns prepared from self-assembled films," *Langmuir*, vol. 20, pp. 974-977, Feb 3 2004.
- [18] A. P. GirardEgrot, R. M. Morelis, and P. R. Coulet, "Direct influence of the interaction between the first layer and a hydrophilic substrate on the transition from Y- to Z-type transfer during deposition of phospholipid Langmuir-Blodgett films," *Langmuir*, vol. 12, pp. 778-783, Feb 7 1996.
- [19] M. Sano, Y. Lvov, and T. Kunitake, "Formation of ultrathin polymer layers on solid substrates by means of polymerization-induced epitaxy and alternate adsorption," *Annual Review of Materials Science*, vol. 26, pp. 153-187, 1996 1996.
- [20] J. B. Schlenoff, H. Ly, and M. Li, "Charge and Mass Balance in Polyelectrolyte Multilayers," *Journal of the American Chemical Society*, vol. 120, pp. 7626-7634, 1998/08/01 1998.
- [21] M. Ferreira, J. H. Cheung, and M. F. Rubner, "Molecular self-assembly of conjugated polyions: a new process for fabricating multilayer thin film heterostructures," *Thin Solid Films*, vol. 244, pp. 806-809, 1994.
- [22] J. B. Schlenoff, "Charge Balance and Transport in Polyelectrolyte Multilayers," in *Multilayer Thin Films*, J. B. S. Gero Decher, Ed., ed: Wiley-VCH Verlag GmbH & Co., 2002 pp. 99-130.
- [23] A. D. Jenkins, P. Kratochvfl, R. F. T. Stepto, and U. W. Suter, "Glossary of basic terms in polymer science (IUPAC Recommendations 1996)," *Pure & Applied Chemistry*, vol. 68, pp. 2287-2311, 1996.
- [24] G. Decher, J. D. Hong, and J. Schmitt, "Buildup of ultrathin multilayer films by a self-assembly process: III. Consecutively alternating adsorption of anionic and cationic polyelectrolytes on charged surfaces," *Thin Solid Films*, vol. 210/21 I, pp. 831-835, 1992.

- [25] S. Yang, Y. Zhang, Y. Guan, S. Tan, J. Xu, S. Cheng, *et al.*, "Water uptake behavior of hydrogen-bonded PVPON–PAA LBL film," *Soft Materials*, vol. 2, pp. 699-704, 2006.
- [26] D. Saeki, M. Imanishi, Y. Ohmukai, T. Maruyama, and H. Matsuyama, "Stabilization of layer-by-layer assembled nanofiltration membranes by crosslinking via amide bond formation and siloxane bond formation," *Journal of Membrane Science*, vol. 447, pp. 128-133, 2013.
- [27] L. Wang, Y. Fu, Z. Wang, Y. Fan, and X. Zhang, "Investigation into an Alternating Multilayer Film of Poly(4-Vinylpyridine) and Poly(acrylic acid) Based on Hydrogen Bonding," *Langmuir*, vol. 15, pp. 1360-1363, 1999/02/01 1999.
- [28] E. C. Hao and T. Q. Lian, "Buildup of polymer/Au nanoparticle multilayer thin films based on hydrogen bonding," *Chemistry of Materials*, vol. 12, pp. 3392-3396, Nov 2000.
- [29] J. A. Lichter, "Assembly and Post-Assembly Manipulation of Polyelectrolyte Multilayers for Control of Bacterial Attachment and Viability " PhD, Materials Science and Engineering, Massachusetts Institute of Technology, 2009.
- [30] M. Elzbiéciak, M. Kolasińska, S. Zapotoczny, R. Krastev, M. Nowakowska, and P. Warszyński, "Nonlinear growth of multilayer films formed from weak polyelectrolytes," *Colloids and Surfaces A: Physicochemical and Engineering Aspects*, vol. 343, pp. 89-95, 2009.
- [31] A. L. Becker, A. P. R. Johnston, and F. Caruso, "Peptide Nucleic Acid Films and Capsules: Assembly and Enzymatic Degradation," *Macromolecular Bioscience*, vol. 10, pp. 488-495, May 14 2010.
- [32] A. P. R. Johnston, E. S. Read, and F. Caruso, "DNA multilayer films on planar and colloidal supports: Sequential assembly of like-charged polyelectrolytes," *Nano Letters*, vol. 5, pp. 953-956, May 2005.
- [33] G. Decher, B. Lehr, K. Lowack, Y. Lvov, and J. Schmitt, "New nanocomposite Films For Biosensors- Layer-by-layer Adsorbed Films of Polyelectrolytes, Proteins or DNA " *Biosensors & Bioelectronics*, vol. 9, pp. 677-684, 1994 1994.
- [34] E. M. Saurer, R. M. Flessner, S. P. Sullivan, M. R. Prausnitz, and D. M. Lynn, "Layer-by-Layer Assembly of DNA- and Protein-Containing Films on Microneedles for Drug Delivery to the Skin," *Biomacromolecules*, vol. 11, pp. 3136-3143, 2010/11/08 2010.
- [35] F. J. Arregui, I. R. Matias, K. L. Cooper, and R. O. Claus, "Fabrication of microgratings on the ends of standard optical fibers by the electrostatic self-assembly monolayer process," *Optics Letters*, vol. 26, pp. 131-133, 2001
- [36] H. Jin, N. Won, B. Ahn, J. Kwag, K. Heo, J.-W. Oh, *et al.*, "Quantum dot-engineered M13 virus layer-by-layer composite films for highly

- selective and sensitive turn-on TNT sensors," *Chemical Communications*, vol. 49, pp. 6045-6047, 2013.
- [37] J. u. M. Corres, A. Sanz, F. J. Arregui, I. R. Mat'ias, and J. i. Roca, "Fiber optic glucose sensor based on bionanofilms," *Sensors and Actuators B* vol. 131, pp. 633-639, 2008.
- [38] I. D. Villar, I. R. Matias, F. J. Arregui, and J. M. Corres, "Fiber optic glucose biosensor," *Optical Engineering*, vol. 45, pp. 104401-1-104401-6, 2006.
- [39] H. Jin, S. Choi, H. J. Lee, and S. Kim, "Layer-by-Layer Assemblies of Semiconductor Quantum Dots for Nanostructured Photovoltaic Devices," *The Journal of Physical Chemistry Letters*, vol. 4, pp. 2461-2470, 2013/08/01 2013.
- [40] S. Rauf, A. Glidle, and J. M. Cooper, "Layer-by-Layer Quantum Dot Constructs Using Self-Assembly Methods," *Langmuir*, vol. 26, pp. 16934-16940, 2010/11/16 2010.
- [41] H. Jin, J. Nam, J. Park, S. Jung, K. Im, J. Hur, *et al.*, "Strong polyelectrolyte quantum dot surface for stable bioconjugation and layer-by-layer assembly applications," *Chemical Communications*, vol. 47, pp. 1758-1760, 2011.
- [42] D. Viegas, J. Goicoechea, J. M. Corres, J. L. Santos, L. A. Ferreira, F. M. Ara'ujo, *et al.*, "A fibre optic humidity sensor based on a long-period fibre grating coated with a thin film of SiO₂ nanospheres," *Measurements Science And Technology*, vol. 20, pp. 1-4, 2009.
- [43] S. Kodaira, S. Korposh, S.-W. Lee, W. J. Batty, S. W. James, and R. P. Tatam, "Fabrication of highly efficient fibre-optic gas sensors using SiO₂/polymer nanoporous thin films," in *3rd International Conference on Sensing Technology*, Tainan, Taiwan, 2008.
- [44] N. A. Kotov, S. Magonov, and E. Tropsha, "Layer-by-Layer Self-Assembly of Alumosilicate–Polyelectrolyte Composites: Mechanism of Deposition, Crack Resistance, and Perspectives for Novel Membrane Materials," *Chemistry of Materials*, vol. 10, pp. 886-895, 1998/03/01 1998.
- [45] D. Lee and T. Cui, "A role of silica nanoparticles in layer-by-layer self-assembled carbon nanotube and In₂O₃ nanoparticle thin-film pH sensors: Tunable sensitivity and linearity," *Sensors and Actuators A: Physical*, vol. 188, pp. 203-211, 2012.
- [46] Y. Liu, A. G. Erdman, and T. Cui, "Acetylcholine biosensors based on layer-by-layer self-assembled polymer/nanoparticle ion-sensitive field-effect transistors," *Sensors and Actuators a-Physical*, vol. 136, pp. 540-545, May 16 2007.

- [47] P. S. Grant and M. J. McShane, "Development of multilayer fluorescent thin film chemical sensors using electrostatic self-assembly," *IEEE Sensors Journal*, vol. 3, pp. 139-146, 2003.
- [48] I. D. Villar, I. R. Matias, and F. J. Arregui, "Enhancement of sensitivity in long-period fiber gratings with deposition of low-refractive-index materials," *Optics Letters*, vol. 30, pp. 2363-2365, 2005.
- [49] Y. Egawa, R. Hayashida, and J.-i. Anzai, "Covalently cross-linked multilayer thin films composed of diazoresin and brilliant yellow for an optical pH sensor " *Polymer*, vol. 48, pp. 1455-1458 2007.
- [50] D. Galbarra, F. J. Arregui, I. R. Matias, and R. O. Claus, "Ammonia optical fiber sensor based on self-assembled zirconia thin films," *Smart Materials and Structures*, vol. 14, pp. 739-745, 2005.
- [51] Y. Liu, A. Rosidian, K. Lenahan, Y.-X. Wang, T. Zeng, and R. O. Claus, "Characterization of electrostatically self-assembled nanocomposite thin films," *Smart Materials & Structures*, vol. 8, pp. 100-105, 1999.
- [52] S. T. Dubas and J. B. Schlenoff, "Factors Controlling the Growth of Polyelectrolyte Multilayers," *Macromolecules*, vol. 32, pp. 8153-8160, 1999/11/01 1999.
- [53] D. L. Feldheim, K. C. Grabar, M. J. Natan, and T. E. Mallouk, "Electron transfer in self-assembled inorganic polyelectrolyte/metal nanoparticle heterostructures," *Journal of the American Chemical Society*, vol. 118, pp. 7640-7641, Aug 14 1996.
- [54] D. Yoo, S. S. Shiratori, and M. F. Rubner, "Controlling bilayer composition and surface wettability of sequentially adsorbed multilayers of weak polyelectrolytes," *Macromolecules*, vol. 31, pp. 4309-4318, 1998.
- [55] S. S. Shiratori and M. F. Rubner, "pH-Dependent thickness behavior of sequentially adsorbed layers of weak polyelectrolytes," *Macromolecules*, vol. 33, pp. 4213-4219, 2000.
- [56] H. G. M. Vandesteeg, M. A. C. Stuart, A. Dekeizer, and B. H. Bijsterbosch, "Polyelectrolyte adsorption: A suitable balance of forces " *Langmuir*, vol. 8, pp. 2538-2546, Oct 1992.
- [57] M. A. C. Stuart and H. Tamai, "Dynamics of adsorbed polymers. 2. Thickness relaxation of poly (ethylene oxide) on glass as a function of segmental binding energy," *Langmuir*, vol. 4, pp. 1184-1188, Sep-Oct 1988.
- [58] R. Montazami, "Fabrication and Characterization of Layer by Layer Assembled Single and Dual-Electrochrome lectrochromic Devices," MSc, Materials Science and Engineering, Virginia Polytechnic Institute and State University, Blacksburg Virginia, 2009.

- [59] Y. Lvov and G. Decher, "Assembly of multilayer ordered films by alternating adsorption of oppositely charged macromolecules," *Crystallography Reports*, vol. 39, pp. 696-616, 1994.
- [60] G. Decher, Y. Lvov, and J. Schmitt, "Proof of multilayer structural organization in self-assembled polycation-polyanion molecular films," *Thin Solid Films*, vol. 244, pp. 772-777, 1994.
- [61] N. G. Hoogeveen, M. A. Cohen Stuart, G. J. Fleer, and M. R. Böhmer, "Formation and Stability of Multilayers of Polyelectrolytes," *Langmuir*, vol. 12, pp. 3675-3681, 1996/01/01 1996.
- [62] M. J. McShane and Y. M. Lvov, "Layer-by-Layer electrostatic self-assembly," in *Dekker Encyclopedia of Nanoscience and Nanotechnology*, ed: Marcel Dekker, 2004.
- [63] M. M. de Villiers, D. P. Otto, S. J. Strydom, and Y. M. Lvov, "Introduction to nanocoatings produced by layer-by-layer (LbL) self-assembly," *Advanced Drug Delivery Reviews*, vol. 63, pp. 701-715, Aug 14 2011.
- [64] J. Goicoechea, F. J. Arregui, J. Corres, and I. R. Matias, "Study and Optimization of Self-Assembled Polymeric Multilayer Structures with Neutral Red for pH Sensing Applications," *Journal of Sensors*, vol. 2008, pp. 1-7, 2008.
- [65] J. Goicoechea, C. R. Zamarréno, I. R. Matías, and F. J. Arregui, "Optical fiber pH sensors based on layer-by-layer electrostatic self-assembled Neutral Red," *Sensors and Actuators B: Chemical* vol. 132, pp. 305-311, 2008.
- [66] A. Chandran, "Self-Assembled Multilayered Dielectric Spectral Filters," Master of Science, Electrical Engineering, Virginia Polytechnic Institute and State University, Blacksburg, Virginia, 2001.
- [67] Y. Egawa, R. Hayashida, and J.-i. Anzai, "Multilayered assemblies composed of brilliant yellow and poly(allylamine) for an optical pH sensor," *Analytical Sciences*, vol. 22, pp. 1117-1119, 2006.
- [68] A. Delcorte, P. Bertrand, E. Wischerhoff, and A. Laschewsky, "Adsorption of polyelectrolyte multilayers on polymer surfaces," *Langmuir*, vol. 13, pp. 5125-5136, Sep 17 1997.
- [69] K. Itano, J. Choi, and M. F. Rubner, "Mechanism of the pH-induced discontinuous swelling/deswelling transitions of poly(allylamine hydrochloride)-containing polyelectrolyte multilayer films," *Macromolecules*, vol. 38, pp. 3450-3461, 2005.
- [70] B. Schoeler, E. Poptoshev, and F. Caruso, "Growth of Multilayer Films of Fixed and Variable Charge Density Polyelectrolytes: Effect of Mutual Charge and Secondary Interactions," *Macromolecules*, vol. 36, pp. 5258-5264, 2003/07/01 2003.

- [71] U. Voigt, V. Khrenov, K. Tauer, M. Hahn, W. Jaeger, and R. v. Klitzing, "The effect of polymer charge density and charge distribution on the formation of multilayers " *Journal of Physics: Condens. Matter*, vol. 15, pp. S213-S218, 2003.
- [72] B.-S. Kim and O. I. Vinogradova, "pH-Controlled swelling of polyelectrolyte multilayer microcapsules," *Journal of Physical Chemistry B*, vol. 108, pp. 8161-8165, 2004.
- [73] D. Lee, A. J. Nolte, A. L. Kunz, M. F. Rubner, and R. E. Cohen, "pH-Induced hysteretic gating of track-etched polycarbonate membranes: swelling/deswelling behavior of polyelectrolyte multilayers in confined geometry," *Journal of the American Chemical Society.* , vol. 128, pp. 8521-8529, 2006.
- [74] N. Kato, P. Schuetz, A. Fery, and F. Caruso, "Thin multilayer films of weak polyelectrolytes on colloid particles," *Macromolecules*, vol. 35, pp. 9780-9787, Dec 17 2002.
- [75] Y. Liu and T. Cui, "Ion-sensitive field-effect transistor based pH sensors using nano self-assembled polyelectrolyte/nanoparticle multilayer films," *Sensors and Actuators B* vol. 123, pp. 148-152, 2007.
- [76] T. Sennerfors, D. Solberg, and F. Tiberg, "Adsorption of Polyelectrolyte–Nanoparticle Systems on Silica: Influence of Ionic Strength," *Journal of Colloid and Interface Science*, vol. 254, pp. 222-226, 10/15/ 2002.
- [77] L. Krasemann and B. Tieke, "Selective ion transport across self-assembled alternating multilayers of cationic and anionic polyelectrolytes," *Langmuir*, vol. 16, pp. 287-290, Jan 25 2000.
- [78] S. T. Dubas and J. B. Schlenoff, "Polyelectrolyte multilayers containing a weak polyacid – construction and deconstruction," *Macromolecules*, vol. 34, pp. 3736–3740, 2001.
- [79] C. C. Buron and C. Filiâtre, "Overshoots of adsorption kinetics during layer-by-layer polyelectrolyte film growth: Role of counterions," *Journal of Colloid and Interface Science*, vol. 413, pp. 147-153, 1/1/ 2014.
- [80] F. Boulmedais, C. S. Tang, B. Keller, and J. Vörös, "Controlled Electrodeposition of Polyelectrolyte Multilayers: A Platform Technology Towards the Surface-Initiated Delivery of Drugs," *Advanced Functional Materials*, vol. 16, pp. 63-70, 2006.
- [81] R. A. Ghostine, R. M. Jisr, A. Lehaf, and J. B. Schlenoff, "Roughness and Salt Annealing in a Polyelectrolyte Multilayer," *Langmuir*, vol. 29, pp. 11742-11750, 2013/09/17 2013.
- [82] N. G. Hoogeveen, M. A. C. Stuart, and G. J. Fleer, "Polyelectrolyte adsorption on oxides .2. Reversibility and exchange," *Journal of Colloid and Interface Science*, vol. 182, pp. 146-157, Sep 1 1996.

- [83] P. R. Van Tassel, "Polyelectrolyte adsorption and layer-by-layer assembly: Electrochemical control," *Current Opinion in Colloid & Interface Science*, vol. 17, pp. 106-113, 4// 2012.
- [84] M. R. Linford, M. Auch, and H. Mohwald, "Nonmonotonic effect of ionic strength on surface dye extraction during dye-polyelectrolyte multilayer formation," *Journal of the American Chemical Society*, vol. 120, pp. 178-182, Jan 14 1998.
- [85] N. G. Hoogeveen, M. A. C. Stuart, and G. J. Fleer, "Polyelectrolyte adsorption on oxides .1. Kinetics and adsorbed amounts," *Journal of Colloid and Interface Science*, vol. 182, pp. 133-145, Sep 1 1996.
- [86] X. Gong and C. Gao, "Influence of salt on assembly and compression of PDADMAC/PSSMA polyelectrolyte multilayers," *Physical Chemistry Chemical Physics*, vol. 11, pp. 11577–11586, 2009.
- [87] J. J. Harris, J. L. Stair, and M. L. Bruening, "Layered Polyelectrolyte Films as Selective, Ultrathin Barriers for Anion Transport," *Chemistry of Materials*, vol. 12, pp. 1941-1946, 2000/07/01 2000.
- [88] B. W. Stanton, J. J. Harris, M. D. Miller, and M. L. Bruening, "Ultrathin, Multilayered Polyelectrolyte Films as Nanofiltration Membranes," *Langmuir*, vol. 19, pp. 7038-7042, 2003/08/01 2003.
- [89] A. V. Dobrynin, M. Rubinstein, and S. P. Obukhov, "Cascade of Transitions of Polyelectrolytes in Poor Solvents," *Macromolecules*, vol. 29, pp. 2974-2979, 1996/01/01 1996.
- [90] P. Linse, "Adsorption of Weakly Charged Polyelectrolytes at Oppositely Charged Surfaces," *Macromolecules*, vol. 29, pp. 326-336, 1996/01/01 1996.
- [91] R. A. McAloney, M. Sinyor, V. Dudnik, and M. C. Goh, "Atomic Force Microscopy Studies of Salt Effects on Polyelectrolyte Multilayer Film Morphology," *Langmuir*, vol. 17, pp. 6655-6663, 2001/10/01 2001.
- [92] G. Decher, "Fuzzy Nanoassemblies: Toward layered polymeric multicomposites," *Science*, vol. 277, pp. 1232-1237, 1997.
- [93] E. R. Kleinfeld and G. S. Ferguson, "Healing of Defects in the Stepwise Formation of Polymer/Silicate Multilayer Films," *Chemistry of Materials*, vol. 8, pp. 1575-1578, 1996/01/01 1996.
- [94] M. Lütt, M. R. Fitzsimmons, and D. Li, "X-ray Reflectivity Study of Self-Assembled Thin Films of Macrocycles and Macromolecules," *The Journal of Physical Chemistry B*, vol. 102, pp. 400-405, 1998/01/01 1998.
- [95] M. Lösche, J. Schmitt, G. Decher, W. G. Bouwman, and K. Kjaer, "Detailed Structure of Molecularly Thin Polyelectrolyte Multilayer Films on Solid Substrates as Revealed by Neutron Reflectometry," *Macromolecules*, vol. 31, pp. 8893-8906, 1998/12/01 1998.

- [96] A. S. Abd-El-Aziz, C. E. Carraher, C. U. Pittman, J. E. Sheats, and M. Zeldin, *Macromolecules Containing Metal and Metal-Like Elements, Organoiron Polymers*: Wiley, 2003.
- [97] E. S. Dragan, *New Trends in Ionic (Co)Polymers and Hybrids*: Nova Science Publishers, 2007.
- [98] C. Yong-Yong, S. Zhong, Z. Shi-Ming, R. Wen-Bin, and D. Jun, "Tunable interface anisotropy in a Pt/Co_{1-x}Fe_x/Pt multilayer," *Chin. Phys. B* vol. 22, pp. 067504-1- 067504-4, 2013.
- [99] T. J. Halthur, P. M. Claesson, and U. M. Elofsson, "Stability of polypeptide multilayers as studied by in situ ellipsometry: Effects of drying and post-buildup changes in temperature and pH," *Journal of the American Chemical Society*, vol. 126, pp. 17009-17015, Dec 29 2004.
- [100] J. M. C. Lourenço, P. A. Ribeiro, A. M. Botelho do Rego, and M. Raposo, "Counterions in layer-by-layer films—Influence of the drying process," *Journal of Colloid and Interface Science*, vol. 313, pp. 26-33, 2007.
- [101] J. Chen, G. Luo, and W. Cao, "The Study of Layer-by-Layer Ultrathin Films by the Dynamic Contact Angle Method," *Journal of Colloid and Interface Science*, vol. 238, pp. 62-69, 6/1/ 2001.
- [102] Y. Lvov, K. Ariga, M. Onda, I. Ichinose, and T. Kunitake, "A careful examination of the adsorption step in the alternate layer-by-layer assembly of linear polyanion and polycation," *Colloids and Surfaces A: Physicochemical and Engineering Aspects*, vol. 146, pp. 337-346, 1/15/ 1999.
- [103] L. Wang, L. Wang, and Z. Su, "Surface defects in polyelectrolyte multilayers: Effects of drying and deposition cycle," *Soft Matter*, vol. 7, pp. 4851-4855, 2011 2011.
- [104] X. Gong, J. Yang, L. Han, and C. Gao, "Influence of drying time of polyelectrolyte multilayers on the compression-induced pattern formation," *Langmuir*, vol. 24, pp. 13925-33, Dec 16 2008.
- [105] N. C. De Souza, J. R. Silva, M. A. Pereira-Da-Silva, M. Raposo, R. M. Faria, J. A. Giacometti, *et al.*, "Dynamic Scale Theory for Characterizing Surface Morphology of Layer-by-Layer Films of Poly(o-methoxyaniline)," *Journal of Nanoscience and Nanotechnology*, vol. 4, pp. 548-552, // 2004.
- [106] J. F. Quinn and F. Caruso, "Thermoresponsive Nanoassemblies: Layer-by-Layer Assembly of Hydrophilic–Hydrophobic Alternating Copolymers," *Macromolecules*, vol. 38, pp. 3414-3419, 2005/04/01 2005.
- [107] D. S. Patel, R. K. Aithal, G. Krishna, Y. M. Lvov, M. Tien, and D. Kuila, "Nano-assembly of manganese peroxidase and lignin peroxidase from P.

- chrysosporium for biocatalysis in aqueous and non-aqueous media," *Colloids and Surfaces B: Biointerfaces*, vol. 43, pp. 13-19, 6/10/ 2005.
- [108] M. Muthukumar, "Theory of counter-ion condensation on flexible polyelectrolytes: Adsorption mechanism," *The Journal of Chemical Physics*, vol. 120, pp. 9343-9350, 2004.
- [109] A. J. Nolte, N. Takane, E. Hindman, W. Gaynor, M. F. Rubner, and R. E. Cohen, "Thin film thickness gradients and spatial patterning via salt etching of polyelectrolyte multilayers," *Macromolecules*, vol. 40, pp. 5479-5486, Jul 24 2007.
- [110] Y. Shimazaki, R. Nakamura, S. Ito, and M. Yamamoto, "Molecular Weight Dependence of Alternate Adsorption through Charge-Transfer Interaction," *Langmuir*, vol. 17, pp. 953-956, 2001.
- [111] Z. Tang, Y. Wang, and N. A. Kotov, "Semiconductor Nanoparticles on Solid Substrates: Film Structure, Intermolecular Interactions, and Polyelectrolyte Effects," *Langmuir*, vol. 18, pp. 7035-7040, 2002.
- [112] J. Dai, A. W. Jensen, D. K. Mohanty, J. Erndt, and M. L. Bruening, "Controlling the Permeability of Multilayered Polyelectrolyte Films through Derivatization, Cross-Linking, and Hydrolysis," *Langmuir*, vol. 17, pp. 931-937, 2001/02/01 2001.
- [113] S. Y. Yang and M. F. Rubner, "Micropatterning of polymer thin films with pH-sensitive and cross-linkable hydrogen-bonded polyelectrolyte multilayers," *Journal of the American Chemical Society*, vol. 124, pp. 2100-2101, Mar 13 2002.
- [114] S. Y. Yang, D. Lee, R. E. Cohen, and M. F. Rubner, "Bioinert solution-cross-linked hydrogen-bonded multilayers on colloidal particles," *Langmuir*, vol. 20, pp. 5978-5981, Jul 6 2004.
- [115] G. Decher, J. D. Hong, and J. Schmitt, "Buildup of ultra thin multi layer films by a self assembly process: II. Consecutively alternating adsorption of anionic and cationic poly electrolytes on charged surfaces," *Thin Solid Films*, vol. 831, pp. 210-211, 1992.

5. pH Indicator Selection

5.1 Introduction

Indicators are chemical dyes that undergo colour changes on interaction with chemical species. The purpose of using so-called indicator chemistry in optical sensing is to convert the concentration of a chemical analyte into a measurable optical signal. In other words, the indicator acts as a transducer for a chemical species that frequently cannot be determined directly by optical means. This has an important implication in that it is the concentration of the indicator species that is measured rather than that of the analyte itself.

As a matter of fact, many indicators cannot be used in fibre optic chemical sensors because of unfavourable analytical wavelengths, poor photo-stability and low molar absorbance. The optical sensor systems are preferably operated between 450-800 nm [1]. Optical pH sensors measure over a limited range of pH and no single indicator is available that allow measurements to be performed over the pH 0 to 14 range unless using combination of different indicators with different values of pK_a which is an important parameter for characterization of a pH indicator. Moreover, the most important pH range is the near neutral (physiological) range. However, few indicators only meet the requirements for

use in pH sensors for neutral range for which the desirable properties are: an appropriate pK_a (7-8), absorption at or above 450 nm to allow the use of inexpensive waveguide optics and light sources, high molar absorbance, photostability and chemical stability and ease of immobilization [1].

Applied pH indicators in optical sensors are mostly weak acids (less often, weak bases) whose colour is different in the dissociated and the associated (protonated) form, respectively. Hence, a pH optical sensor is based on the pH-dependent changes of the optical properties of an indicator-dyed layer attached to the tip or surface of an optical light guide through which these changes are detected. Numerous optical sensors for pH have been reported [2-9]. They differ mainly in the kind of chemical transducer and the optical sensing scheme employed. Most of the work to date has been on sensors based on absorbance, reflectivity, fluorescence and optical power [10-16]. However, there is no wavelength-based pH sensor available to date. Sensors based on peak wavelength shift are more reliable as these sensors are independent of the light source. When the pH-dependent change in colour is significantly great, the shift in peak wavelength between two successive pH is significant and the indicator that provides this wavelength shift can be a good choice for fabrication of a wavelength-dependent pH sensor which is the novelty of this research work. In case of using LbL deposition technique, to date a limited number of pH indicators such as neutral red, methylene blue, brilliant yellow and prussian blue have been deposited onto the optical fibre to create pH sensors [3, 7, 17-20]. In this work in order to identify the suitable pH indicator which shows better

performance based on wavelength change with narrow intervals based on colourimetric measurements, some indicators have been examined and compared with others. The common properties of pH indicators that are suitable for deposition using LbL technique are:

- Charged molecules
- Easily water soluble
- The high variation colour in the presence of acidic to alkali solutions
- The pH range is between 3 and 10 (The multilayers film may be destructed in high or low pHs)

5.2 Materials and method

5.2.1 Materials

Based on the characteristics mentioned above some indicators were selected for which the properties are listed below. Few drops of the dilute solutions of these selected indicators were added to the pH buffer solution and their absorbance spectra versus pH were recorded.

Neutral Red (NR):

- Molecular Weight: 288.78 g/mol
- pH Range: 6.8–8.0
- Colour Change at pH: Red (6.8) to yellow (8.0)
- pK_a: 7.4
- Solubility: Soluble in water
- UV-Visible (λ_{max}): 522 nm
- Charge: Positive charge

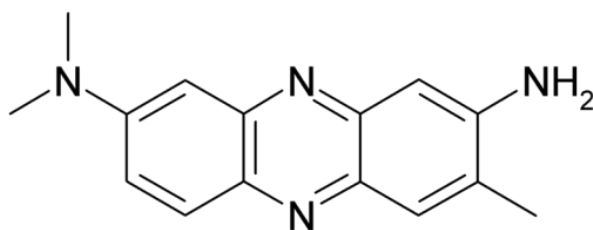


Fig 5-1 Neutral red's chemical structure.

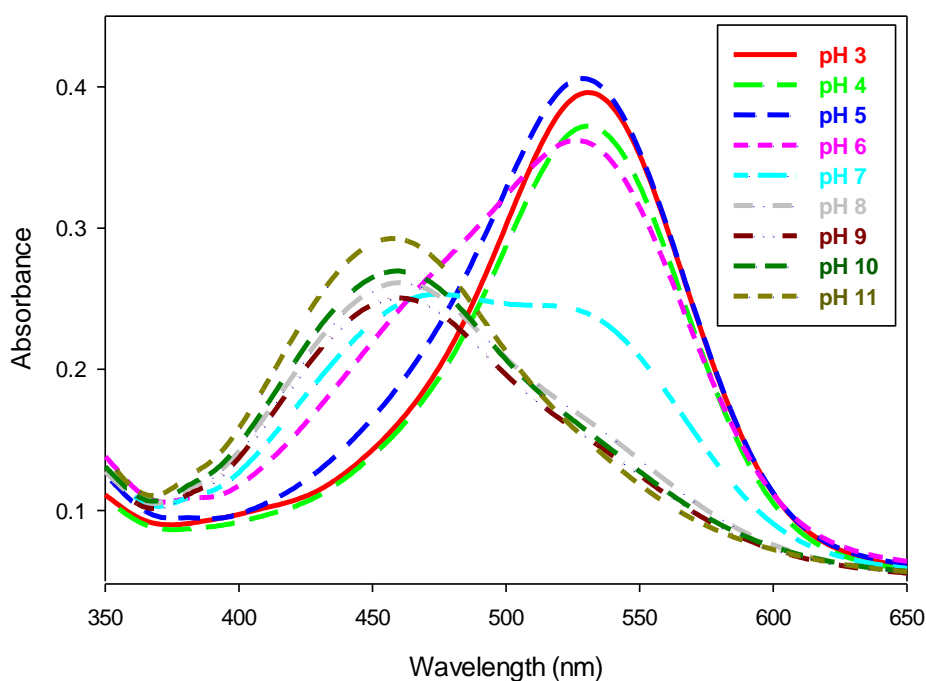


Fig 5-2 Absorbance spectra for NR at different pH buffer solutions

Brilliant Yellow (BY):

- Molecular Weight: 624.56 g/mol
- pH Range: 6.6–8.0
- Colour Change at pH: Yellow (6.6) to red-orange (8.0)
- pK_a : 7.2
- Solubility: Soluble in water
- UV-Visible (λ_{max}): 497 nm
- Charge: Negative charge

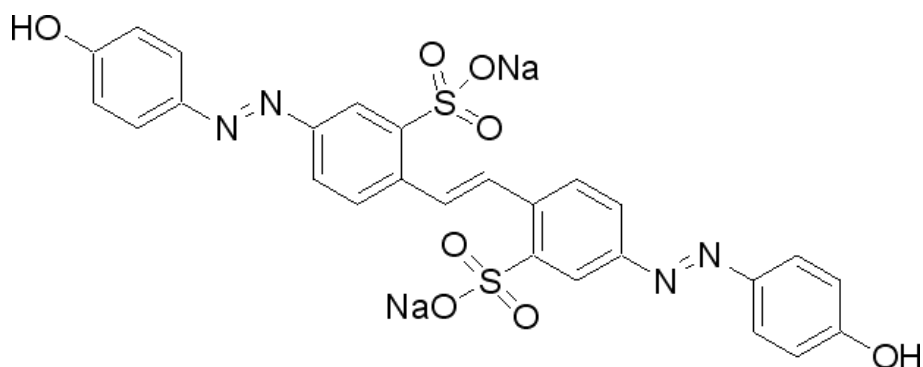


Fig 5-3 Chemical structure of brilliant yellow.

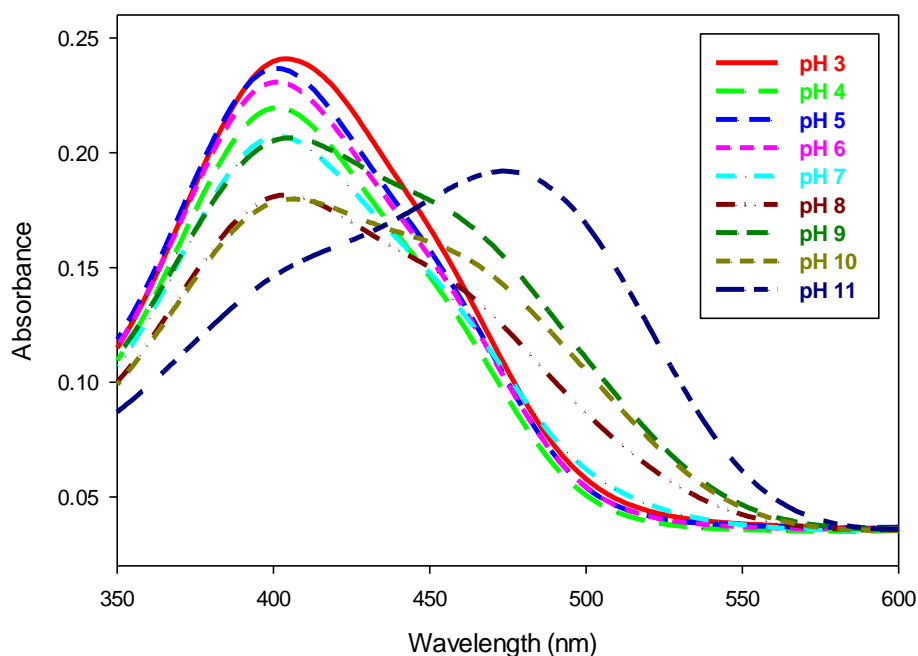


Fig 5-4 Absorbance spectra for brilliant yellow in different pH buffer solutions.

Alizarin Red S (ARS)

- Molecular Weight: 342.26 g/mol
- pH Range: 3.5–6.5; 9.4–12.0
- Colour Change at pH: Yellow (3.5) to red (6.5)
Orange (9.4) to violet (12.0)
- pK_a: 4.5, 11
- Solubility: Freely soluble in water
- UV-Visible (λ_{max}): 596 nm, 556 nm, 546 nm, 423 nm
- Charge: Negative charge

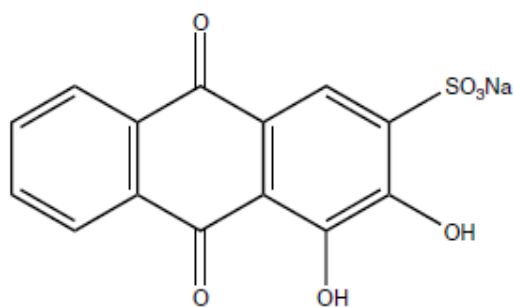


Fig 5-5 Chemical structure of alizarin red S.

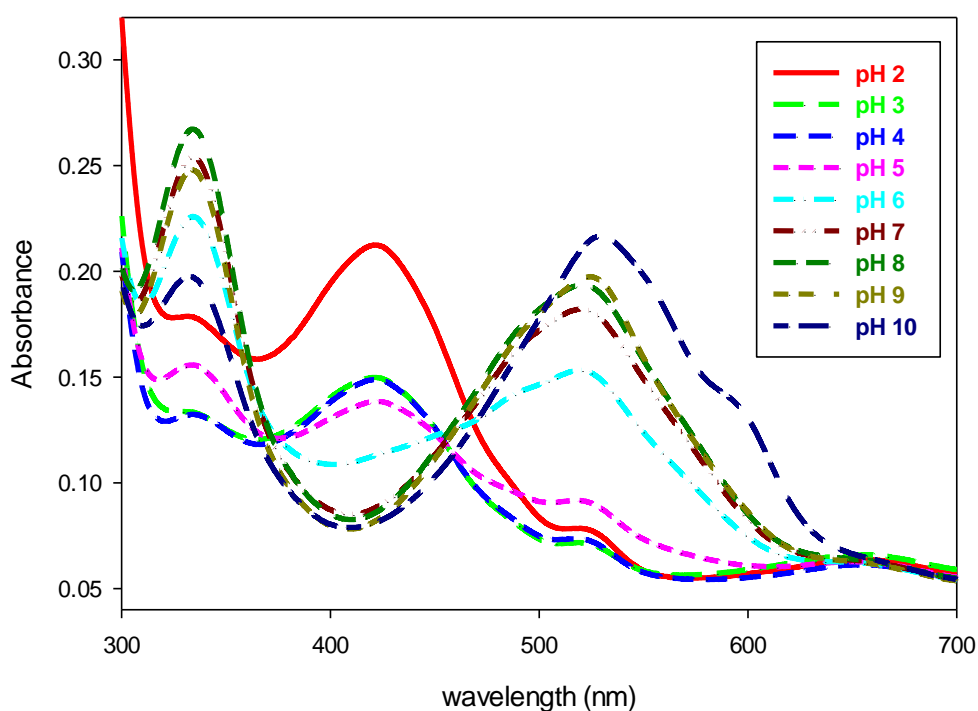


Fig 5-6 Absorbance spectra for ARS in different pH buffer solutions.

Litmus

- Molecular Weight: unknown
- pH Range: 4.5 - 8.3
- Colour Change at pH: Red (4.5) to blue (8.3)
- pK_a: 7
- Solubility: soluble in water
- Charge: Negative charge

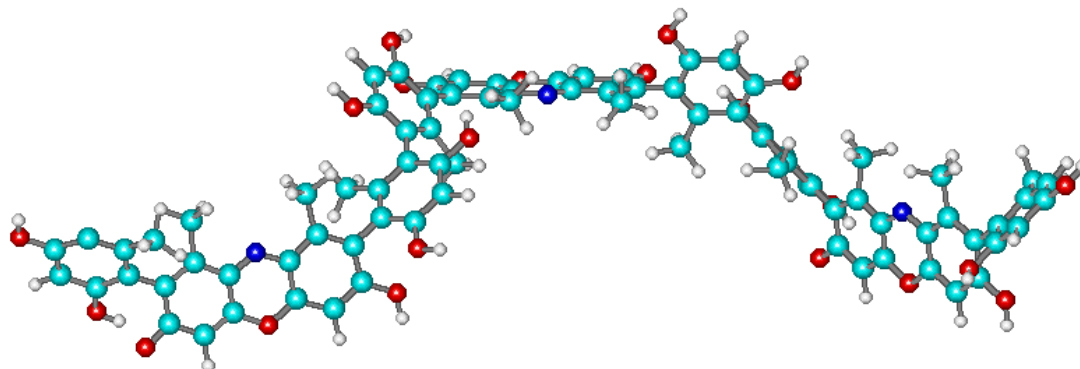


Fig 5-7 Suggested chemical structure for litmus. The repeating unit consists of a substituted phenoxazone and two orcinol residues [21].

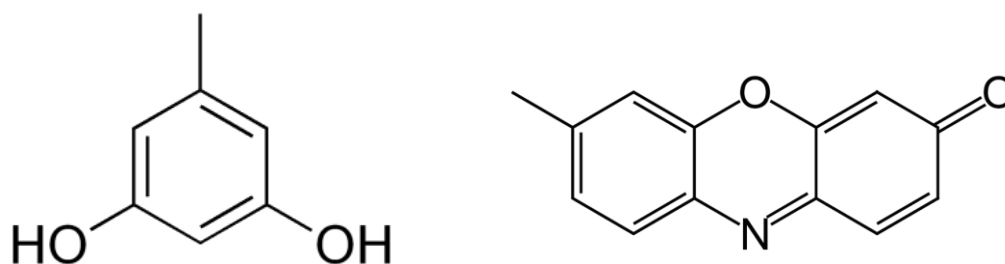


Fig 5-8 Orcinol(left) and phenoxizone (right) chemical structures.

Poly (aniline)

- Molecular Weight: average >15,000 g/mol
- pH Range: 4.0–12.0
- Solubility: partially soluble in water
- UV-Visible (λ_{\max}): 600 nm, 840 nm
- Charge: negative charge in high pH and positive charge in low pH

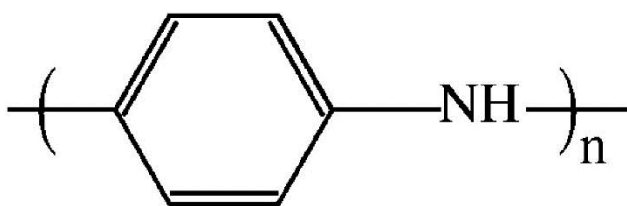


Fig 5-9 Chemical structure of poly (aniline).

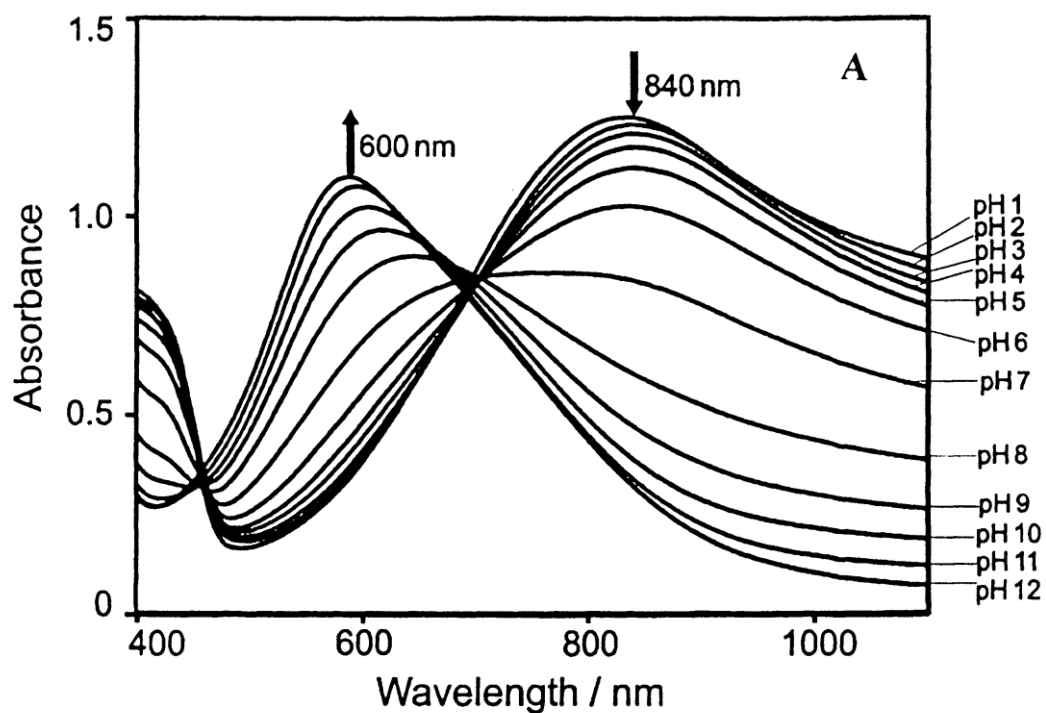


Fig 5-10 Absorbance spectra for poly (aniline) in different pH buffer solutions [22].

Congo Red (CR):

- Molecular Weight: 696.67 g/mol
- pH Range: 3.0–5.0
- Colour Change at pH: Blue (3.0) to red (5.0)
- pK_a: 4.1
- Solubility: Soluble in water
- UV-Visible (λ_{max}): 595 nm, 497 nm, 488 nm
- Charge: Negative charge

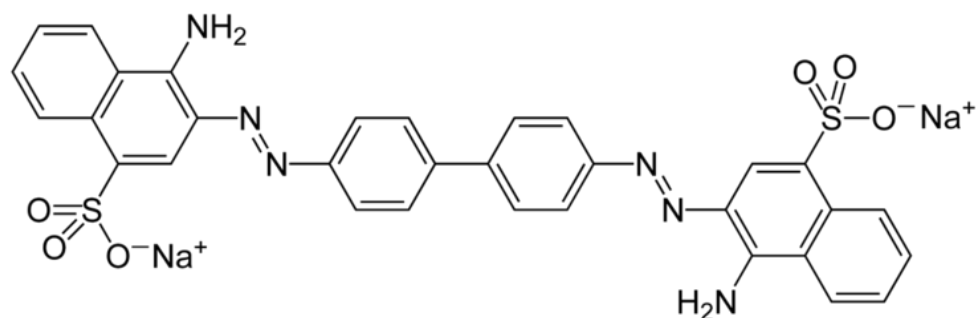


Fig 5-11 Chemical structure of congo red.

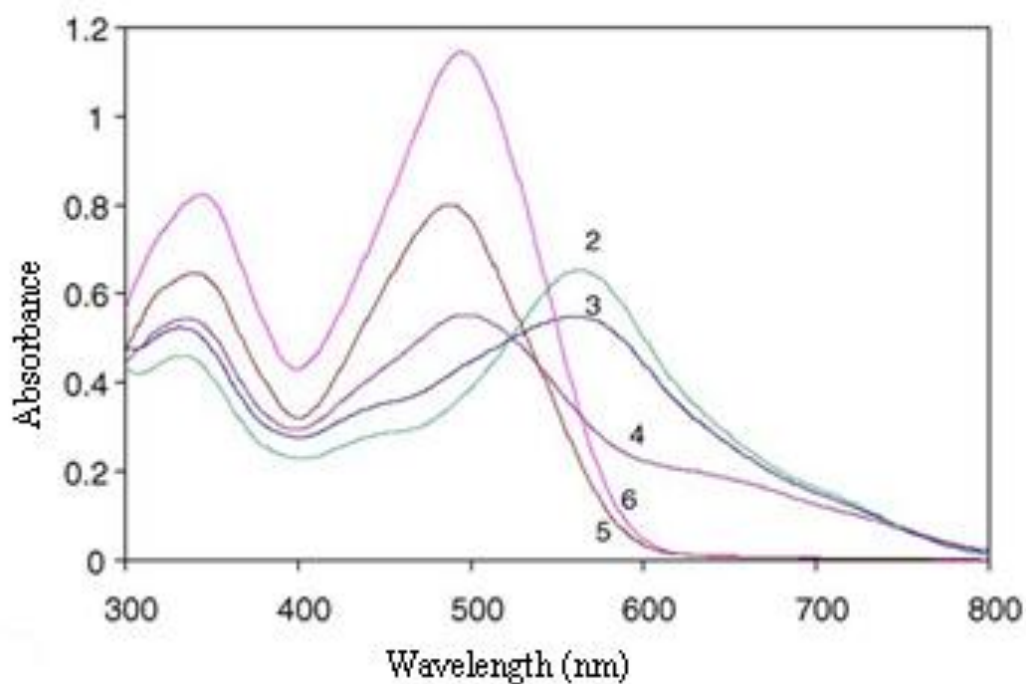


Fig 5-12 Absorbance spectra for congo red at different pH buffer solutions [23].

5.2.2 Methodology

In order to study the behavior of immobilized dye in different pH solutions and to find out the suitable reagent that shows high colour variation with significant

peak wavelength shift in a wider range of pH the named components were deposited on the glass slide and the optical fibre using LbL technique and then absorbance spectra in different pH buffer solution were studied according to the procedure described in Section 3.5.

Neutral red, brilliant yellow and alizarin red S were selected among the mentioned indicators. Polyaniline and litmus can indicate a wide range of pH of a solution with great change colour and consequently big wavelength shift. However, polyaniline has commonly been used as a conductive electrode [24, 25] and has been used to develop a gas sensor [26]. It has been used in membranes [12, 16, 27] and in a Quartz Crystal Microbalance (QCM) device [28] as a pH sensor. It is also utilized in the specific measurement of pH [29]. It is negatively charged in high pH and positively charged in low pH [25]. Therefore in the case of pH measurement discharging happens especially when it is deposited by LbL technique.

The molecules of litmus carry negative charge and can be used as a polyanion, then PAH was applied as a polycation. The absorbance spectra of water-based solution of litmus showed a pick at 581 nm wavelength. Nonetheless, the multilayers of (PAH/Litmus) did not show any acceptable absorbance spectra, as the absorbance for a thin film comprising 15 bilayers of (PAH/Litmus) was only 0.04. Despite the molecular structure of litmus which carries two negative functional groups, it is likely that its molecules were not able to get attracted to the surface properly.

congo red is water soluble, yielding a colloidal solution; its solubility is better in organic solvents such as ethanol.

Eventually, BY, NR, ARS and their combinations (for a wider range of pH recognition) were selected as pH indicators among the indicators listed above. PAH and PAA were also used as cross-linker. For those indicators with positive charge functional groups PAA was applied as an alternate layer and PAH was utilized between layers of indicators with negative charge functional group. The compounds that are selected for coating are listed below.

❖ PAH/BY

Polycation: PAH

Polyanion: BY

❖ NR/PAA

Polycation: NR

Polyanion: PAA

❖ PAH/ARS

Polycation: PAH

Polyanion: ARS

❖ PAH/(ARS+BY)

Polycation: PAH

Polyanion: ARS & BY

❖ (PAH+NR)/ARS

Polycation: PAH & NR

Polyanion: ARS

PAH and PAA were used as cross-linker while other components were applied as pH indicators.

The concentrations of the polymers were constant at 2.5 mM in saline solution with 150 mM NaCl. However the dyes had different concentrations (0.25 mM and 0.5 mM) in saline solution (150 mM NaCl) depending on the type of reagent. The concentration of polymers, reagents and salt were selected based on some preliminary experiments which gave a good homogenous coating with considerable absorbance. The dipping time for all stages of the coating was 5 minutes for each stage without drying. To enhance the stability of the bilayers heat treatment was used after carrying out the deposition as the fibre was cured at 120°C for 4 hours. In order to prepare a fibre optic sensor the procedures mentioned in Sections 3.4 and 3.5 were carried out. The length of the mirror created at the tip of the fibre was kept constant at 2.5 mm for all probes and the length of the sensor was adjusted to 21 mm (Fig 5-13). As already mentioned the Dose-Response curve fitting model was applied to fit curves of the peak wavelength with pH values of buffer solutions. Curve gradient in the inflection point can present the peak wavelength shift per pH unit in which higher absolute value shows greater sensitivity.

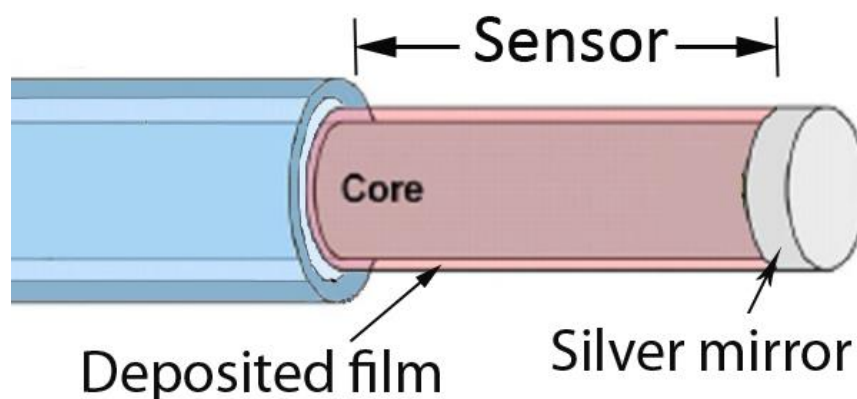


Fig 5-13 The sensor part is a coated core which ended by a silver mirror.

5.2.3 The performance of the selected indicators

➤ *Brilliant yellow*

Brilliant yellow (BY) is one of the indicators which is suitable for coating using the layer-by-layer technique. Before examining each indicator on an optical fibre, the changes of absorbance and peak wavelength versus number of bilayers of (PAH/BY)_n were studied. Having plotted the absorbance and peak wavelength as a function of number of bilayers, the results based on number of bilayers which gives the considerable absorbance with stable peak wavelength lead to a suitable number of deposited bilayers as shown in

Fig 5-14.

The thickness of the film progressively increases when adding bilayers on the surface and as a consequence absorbance increases. In contrary the peak wavelength shifts to higher values with low number of bilayers. However, when adding higher number of bilayers the peak wavelength shift is negligible.

The optical fibre was coated using brilliant yellow and was examined over a range of pH values from pH 3 to pH 10. The results illustrated in Fig 5-15 and Fig 5-16 show that to what extent this indicator demonstrates a good wavelength shift when pH of the solution surrounding the sensing region of the fibre differs. The parameters for curve fitting based on Dose-Response model for this probe is given in Table 5-1.

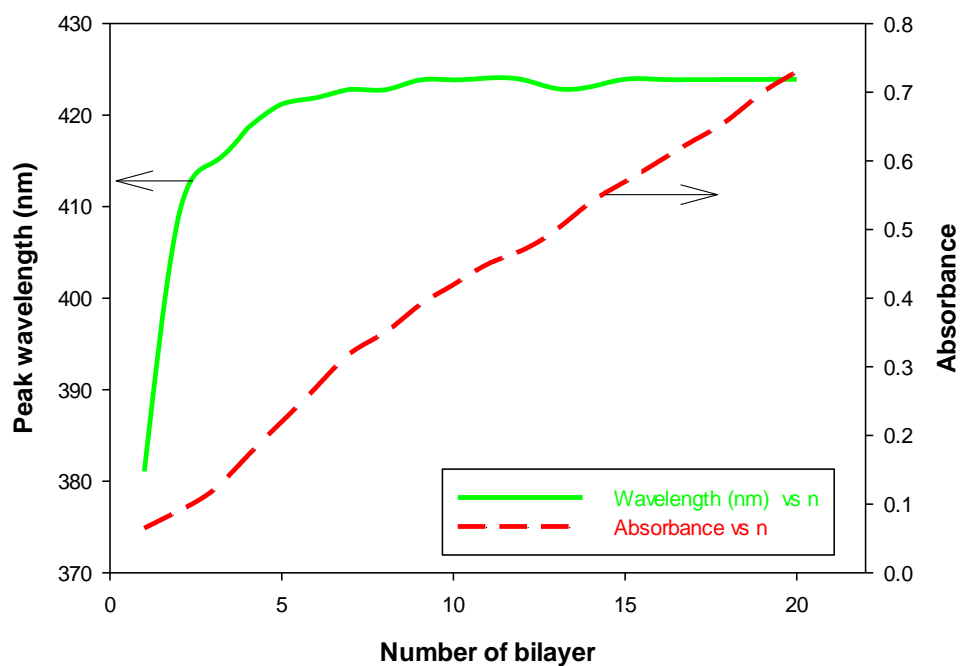


Fig 5-14 The peak wavelength value and absorbance changes when adding bilayers on the surface for $(\text{PAH/BY})_n$ deposited on the glass slide.

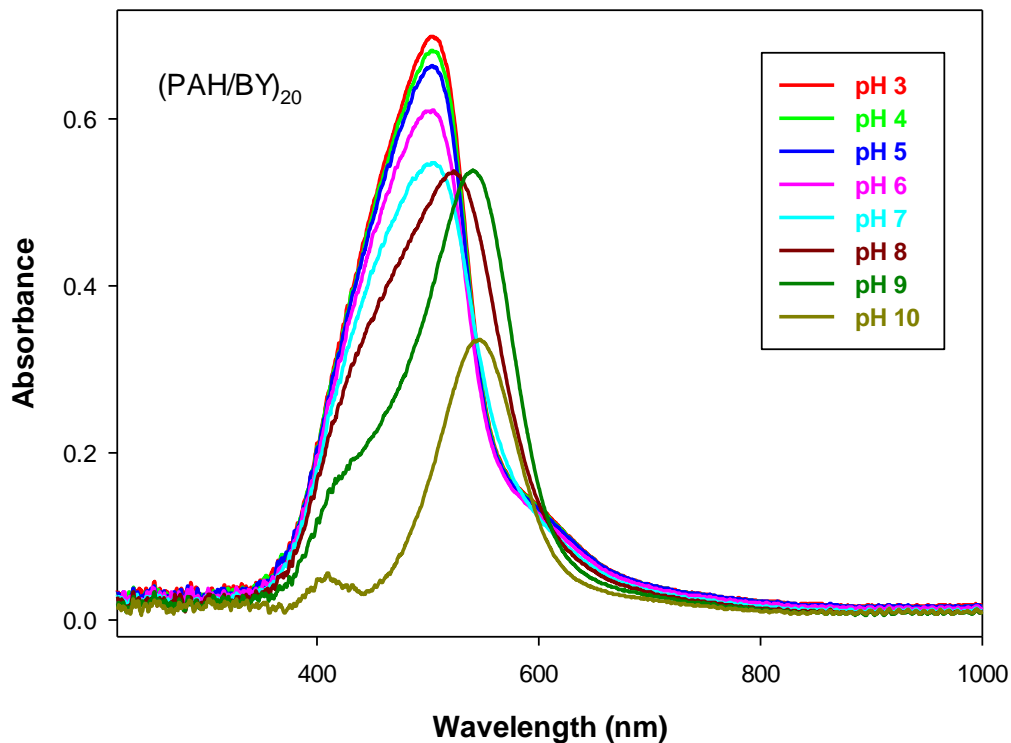


Fig 5-15 The absorbance spectra for a probe coated with $(\text{PAH/BY})_{20}$. The concentration of BY and PAH solutions was 0.25 mM and 2.5 mM respectively. (Probe code: OFBY)

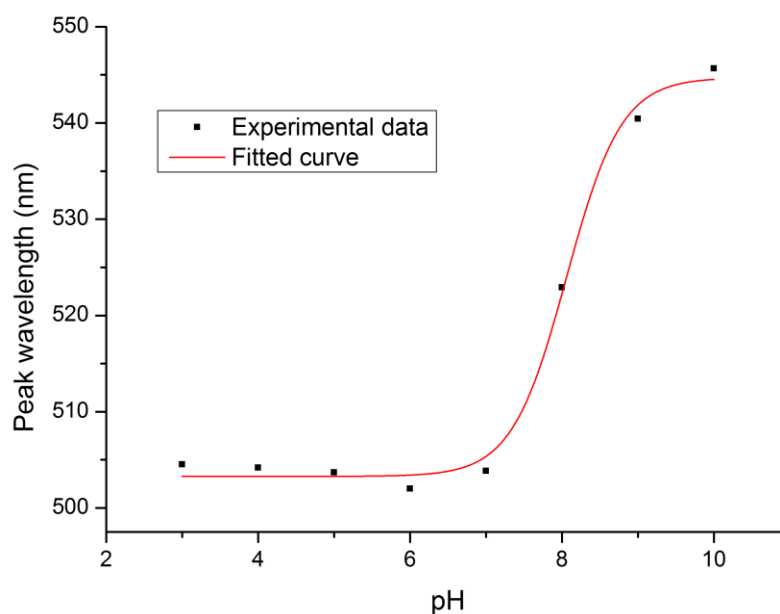


Fig 5-16 The peak wavelength as a function of the pH value of the buffer solution for a probe coated with (PAH/BY)₂₀ (Probe code: OFBY).

➤ **Neutral red**

Neutral red which carries a positive functional group applied with PAA which is negatively charged to create a multilayer thin film. The absorbance and peak wavelength as a function of number of bilayers of (NR/PAA)_n deposited on glass slide is shown in Fig 5-17. As can be seen from this graph, the peak wavelength shows a slight change (~7 nm) when the number of bilayers added is increased from 5 to 27 bilayers while the absorbance increases from 0.13 to 0.74.

The optical fibre was coated with 15 bilayers (NR/PAA) to create a sensor which was tested in the range of pH 4.5 to 9.5. Fig 5-18 shows its spectroscopic properties. The Dose-Response curve fitting in Fig 5-19 demonstrates that the peak wavelength shift has a remarkable jump in the pH 6 to 7 range.

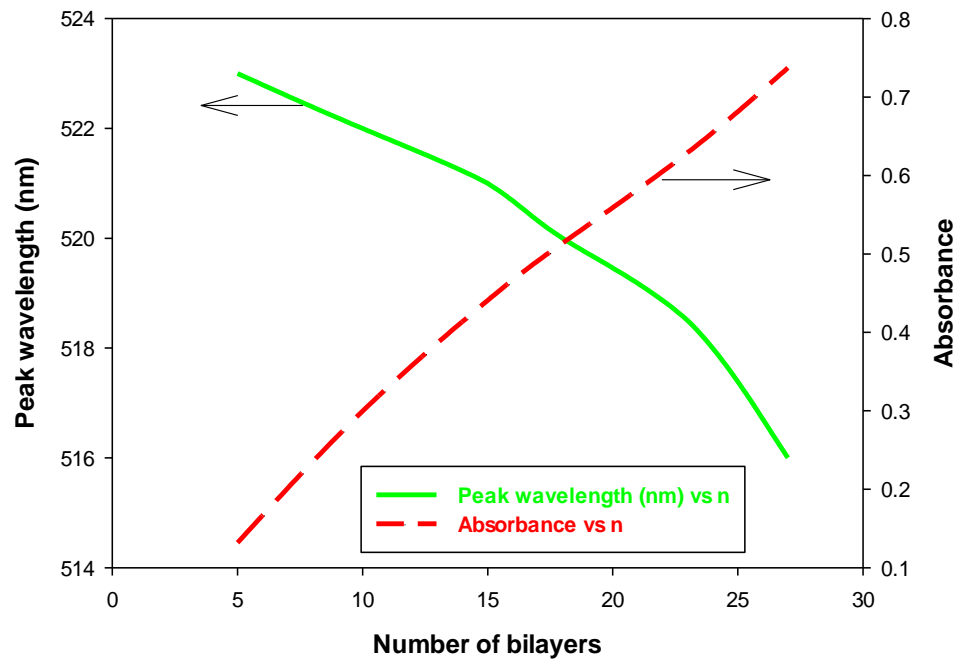


Fig 5-17 The peak wavelength value and absorbance changes when adding bilayers on the surface for $(NR/PAA)_n$ deposited on the glass slide.

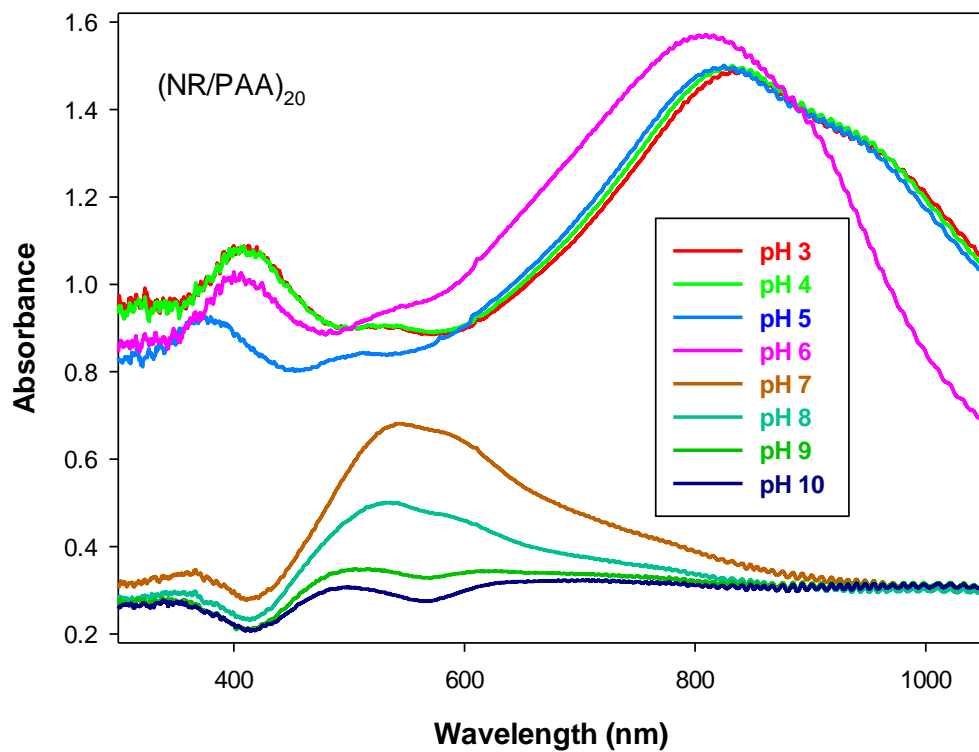


Fig 5-18 The optical fibre coated with NR in different pH buffer solutions from pH 3 to pH 10. The concentration of NR and PAA solutions was 0.25 mM and 2.5 mM respectively. (Probe code: OFNR)

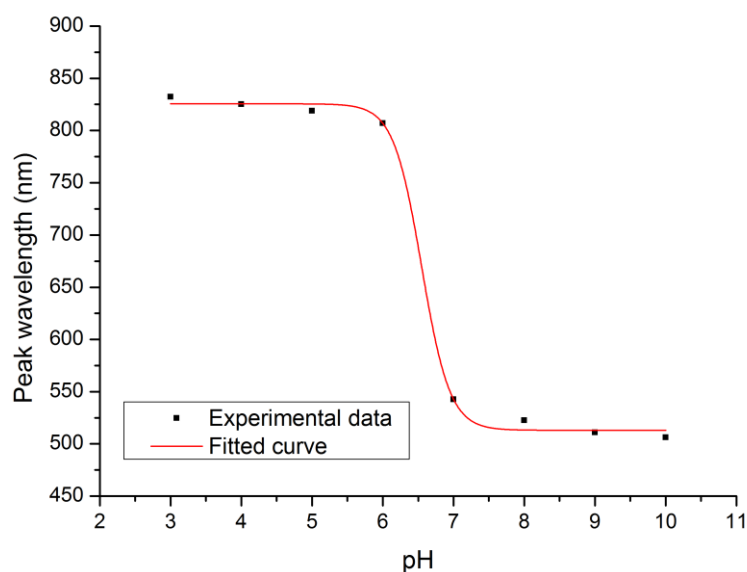


Fig 5-19 The peak wavelength for each spectrum in respect to pH for Fibre OFNR.

➤ *Alizarin red S*

Alizarin red S (ARS) is the third indicator that was examined in this study. The changes of the peak wavelength and the absorbance with respect to number of bilayers of (PAH/ARS)_n deposited on glass slide is shown in Fig 5-20. Adding multilayer thickness caused an increase in the absorbance and shortened the peak wavelength which is similar to the behavior observed in neutral red. ARS was examined by a probe which was deposited with 20 bilayers (PAH/ARS) in the pH range 3 to 9. The related spectroscopic graphs are shown in Fig 5-21. The Dose-Response curve fitting (Fig 5-22) demonstrates two different indicating ranges in which one of them is located around pH 3.5 to 5.5 and the other one starts from a pH of 7.5 and it is expected to continue as high as 9. However, since discharging and later damaging of the layers happens in very low and very high pH, it is not desirable to carry out measurements beyond pH 9.

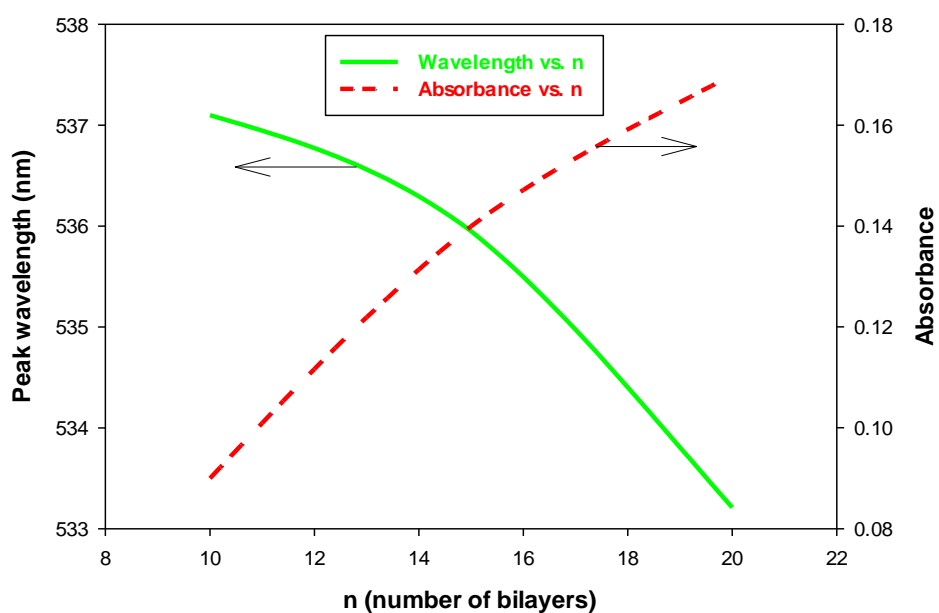


Fig 5-20 The peak wavelength value and absorbance changes when adding bilayers on the surface for $(\text{PAH/ARS})_n$ deposited on the glass slide.

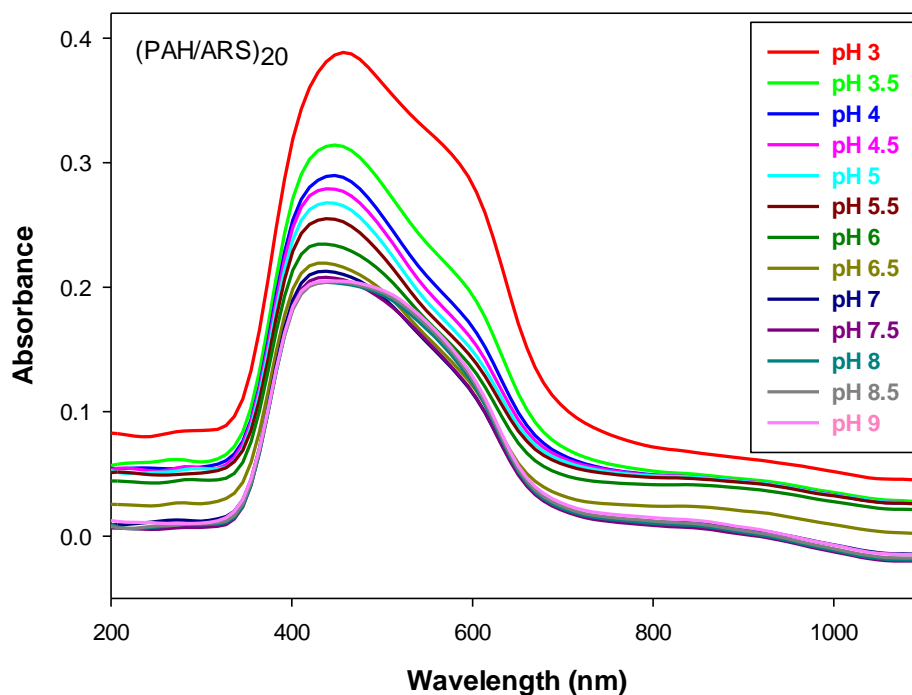


Fig 5-21 The optical fibre coated with ARS in different pH buffer solutions from pH 3.0 to pH 9.0. The concentration of ARS and PAH solutions was 0.5 mM and 2.5 mM respectively. (Probe code: OFARS)

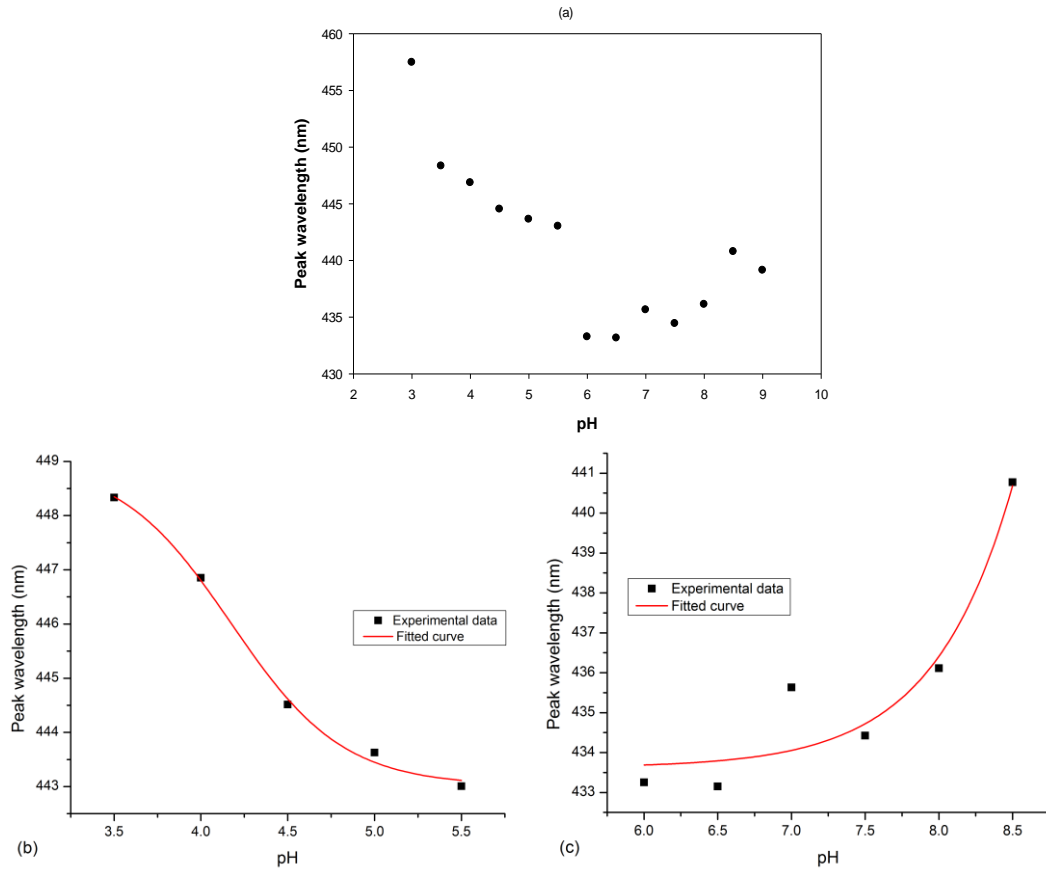


Fig 5-22 The peak wavelength for each spectrum in respect to pH for Fibre OFARS. (a) for range of pH from 3.0 to 9.0 (b) for low pHs (c) for high pHs.

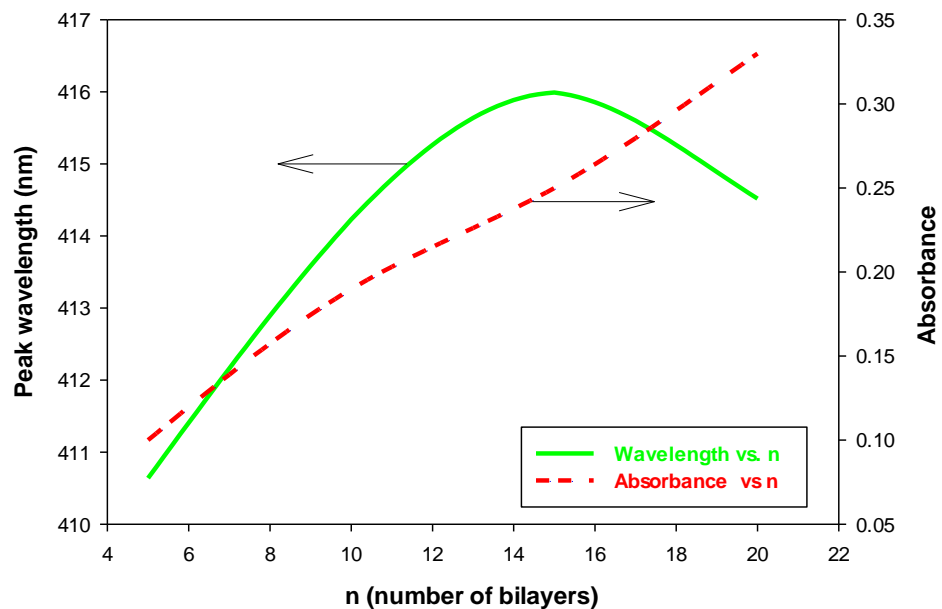


Fig 5-23 The wavelength value and absorbance changes when adding bilayers on the surface for $(\text{PAH}/(\text{ARS}+\text{BY}))_n$ deposited on the glass slide.

➤ **Alizarin red S and brilliant yellow**

Next set of experiments were done on the basis of combination of BY and ARS in order to enhance the sensing range of pH based on peak wavelength shift. Concerning the range of pH of brilliant yellow and Alizarin red S (the pH range for BY is 6.4 to 8.0 and for ARS is 3.5 to 6.5 and 9.4 to 12), it was expected that there was a regular change in peak wavelength in a wider range of pH from pH 3.5 to pH higher than 9. The variation of peak wavelength shift and the absorbance as a function of number of bilayers of $(\text{PAH}/(\text{BY}+\text{ARS}))_n$ coated on the glass slide is illustrated in Fig 5-23. As can be seen from these graphs, peak wavelength differs up to 6 nm when increasing the thickness of the multilayers from 5 to 14 bilayers.

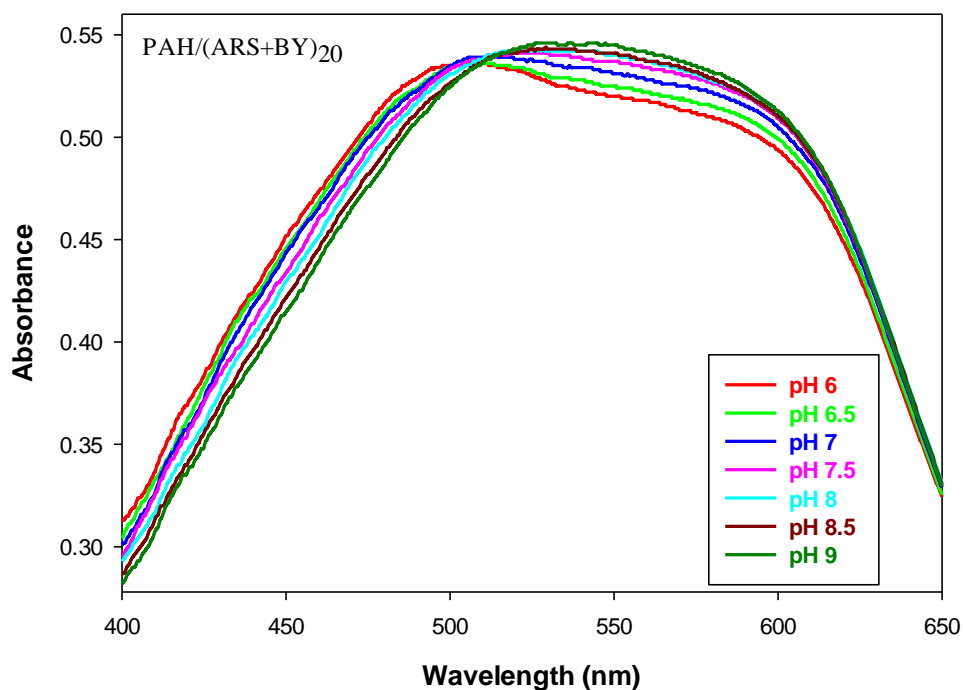


Fig 5-24 Absorbance spectra for the optical fibre coated with $(\text{PAH}/(\text{ARS}+\text{BY}))_{20}$ in different pH buffer solutions from pH 6.0 to pH 9.0 (Probe code: OFABY).

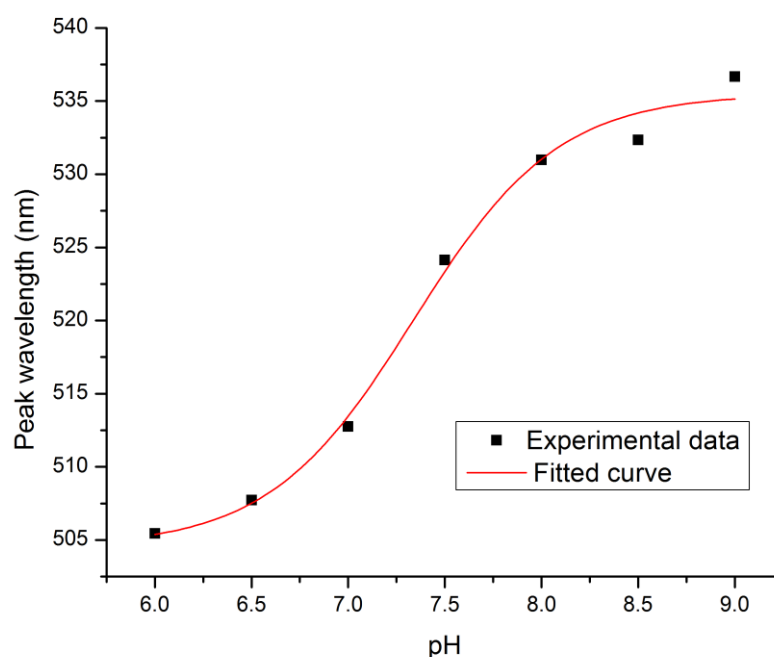


Fig 5-25 The optical fibre coated with (PAH/(ARS+BY))₂₀ in different pH buffer solutions from pH 6.0 to pH 9.0. (Probe code: OFABY)

➤ *Alizarin red S and neutral red*

The combination of alizarin red S (ARS) and neutral red (NR) was applied to coat the distal end of an optical fibre. Again, the combination of these two indicators was applied to cover a wider range of pH (the pH range for NR is 6.8 to 8.0 and for ARS is 3.5 to 6.5 and 9.4 to 12) values. The prepared probe was examined in pH buffer solutions from pH 6 to pH 9. The absorbance spectra for this probe are shown in Fig 5-26. In light of the fact, that NR is positively charged and has a stronger functional group as compared to ARS, it is expected that the Dose-Response model demonstrates a negative slope as shown in Fig 5-27.

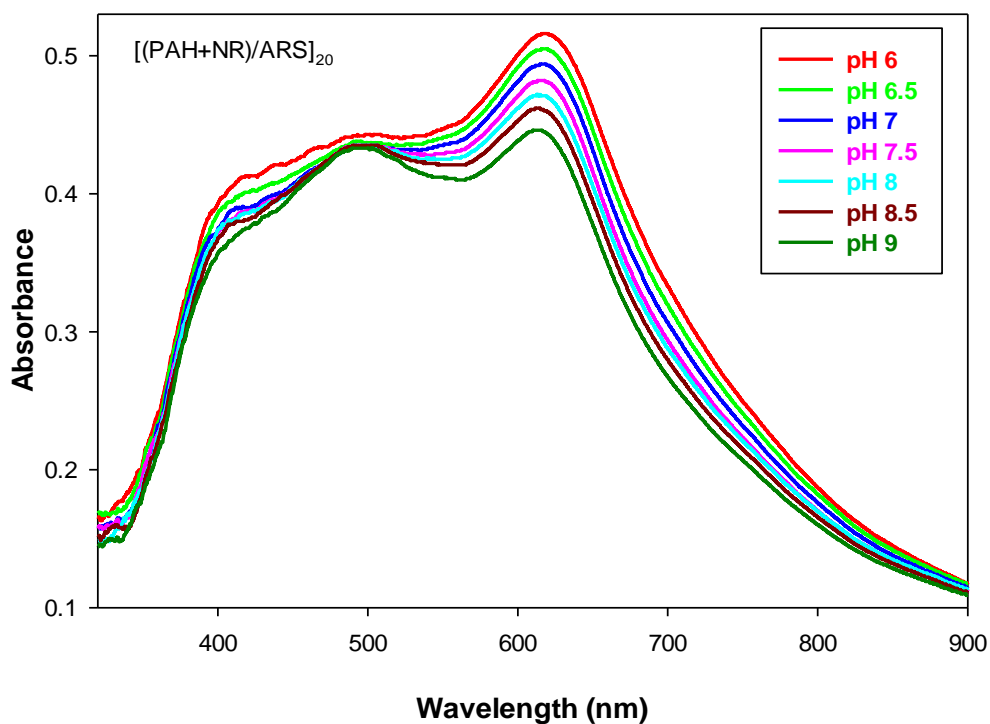


Fig 5-26 The absorbance spectra for the optical fibre coated with $((\text{PAA}+\text{NR})/\text{ARS})_{20}$ in different pH buffer solutions from pH 6.0 to pH 9.0. The concentration of ARS, NR and PAH solutions was 0.5 mM, 0.5 mM and 2.5 mM respectively. (Probe code: OFANR)

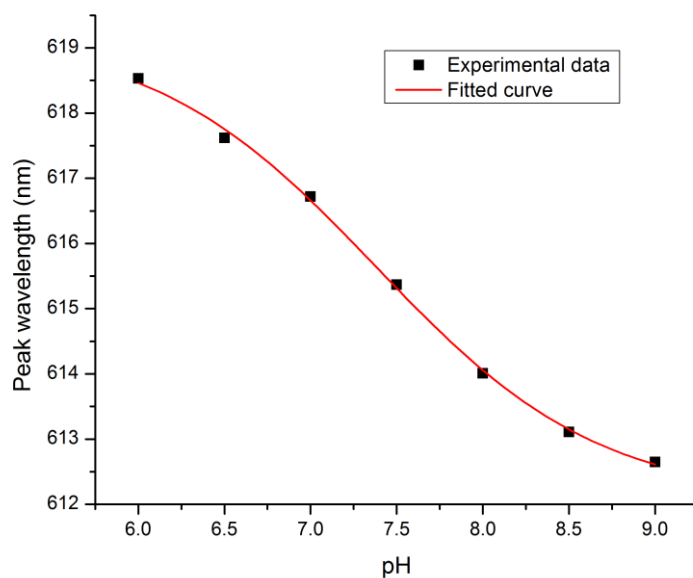


Fig 5-27 The optical fibre coated with $((\text{PAA}+\text{NR})/\text{ARS})_{20}$ in different pH buffer solutions from pH 6.0 to pH 9.0. (Probe code: OFANR)

Table 5-1 The parameters for curve fitting based on Dose-Response model for the created probe. A1 and A2 are lowest and highest values of peak wavelength respectively, p is the slope factor, pK_a is the acid dissociation constant and Y is curve gradient in the inflection point.

Probe	n	A1		A2		pK_a		p		Adj. R-Square	Y (nm/pH unit)
		Value	Standard Error	Value	Standard Error	Value	Standard Error	Value	Standard Error		
OFBY	20	503.27	0.803	544.72	1.648	8.060	0.069	1.204	0.2844	0.992	114.78
OFNR	20	513.07	4.330	825.57	4.329	6.55	0.056	-2.17	0.489	0.247	-1559
OFABY	20	504.55	1.914	535.50	1.474	7.34	0.086	1.165	0.264	0.986	82.93
OFANR	20	612.06	0.268	619.24	0.337	7.379	0.062	-0.66	0.0842	0.9978	-10.99

Table 5-2 Cross comparison of the prepared sensors.

Probe	pH range sensing	Peak wavelength shift (nm)
OFBY	7.0 – 10.0	40
OFNR	6.0 - 7.0	270
OFARS	3.5 - 5.5	5
	6.5 - 9.5	7
OFABY	6.0 – 9.0	30
OFANR	6.0 - 9.0	6

5.3 Results and discussion

Brilliant yellow, neutral red and alizarin red S were the three pH indicators that are applied individually and as a combination to coat the distal end of optical fibre to create a pH optical sensor using the layer-by-layer deposition technique. The performance of these indicators under the same criteria was investigated based on the variation of peak wavelength with respect to pH values of the

solutions surrounding the probe. The indicator which achieved the highest peak wavelength shift over wider range of pH can be a suitable candidate for wavelength dependent pH sensor. The results of these experiments are summarized in Table 5-1 and Table 5-2. The optical fibre coated by neutral red shows a dramatic peak wavelength shift specifically when the probe is transferred from the buffer solution with pH 6 to the buffer solution with pH 7 and the peak wavelength reduces by 270 nm. Moreover, the absolute value of the curve gradient at the inflection point (at pH 6.55) is 1559 nm/pH unit. This probe can be an excellent candidate for a peak wavelength based sensor operating in the range of pH 6 to pH 7.

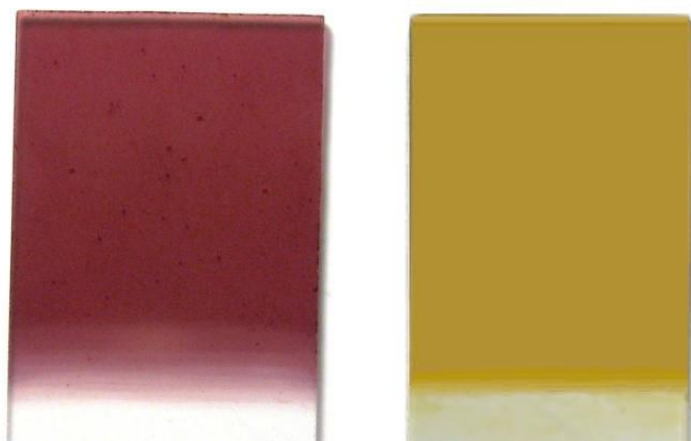


Fig 5-28 Dark and fine spots on the surface of the coated glass slide with (NR/PAA)₁₅ while the surface coated with (PAH/BY)₁₆ is totally homogenous.

However, on the surface of all samples either the glass slides or optical fibres coated with (NR/PAA)_n many dark and fine spots had been seen as shown in Fig 5-28. Although, by replacing the polymer (PAA) with a lower molecular weight one can decrease the number of spots. However, some fine spots still remain on

the surface. In conclusion, using the short-chain polymer improved the surface homogeneity but it did not have a significant effect on removing the fine spots and producing the highly homogenous coating. In contrast, the surface coated with brilliant yellow looked totally homogenous as shown in Fig 5-28. The optical fibre coated with brilliant yellow shows a good fit with the Dose-Response curve fitting model. Furthermore, it is observed that this probe is more sensitive in the pH range of 7.0 to 10.0. Although, the curve gradient in inflection point for OFBY is around 115 nm/pH unit and it is not comparable to that of for OFNR which is around 1560 nm/pH unit, the fibre coated with (PAH/BY) multilayers had a better practical behaviour and a regular spectra configuration compared to the fibre coated with (NR/PAA) multilayer. The sensors prepared by coating the fibre with alizarin red S and its combinations with brilliant yellow and neutral red did not show any significant wavelength shift and were not suitable for a wavelength dependent sensor.

5.4 Summary

A variety of probes with similar deposition conditions were prepared based on three indicators and their combinations. Brilliant yellow showed good sensitivity based on peak wavelength shift for a pH range of pH 7.0 to 10.0 compared to other indicators. Although neutral red illustrated a dramatic slope at the inflection point, it shows high sensitivity for a narrower pH range of 6 to 7. BY is the second good-performer indicator with wider pH range sensing and a slope of 115 nm/pH unit. Consequently brilliant yellow was selected as the pH

indicator to provide a high resolution sensor for wider range of pH values. To investigate the performance of the sensor prepared by brilliant yellow some further experiments are undertaken which are discussed in the Chapter 6.

References

- [1] O. S. Wolfbeis, "Chemical sensing using indicator dyes," in *Optical Fiber Sensors*, vol. IV, J. Dakin and B. Culshaw, Eds., ed Boston-London: Artech House, 1997, pp. 53-107.
- [2] P. Hashemi, R. A. Zarjani, M. M. Abolghasemi, and A. k. Olin, "Agarose film coated glass slides for preparation of pH optical sensors," *Sensors and Actuators B*, vol. 121, pp. 396-400, 2007
- [3] J. M. Corres, I. R. Matias, I. D. Villar, and F. J. Arregui, "Design of pH sensors in long-period fiber gratings using polymeric nanocoatings," *IEEE Sensors Journal*, vol. 7, pp. 455-463 2007.
- [4] P. S. Grant and M. J. McShane, "Development of multilayer fluorescent thin film chemical sensors using electrostatic self-assembly," *IEEE Sensors Journal*, vol. 3, pp. 139-146, 2003.
- [5] G. Beltrán-Pérez, F. López-Huerta, S. Muñoz-Aguirre, J. Castillo-Mixcóatl, R. Palomino-Merino, R. Lozada-Morales, *et al.*, "Fabrication and characterization of an optical fiber pH sensor using sol-gel deposited TiO₂ film doped with organic dyes," *Sensors and Actuators B: Chemical*, vol. 120, pp. 74-78, 2006.
- [6] J. M. Corres, I. d. Villar, I. R. Matias, and F. J. Arregui, "Fiber-optic pH-sensors in long-period fiber gratings using electrostatic self-assembly," *Optics Letters*, vol. 32, pp. 29-31, 2007
- [7] F. J. Arregui, I. L. I. R. Matias, and R. Claus, "An optical fiber pH sensor based on the electrostatic self-assembly method," *IEEE Sensors Conference Proceedings*, pp. 107-110, 2003.
- [8] A. Lobnik, I. Oehme, I. Murkovic, and O. S. Wolfbeis, "pH optical sensors based on sol-gels: chemical doping versus covalent immobilization," *Analytica Chimica Acta*, vol. 367, pp. 159-165, 1998.
- [9] J. Lin, "Recent development and applications of optical and fiber-optic pH sensors," *Trends in Analytical Chemistry*, vol. 19, pp. 541-552, 2000.
- [10] W. J. Stephen and P. T. Ralph, "Fibre optic sensors with nano-structured coatings," *Journal of Optics A: Pure and Applied Optics*, vol. 8, pp. S430-S435, 2006.
- [11] Z. Hotra, O. Aksimenteva, I. Hlushyk, V. Cherpak, and P. Stakhira, "Fibre-optic pH sensor," *Modern Problems of Radio Engineering, Telecommunications, and Computer Science (TCSET): International Conference (TCSET)*, vol. 4, pp. 673-674, 2006.
- [12] Z. Jin, Y. Su, and Y. Duan, "An improved optical pH sensor based on polyaniline," *Sensors and Actuators B* vol. 71, pp. 118-122, 2000.

- [13] Y. Liu and T. Cui, "Ion-sensitive field-effect transistor based pH sensors using nano self-assembled polyelectrolyte/nanoparticle multilayer films," *Sensors and Actuators B* vol. 123, pp. 148-152, 2007.
- [14] A. Armin, M. Soltanolkotabi, and P. Feizollah, "On the pH and concentration response of an evanescent field absorption sensor using a coiled-shape plastic optical fiber," *Sensors and Actuators a-Physical*, vol. 165, pp. 181-184, Feb 2011.
- [15] H. Nguyen, T. Venugopalan, T. Sun, and K. T. V. Grattan, "Development of intrinsic optical fiber pH sensors for industrial applications," *IEEE Sensors* vol. 1-3, pp. 89 - 94 2009.
- [16] T. Lindfors and A. Ivaska, "pH sensitivity of polyaniline and its substituted derivatives," *Journal of Electroanalytical Chemistry* vol. 531, pp. 43-52, 2002.
- [17] J. Goicoechea, C. R. Zamarreño, I. R. Matias, and F. J. Arregui, "Utilization of white light interferometry in pH sensing applications by mean of the fabrication of nanostructured cavities," *Sensors and Actuators B: Chemical* vol. 138, pp. 613-618, 2009.
- [18] J. Goicoechea, C. R. Zamarreño, I. R. Matías, and F. J. Arregui, "Study on White Light Optical Fiber Interferometry for pH Sensor Applications," in *IEEE Sensors Conference Proceedings*, 2007.
- [19] J. Goicoechea, C. R. Zamarreño, I. R. Matías, and F. J. Arregui, "Optical fiber pH sensors based on layer-by-layer electrostatic self-assembled Neutral Red," *Sensors and Actuators B: Chemical* vol. 132, pp. 305-311, 2008.
- [20] Y. Egawa, R. Hayashida, and J.-i. Anzai, "Multilayered assemblies composed of brilliant yellow and poly(allylamine) for an optical pH sensor," *Analytical Sciences*, vol. 22, pp. 1117-1119, 2006.
- [21] <http://www.chriscooksey.demon.co.uk/lichen/litmus2.htm>.
- [22] E. Pringsheim, E. Terpetsching, and O. S. Wolfbeis, "Optical sensing of pH using thin film of substituted polyanilines," *Analytica Chimica Acta*, vol. 357, pp. 247-252, 1997.
- [23] P. Hashemi and M. M. Abolghasemi, "Preparation of a novel optical sensor for low pH values using agarose membranes as support," *Sensors and Actuators B-Chemical*, vol. 115, pp. 49-53, 2006.
- [24] J.-H. K. Kouji Fujimoto, Kiwako Ohmori, Akinobu Ono, Seimei Shiratori, "Flexible multilayer electrode films consisted of polyaniline and polyelectrolyte by layer-by-layer self-assembly," *Colloids and Surfaces A: Physicochem. Eng. Aspects* vol. 313-314 pp. 387-392, 2008.
- [25] N. Sarkar, M. K. Ram, A. Sarkar, R. Narizzano, S. Paddeu, and C. Nicolini, "Nanoassemblies of sulfonated polyaniline multilayers," *Nanotechnology*, vol. 11, pp. 30-36, Mar 2000.

- [26] F. J. Arregui, X. Liu, I. R. Matias, and R. O. Claus, "Optical fiber humidity sensor using a nano Fabry–Perot cavity formed by the ionic self-assembly method," *Sensors and Actuators B: Chemical* vol. 59, pp. 54-59, 1999.
- [27] Y. T. Tsai, T. C. Wen, and A. Gopalan, "Tuning the optical sensing of pH by poly(diphenylamine)," *Sensors and Actuators B*, vol. 96, pp. 646-657, 2003.
- [28] M. M. Ayad, N. A. Salahuddin, M. O. Alghaysh, and R. M. Issa, "Phosphoric acid and pH sensors based on polyaniline films," *Current Applied Physics* vol. 10, pp. 235-240, 2010.
- [29] L. H. Tom Lindfors, and Ari Ivaska, "Optical pH measurements with water dispersion of polyaniline nanoparticles and their redox sensitivity," *Analytical Chemistry*, vol. 78, pp. 3019-3026, 2006.

6. Enhanced Sensitivity of a Fibre Optic pH Sensor Coated with Brilliant Yellow

6.1 Introduction

A sensor is a device which detects or measures a physical property and records, indicates, or otherwise responds to it. In other words, a sensor is a device, which responds to an input quantity by generating a functionally related output usually in the form of an electrical or optical signal. Optical sensors which are a type of sensor is usually based on optical fibres.

The fibre optic chemical sensor is a sensor that measures a particular measurand when an indicator or chemical reagent coats the surface of the optical fibre using a mediator to produce an observable optical signal. Typically, conventional techniques, such as absorption spectroscopy are employed to measure changes in the optical signal. It is well known that different structures of fibres that may be used and their various materials employed, as well as different shapes of the probe formed from the fibre can all demonstrate individual behaviour in a range of sensor applications [1-4]. Hence optimizing

the type of the fibre and the coating method used can be crucial steps in producing the most suitable probes for different sensing applications and ranges. The sensitivity of a sensor indicates how much the sensor's output changes when the measured quantity changes. Sensors that measure very small changes must have very high sensitivities. Several properties of the fibre can be used to enhance its sensitivity.

Sensitivity not only depends on the choice of materials of deposited film, but also on the geometry of the fibre, the thickness of the coated thin layer, fibre core radius and refractive index of both the fibre and its coating [5-8] which is strongly dependent upon the fibre bend radius and the thickness of the thin film [7, 9]. Sensitivity can be enhanced by bending fibres. The curvature of the sensing fibre enhances the interaction of the incident light with the sensing film because the intensity of the evanescent wave increases with curving the sensing fibre [10, 11].

However, when the bending radius decreases below a certain value, the sensitivity of the sensor may start to decrease due to the reason that the incident angle of light is less than the critical angle required for light to be guided in the bending region. Therefore, the maximum sensitivity of the U-shaped sensor can be obtained at an optimum value of the bending radius [12, 13].

While many researchers have shown that the higher sensitivity of a fibre optic sensor can be achieved by increasing the thickness of the sensing region [14-16], other scholars have demonstrated that the thickness optimization which is

achieved by the control of number of bilayers is necessary to obtain the highest pH sensitivity [17, 18].

Sensitivity also varies with the amount of adsorbed material which can be controlled by concentration of polyions solutions using the layer-by-layer approach [9, 19]. The optical sensors which work at shorter wavelength show higher sensitivity [20].

To date, in most of the pH sensors developed, their sensitivity has been determined through intensity-based measurements which can be prone to errors. Few researchers have studied optical sensors which are based on wavelength shift. However, the highest sensitivity for their sensors was not very significant e.g. 0.32 nm/pH unit and -0.45 nm/pH unit for acid and alkali solutions, respectively [21], or 0.6 nm/pH unit and -0.85 nm/pH unit for acidic and alkaline solutions, respectively [15]. However, in the current work, the design and characteristics of novel and high sensitive wavelength-dependent pH optical sensors have been studied and reported. This allows the sensor mechanism to be independent of any source variation or any perturbation, other than the pH change being measured. In the present study, brilliant yellow was chosen and was applied as an indicator because of the greater wavelength shift observed with pH change, compared to the use of other indicators.

Reviewing the response to wavelength change, the sensitivity of the probes is limited and significant over the pH values from pH 7 to pH 9 for almost all probes coated with PAH/BY and in this pH range the wavelength shift is clearly

measurable. Hence wavelength shift can be considered as an index for sensitivity.

This chapter focuses particularly on key fabrication parameters including effects and influence of the concentration of the indicator, the fibre core diameter and the bending radius of the fibre that was used. The wavelength shift and the sensitivity of the probes prepared in this work – the key measurand-related parameters – demonstrate the advantage of this approach and the level of sensitivity achievable. The work provides a framework for the optimization of the design and structure of the pH sensor, where key information on several parameters, such as number of deposited layers, the concentration of the indicator solution, fibre core diameter and the shape (straight and U-bend) of the probe have been investigated and results on the sensor performance are reported.

In all experiments changing the effective parameters influences the nature of the coating comprising of components which are active at a specific wavelength.

6.2 Materials and methods

6.2.1 Materials

In order to create an effective optical pH sensor, brilliant yellow (BY) was selected as the pH indicator, as discussed earlier. This molecule is negatively

charged and can be used as a polyanion. Poly (allylamine hydrochloride) [PAH] is a positively charged molecule and was used as a polycation.

6.2.2 Fabrication of the sensors

To design and develop the sensor probe, a silica multimode fibre with a core diameter of 1mm and cladding thickness of 10mm was used, as supplied by Thorlabs. To create a straight evanescent sensor, the distal end of the fibre was stripped of the jacket coating and the fibre was polished with 5 μm , 3 μm , 1 μm and 0.3 μm stone-papers respectively to achieve a smooth finish. As the cladding is acetone soluble, it was easily removable. To create an evanescent field U-bend sensor, a part of the fibre also was stripped off its jacket and cladding. A flame was then applied to soften the glass, so that if required the fibre could be slowly bent to create the U-shape, following which the fibre was cleaned and the surface functionalized. Following that the bare core was soaked in piranha solution (a 30:70 (v/v) mixture of oxygen peroxide (H_2O_2) (30%) and concentrated sulfuric acid (H_2SO_4)) for 60 minutes to produce the negatively charged surface and it was then rinsed in distilled water. To reflect the radiated light back and guide it to the other end of the fibre in the straight probe, a mirror was created at the tip of the fibre. Both fibres were then coated with positively charged molecules. The layer-by-layer technique used is based on the successive deposition of oppositely charged molecules onto the solid surface; here the negatively charged fibre was dipped into the polycation solution for 5 minutes. As a result, a thin layer of the positive molecules was adsorbed onto

the surface. Following that, the fibre was then dipped into distilled water for 5 minutes to remove any unbounded molecules from its surface and the substrate was alternately placed into the polyanion solution for another 5 minutes which further allowed any unbound molecules to be washed out, again using distilled water. This procedure was repeated and as a result a multilayer coating was built up. To improve the stability of the film and to avoid progressive degradation of the indicator, the coated substrate was cured at 120°C for 4 hours.

6.2.3 Experiments

To study the performance of the sensors which had been prepared by building up the layers of the pH indicator on the glass core of the optical fibre and to optimize the conditions for the use of the sensor, a number of key parameters such as the number of bilayers used (one layer of brilliant yellow and one layer of PAH constitutes a bilayer), the concentration of the brilliant yellow indicator, the size of the core and the shape of the fibre were examined. The concentration of the PAH solution (in 150 mM saline solution) was identical at 2.5mM for all samples considered, while two different concentrations for the BY solution (in 150 mM saline solution) were examined, these being 0.25 mM and 0.5 mM. The pH of the polyanion solutions was adjusted at pH 6 for BY and pH 5 for PAH solutions. The sensing length was 22 mm for both the U-bend and the straight probes while radii of the U-bend probes were different, at 1.15 mm and 1.55 mm. These two configurations shown in Fig 6-1.

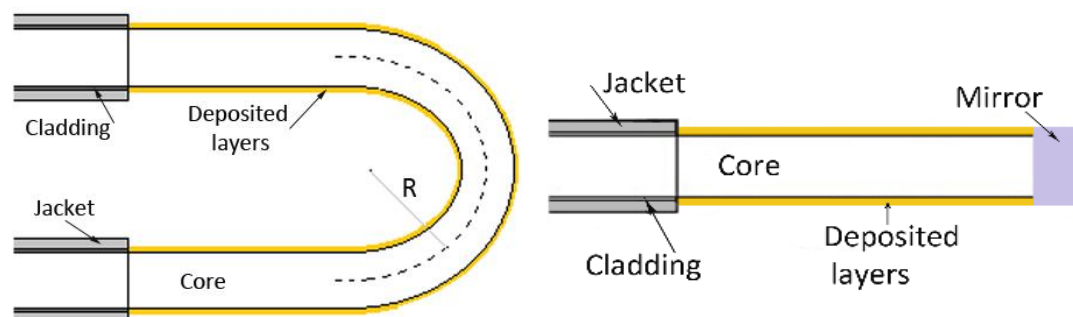


Fig 6-1 Schematic of the U-bend and straight probes.

The layer-by-layer technique was employed to coat the uncladded silica core of all the probes alternately with PAH and BY. The probes thus prepared were tested and evaluated in buffer solutions of known pH over a range of 6.6 to 9.4. To measure the absorbance spectra of the coated optical fibre, an experimental setup was designed and developed for this purpose, and shown schematically in Fig 6-2.

All measurements took place in stable conditions and each spectrum was recorded after achieving stable results (about 50- 60 second). No cleaning, washing or heating steps between measurements were done.

Measuring the absorbed light as a function of wavelength for different pH buffer solutions using a spectrophotometer gave a series of spectra. Following that, the wavelength of the maximum absorbance for each graph was plotted with respect to pH so that the generated graph was seen to obey the appropriate Dose-Response curve fitting model.

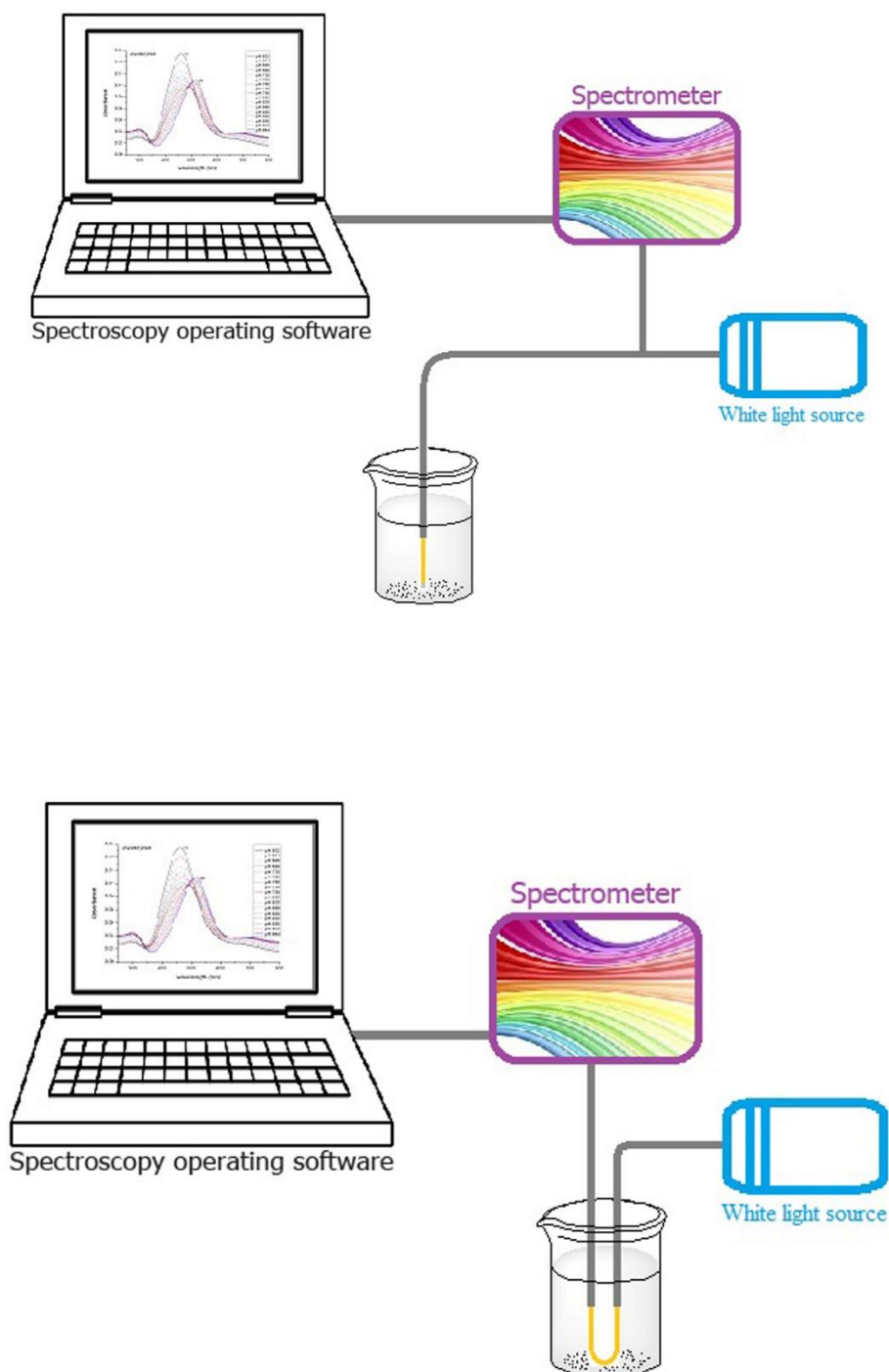


Fig 6-2 The experimental set up for straight probes (up) and U-bend probes (down).

In addition, layers of PAH and BY were built up on the straight optical fibre (with 600 μm core diameter) using a range of different bilayers (numbered here

from 3.5 to 9.5) such that probes with whole numbers of layers end with BY whereas those with fractional (decimal) numbers of bilayers end with PAH.

Two series of experiments were carried out on U-bend and straight probes (of which the core diameter was identical at 1000 μ m), and the concentration of the BY solutions was varied from 0.25 mM to 0.5 mM.

Six double layers of (PAH/BY) were built up on the glass core. Having examined the probes in the pH buffer solutions, the conclusions obtained from the respective Dose-Response graph for every probe are summarized in Table 6-1. The results of each experiment will show and compare graphically in each relevant section separately.

6.3 Results and discussion

In the present chapter, using the layer-by-layer technique, brilliant yellow as a pH indicator and poly (allylamine hydrochloride) [PAH] as a cross-linker have been deposited on an uncladded silica fibre to create a wavelength dependent pH sensor. The wavelength shift can be demonstrated by the slope of Dose-Response graph and is the basis of the index for sensitivity used. The inflection point in the Dose-Response graph demonstrates the pK_a of the thin film, which is a function of the degree of ionization, revealing the pH at which 50% of the thin film functional groups are ionized [22, 23]. The pK_a is given by $-\log_{10}K_a$ where K_a is the acid dissociation constant which is the equilibrium constant of the dissociation reaction in the context of the acid-base reaction, in which an acid is ionized reversibly into its conjugate base and the hydrogen ion.

Table 6-1 Dose-Response curve properties for the prepared probes.

Probe Code	Shape		Core diameter (μm)	C_{ev} (mM)	Number of kilauers (L)	pH at inflection point (pKa)	gradient in the inflection point	Adj. R-square	Wavelength		Wavelength shift/0.2 pH units	pH units/ μm		
									at pH 7	at pH 9				
P01	Straight		600	0.25	3.5	7.96	119.868	0.998	457.28	494.78	3.749	0.053		
P02			"	"	4	7.69	128.224	0.997	461.66	499.71	3.804	0.053		
P03			"	"	5	7.65	150.724	0.996	457.31	497.15	3.984	0.050		
P04			"	"	5.5	7.74	177.610	0.994	462.96	504.79	4.182	0.048		
P05			"	"	6	7.56	148.703	0.996	459.46	505.98	4.654	0.043		
P06			"	"	6.5	7.81	155.845	0.998	467.87	512.64	4.477	0.045		
P07			"	"	7.5	7.83	127.530	0.999	471.79	513.82	4.203	0.047		
P08			"	"	8	7.71	126.514	0.996	471.85	511.32	3.947	0.051		
P09			"	"	8.5	7.84	89.201	0.996	482.97	514.10	3.113	0.064		
P10			"	"	9	7.72	85.397	0.998	487.28	515.20	2.792	0.072		
P11			"	"	9.5	7.87	82.238	0.999	491.61	517.37	2.575	0.078		
P12			"	"	1000	"	6	8.21	203.929	0.998	457.34	503.18	4.583	0.047
P13			"	"	"	0.5	6	8.46	183.690	0.997	456.52	499.31	4.279	0.044
P14	U-bend		"	0.25	6	8.03	111.826	0.994	474.01	513.7	3.969	0.063		
P15			"	0.5	6	8.36	79.361	0.996	477.97	509.78	3.181	0.051		
P16			"	0.25	6	8.00	193.694	0.994	450.94	505.39	5.446	0.039		
P17			"	0.5	6	8.21	161.422	0.998	452.13	503.76	5.163	0.037		

There are many evidences that illustrated [16, 23-28] that the effective pK_a of a polyelectrolyte substantially differs from solution state value when incorporated into a multilayer film. Reviewing the device response to wavelength change, the sensitivity of the probes is limited. However, levels of sensitivity are significant over the pH range from 7 to 9, for almost all probes used that were coated with

PAH/BY. In this pH range the wavelength shift is clearly measurable, demonstrating that the wavelength shift can be considered as an effective measure of sensitivity.

Two main properties are discussed in this section; the sensitivity and pK_a . In all the experiments carried out, changing the nature of the coating (comprising of components which are active at a specific wavelength) changes the performance of the probes. Changing key factors such as the number of bilayers used, the thickness of these layers and the number of molecules (the density) constituting the layers (resulting from changing the concentration of the polyelectrolyte solution) and also the shape of the probe causes a change in the polarity of the micro-environment and thus the measurements made with the probe, allowing for the optimization of the device sensitivity.

6.3.1 Number of layers

The set of experiments undertaken initially used probes with 600 micron core diameter deposited with 3.5 bilayers to 9.5 bilayers of (PAH/BY) in which concentration of BY solution was 0.25mM. The absorbance spectra for these sensors are shown in Fig 6-3, Fig 6-4, Fig 6-5, Fig 6-6, Fig 6-7 and Fig 6-8 and Dose-Response graphs are presented in Fig 6-9, Fig 6-10, Fig 6-11 and Fig 6-12. The single most striking observation to emerge from the graphs is working at higher wavelengths once the number of bilayers increases, nonetheless it can be seen that the slope of graphs are decreasing.

The slope of Dose-Response graph in inflection point for the probe with 3.5 bilayers coded as P01 is ~ 120 nm/pH unit. The second probe with 4 bilayers shows a greater sensitivity, since its slope increases to ~ 128 nm/pH unit. This amount proportionally increases with number of bilayers to maximum 178 nm/pH unit for a probe with 5.5 bilayers. However, the probe with 6 bilayers shows a sensitivity that begins to decrease with a slope of 149 nm/pH unit.

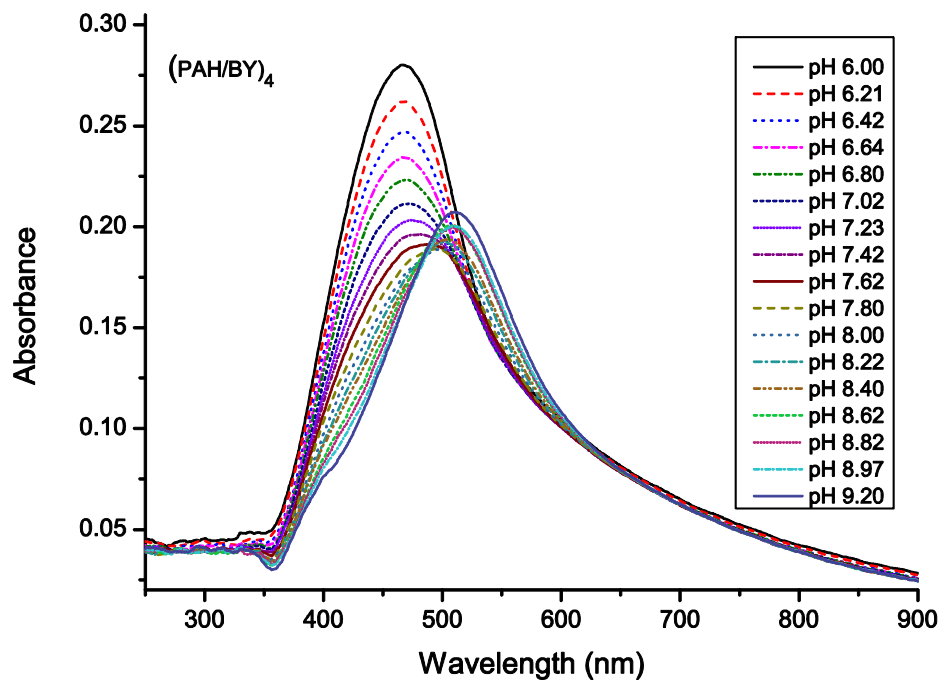


Fig 6-3 Absorbance spectra for the straight optical fibre coated using 4 bilayers of (PAH/BY) in different pH buffer solutions.

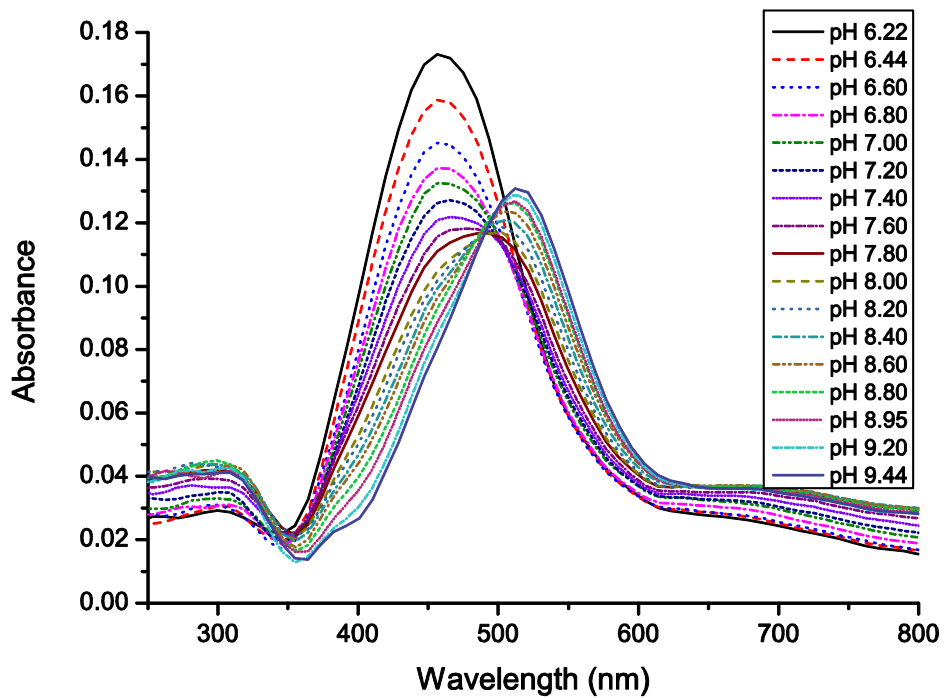


Fig 6-4 Absorbance spectra for the straight optical fibre coated using 5.5 bilayers of (PAH/BY) in different pH buffer solutions.

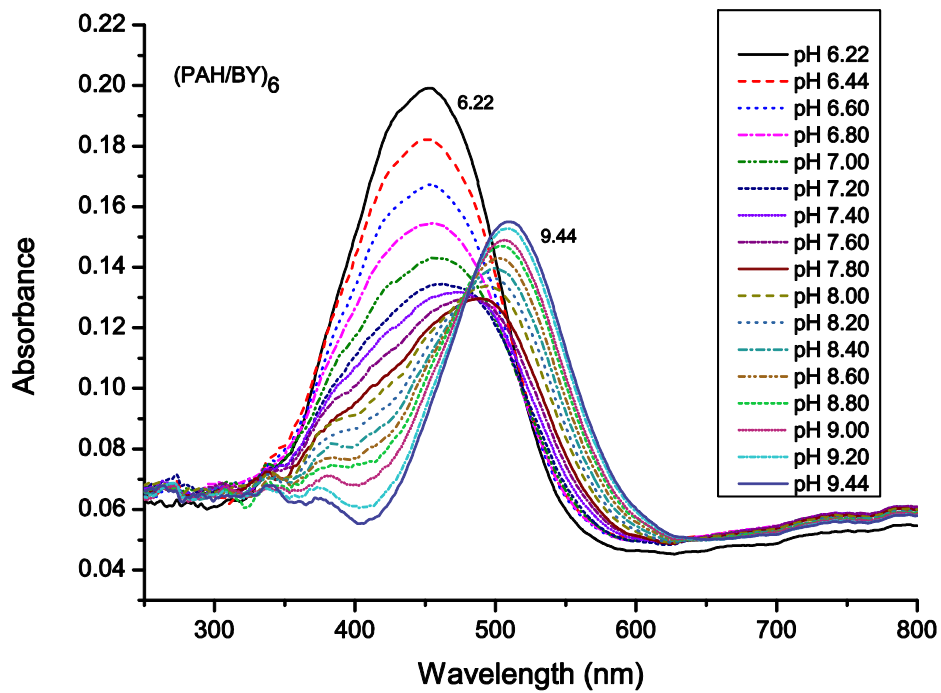


Fig 6-5 Absorbance spectra for the straight optical fibre coated using 6 bilayers of (PAH/BY) in different pH buffer solutions.

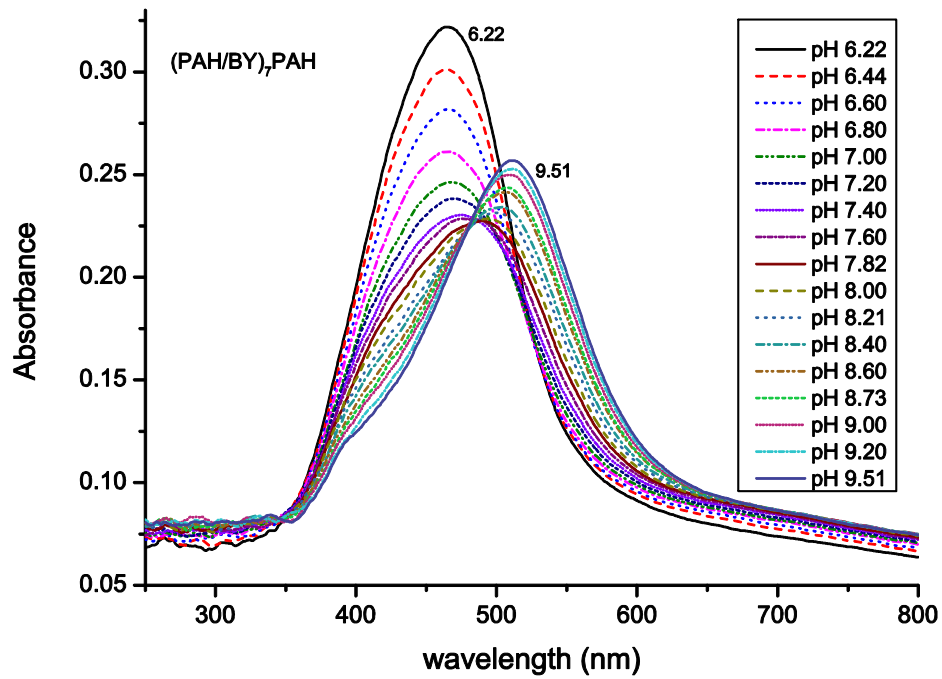


Fig 6-6 Absorbance spectra for the straight optical fibre coated using 7.5 bilayers of (PAH/BY) in different pH buffer solutions.

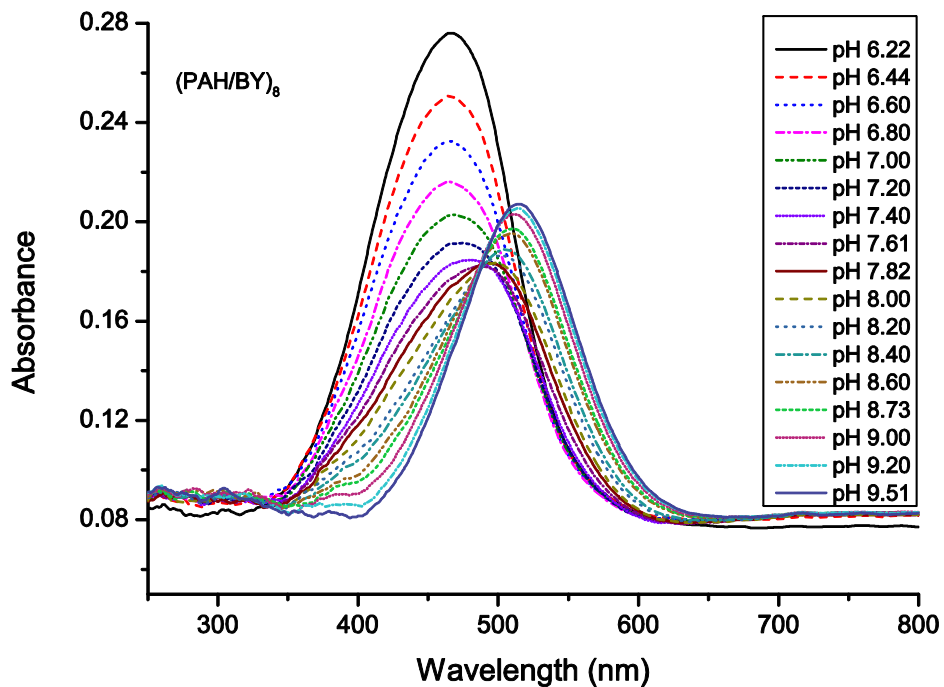


Fig 6-7 Absorbance spectra for the straight optical fibre coated using 8 bilayers of (PAH/BY) in different pH buffer solutions.

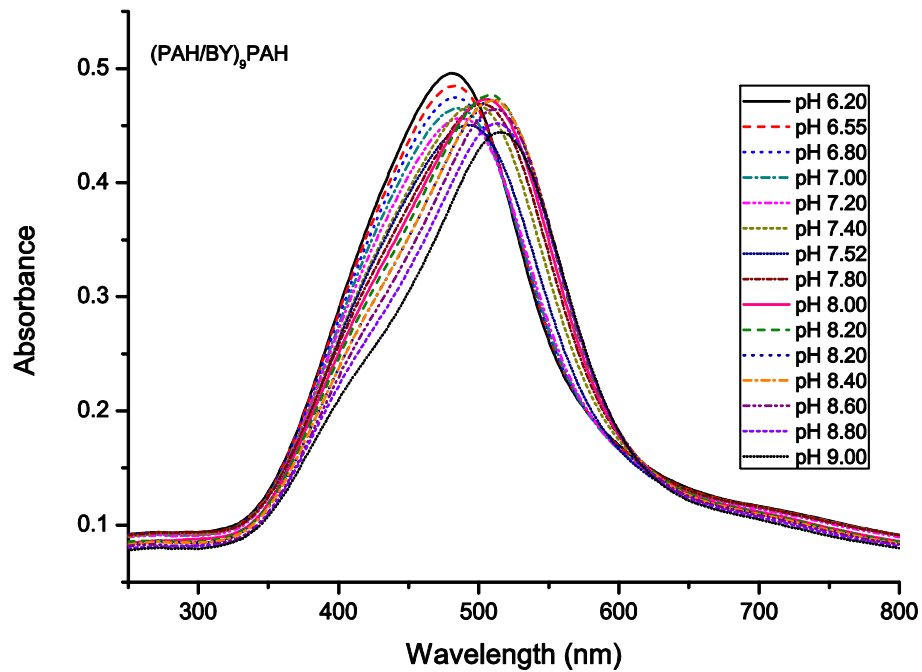


Fig 6-8 Absorbance spectra for the straight optical fibre coated using 9.5 bilayers of (PAH/BY) in different pH buffer solutions.

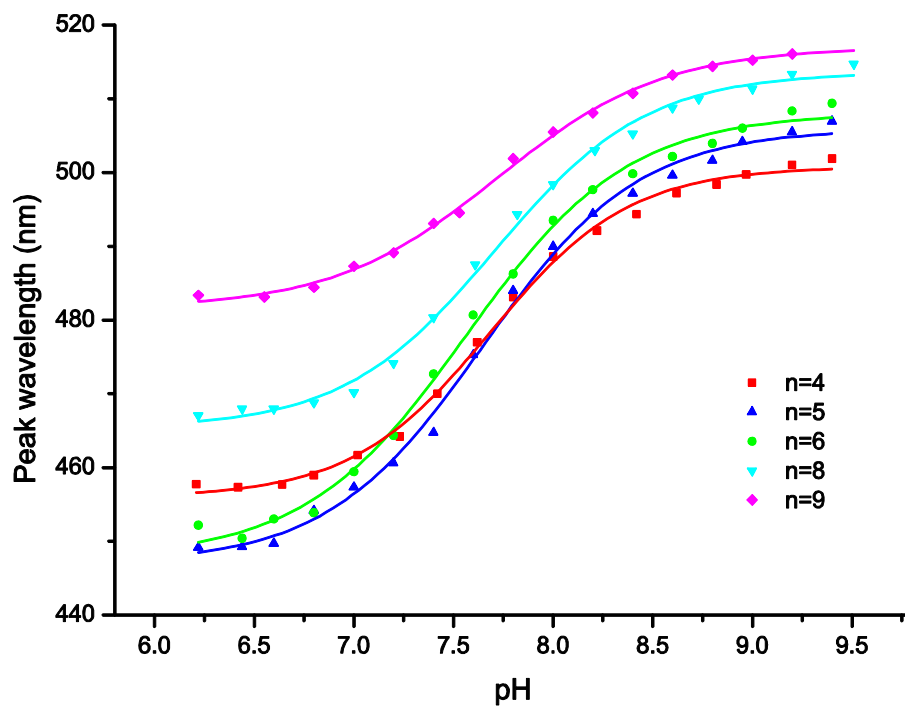


Fig 6-9 The peak wavelength for each spectrum with respect to pH for probes with different number of bilayers.

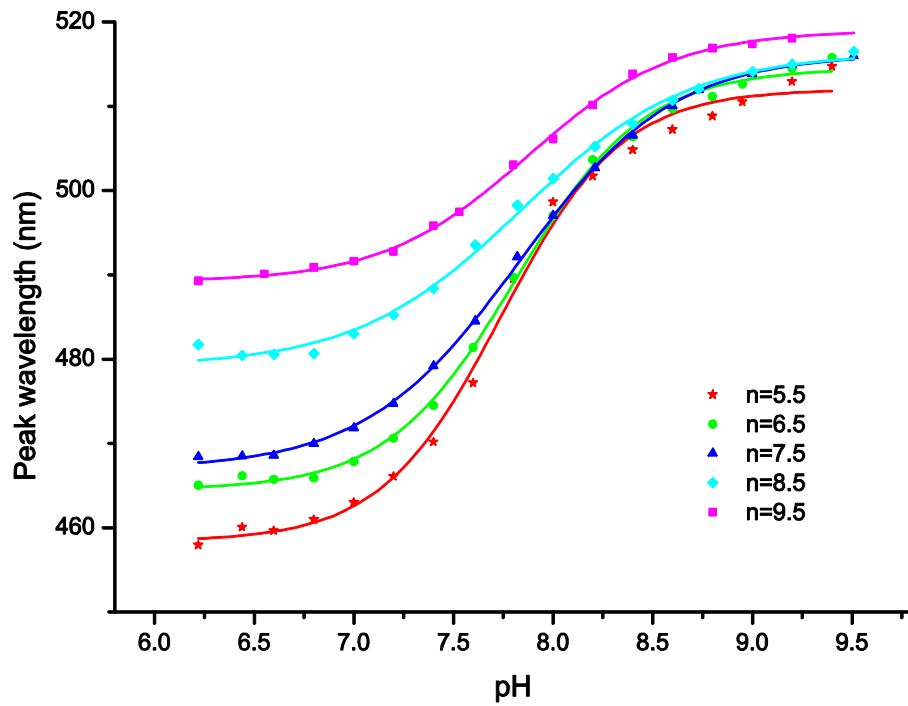


Fig 6-10 The peak wavelength for each spectrum with respect to pH for probes with different number of bilayers.

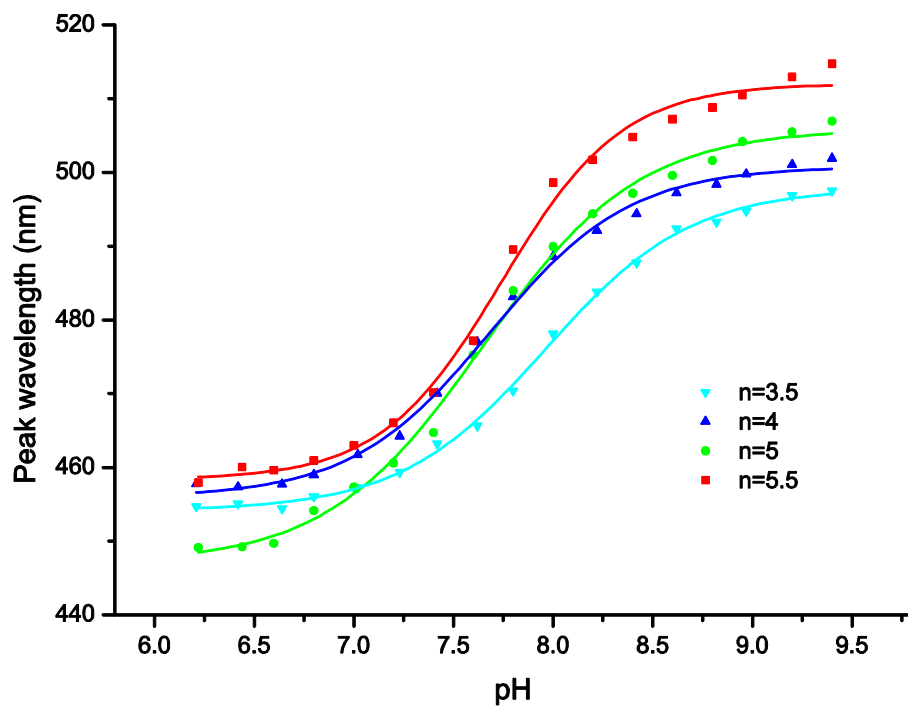


Fig 6-11 The peak wavelength for each spectrum with respect to pH for probes with different number of bilayers.

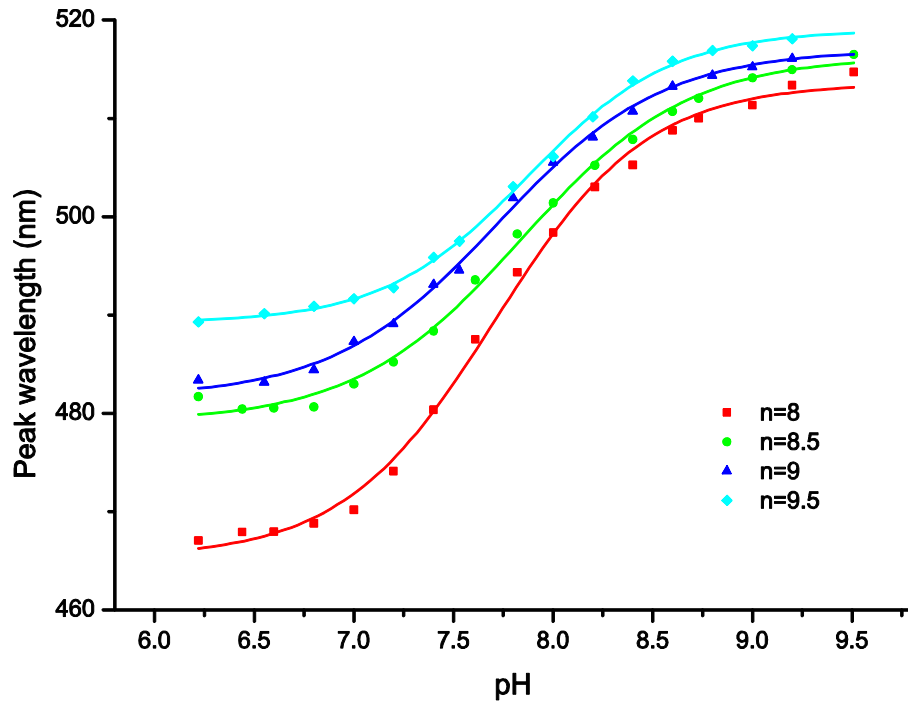


Fig 6-12 The peak wavelength for each spectrum with respect to pH for probes with different number of bilayers.

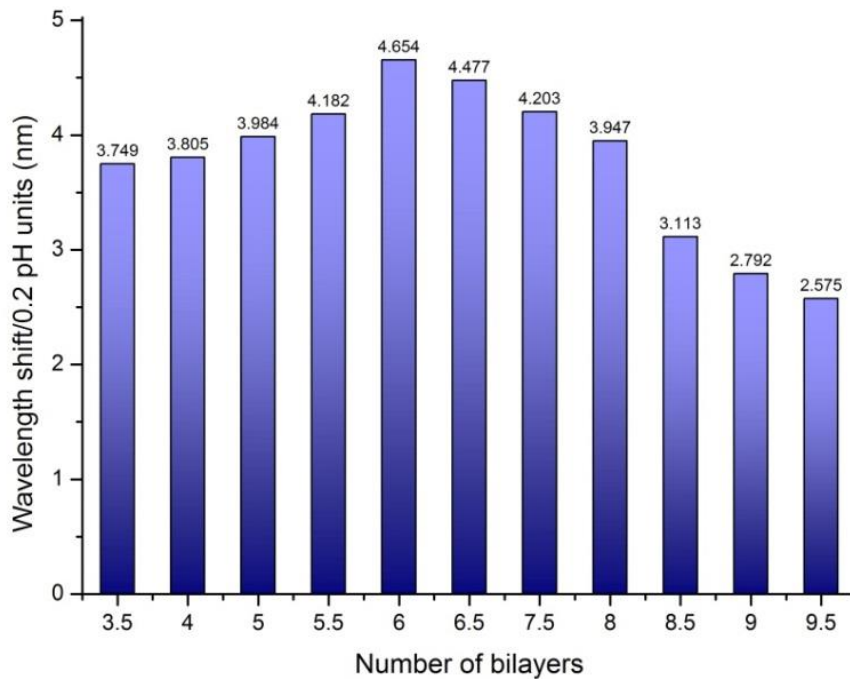


Fig 6-13 The average wavelength shift for a sample of 0.2 pH units at each measurement from pH 7 to pH 9 for the probes with 600 micron core diameter and 0.25mM of BY solution and different number of bilayers.

The slope for all probes beyond this shows a downward trend, as shown in Fig 6-13, whilst the slope reduction for the last three probes is somewhat less than other probes. Although it is expected that the sensitivity of the probe could be improved with the addition of more bilayers [29, 30] this series of experiments shows that a different behaviour is evident.

The sensitivity of a pH sensor is, of course, a measure of the degree of change in the sensor output with change in the solution pH. In optical sensors this transduction effect (that can then be related to the measurand) typically can be absorbance [31-33], reflected optical power [29, 30], transmitted power [34] or the wavelength at maximum absorbance [35], for example, and indeed other effects can be used. Therefore, the sensitivity of the device will depend on the optimum choice of this transduction mechanism – where for example, a cross-comparison of graphs in Fig 6-7 shows a significant change in absorbance from pH 6.22 to 7.20 for the probe coated with eight bilayers and the least change for the probe with 9.5 bilayers. Hence, an eight bilayer-deposited fibre creates a more sensitive device for use over the pH range 6.2 to 7.2 than it does with other number of bilayers coated fibre. Reviewing its response to wavelength, the sensitivity of these probes is limited over the range considered but for the higher pH range the wavelength shift is clearly measurable, especially for the probe coated with 5.5 to 6.5 bilayers which shows the highest slope and thus device sensitivity. This means that the sensitivity is significant over the pH values from pH 7 to pH 9 for all probes coated with BY.

As far as the average peak wavelength shift for 0.2 pH units is concerned, it varies from 2.57 nm for the probe P11 to 4.65 for the probe P05 and the best sensitivity (measured per nm shift) is 0.043 pH units for the probe P05, with the least sensitivity seen being 0.08 pH units for the probe P11. The conclusion from this experiment is that increasing the number of bilayers does not necessarily increase the sensitivity and, in addition, the sensitivity can even decrease when the number of bilayers on the fibre is increased. Fig 6-13 confirms a continuous reduction of sensitivity for the probes ranging from P06 to P11 and there is a dramatic decline in sensitivity for the probes from P08 to P11, although, the probes with fewer than 5 bilayers are not as sensitive as the probes P04, P05 and P06. This may arise due to lower stability of the layers as the thin film may not be sufficiently stable in cases of both very high and very low thickness values [29, 30]. Considering the data shown in Fig 6-11 and Fig 6-12 the probes coated with more than 6 bilayers demonstrate a slightly different behaviour in comparison to those probes with fewer than 6 bilayers. With the higher number of bilayers ($n > 6$), each probe with more coated layers (than 6) has a peak which tends to move up to a higher wavelength. The onset point for each graph (as a function of the number of bilayers) varies both up and down as a probe with more deposited layers starts from the greater peak wavelength at lower pH region by contrast all the graphs approach convergence in the higher pH regions.

In spite of the fact that all the probes considered demonstrate their peak sensitivity in the pH range 7 to 9, they do not have the same inflection point

and, as a result, the same pK_a . With reference to Table 6-1, the value of pK_a varies from one probe to another. The outer layer in the thin film directly effects the pK_a ; overall, a thin film terminated with a PAH shows a higher pK_a compared to a probe terminated with BY, as shown in Fig 6-14.

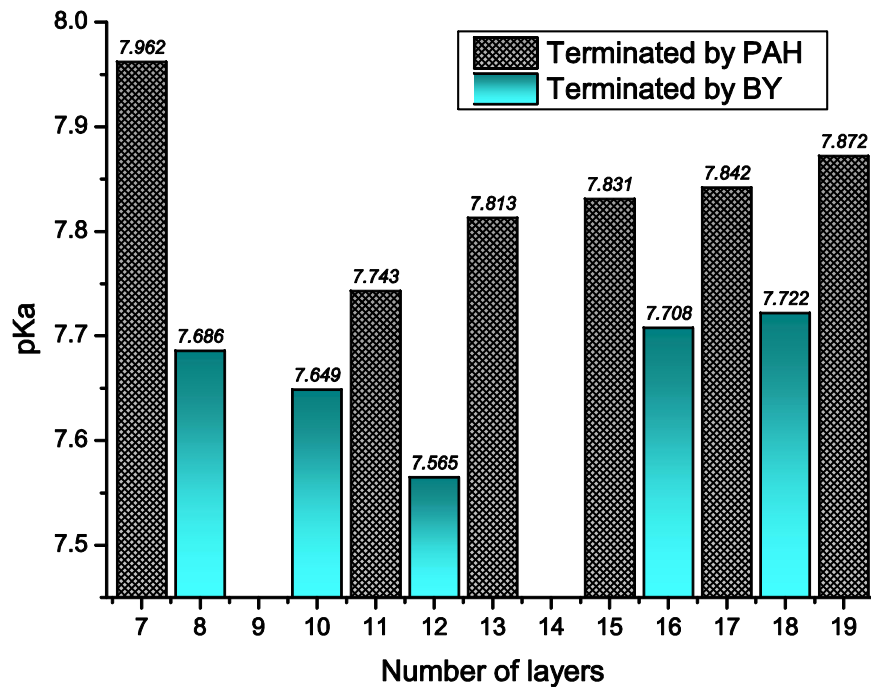


Fig 6-14 The value of pK_a for each probe versus number of layers.

The PAH film is individually applied as a pH indicator [23, 32, 35] for which the value of pK_a is reported to be between 8.0 and 8.8 [23, 36-39], whereas the pK_a value for BY is 7.2 [40]. It is clear that they substantially influence each other and the pK_a of the multilayer built up with their combination between pK_a values of PAH and BY. The values obtained from this series of experiments (represented in Table 6-1) confirm this claim. The average pK_a value for an odd number of layers (where the PAH is the outer layer) is 7.84 whilst for an even

number of layers (where the BY is outer layer) is 7.66. However, an interesting observation is that the pK_a value for both the odd and even number of layers decreases with an increase in the thickness of the thin film from 5.5 to 6 bilayers, whilst beyond this the pK_a value starts to go up with an increasing number of bilayers. This means that the sensitivity of the probes slightly shifts to the alkaline region when more layers are deposited onto the fibre. In addition, when the PAH is applied as the outer layer, the pK_a of the multilayer film rises to reach a higher level; in other words, when there is one more layer of PAH than BY, the probe shows greater sensitivity in the alkaline region because of higher association constant of the PAH compared to the BY.

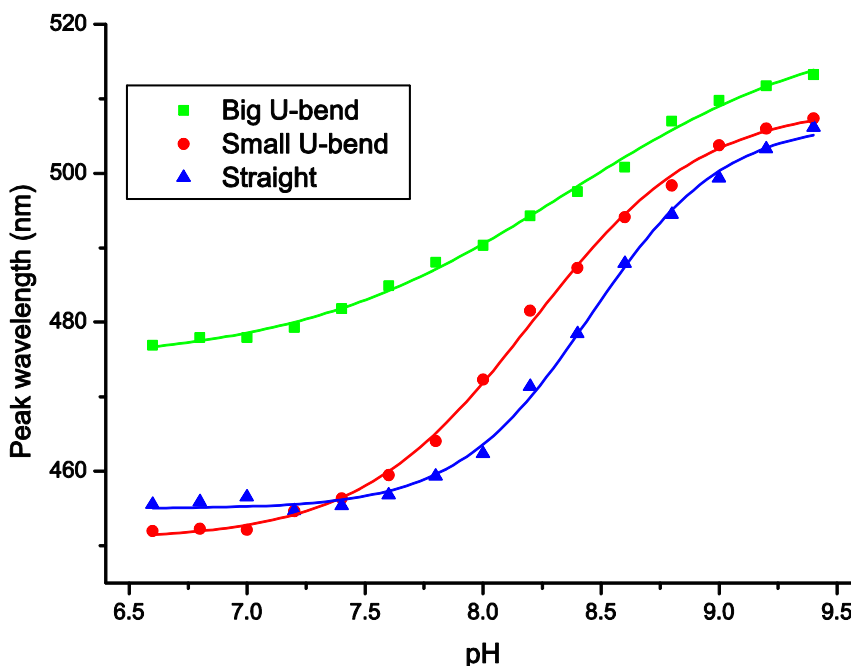


Fig 6-15 The peak wavelength for each spectrum with respect to pH for probes with different shapes when concentration of BY solution is 0.5 mM.

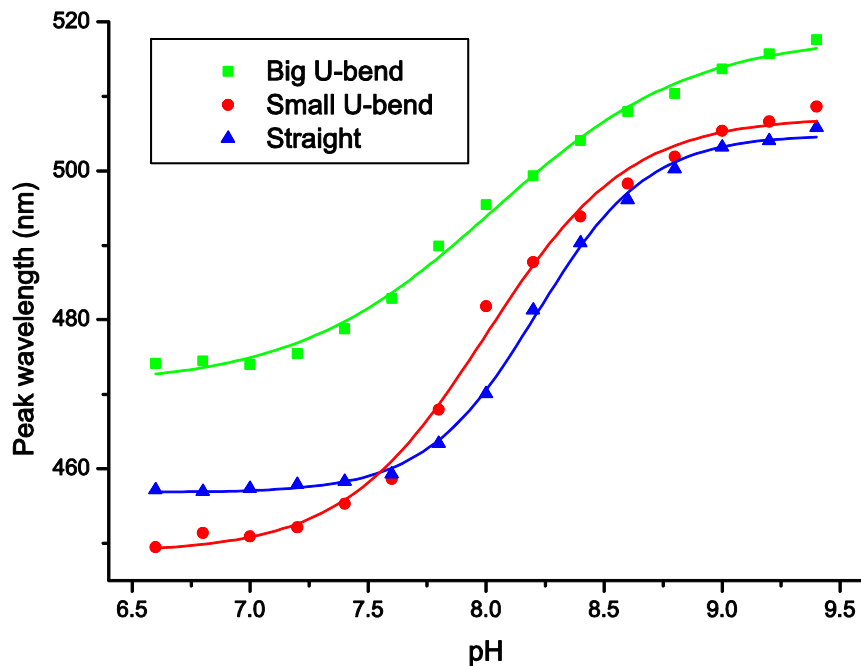


Fig 6-16 The peak wavelength for each spectrum with respect to pH for probes with different shapes when concentration of BY solution is 0.25 mM.

6.3.2 Shape of the probe

A series of experiments was carried out with the probes constructed using 1000 μ m core diameter and different shapes; both straight and U-bend with two different radii of 1.15 mm and 1.55 mm, as seen in Fig 6-1. The performance of these probes is summarised in Fig 6-15, Fig 6-16 and Fig 6-17 confirms that the two different sizes of the U-bend probes developed and fabricated demonstrate two different levels of sensitivity: the sensitivity of the larger radius ('big') U-bend not only is not as large as the sensitivity of the smaller radius ('small') U-bend – but it is also less than that of the straight probe. As is seen in Fig 6-17 probes P14 and P15 have the least sensitivity when compared to other probes.

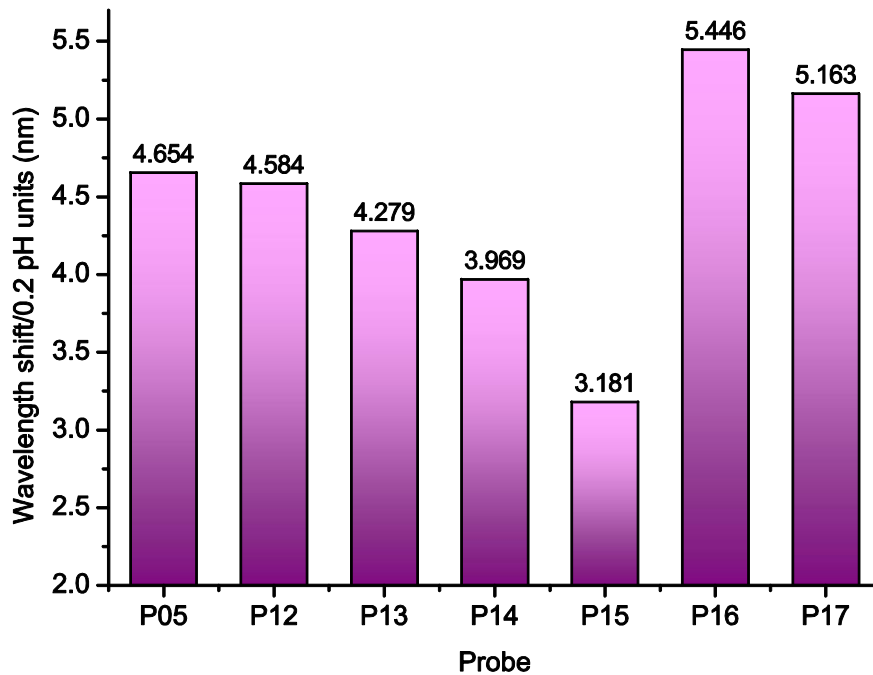


Fig 6-17 The average wavelength shift for a sample of 0.2 pH units at each measurement from pH 7 to pH 9 for the probes coated with (PAH/BY)₆ and variable properties.

Further, probes P16 and P17 display the greatest sensitivity with 5.45 and 5.14 nm wavelength shifts for just 0.2 pH units. The observation of decreasing sensitivity with increasing probe bend diameter has been discussed in a number of research papers [3, 12, 41, 42]. In contrast, it is also been reported in literature [1, 43-45] that there is an *increasing sensitivity with probe bend diameter*. Clearly in this body of work there are other factors at work than the probe bend diameter to influence the overall sensitivity of the system and the bending of the fibre plays a relatively minor role. The results obtained from this study show that the sensitivity of the sensor does not necessarily increase when the probes are bent into a U-shape despite the obvious attempts through that

geometry to increase the interaction between the optical wave and the analyte in the sensing region [44-47]. A further approach to achieving this is to coat the distal end of a straight fibre with a mirror surface, as was also done in this study. As Klepáček has shown in [48] that the *gradient* of refractive index of the core and the coated layers are effective parameters in optimizing the interaction of the light with the material, in addition to the effect of the radius of the bend and the overall fibre diameter. The interaction region in the U-bend probe is typically greater than for the straight probe, as the slope (measured at the inflection point) for the straight probes are 203 nm/pH unit and 184 nm/pH unit – this is seen to reduce in the cases of the ‘small’ and ‘big’ U-bend probes.

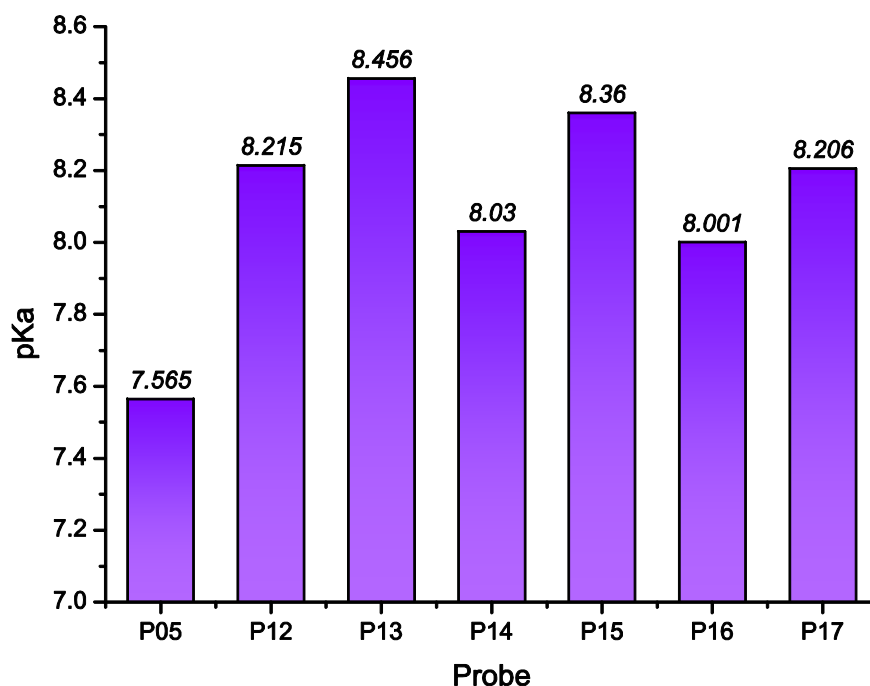


Fig 6-18 The value of pKa for each probe versus shape of the probes at different core diameter and concentration of BY.

Nonetheless, regardless the concentration of the BY solution used, the straight probes show the highest sensitivity in the pH range between 7.6 to 9.0, whereas the U-bend probes show a slightly wider range of sensitivity (from around pH 7.0 to 9.0). The values of pK_a (compared in Fig 6-18) also show that the straight probe shows the highest measured value while the ‘small’ U-bend probes have lower values of pK_a , when compared to the ‘big’ U-bend probes. Comparing the situation overall where all the parameters are the same for all the probes, it would appear that by increasing the probe radius, the most sensitive region shifts to a higher pH region and hence in the extreme where the probe is effectively straight (an infinite radius), the region of maximum sensitivity tends move towards the alkaline region.

6.3.3 Concentration of BY solution

To study the effect of the concentration of the indicator solution on the sensor performance, polyanion solutions of two different concentrations were utilized. Fig 6-19, Fig 6-20 and Fig 6-21 show a comparison of the performance of probes on which were deposited 6 bilayers of PAH/BY in which the BY concentration was 0.25 mM and then 0.5 mM, while the PAH concentration was 2.5 mM for both probes. As the graphs show, increasing the concentration shifts the response towards the higher pH region. Thus, the probes prepared with the low concentration of BY are active at a higher wavelength, at a specific values of pH. For instance, the U-bend fibre probes using 0.25 mM of BY solution is the basis of a device particularly sensitive for use over the pH range 7.2 to 9.0, while this most sensitive region is shifted to the pH range 7.4 to 9.2

for similar probes prepared using 0.5 mM of BY solution. This aligns with the pK_a values stated in Table 6-1. As illustrated by Table 6-1 and Fig 6-18, the value of pK_a increases when the concentration of BY is increased and the sensitive area moves towards the more alkaline i.e. the value of pK_a increases from 0.21 for the ‘small’ U-bend probe to 0.36 for the ‘big’ U-bend. For the straight probe, this quantity also shifts by 0.25 towards the alkaline region. Considering the data shown in Fig 6-19 to Fig 6-21 and Table 6-1, the sensors prepared with the lower concentration of BY show higher slopes of the Dose-Response graphs, consequently demonstrating higher sensitivity. Thus an enhancement of the sensitivity can be achieved by either decreasing the number of bilayers or lowering the concentration of the indicator solution.

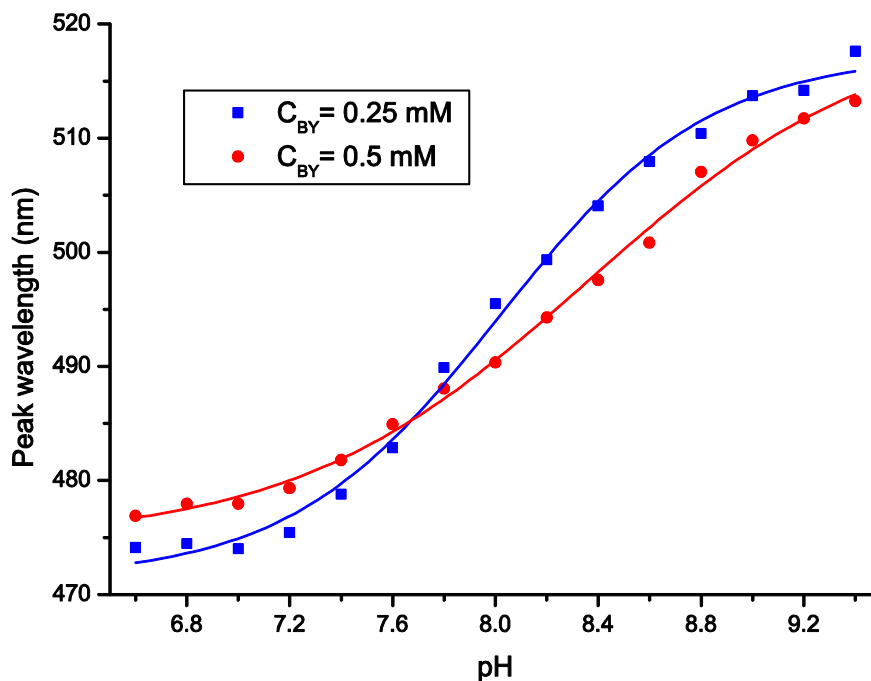


Fig 6-19 The peak wavelength for each spectrum with respect to pH in different concentrations of brilliant yellow solutions for big U-bend sensors.

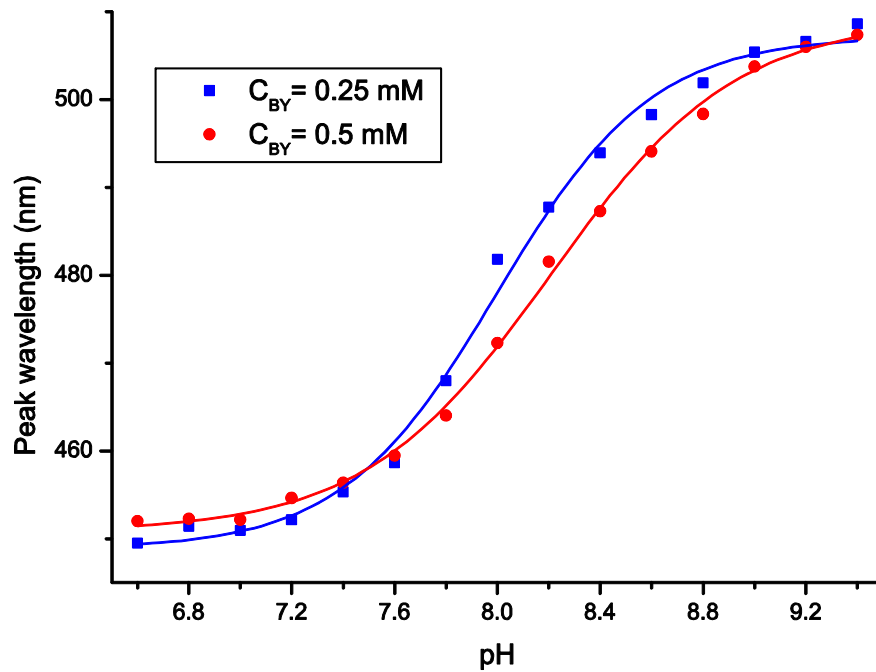


Fig 6-20 The peak wavelength for each spectrum with respect to pH in different concentrations of brilliant yellow solutions for small U-bend sensors.

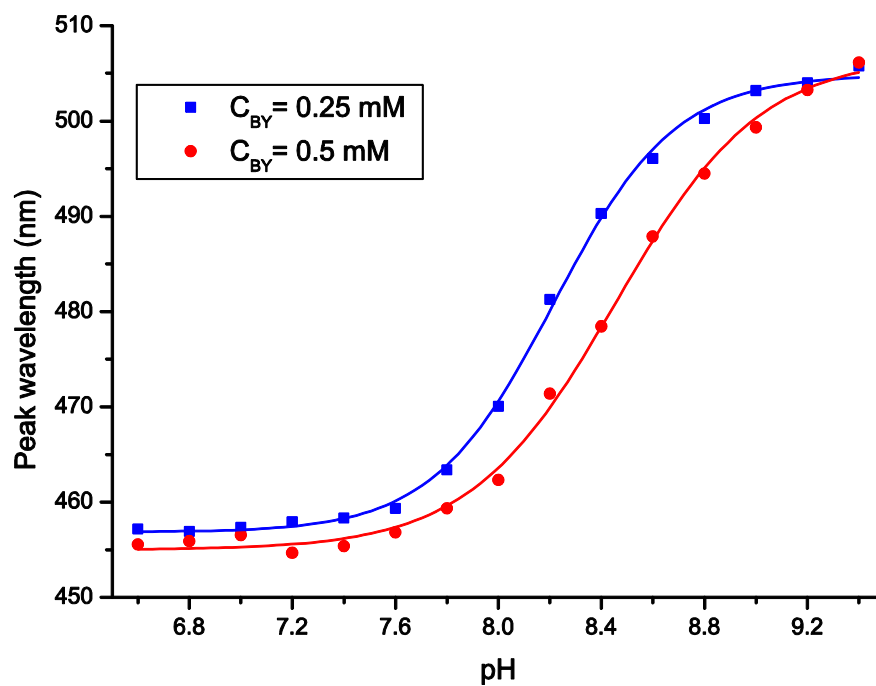


Fig 6-21 The peak wavelength for each spectrum with respect to pH in different concentrations of brilliant yellow solutions for straight sensors.

6.3.4 Fibre core diameter

To determine the effect of the optical fibre core diameter on the probe performance, experiments were carried out on probes fabricated using two different core size fibres. Fig 6-22 shows a comparison of the performance of these two fibre optic sensors deposited with 6 bilayers of PAH/BY while the concentration of BY solution was maintained at 0.25 mM for both probes. As can be seen in the figure, the sensitivity of the sensor fabricated from 1mm core diameter fibre is limited over pH values from pH 7.6 to pH 9.0, when compared to the sensor using narrow core fibre for which the sensitivity is optimal over the wider range from pH 6.6 to pH 9.2. Considering the slope at the inflection point from Table 6-1, the probe fabricated with the narrow fibre displays a lower slope compared to the one with greater fibre diameter. However, the average wavelength shifts for a sample of 0.2 pH units (in the region from pH 7 to pH 9) is 4.65 and 4.28 for the probes using the narrow and the large core fibres respectively, as shown in Fig 6-17. Thus although the narrow core fibre can give a satisfactory sensitivity over a wide pH range, the large core fibre enables a more sensitive device, over a smaller pH range to be created – this also showing a greater slope and higher resolution for the higher pH region. In contrast, Khijwania and Gupta showed in their work [49] that an enhanced sensitivity is achieved by decreasing the core size. Referring to Fig 6-18 and comparing the value of pKa for different probes, P05 demonstrates a value of 7.57 for the pKa, while for P12 it rises to 8.22. Hence the larger diameter probe can create a sensor working efficiently. However, this is over a small pH range

centred around a value of 8.2. On the other hand, examining the region from pH 7 onwards, for the same pH values, the sensor with the narrow fibre core tends to operate at a higher wavelength value.

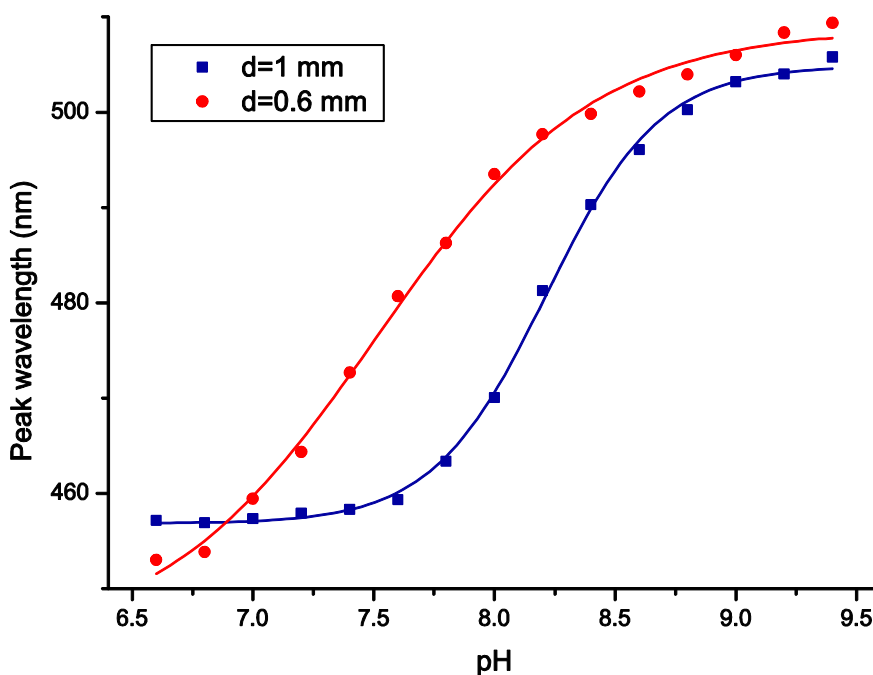


Fig 6-22 The peak wavelength for each spectrum with respect to pH for probes with different core diameter. The wide fibre (P12) and the narrow one (P05).

6.4 Summary

In this chapter, the design and performance of a number of pH-sensitive probes using brilliant yellow as the pH indicator, with PAH being utilized as a cross-linker, were studied and evaluated. The absorbance spectra as a function of wavelength for each probe at different buffer pH solutions was plotted and

discussed, for each a Dose-Response graph from the peak wavelength points was created and studied. The key design parameters such as the number of bilayers, the shape of the probe, the concentration of the indicator solution and the core diameter of the optical fibre used were all studied and their effects on performance evaluated. Key findings from this study can be summarized as follows:

- Those probes with 5 to 6 bilayers demonstrated the best performance. It has also been observed that the sensitivity of the probes improves with an increasing number of bilayers (optimizing typically at about 5 to 6 bilayers) and beyond this a reduction of sensitivity occurs with an increasing number of bilayers.
- The sensitivity can be enhanced by curving the fibre to a U-shape – in this case with a smaller radius for better performance. A lower sensitivity was observed for a larger curve radius, by comparison to the performance of a ‘straight’ sensor.
- With only two samples available in this work (at concentrations of (0.25 and 0.5 mM)) it would appear that further improvement in sensitivity would be achieved where the concentration of the indicator solution was lower. For a higher concentration (of BY solution), the devices are less sensitive. However this needs further experiments with a wider range of samples of different concentrations.
- In addition, a design utilizing a narrow core fibre leads to a sensor with a wider sensitivity range, compared to a larger core fibre. With this design, a

highly sensitive sensor but working over a smaller pH range and with a sharper slope and higher resolution is seen.

The second major finding was that pK_a value varies from one probe design to another. The pK_a slowly rises with an increasing number of layers, with the contrary behaviour seen for a smaller number of layers and further, the outer layer of thin film also clearly influences the pK_a value. In summary:

- Increasing the number of layers shifts the sensitivity towards higher pH and the more alkaline region.
- ‘Straight’ probes work best in the more alkaline region compared to U-bend probes
- For probes with a bigger radius the value of pK_a tends to slightly higher values.
- In addition, the role of the concentration of the BY solution must be considered since preparing the sensors with a low concentration of BY leads to lower pK_a values while the sensors prepared with higher concentration of polyanion solution work best in the higher pH region due to higher pK_a values.

References

- [1] M. Fabian, E. Lewis, T. Neue, S. Lochmann, and I. Mueller, "Investigation of ethanol and methanol water mixtures in the visible wavelength area using fibre-optic evanescent field absorption sensors based on a U-shaped, a coil-shaped and a meander-shaped probe," in *IEEE Sensors Applications Symposium* Atlanta, GA, 2008.
- [2] A. Armin, M. Soltanolkotabi, and P. Feizollah, "On the pH and concentration response of an evanescent field absorption sensor using a coiled-shape plastic optical fiber," *Sensors and Actuators A* vol. 165, pp. 181-184, 2011.
- [3] B. D. Gupta and N. K. Sharma, "Fabrication and characterization of U-shaped fiber-optic pH probes," *Sensors and Actuators B* vol. 82, pp. 89-93, 2002.
- [4] F. Wassmann, "Modal field analysis of circularly bent single-mode fibers," *Journal Of Lightwave Technology*, vol. 17, pp. 957-968, 1999.
- [5] V. L. Paul, "Integrated optical sensors for the chemical domain," *Measurement Science and Technology*, vol. 17, p. R93, 2006.
- [6] N. G. Hoogeveen, M. A. C. Stuart, and G. J. Fleer, "Polyelectrolyte adsorption on oxides .1. Kinetics and adsorbed amounts," *Journal of Colloid and Interface Science*, vol. 182, pp. 133-145, Sep 1 1996.
- [7] J. A. Jay., An Overview of Macrobending and Microbending of Optical Fibers 1-21, www.corning.com/opticalfiber, 2010
- [8] A. Salimi and A. Noorbakhsh, "Layer by layer assembly of glucose oxidase and thiourea onto glassy carbon electrode: Fabrication of glucose biosensor," *Electrochimica Acta*, vol. 56, pp. 6097-6105, 7/1/ 2011.
- [9] S. C. Howard, V. S. J. Craig, P. A. FitzGerald, and E. J. Wanless, "Swelling and Collapse of an Adsorbed pH-Responsive Film-Forming Microgel Measured by Optical Reflectometry and QCM," *Langmuir*, vol. 26, pp. 14615-14623, Sep 21 2010.
- [10] Y. Mendelson, "Optical Sensors," in *The Biomedical Engineering Handbook*, E. Joseph and D. Bronzino, Eds., Second Edition ed: CRC Press LLC, 2000.
- [11] S. Otsuki, K. Adachi, and T. Taguchi, "A novel fiber-optic gas-sensing configuration using extremely curved optical fibers and an attempt for optical humidity detection," *Sensors and Actuators B* vol. 53, pp. 91-96, 1998.
- [12] R. K. Verma and B. D. Gupta, "Theoretical modelling of a bi-dimensional U-shaped surface plasmon resonance based fibre optic sensor for sensitivity enhancement," *Journal of Physics D: Applied Physics*, vol. 41, p. 095106, 2008.

- [13] B. D. Gupta, H. A. Dodeja, and K. Tomar, "Fibre-optic evanescent field absorption sensor based on a U-shaped probe " *Optical and Quantum Electronics*, vol. 28, pp. 1629-1639 1996.
- [14] S. T. Lee, J. Gin, V. Nampoore, C. Vallabhan, N. V. Unnikrishnan, and P. Radhakrishnan, "A sensitive fibre optic pH sensor using multiple sol-gel coatings," *J. Opt. A: Pure Appl. Opt.*, vol. 3, pp. 355-359, 2001.
- [15] M. Yin, B. Gu, Q. Zhao, J. Qian, A. Zhang, Q. An, *et al.*, "Highly sensitive and fast responsive fiber-optic modal interferometric pH sensor based on polyelectrolyte complex and polyelectrolyte self-assembled nanocoating," *Analytical and Bioanalytical Chemistry*, vol. 399, pp. 3623-3631, 2011/04/01 2011.
- [16] H. H. Qazi, A. B. bin Mohammad, and M. Akram, "Recent Progress in Optical Chemical Sensors," *Sensors* vol. 12, pp. 16522-16556, 2012.
- [17] L.-Y. Shao, M.-J. Yin, H.-Y. Tam, and J. Albert, "Fiber Optic pH Sensor with Self-Assembled Polymer Multilayer Nanocoatings," *Sensors*, vol. 13, pp. 1425-1434, 2013.
- [18] Y. Zhiyong, E. Mielczarski, J. Mielczarski, D. Laub, P. Buffat, U. Klehm, *et al.*, "Preparation, stabilization and characterization of TiO₂ on thin polyethylene films (LDPE). Photocatalytic applications," *Water Research* vol. 41, pp. 862 - 874, 2007.
- [19] S. Prakash, T. Chakrabarty, A. K. Singh, and V. K. Shahi, "Polymer thin films embedded with metal nanoparticles for electrochemical biosensors applications," *Biosensors and Bioelectronics*, vol. 41, pp. 43-53, 2013.
- [20] G. Beltrán-Pérez, F. López-Huerta, S. Muñoz-Aguirre, J. Castillo-Mixcóatl, R. Palomino-Merino, R. Lozada-Morales, *et al.*, "Fabrication and characterization of an optical fiber pH sensor using sol-gel deposited TiO₂ film doped with organic dyes," *Sensors and Actuators B: Chemical*, vol. 120, pp. 74-78, 2006.
- [21] B. Gu, M.-J. Yin, A. P. Zhang, J.-W. Qian, and S. He, "Low-cost high-performance fiber-optic pH sensor based on thin-core fiber modal interferometer," *Optics Express*, vol. 17, pp. 22296- 22302, 2009.
- [22] D. Yoo, S. S. Shiratori, and M. F. Rubner, "Controlling bilayer composition and surface wettability of sequentially adsorbed multilayers of weak polyelectrolytes," *Macromolecules*, vol. 31, pp. 4309-4318, 1998.
- [23] M. F. R. Jeeyoung Choi, "Influence of the Degree of Ionization on Weak Polyelectrolyte Multilayer Assembly," *Macromolecules*, vol. 38, pp. 116-124, 2005.
- [24] A. J. Nolte, N. Takane, E. Hindman, W. Gaynor, M. F. Rubner, and R. E. Cohen, "Thin film thickness gradients and spatial patterning via salt etching of polyelectrolyte multilayers," *Macromolecules*, vol. 40, pp. 5479-5486, Jul 24 2007.

- [25] F. Boulmedais, C. S. Tang, B. Keller, and J. Vörös, "Controlled Electrodeposition of Polyelectrolyte Multilayers: A Platform Technology Towards the Surface-Initiated Delivery of Drugs," *Advanced Functional Materials*, vol. 16, pp. 63-70, 2006.
- [26] B. Schoeler, E. Poptoshev, and F. Caruso, "Growth of Multilayer Films of Fixed and Variable Charge Density Polyelectrolytes: Effect of Mutual Charge and Secondary Interactions," *Macromolecules*, vol. 36, pp. 5258-5264, 2003/07/01 2003.
- [27] K. A. Hunter, *Acid-base chemistry of aquatic systems*. Dunedin, New Zealand: University of Otago, 1998.
- [28] O. Mermut and C. J. Barrett, "Stable sensor layers self-assembled onto surfaces using azobenzene-containing polyelectrolytes," *Analyst*, vol. 126, pp. 1861-1865, 2001.
- [29] I. D. Villar, I. R. Matias, and F. J. Arregui, "Fiber-optic chemical nanosensors by electrostatic molecular self-assembly," *Current Analytical Chemistry*, vol. 4, pp. 341-355, 2008.
- [30] I. D. Villar, I. R. Matías, F. J. Arregui, and R. O. Claus, "ESA-based in fiber nanocavity for hydrogen peroxide detection," *IEEE Transactions On Nanotechnology*, vol. 4, pp. 187-193, 2005.
- [31] J. Lin, "Recent development and applications of optical and fiber-optic pH sensors," *Trends in analytical chemistry*, vol. 19, pp. 541-552, 2000.
- [32] J. Goicoechea, C. R. Zamarreño, I. R. Matías, and F. J. Arregui, "Optical fiber pH sensors based on layer-by-layer electrostatic self-assembled Neutral Red," *Sensors and Actuators B: Chemical* vol. 132, pp. 305-311, 2008.
- [33] S. Kodaira, S. Korposh, S.-W. Lee, W. J. Batty, S. W. James, and R. P. Tatam, "Fabrication of highly efficient fibre-optic gas sensors using SiO₂/polymer nanoporous thin films," in *3rd International Conference on Sensing Technology*, Tainan, Taiwan, 2008.
- [34] I. R. Matias, F. J. Arregui, J. M. Corres, and J. Bravo, "Evanescent field fiber-optic sensors for humidity monitoring based on nanocoatings," *IEEE Sensors Journal*, vol. 7, pp. 89-95, 2007.
- [35] C. R. Zamarreño, M. Hernández, I. D. Villar, I. R. Matías, and F. J. Arregui, "Optical fiber pH sensor based on lossy-mode resonances by means of thin polymeric coatings," *Sensors Actuat B-Chem* vol. 155, pp. 290-297, 2011.
- [36] M. M. Fang, C. H. Kim, G. B. Saupe, H. N. Kim, C. C. Waraksa, T. Miwa, *et al.*, "Layer-by-layer growth and condensation reactions of niobate and titanoniobate thin films," *Chemistry of Materials* vol. 11, pp. 1526-1532, 1999.

- [37] Y. Yoshikawa, H. Matsuoka, and N. Ise, "Ordered structure of polyallylamine hydrochloride in dilute-solutions as studies by small-angle X-ray-scattering," *Brit Polym J* vol. 18, pp. 242-246, 1986.
- [38] H. Ochiai, Y. Anabuki, O. Kojima, K. Tominaga, and I. Murakami, "Dissociation of poly(allylammonium) cations in salt solutions," *Journal of Polymer Science Part B: Polymer Physics*, vol. 28, pp. 233–240, 1990.
- [39] A. I. Petrov, A. A. Antipov, and G. B. Sukhorukov, "Base-acid equilibria in polyelectrolyte systems: From weak polyelectrolytes to interpolyelectrolyte complexes and multilayered polyelectrolyte shells," *Macromolecules*, vol. 36, pp. 10079-10086, 2003.
- [40] R. W. Sabnis, *Handbook of acid-base indicators*: Taylor & Francis Group, 2008.
- [41] P. Nath, "Enhanced sensitivity fiber-optic sensor with double pass evanescent field absorption," *Microwave And Optical Technology Letters*, vol. 51, pp. 3004-3006, 2009.
- [42] B. D. Gupta, H. Dodeja, and A. K. Tomar, "Fibre-optic evanescent field absorption sensor based on a U-shaped probe," *Optical and Quantum Electronics*, vol. 28 pp. 1629-1639, 1996.
- [43] Dgardner. (Oct 23, 2012). *0.37 NA and 0.39 NA Step-Index Multimode Fibers*.
- [44] S. K. Khijwania, K. L. Srinivasan, and J. P. Singh, "An evanescent-wave optical fiber relative humidity sensor with enhanced sensitivity," *Sensors and Actuators B*, vol. 104, pp. 217-222, 2005.
- [45] P. K. Choudhury and T. Yoshino, "On the pH response of fiber optic evanescent field absorption sensor having a U-shaped probe: An experimental analysis," *Optik* vol. 114, pp. 13-18, 2003.
- [46] B. D. Gupta and Ratnanjali, "A novel probe for a fiber optic humidity sensor," *Sensors and Actuators B*, vol. 80, pp. 132-135, 2001.
- [47] R. Jindal, S. Tao, J. P. Singh, and P. S. Gaikwad, "Fast-Responsive opticalFiber relative humidity sensor," in *Fiber Optic Sensor Technology and Applications 2001*, pp. 314-319.
- [48] R. Klepáček and L. Kalvoda, "Monte Carlo simulation of light propagation in U-bent optical fiber," in *Optical Sensors 2011; and Photonic Crystal Fibers V*, 2011.
- [49] S. K. Khijwania and B. D. Gupta, "Fiber optic evanescent field absorption sensor: Effect of fiber parameters and geometry of the probe," *Optical and Quantum Electronics*, vol. 31, pp. 625-636, 1999.

7. Stabilization and Reusability

7.1 Introduction

The layer-by-layer technique is one of the deposition methods widely used to coat thin films on to optical substrates and optical fibres. The layer-by-layer (LbL) technique is used to build up a sufficient thickness of such material on the fibre and is based on the electrostatic attraction between oppositely charged molecules to create the layers and thereby increase the overall coating thickness [1]. The principal advantage of the use of this technique is the ability to create stable deposited thin films with well-organized structure and controlled nanometer thicknesses on substrates of various shapes and sizes [2-7]. Generally, the thin films created by using the LbL technique are stable [2, 8], and it is difficult to remove them from a solid substrate. There are two main methods to remove LbL deposited films, should this be needed. First, a solution of high pH can be used which will attack the first polycation layer and destroy the ionic bonds that stabilize the films. A second method is to expose the LbL multilayers to a solution with very high ionic strength, such as 3M NaCl, under sonication for approximately 2– 3 hours [9]. Destruction of the layers happens when the coated surface is immersed into the high pH buffer solution. For practical applications, especially those needing continuous monitoring, it is

critical to have a pH probe that can give consistent results and survive for as long as possible. However, the destruction of the layers limits the life of the probe and does not make it as suitable for continuous monitoring. A variety of techniques has been proposed to improve the stability of the film and to avoid progressive destruction of the coating. Ionic strength, pH, concentration of the polyion solutions and the presence of a copolymer such as salt affect the LbL assembly, the film thickness and its stability [2, 3]. Heat treatment is also an important process which has been discussed in many works in the literature [10-12] to achieve a higher stability of the thin films and avoid problems with the destruction of the films when they are immersed in buffer solutions of different values of pH [13, 14]. However this sort of treatment affects the sensor performance and decreases its sensitivity [14], as well as allowing for a degradation of the indicator dyes used which happens at high temperatures.

The stability of thin films thus generated does depend on the interaction between the layers, such as through the formation and destruction of hydrogen bonds. Hence, the stabilization of the LbL-assembled films via polyamide bond formation was a further method reported in the literatures [15-17]. The amine coupling reaction can easily allow a cross-linkage of an amino group to a cationic polyelectrolytes and a carboxyl group on anionic polyelectrolytes via amide bond formation. There is a further report in the literature [18] which focused on the film stability under chlorine treatment as a means to improve the stability of the LbL-assembled nanofiltration membranes in combined high ionic strength conditions and under chlorine treatment. In another approach, the

stabilizing of the thin film is achieved by forming siloxane bonds owing to a silane coupling reaction between oppositely charged polyelectrolytes which leads to the crosslinking between the silane groups [18, 19]. Egawa et al. demonstrated [20] crosslinking between the sulfonate group in the polyanion and the diazonium ion in polycation due to exposure to UV light.

An alternative approach is to build up several capping layers using different materials such as nanoparticles to enhance the film stability. Prakash et al. [21] discussed applying nanoparticles to achieve an adequate sensitivity and stability with the modification of the sensors (or biosensors) with nanomaterials such as gold and/or silver nanoparticles [6, 22, 23], carbon nanomaterials [24, 25] and silica nanoparticles [26] and these have shown considerable promise. Putzbach et al. reported that the immobilization of enzymes improves stability of the biosensor discussed [27]. In further work reported in the literature [28], a coating of 5 nm layers of Al or 1 nm layers of EuS (Europium (II) sulfide) was applied as a covering layer to stabilize ultrathin tin films and reduce the diffusion of tin atoms. Abdelghani et al. used long chain alkanethiols to protect a silver film from oxidation and thus increase its stability [23]. Ng et al. employed three different drug stabilization approaches in the study presented in literature [29] through changing the architectures of the films. In their work, in the first approach, a solid dispersion film of the drug and polymer was prepared. A second approach involved coating the surface of a freshly prepared drug thin film with a thin polymer film, whereas for the third approach, the solid substrate surface was modified with a polymer coating prior to the laying of the pure drug

thin film on top. A cross comparison of these three stabilization approaches was carried out and it was found that the polymer thin film coatings were more effective for the model drugs tested in their study.

The application of silica nanoparticles (SiO_2) has drawn considerable attention for surface modification, due to its use as an enhancer for the sensitivity, selectivity and strength of the thin films as well as its use as a pH indicator in many research situations and in industry [30-35]. In the work published by Lee et al. [36], pH-sensitivity of the nanomaterial thin film chemo-resistor and transistors was tuned by depositing a SiO_2 nanoparticles layer on top of a semiconducting nanomaterial multilayer fabricated by using a layer-by-layer self-assembly in which the silica nanoparticles play the role of the charge collector, influencing the conductance of the semiconducting layers of the carbon nanotubes and the indium oxide nanoparticles. Liu et al. also used a silica nanoparticle layer on top of further layers of indium oxide nanoparticles and poly (styrene sulfonate) (PSS) as an insulating layer, in the approach published in [30]. Selectivity for hydrogen gas was obtained by deposition of a thin film of silica nanoparticles on top of the $\text{SnO}_2\pm\text{Cu}/\text{Pt}$, in a mixture of the two gases [10].

The use of silica nanoparticles can create a very strong thin film if they are used to cover the indicator multilayers. The work presented in this chapter thus takes advantage of this and compares and contrasts three different stabilization approaches with the aim of creating a stable pH sensor which is re-usable and stable under storage. In the course of the investigation and optimization of the

sensor system developed, aspects of the fabrication process such as heat treatment, the deposition of two layers of PAH/SiO₂ as thin film ‘topping’ layers and the deposition of two layers of APTMS/SiO₂ as similar ‘topping’ layers have been investigated and the resulting sensors characterized to determine the best approach to creating a sensor which is stable and reliable in operation: thus giving the same calibration, in terms of the value of the peak wavelength for a particular value of pH, and doing so in a reproducible way. Further aspects which relate to improved sensor performance, such as longer shelf-life, better stability and sensor re-usability after cleaning for a sensor prepared using the LbL technique in this work are considered and reported, showing the importance of the approach taken in this research.

7.2 Materials and methods

7.2.1 Chemicals

In order to create an effective optical pH sensor, brilliant yellow (BY) was selected as the pH indicator to be used, as discussed in prior chapters. This indicator dye was chosen for its wavelength variation and ease of use and it was cross-linked to poly (allylamine hydrochloride) [PAH] which is a positively charged molecule and was used as a polycation. 3-Aminopropyl-trimethoxy silane (APTMS) (99%) as a silane coupling agent and SM-30 containing 30 wt% SiO₂ nanoparticles in H₂O as a strength enhancer were used. The structures of these molecules are shown schematically in Fig 7-1.

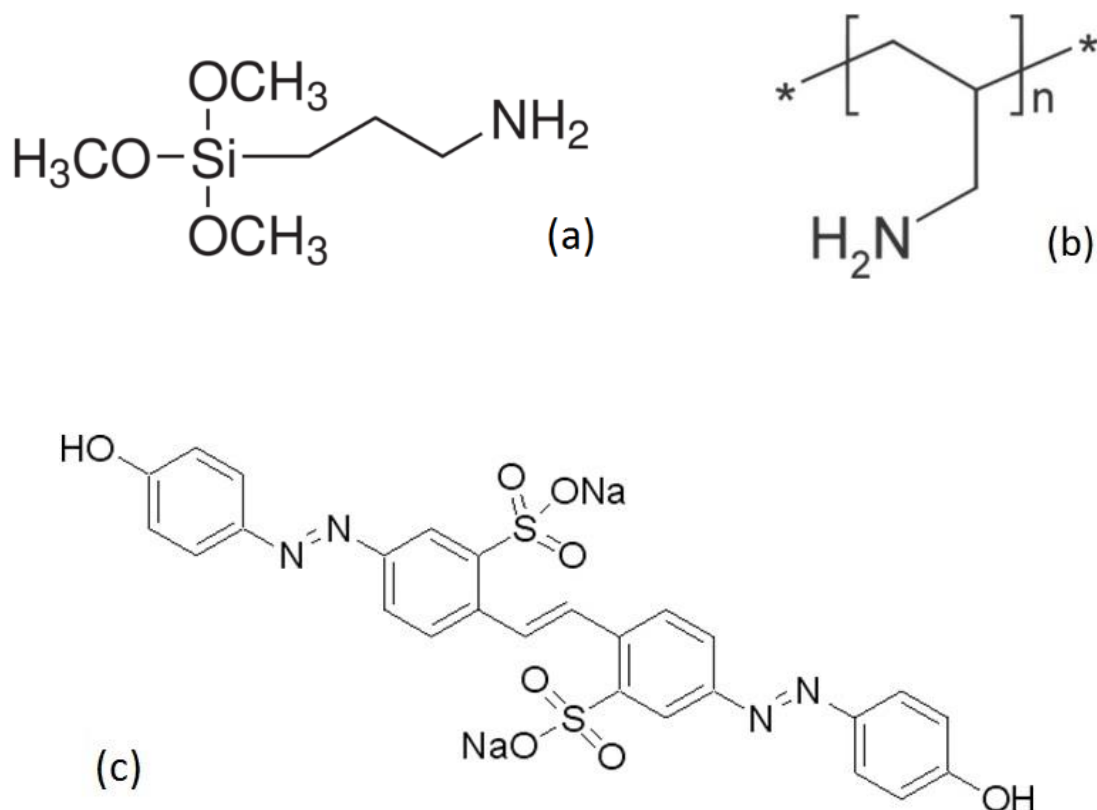


Fig 7-1 Chemical structure of (a) APTMS, (b) Poly (allylamine) hydrochloride [PAH] and (c) brilliant yellow.

7.2.2 Procedures

The multilayer coating which was deposited by using a self-assembly, layer-by-layer (LbL) technique was carried out using a glass microscope slides of dimensions 76×26 mm, with thickness of 1.0 mm. The glass slide used was treated with Piranha solution (30:70 (v/v) mixture of hydrogen peroxide (H₂O₂) (30%) and concentrated sulfuric acid (H₂SO₄)) for 60 minutes to produce the negatively charged surface and was then rinsed with distilled water, followed by drying with compressed nitrogen. The glass slide was then ready to be coated with positively charged molecules. The layer-by-layer technique is based on the successive deposition of oppositely charged molecules onto a solid surface. In

this technique, the functionalized surface of a glass slide dipped into PAH solution for 5 minutes to create a polycation layer. The glass slide was then dipped into distilled water for 5 minutes to wash off the un-bonded molecules. This glass slide was then dipped in BY solution for 5 minutes to construct the polyanion layer above the PAH layer. To wash away the un-bonded molecules, the glass slide was then immersed in fresh distilled water for 5 minutes. This operation was then repeated several times to build up the layers and thus increase the thickness of the thin film deposited on the glass slide, which was then ready to be used as the active element in the sensor system, tested by being used for measurement of the pH of a buffer solution. The performance of the sensor prepared was examined through the measurement and the evaluation of the change in the peak wavelength of the absorption when the sensor was evaluated by being dipped into buffer solutions of different and varying pH. The process was carried out by dipping the sensor slide into the pH solution for a few minutes, following which the absorbed light versus wavelengths is measured by use of the PerkinElmer spectrophotometer. The glass slide was then taken out of the solution and was immersed in another, fresh buffer solution (of different and known pH), this being followed by a measurement of the absorbance spectra. The measurement was carried out several times, using fresh buffer solutions increasing from pH 6 to 9, and then decreasing from pH 9 to 6, this being repeated several times for a number of such samples. The maximum value of the absorbance was normalized by dividing by the minimum value and the results were plotted as a graph of relative absorbance versus pH.

For consistency, the preparation conditions and the concentration of the polyion solutions used were the same in all these experiments. However, it was found that to achieve a sensor performance that is consistent and shows the same values of peak wavelength for an identical pH, especially after several times of use, further operations on the design and construction of the sensor are needed and this is discussed in the following work.

7.2.3 Experiments

Following the approach in previous chapters, a glass slide was prepared on which alternate layers of brilliant yellow (BY) (acting as a pH indicator) and poly (allylamine hydrochloride) [PAH] (acting as a cross-linker of the layers of brilliant yellow) was deposited, using layer-by-layer coating technique. To determine the stability of thin film, initially neither heat treatment nor drying was used in the process of coating of glass slide with a total of 8 bilayers of (PAH/BY); this configuration is denoted by (PAH/BY)₈. As high pH can discharge the first polycation layer and destroy the ionic bonds that stabilize the films, to prevent this action solutions with a pH in the range from 6 to 8 (over the neutral pH range) only were examined. The results of several (three) successive measurements using this sensor approach are shown in Fig 7-2.

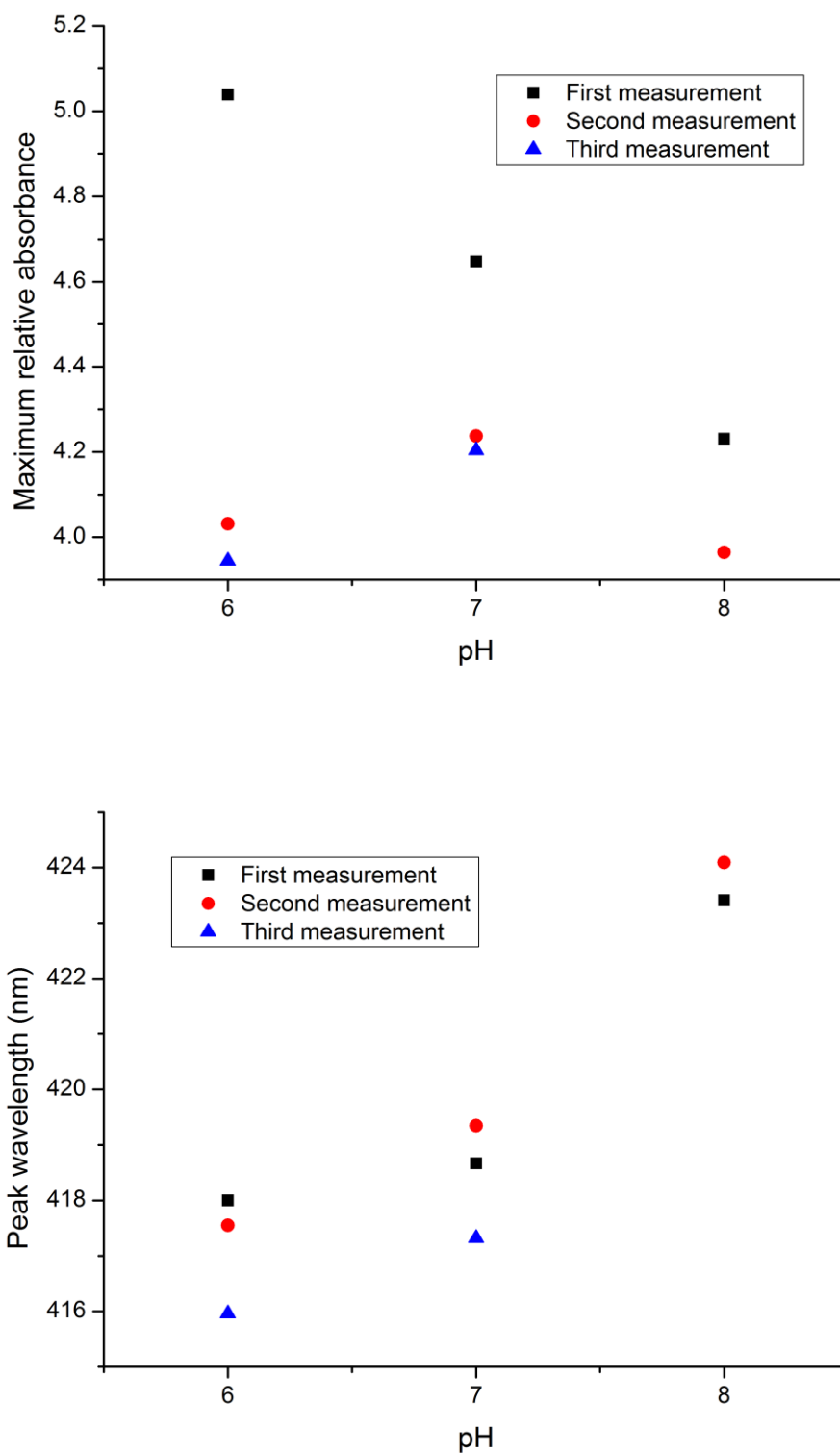


Fig 7-2 The maximum value of the relative absorbance (up) and the peak wavelength (down) versus pH for the consecutive measurements of the pH solutions for (PAH/BY)₈ on the glass slide. No heat treatment or drying was used in the process. (The sample is designated GS01)

However, it can be seen that the stability of the bilayer system thus prepared could be enhanced and this was achieved by further operations including heat treatment or applying a capping layer, such as a layer of silica nanoparticles. In order to determine the most efficient method of stabilizing the deposited layers, a number of different methods were considered and applied including a) heat treatment b) covering the layers with PAH and silica nanoparticles and c) covering the layers with 3-Aminopropyl-trimethoxysilane (APTMS) and silica nanoparticles. These are discussed in the next section.

7.2.4 Heat treatment

In order to make a stable thin film, two glass slides coated as indicated with (PAH/BY)₁₆ and (PAH/BY)₆ and cured in 120°C for 4 hours were examined. The glass slide coated with (PAH/BY)₁₆ was investigated using buffer solutions with pH varying from 6 to 8 and then back from 8 to 6, while the other slide was tested in a similar way with buffer solutions ranging from 6 to 9. The maximum value of the relative absorbance and the peak wavelength versus pH for the consecutive measurements of the pH of the solutions investigated for these two samples are shown in Fig 7-3 and Fig 7-4.

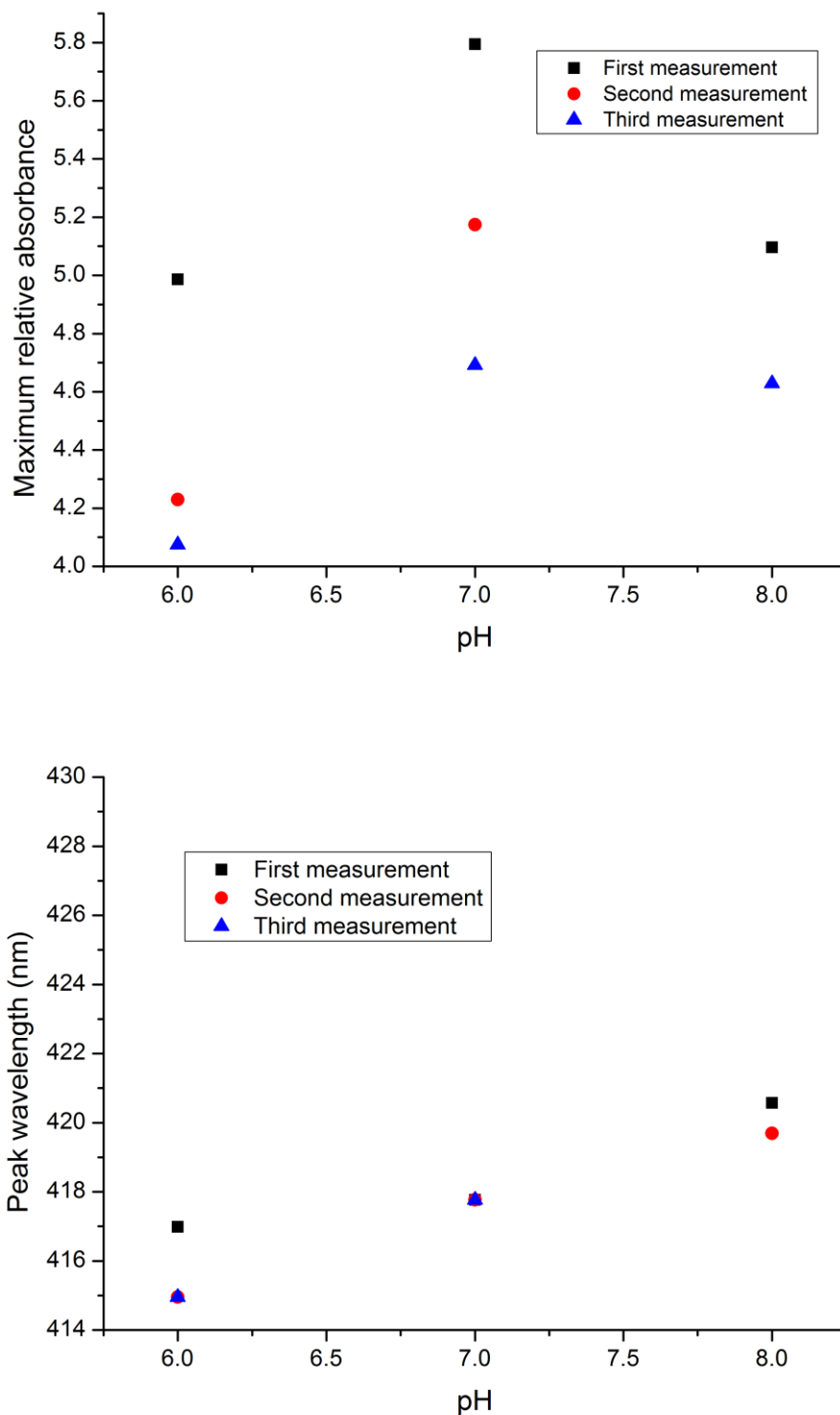


Fig 7-3 The maximum value of the relative absorbance (up) and the peak wavelength (down) versus pH for the consecutive measurements of the pH solutions for (PAH/BY)₁₆ on the glass slide. The sample was cured at 120°C for 4 hours. (The sample is designated GS02)

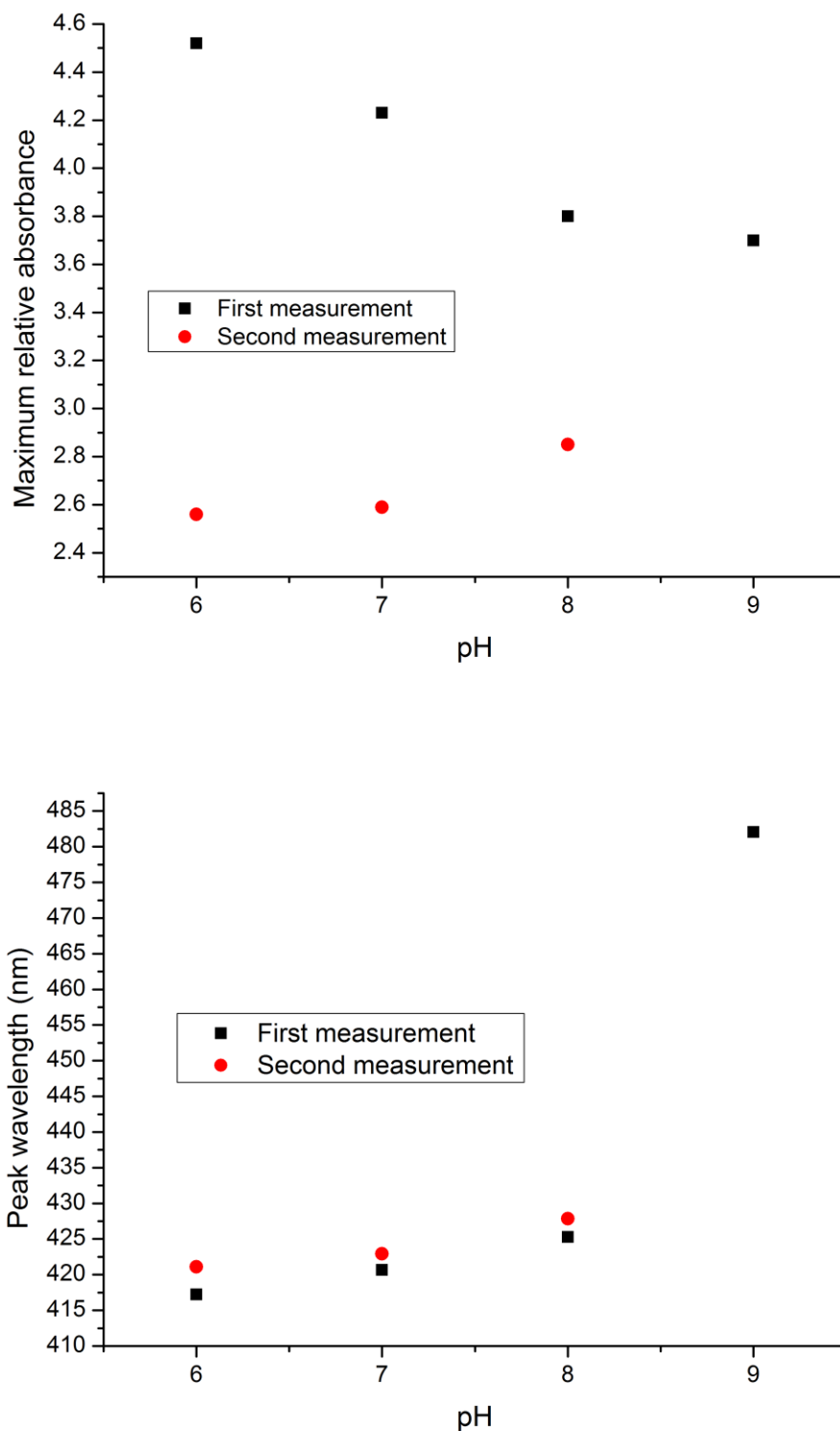


Fig 7-4 The maximum value of the relative absorbance (up) and the peak wavelength (down) versus pH for the consecutive measurements of the pH solutions for (PAH/BY)₆ on the glass slide. The sample was cured at 120°C for 4 hours. (The sample is designated GS03)

7.2.5 Using PAH and silica nanoparticle coatings

The use of silica nanoparticles covering the indicator multilayers is designed to enhance the strength of the film. Therefore, a series of experiments was carried out and discussed below in which layers of silica nanoparticles were built up on a glass slide already coated with 6 bilayers of (PAH/BY), i.e. (PAH/BY)₆. Different methods of curing were examined to find out the most appropriate way to develop the most stable coating. The silica solution used (SiO₂) was prepared at 1 wt.% (1.7 mM) concentration. As the SiO₂ solution is strongly alkaline (with pH 10.5), it causes the destruction of the BY layers; hence the pH of the SiO₂ solution was adjusted to pH 7 by adding some drops of HCl to the solution before the deposition of the layers was commenced. The glass slide thus prepared with (PAH/BY)₆ was then functionalized by using two bilayers of (PAH/SiO₂) followed by curing at 120°C for four hours (this sample being designated GS04). The results of the measurements taken using this sensor sample, over the range from pH 6 to pH 9 and from 9 back to 6, is shown in Fig 7-5. In a further experiment, the temperature used for the annealing of the thin film coating and comprising the following combination (PAH/BY)₆(PAH/SiO₂)₂ was heat treated for a longer period, of to 7 hours, at 130°C (with this sample being designated GS05) was and exposed to the buffer solutions. Experiment has shown that higher temperatures cannot be applied successfully because of the degradation caused to the BY material. The results of the measurements carried out using this sample is shown in Fig 7-6.

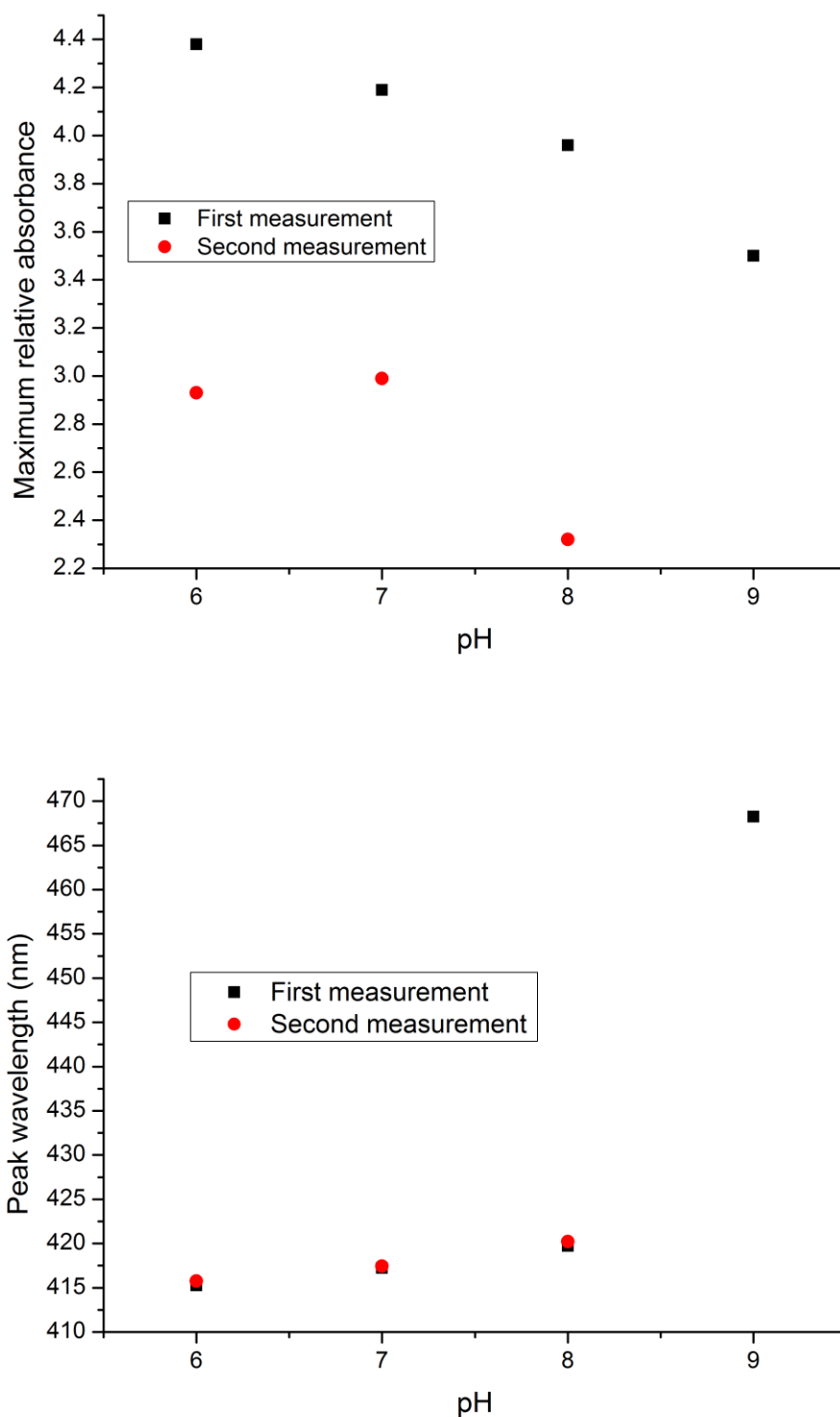


Fig 7-5 The maximum value of the relative absorbance (up) and the peak wavelength (down) versus pH for the consecutive measurements of the pH solutions for $(\text{PAH}/\text{BY})_6(\text{PAH}/\text{SiO}_2)_2$ on the glass slide. (The sample designated as GS04)

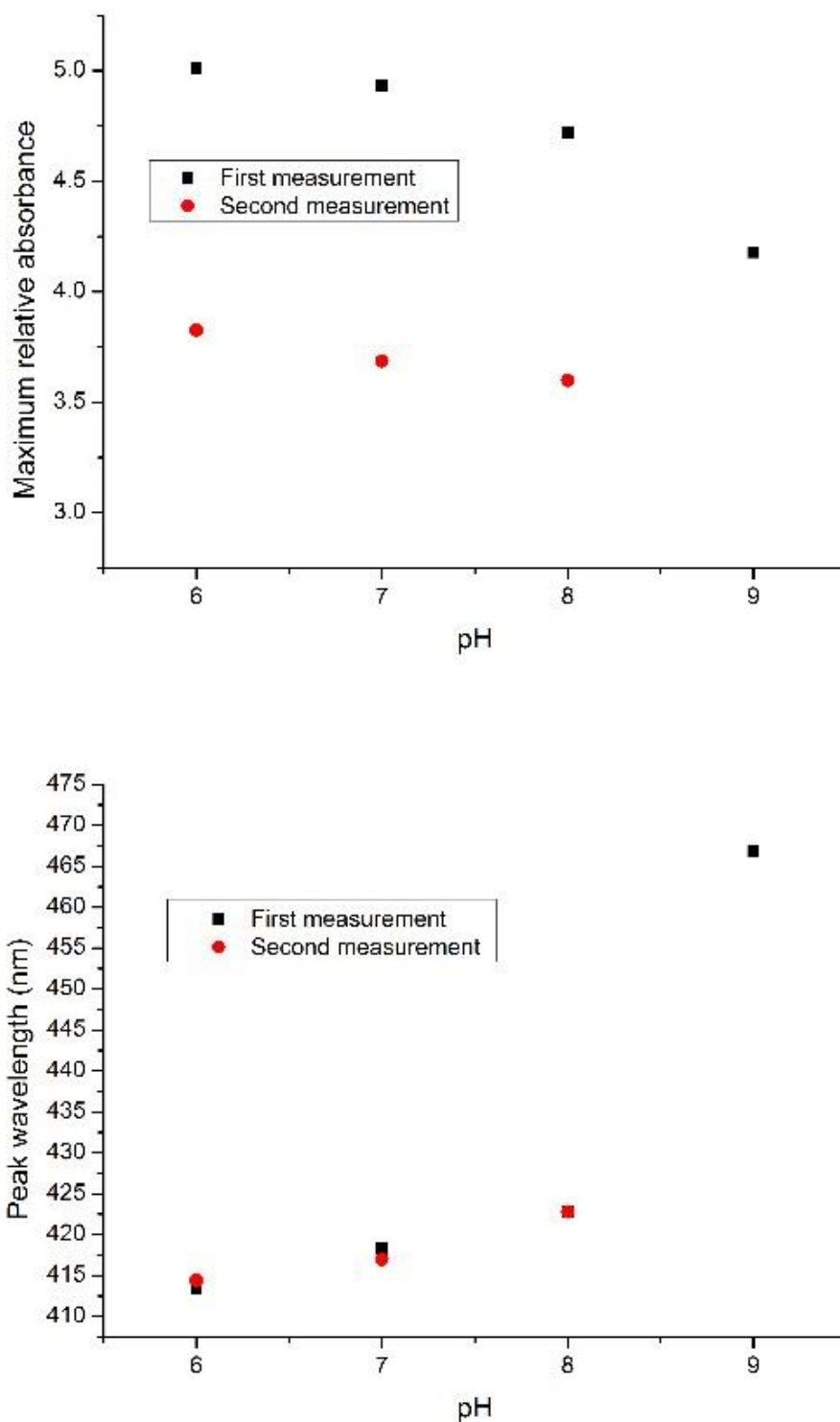


Fig 7-6 The maximum value of the relative absorbance (up) and the peak wavelength (down) versus pH for the consecutive measurements of the pH solutions for $(\text{PAH/BY})_6(\text{PAH/SiO}_2)_2$ on the glass slide. The sample was cured at 130°C for 7 hours. (The sample designated as GS05)

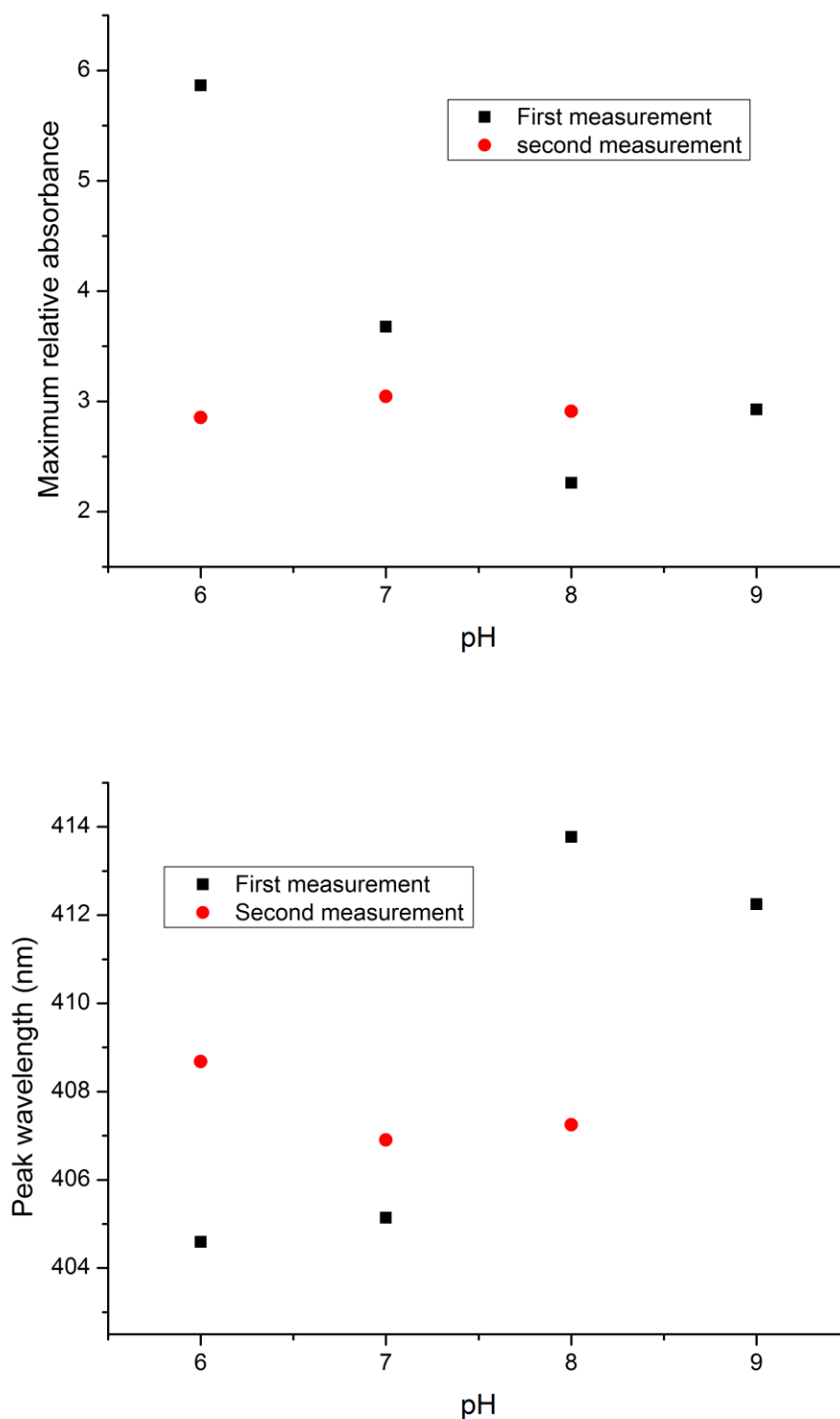


Fig 7-7 The maximum value of the relative absorbance (up) and the peak wavelength (down) versus pH for the consecutive measurements of the pH solutions for $(\text{PAH/BY})_6(\text{PAH/SiO}_2)_2$ on the glass slide. The sample was cured at 130°C for 7 hours and exposed to UV light for 20 minutes. (The sample designated as GS06)

In the next experiment, UV irradiation was utilized to provide energy to cause the layers to form a stronger bond, in addition to the electrostatic attraction present. The silica nanoparticle coating is a photosensitive material and the ionic bonds between the SiO₂ and PAH may be converted to covalent bonds by use of this UV irradiation. To do so, the sample was exposed to the UV light (irradiation intensity: 1112 mWcm⁻² at 365 nm) for 20 minutes, after annealing at 130°C for 7 hours and then the sensor was exposed to the different pH buffer solutions. The results of the spectra recorded for this sample (designated GS06) are shown in Fig 7-7.

The silica nanoparticles act as polyanions in the same way as the BY material. It can be speculated that if the silica molecules are located amongst the molecules of brilliant yellow (BY), then the formation of the molecular bonds between the silica and the PAH molecules would create a bilayer which would surround the BY molecules in each layer. Therefore, a further set of experiments was carried out in which a silica nanoparticle solution was added to a BY solution (1.7 mM SiO₂: 0.25 mM BY) and the pH of the solution was adjusted to pH 6. Having coated the glass slide sensor in this way to create (PAH/(BY+SiO₂))₆, then annealing at 120°C for 4 hours, the deposited glass slide (designated GS07) was examined under various buffer solutions of different values of pH. The results of this test and thus the recorded spectra are shown in Fig 7-8.

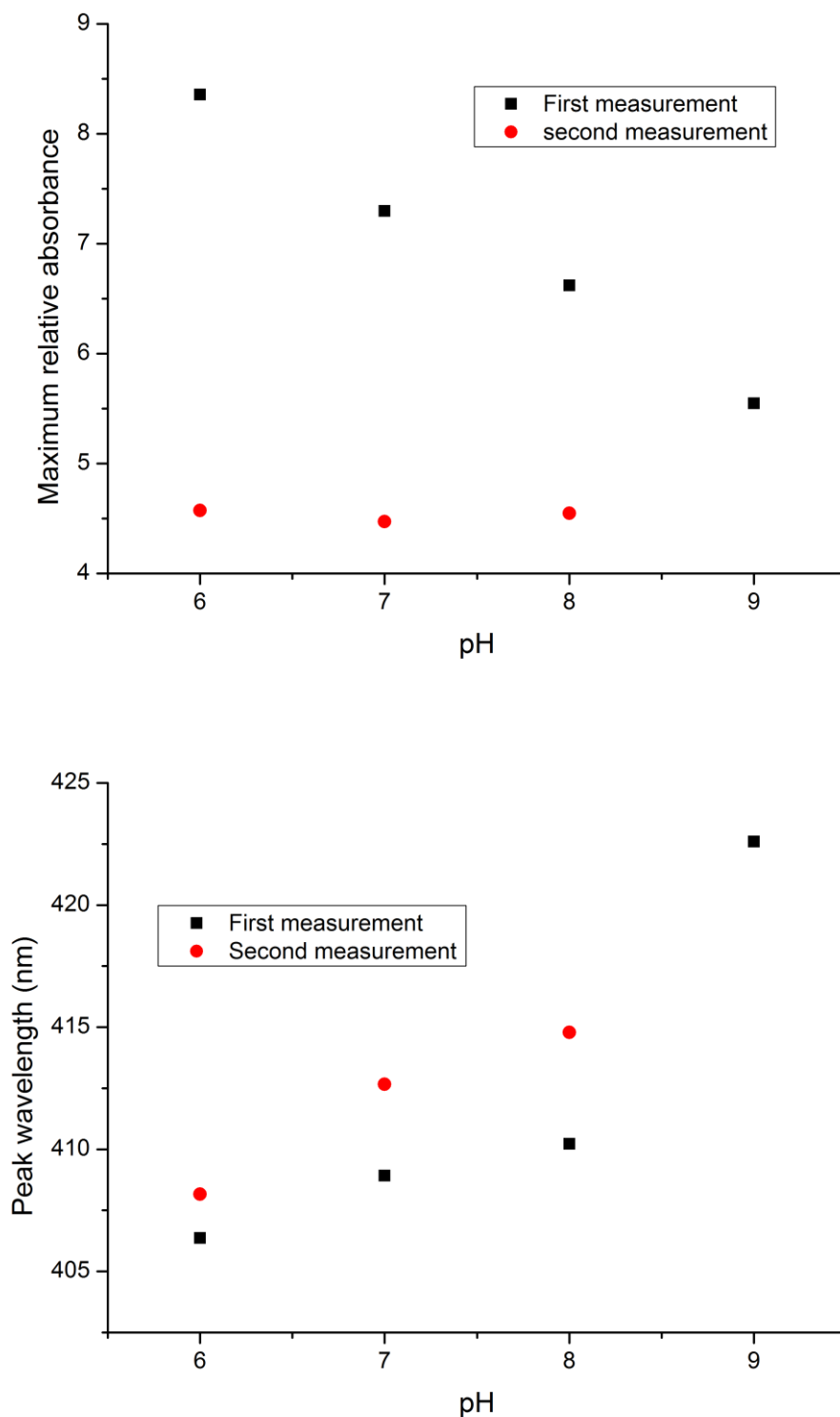


Fig 7-8 The maximum value of the relative absorbance (up) and the peak wavelength (down) versus pH for the consecutive measurements of the pH solutions for $(\text{PAH}/(\text{BY}+\text{SiO}_2))_6$ on the glass slide. The sample was cured at 120°C for 4 hours. (The sample designated GS07)

7.2.6 Use of APTMS and silica nanoparticles

Further experimentation was carried out by replacing the polycation; PAH; with 3-Aminopropyl-trimethoxysilane (APTMS) in the capping layers. APTMS is known as a silane coupling agent in which a water based solution is polymerized after hydrolysis, as shown schematically in Fig 7-9. The surface of the SiO₂ nanoparticle thin film contains hydroxyl groups in the form of SiOH. These groups may donate or accept a proton from the solution, leaving a negatively charged or a positively charged surface group respectively [30]. Therefore, there are two possibilities that the molecules of APTMS bond to the silica nanoparticles; the molecule constitutes of an amine group as a positive charge supplier and hydroxyl groups as negative charges supplier which bond to silicon, as shown in Fig 7-10. In the experiment, the solution of 1 wt.% APTMS in H₂O (1.4 mM) used was strongly alkaline (with pH 10.8) and should thus be adjusted to the neutral pH that is best suited for use as polyelectrolyte in the LbL technique. Hence several drops of HCl were added to both solutions of the polycation and polyanion to adjust their pH value to pH 6. Two glass slide sensor samples coated with (PAH/BY)₆(APTMS/SiO₂)₂ were prepared; one of them was examined the same day of preparation (the sample designated GS08) and the second (the sample designated GS09) was evaluated a week later. The results of the tests carried out are shown in Fig 7-11 and Fig 7-12 respectively.

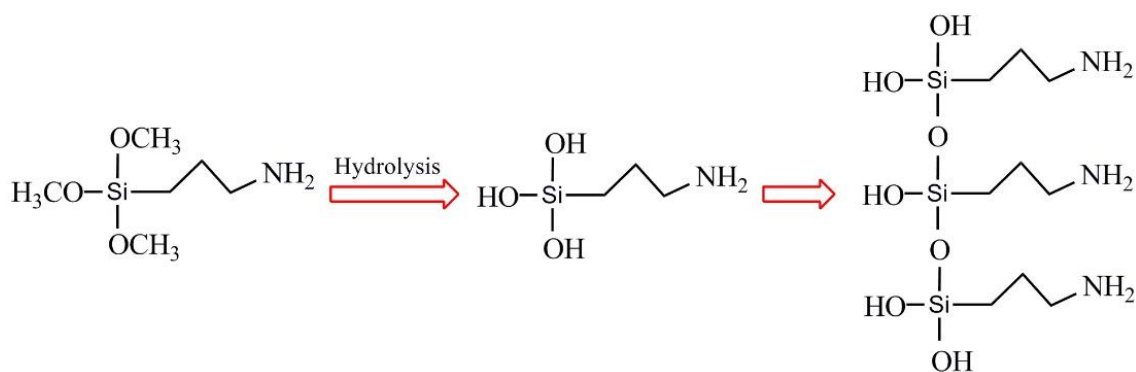


Fig 7-9 APTMS is polymerized in aqueous solution after hydrolysis.

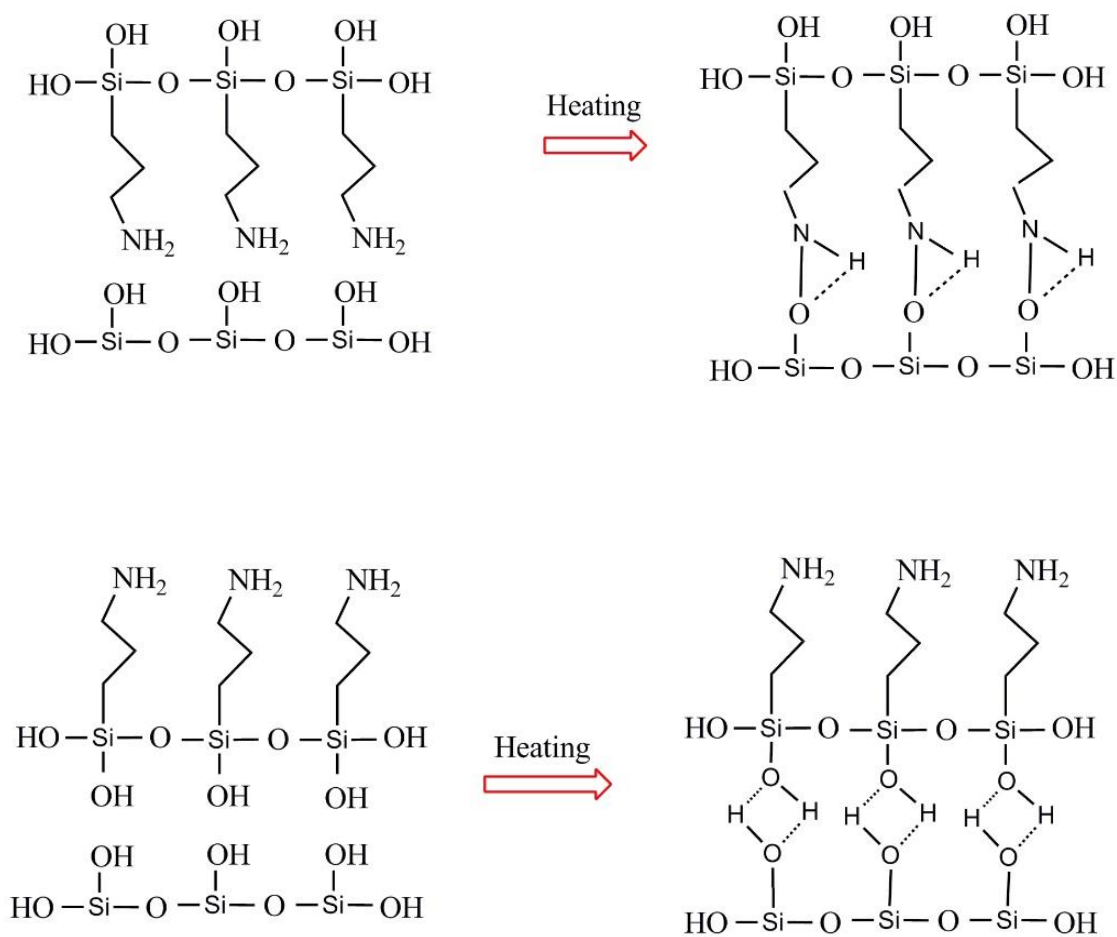


Fig 7-10 Two possibilities reaction between molecules of APTMS and silica nanoparticles.

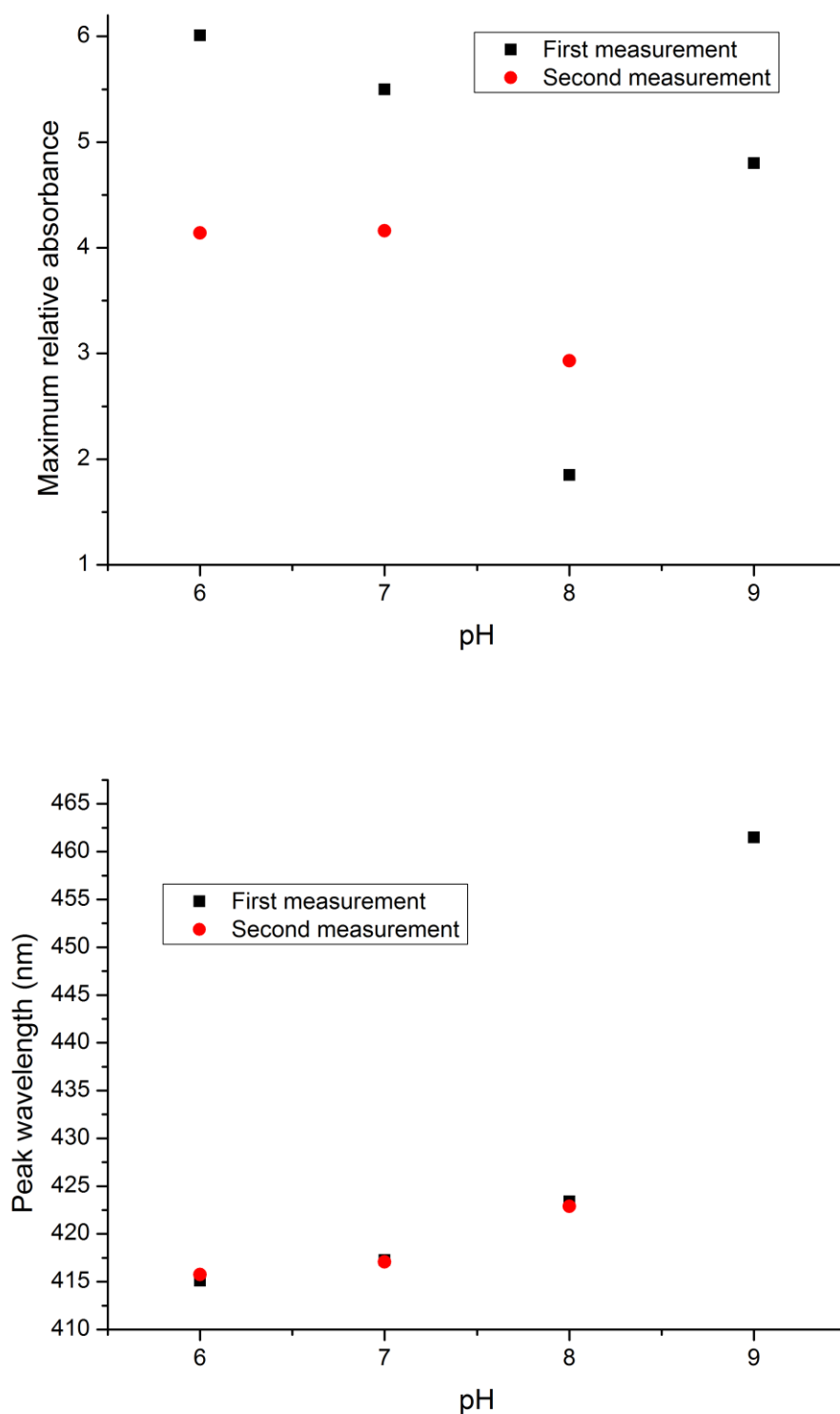


Fig 7-11 The maximum value of the relative absorbance (up) and the peak wavelength (down) versus pH for the consecutive measurements of the pH solutions for $(\text{PAH/BY})_6(\text{APTMS/SiO}_2)_2$ on the glass slide. The sample was cured at 120°C for 4 hours. (The sample designated GS08)

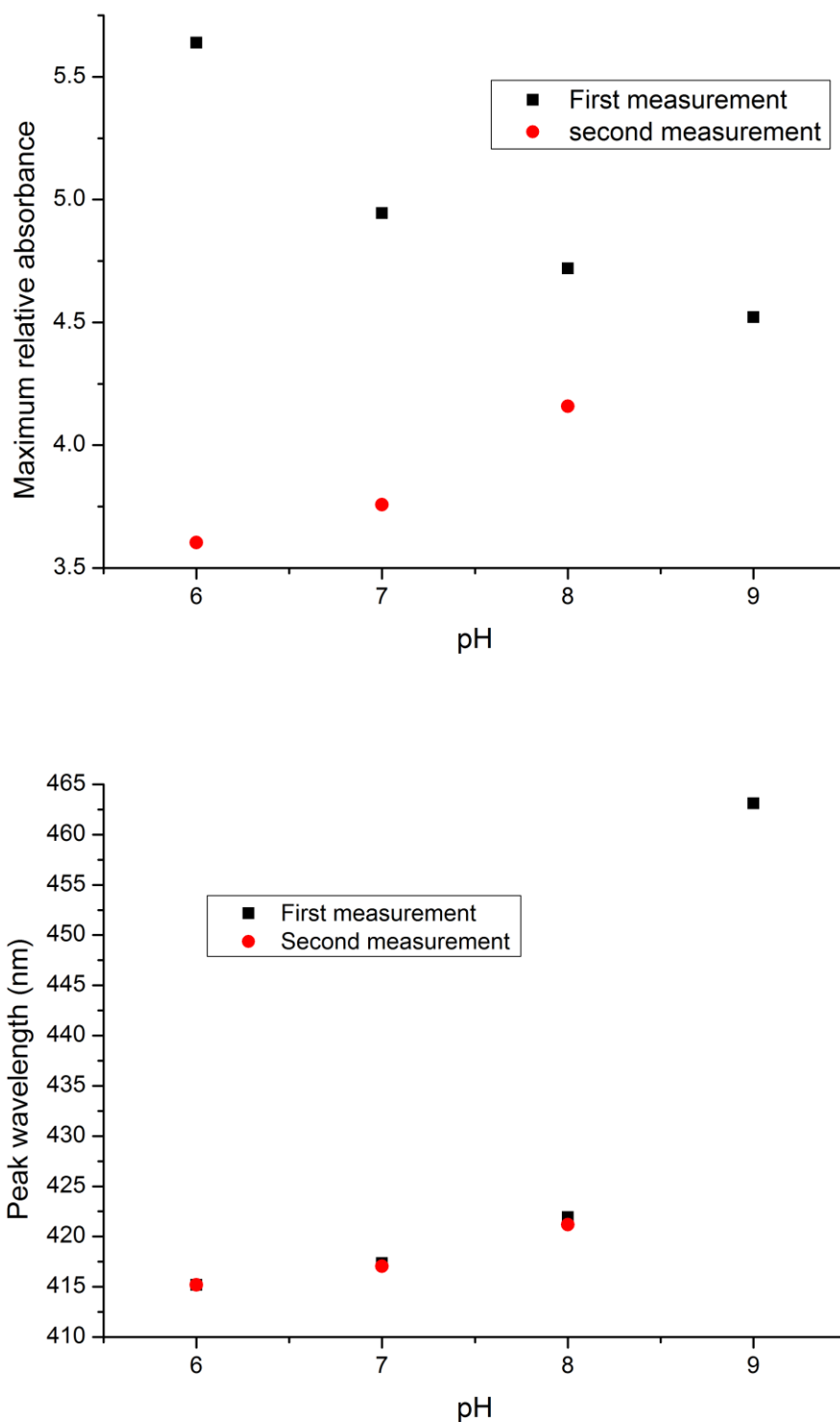


Fig 7-12 The maximum value of the relative absorbance (up) and the peak wavelength (down) versus pH for the consecutive measurements of the pH solutions for $(\text{PAH/BY})_6(\text{APTMS/SiO}_2)_2$ on the glass slide. The sample was cured at 120°C for 4 hours and examined after a week. (The sample designated GS09)

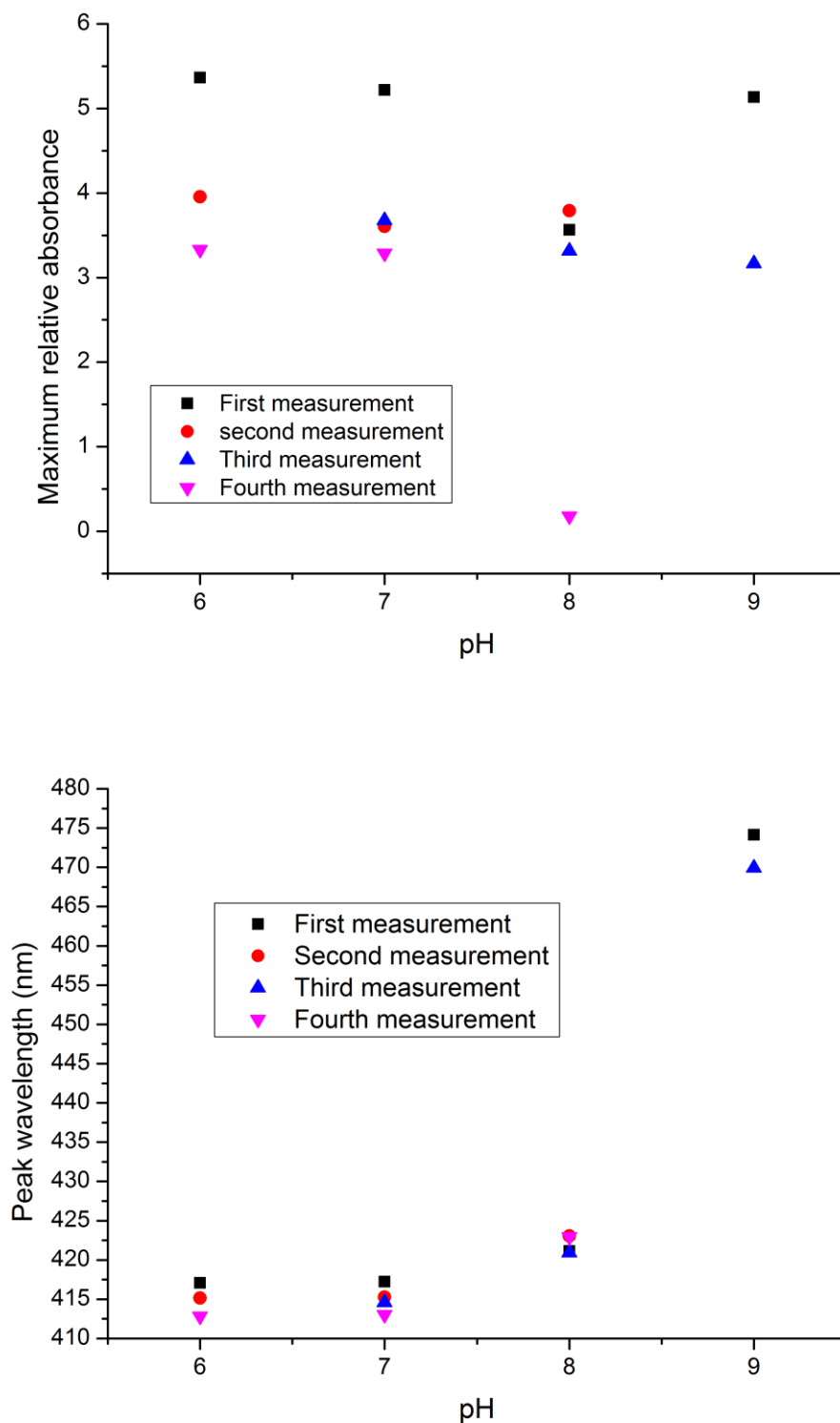


Fig 7-13 The maximum value of the relative absorbance (up) and the peak wavelength (down) versus pH for the consecutive measurements of the pH solutions for $(\text{PAH/BY})_6\text{APTMS}$ on the glass slide. The sample was cured at 120°C for 4 hours. (The sample designated GS10)

To investigate the effect of the use of APTMS alone, a thin film comprising 6 bilayers of (PAH/BY), dipped in APTMS solution for 30 minutes, followed by dipping in distilled water for 5 minutes, then cured at 120°C for 4 hours was examined. The results of this experiment are shown in Fig 7-13.

7.2.7 Reusability and aging

To investigate the effect on sensor stability of the storage of the glass slides, different coated glass slides of different types were examined. Thus in this investigation, initially the glass slide with a coating was dipped into a fresh buffer solution with constant pH for 60 minutes and after this time the absorbance spectra was recorded as a reference. Following that the glass slide was removed from that solution and then was immersed into another solution (with the same pH) for a further 60 minutes and a second absorbance spectra was recorded. This operation was repeated for a third time. Several different slides with different films were recorded: the stability and thus the re-usability of the multilayer thin film slides using two different samples with different structures, these being $(\text{PAH/BY})_6$ and $(\text{PAH/BY})_6(\text{APTMS/SiO}_2)_2$ were examined at two different values of pH; pH 6 and 8, separately.

The results of this test are shown in Fig 7-14 and Fig 7-15 and the positive results obtained imply the stability of these two sensor samples under exposure to these solutions for the times indicated.

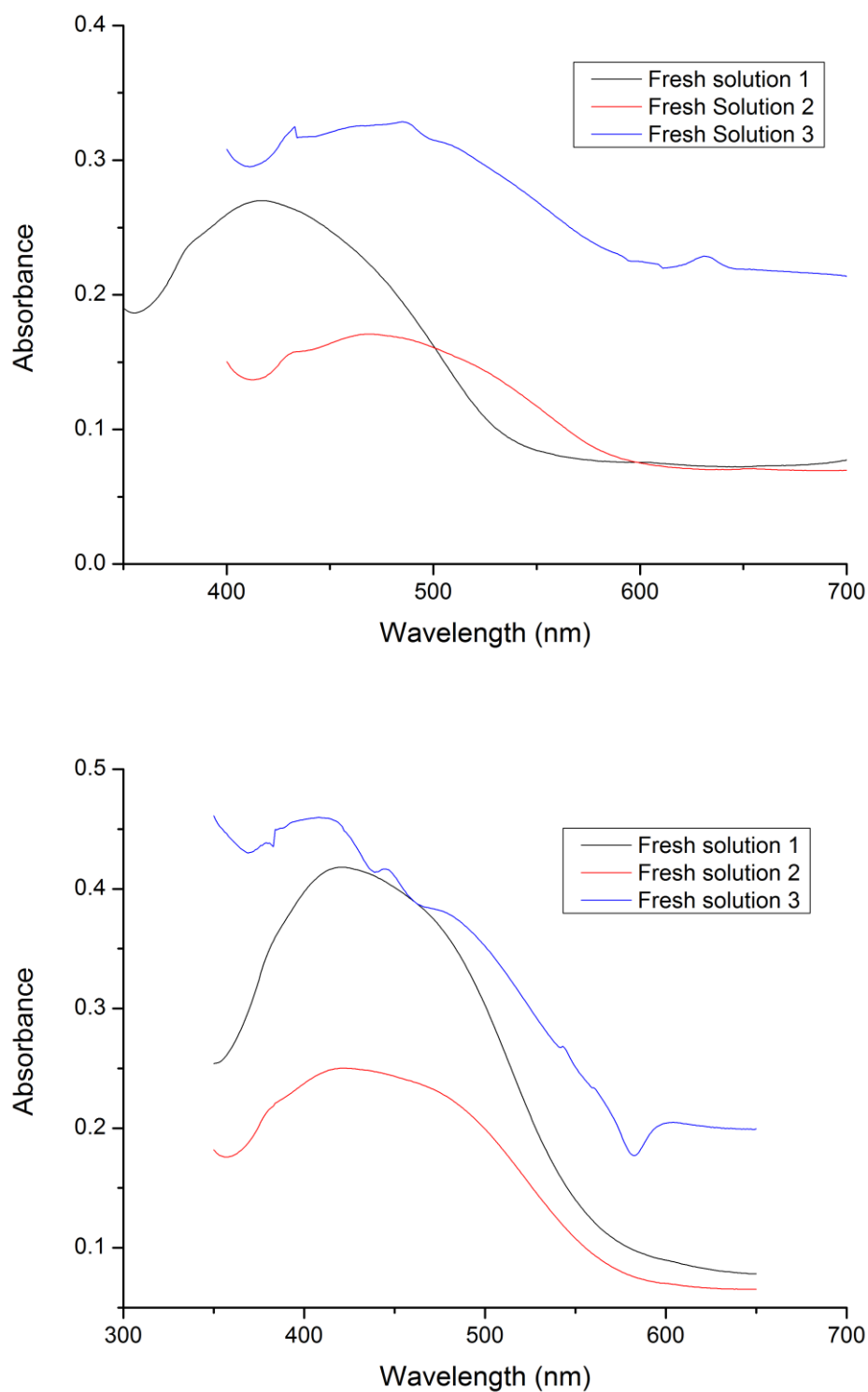


Fig 7-14 The spectra for the coated glass slides with $(\text{PAH/BY})_6$ dipped into the fresh buffer solution for three times and each time for 60 minutes. Up: pH 6 (The sample designated GS11), Down: pH 8 (The sample is designated GS12). The samples were cured at 120°C for 4 hours.

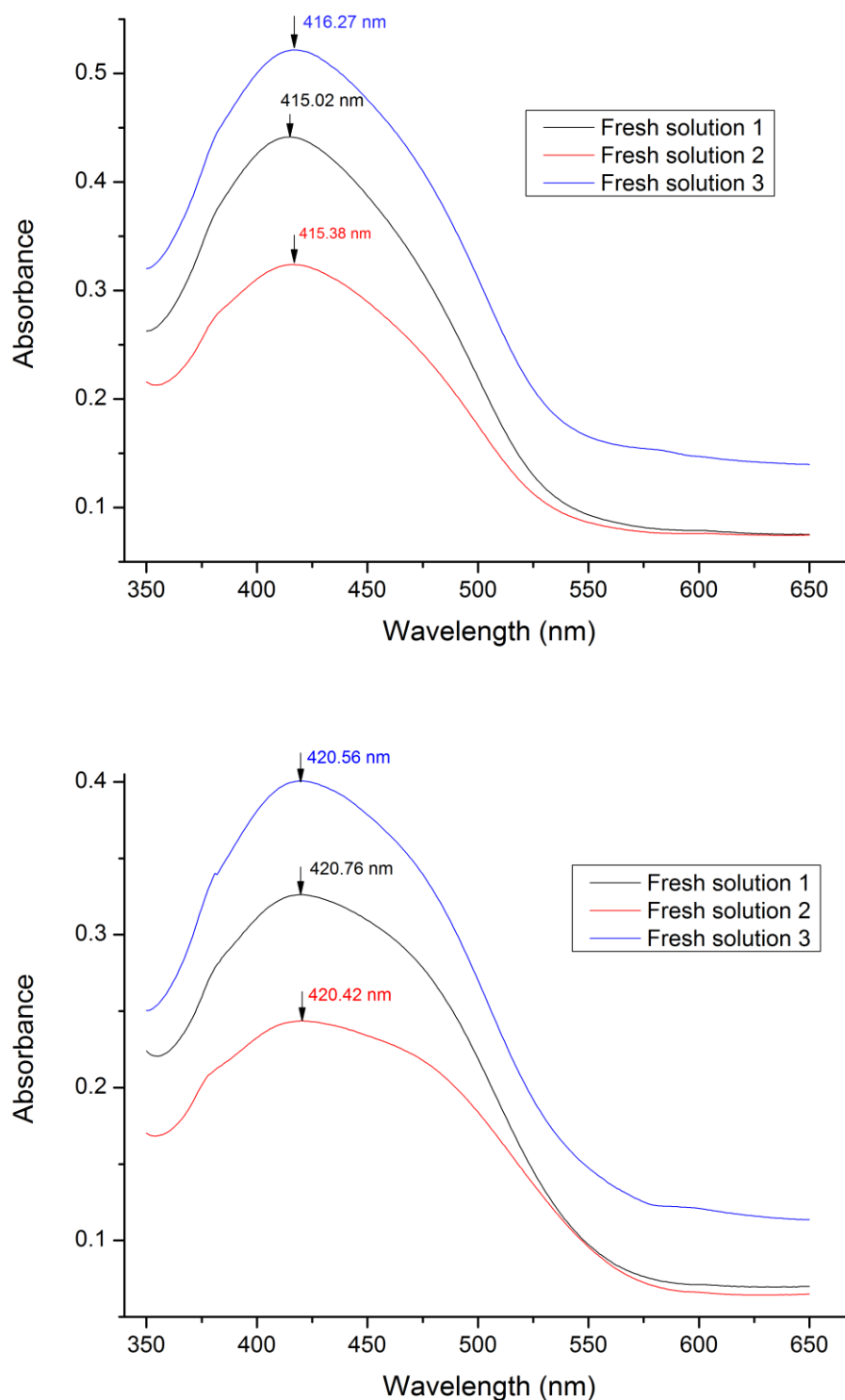


Fig 7-15 The spectra for the coated glass slides with $(\text{PAH/BY})_6(\text{APTMS/SiO}_2)_2$ dipped into the fresh buffer solution for three times and each time for 60 minutes. Up: pH 6 (The sample is designated GS13), Down: pH 8 (The sample is designated GS14). The samples were cured at 120°C for 4 hours.

7.3 Results and discussion

In the layer-by-layer coating technique, the stability of the layers is seen to depend on type and concentration of the salt, the strength of ions and polyelectrolytes, the polymer molecular weight, the pH of the solutions and the thermal energy.

In order to form a stable multilayer thin film, a minimum charge density in each layer is needed. This minimum charge density depends on the salt concentration and the salt type; this was investigated in chapter 3 and also it was shown that to rely very strongly on the chemical identity of the charged units involved in forming the thin film [37]. Stronger ion pairing will also yield more stable multilayers [2] and moreover, high molecular weight polymers promote the stability of the layers [38-40]. High and low pH solutions can potentially discharge the ions and destroy the layers, while heat treatment causes a chemical reaction between the molecules of two adjacent layers and makes the bonds stronger and creates a more stable multilayer film, as can be seen in the first three experiments discussed (shown in Fig 7-2, Fig 7-3 and Fig 7-4). As the figures show, in this series of experiments there is a continuous decrease in the maximum absorbance for each pH buffer solution for two successive measurements while the values of the peak wavelength show a significant change from the first to the second measurement for the sample without heat treatment, and this represents an increase in stability of the thin film because of the thermal effect on the sample.

In the sample designated GS03 and examined in solutions ranging from pH 6 to pH 9, a dramatic decline in the maximum absorbance was seen, compared to other samples examined over the range from pH 6 to pH 8. The reduction in absorbance is a clear proof that leaching of the indicator is occurring and the decrease of the thickness of the thin film. In particular, in the case where a pH 9 solution is used, which causes greater destruction of the layers, a noticeable decrease takes place in the absorbance from the first to the second measurement. In addition to the absorbance, in all the samples studied the wavelength has not stayed stable during consecutive measurements and a small change of around 0 to 2 nm in the peak wavelength was observed; although with increasing the number of bilayers the amount of this change becomes reduced.

Covering the sensitive thin film with a couple of layers of silica nanoparticles leads to a coating which creates such a stable film that the wavelength continues to remain constant for a certain known pH, while the absorbance decreases irregularly during the several cycles of measurement, as shown in Fig 7-5. Referring to Fig 7-6, the duration and the temperature of thermal treatment used did not have any significant effect on the stability of the film as the values of the peak wavelengths for the first and the second measurements for both samples used, designated GS04 and GS05, were roughly the same. However, exposing the samples to UV light did not modify the molecular bonds. As Fig 7-7 shows there is not a regular change in the peak wavelength but a drastic decline is seen in both the absorbance and the peak wavelength values compared to previous experiments and also a dramatic absorbance reduction was observed in the first

measurement. This means that by applying UV irradiation, an increase in the strength of the inter-molecular bonds occurs temporarily. However, these inter-molecular forces are lost after a few times of dipping the sensor slide into the buffer solutions. As a result, the molecules of BY start to leach out from the sensitive thin film and this causes a steep decrease in absorbance and a very undesirable situation for a sensor system.

Adding silica nanoparticles to BY solutions shifts the absorbance spectra to the lower peak wavelength values, as shown in Fig 7-8. It can be seen in this figure that the absorbance has increased significantly compared to that of the other samples; however, the values of both the absorbance and the peak wavelength in the second measurement become close to the values seen from the previous tests. Looking more closely, it can be said that the higher values of maximum absorbance in the first measurement imply a larger number of molecules of brilliant yellow in the deposited layers. In other words, the SiO₂-PAH bilayers can protect the BY from significant damage, but not for a long time.

When the PAH was replaced by APTMS in the capping layers, the results showed that the peak wavelength for each pH solution used demonstrated almost same values as shown in Fig 7-12. Table 7-1 compares the peak wavelengths of three slides (designated GS04, GS08 and GS09) for two successive measurements over the range from pH 6 to pH 9 and then from 9 to 6. It is noticeable that the APTMS does not cause any significant changes to the peak wavelengths, compared to the use of PAH and the three tests carried out exhibited the same peak wavelengths, in spite of the difference in the peak

intensity. The most striking result of this series of experiments is the remarkable reduction of the degradation of the probes and thus the improvement that would be seen to their shelf-life, as well as their re-usability, which are key considerations for the use of this type of coating in an industrial sensor system. Fig 7-13 shows that when the sensitive film is coated with a layer of APTMS, the peak wavelength for each pH value changes during successive measurements and also there is not a regular shift at different times of measurements. This therefore implies that the stability of the measured wavelength cannot be maintained because of the polycation properties. Moreover, the influence of SiO₂ is more effective in creating a stable sensor than does the polycation. However, the cross-comparison of the two sensor samples (designated as GS03 (without APTMS) and GS10 (with a layer of APTMS)) and shown in Fig 7-4 and Fig 7-13 confirms that the effect of APTMS on stability cannot be ignored. Indeed, as Table 7-1 shows, there is no significant difference in the stability observed between the situations where two capping layers of (PAH/SiO₂) and (APTMS/SiO₂) are applied. This may arise because of the similarity between the functional groups (amine groups) in both the PAH and the APTMS and thus the same interaction occurring between the polyanion and the polycation species.

In addition, a comparison of the last two columns of Table 1 shows that storing the samples for a week has had a negligible effect on the peak wavelength values. Applying these capping layers not only improved the sensor shelf-life but also enhances the re-usability of the sensor, as can be seen when sensors

designated GS11 and GS12 are compared to GS13 and GS14, as illustrated in Fig 7-14 and Fig 7-15, respectively. Fig 7-14 shows a result which implies that destroying the deposited layers after 60 minutes exposure to the buffer solution results in the peak wavelength staying constant for those samples covered with two layers of APTMS/SiO₂, even after immersion on two separate occasions in the buffer solutions, for periods of 60 minutes in each case.

Table 7-1 The peak wavelength for two times consecutive measurements for the glass slides, designated GS04, GS08 and GS09 in pH solutions from 6 to 9 and then from 9 to 6.

pH	Measurement	Peak wavelength (nm)					
		GS04		GS08		GS09	
		(PAH/BY) ₆ (PAH/SiO ₂) ₂		(PAH/BY) ₆ (APTMS/SiO ₂) ₂		(PAH/BY) ₆ (APTMS/SiO ₂) ₂	
			error		error		error
6	First	415.26	-	415.10	-	415.18	-
7	First	417.24	-	417.26	-	417.36	-
8	First	423.19	-	423.4	-	421.92	-
9	First	468.25	-	461.5	-	463.12	-
8	Second	423.09	-0.02%	422.9	-0.1%	421.17	-0.2%
7	Second	417.45	0.05%	417.06	-0.08%	417.06	-0.07%
6	Second	415.75	0.1%	415.75	0.1%	415.18	0%

7.4 Summary

In this study, the stability and the deterioration of wavelength-dependent optical sensor devices to pH changes using techniques to build up a series of nanolayer coatings was investigated and the results reported.

The stability of the pH sensors thus fabricated was studied using different pH buffer solutions. A variety of techniques was proposed and investigated to improve the stability of the film and to avoid progressive destruction of the indicator layer. One technique explored extensively was to build up capping bilayers using different materials i.e. silica nanoparticles as the polyanion and PAH or APTMS as the polycation. Another approach investigated was to apply thermal treatment after the layer building process and an alternative method considered was applying UV light irradiation.

The results of the experiments carried out, including covering the sensitive thin film with two layers of (APTMS/silica) nanoparticles was shown to improve the stability of the sensor (indicated by the stability of the peak wavelength) and also to enhance the stability and potential shelf life of the sample, when the nanolayers are deposited on the glass slide substrates. The most striking result is that the peak wavelength continues to remain constant for a particular pH while the layers were affected during several repeated measurements.

The durability of the sensors thus created makes the probe a suitable wavelength-dependent measurement device which is well suited to use as a high resolution pH sensor. To do so, the layers described can be coated directly onto optical fibres of various diameters or alternatively coated glass substrates can be attached to the distal end of the fibre probes created. In that way compact optical fibre sensors can be created for a range of applications and as the work has shown, stored for some time before use.

References

- [1] G. Decher, J. D. Hong, and J. Schmitt, "Buildup of ultra thin multi layer films by a self assembly process: II. Consecutively alternating adsorption of anionic and cationic poly electrolytes on charged surfaces," *Thin Solid Films*, vol. 831, pp. 210-211, 1992.
- [2] G. Decher and J. B. Schlenoff, *Multilayer Thin Films*: Wiley-VCH Verlag GmbH & Co., 2002.
- [3] H. Ai, S. A. Jones, and Y. M. Lvov, "Biomedical applications of electrostatic layer-by-layer nano-assembly of polymers, enzymes, and nanoparticles," *Cell Biochemistry and Biophysics*, vol. 39, pp. 23-43, 2003 2003.
- [4] A. P. R. Johnston, C. Cortez, A. S. Angelatos, and F. Caruso, "Layer-by-layer engineered capsules and their applications," *Current Opinion in Colloid & Interface Science*, vol. 11, pp. 203-209, Oct 2006.
- [5] T. Cassagneau, T. E. Mallouk, and J. H. Fendler, "Layer-by-layer assembly of thin film zener diodes from conducting polymers and CdSe nanoparticles," *Journal of the American Chemical Society*, vol. 120, pp. 7848-7859, Aug 12 1998.
- [6] S. T. Dubas, P. Kumlangdudsana, and P. Potiyaraj, "Layer-by-layer deposition of antimicrobial silver nanoparticles on textile fibers," *Colloids and Surfaces A: Physicochemical and Engineering Aspects*, vol. 289, pp. 105-109, 2006.
- [7] Y. J. Liu, Y. X. Wang, and R. O. Claus, "Layer-by-layer ionic self-assembly of Au colloids into multilayer thin-films with bulk metal conductivity," *Chemical Physics Letters*, vol. 298, pp. 315-319, Dec 18 1998.
- [8] M. M. de Villiers, D. P. Otto, S. J. Strydom, and Y. M. Lvov, "Introduction to nanocoatings produced by layer-by-layer (LbL) self-assembly," *Advanced Drug Delivery Reviews*, vol. 63, pp. 701-715, Aug 14 2011.
- [9] M. J. McShane and Y. M. Lvov, "Layer-by-Layer electrostatic self-assembly," in *Dekker Encyclopedia of Nanoscience and Nanotechnology*, ed: Marcel Dekker, 2004.
- [10] R. K. Sharma, P. C. H. Chan, Z. Tang, G. Yan, I. M. Hsing, and J. K. O. Sin, "Sensitive, selective and stable tin dioxide thin-films for carbon monoxide and hydrogen sensing in integrated gas sensor array applications," *Sensors and Actuators B: Chemical*, vol. 72, pp. 160-166, 2001.

- [11] R. Singh, T. C. Goel, and S. Chandra, "RF magnetron sputtered La³⁺-modified PZT thin films: Perovskite phase stabilization and properties," *Materials Chemistry and Physics*, vol. 110, pp. 120-127, 2008.
- [12] G. Decher, Y. Lvov, and J. Schmitt, "Proof of multilayer structural organization in self-assembled polycation-polyanion molecular films," *Thin Solid Films*, vol. 244, pp. 772-777, 1994.
- [13] I. D. Villar, I. R. Matías, F. J. Arregui, and R. O. Claus, "ESA-based in fiber nanocavity for hydrogen peroxide detection," *IEEE Transactions On Nanotechnology*, vol. 4, pp. 187-193, 2005.
- [14] I. D. Villar, I. R. Matias, and F. J. Arregui, "Fiber-optic chemical nanosensors by electrostatic molecular self-assembly," *Current Analytical Chemistry*, vol. 4, pp. 341-355, 2008.
- [15] I. Ichinose, S. Muzuki, S. Ohno, H. Shiraishi, and T. Kunitake, "Preparation of cross-linked ultrathin films based on layer-by-layer assembly of polymers," *Polymer Journal*, vol. 31, pp. 1065-1070, 1999.
- [16] H. Yamada, T. Imoto, K. Fujita, K. Okazaki, and M. Motomura, "Selective modification of aspartic acid-101 in lysozyme by carbodiimid reaction", *Biochemistry*, vol. 20, pp. 4836-4842, 1981.
- [17] Q. Li, J. F. Quinn, and F. Caruso, "Nanoporous Polymer Thin Films via Polyelectrolyte Templating," *Advanced Materials*, vol. 17, pp. 2058-2062, 2005.
- [18] D. Saeki, M. Imanishi, Y. Ohmukai, T. Maruyama, and H. Matsuyama, "Stabilization of layer-by-layer assembled nanofiltration membranes by crosslinking via amide bond formation and siloxane bond formation," *Journal of Membrane Science*, vol. 447, pp. 128-133, 2013.
- [19] A. K. Sen, B. Mukherjee, A. S. Bhattacharyya, P. P. De, and A. K. Bhowmick, "Kinetics of silane grafting and moisture crosslinking of polyethylene and ethylene propylene rubber," *Journal of Applied Polymer Science*, vol. 44, pp. 1153-1164, 1992.
- [20] Y. Egawa, R. Hayashida, and J.-i. Anzai, "Covalently cross-linked multilayer thin films composed of diazoresin and brilliant yellow for an optical pH sensor " *Polymer*, vol. 48, pp. 1455-1458 2007.
- [21] S. Prakash, T. Chakrabarty, A. K. Singh, and V. K. Shahi, "Polymer thin films embedded with metal nanoparticles for electrochemical biosensors applications," *Biosensors and Bioelectronics*, vol. 41, pp. 43-53, 2013.
- [22] Y.-l. Su and C. Li, "Stable multilayer thin films composed of gold nanoparticles and lysozyme," *Applied Surface Science*, vol. 254, pp. 2003-2008, 2008.
- [23] A. Abdelghani, C. Veillas, J. M. Chovelon, N. Jaffrezic-Renault, and H. Gagnaire, "Stabilization of a surface plasmon resonance (SPR) optical fibre sensor with an ultra-thin organic film: application to the detection

- of chloro-fluoro-carbon (CFC)," *Synthetic Metals*, vol. 90, pp. 193-198, 1997.
- [24] K. J. Loh, J. Kim, J. P. Lynch, N. W. Shi Kam, and N. A. Kotov, "Multifunctional layer-by-layer carbon nanotube-polyelectrolyte thin films for strain and corrosion sensing," *Smart Materials & Structures*, vol. 16, pp. 429-438, Apr 2007.
- [25] E. Llobet, "Gas sensors using carbon nanomaterials: A review," *Sensors and Actuators B* vol. 179, pp. 32- 45, 2013.
- [26] D. Wang, H. Shakeel, J. Lovette, G. W. Rice, J. R. Heflin, and M. Agah, "Highly Stable Surface Functionalization of Microgas Chromatography Columns Using Layer-by-Layer Self-Assembly of Silica Nanoparticles," *Analytical Chemistry*, vol. 85, pp. 8135-8141, 2013/09/03 2013.
- [27] W. Putzbach and N. Ronkainen, "Immobilization Techniques in the Fabrication of Nanomaterial-Based Electrochemical Biosensors: A Review," *Sensors*, vol. 13, pp. 4811-4840, 2013.
- [28] H. P. Kehler, "Stabilisation of thin tin films," *Thin Solid Films*, vol. 7, pp. R43-R47, 1971.
- [29] Y. C. Ng, Z. Yang, W. J. McAuley, and S. Qi, "Stabilisation of amorphous drugs under high humidity using pharmaceutical thin films," *European Journal of Pharmaceutics and Biopharmaceutics*, vol. 84, pp. 555-565, 2013.
- [30] Y. Liu and T. Cui, "Ion-sensitive field-effect transistor based pH sensors using nano self-assembled polyelectrolyte/nanoparticle multilayer films," *Sensors and Actuators B* vol. 123, pp. 148-152, 2007.
- [31] G. Nallathambi, T. Ramachandran, V. Rajendran, and R. Palanivelu, "Effect of silica nanoparticles and BTCA on physical properties of cotton fabrics," *Materials Research*, vol. 14, pp. 552-559, 2011.
- [32] V. V. Potapov, E. S. Shitikov, N. S. Trutnev, V. A. Gorbach, and N. N. Portnyagin, "Influence of silica nanoparticles on the strength characteristics of cement samples," *Glass Physics and Chemistry*, vol. 37, pp. 98-105, 2011/02/01 2011.
- [33] J. Vivero-Escoto, *Silica Nanoparticles: Preparation, Properties and Uses*: Nova Science Pub Incorporated, 2011.
- [34] D. Lee and T. Cui, "A role of silica nanoparticles in layer-by-layer self-assembled carbon nanotube and In₂O₃ nanoparticle thin-film pH sensors: Tunable sensitivity and linearity," *Sensors and Actuators A: Physical*, vol. 188, pp. 203-211, 2012
- [35] I. A. Rahman and V. Padavettan, "Synthesis of Silica Nanoparticles by Sol-Gel: Size-Dependent Properties, Surface Modification, and Applications in Silica-Polymer Nanocomposites—A Review," *Journal of Nanomaterials*, vol. 2012, pp. 1-15, 2012.

- [36] D. Lee and T. Cui, "A role of silica nanoparticles in layer-by-layer self-assembled carbon nanotube and In₂O₃ nanoparticle thin-film pH sensors: Tunable sensitivity and linearity," *Sensors and Actuators A: Physical*, vol. 188, pp. 203-211, 2012.
- [37] P. Bertrand, A. Jonas, A. Laschewsky, and R. Legras, "Ultrathin polymer coatings by complexation of polyelectrolytes at interfaces: suitable materials, structure and properties," *Macromolecular Rapid Communications*, vol. 21, pp. 319-348, 2000.
- [38] Y. Shimazaki, R. Nakamura, S. Ito, and M. Yamamoto, "Molecular Weight Dependence of Alternate Adsorption through Charge-Transfer Interaction," *Langmuir*, vol. 17, pp. 953-956, 2001.
- [39] Z. Tang, Y. Wang, and N. A. Kotov, "Semiconductor Nanoparticles on Solid Substrates: Film Structure, Intermolecular Interactions, and Polyelectrolyte Effects," *Langmuir*, vol. 18, pp. 7035-7040, 2002.
- [40] N. A. Kotov, S. Magonov, and E. Tropsha, "Layer-by-Layer Self-Assembly of Aluminosilicate–Polyelectrolyte Composites: Mechanism of Deposition, Crack Resistance, and Perspectives for Novel Membrane Materials," *Chemistry of Materials*, vol. 10, pp. 886-895, 1998/03/01 1998.

8. Conclusions and Future Work

This research work reported in this thesis was undertaken to design and prepare novel, sensitive and reliable pH fibre optic sensors which were based on peak wavelength measurement that allows the sensor to function effectively and independently of any source variations or other system perturbations than pH change. The sensor benefited of high resolution in wider range of pH sensitivity from neutral to alkaline with an accuracy of ± 0.2 . In order to prepare such a probe, the fibre optic used was selected due to its rapid response to the smallest change in media and the layer-by-layer technique was chosen to coat an indicator on the fibre, due to its low process cost as well as its ease of control of the thickness of the coating with this technique.

Based on the results obtained from this research, the following assessment of the present study can be made.

8.1 Conclusion and overview of the work

In Chapter 2 of this thesis a brief literature review on the deposition techniques and self-assembly multilayer coating was given along with the advantages and disadvantages of each method. Longmuir-Blodgett, sol-gel, covalently multilayer self-assembly and layer-by-layer approaches were systematically

introduced in this review, accompanied by appropriate comparisons and discussions.

Chapter 3 has summarised in a review all the key components and instruments prepared and used in this research work such as chemical reagents, fibre optic, connectors and detectors. This chapter has also covered the preparation method of the sensor, the setup of a system for examination of the probe, the method of data analysis and the software employed.

Chapter 4 explored the operational principles of layer-by-layer deposition technique and the important parameters on the deposition technique and their effects on the properties of the immobilized layers based on a great number of related references. Subsequently, some preliminary experiments were carried out on the glass slide coated with neutral red and poly (acrylic acid).

As a conclusion, it was decided to prepare the probes in the presence of salt molecules as a copolymer to distribute charges uniformly. The deposition was carried out on wet layers instead of dry. Although drying caused a higher light absorbance, wet layers benefited from more homogeneity. Applying heat treatment after completing the coating creates stronger immobilized multilayers.

A variety of dyes, as pH indicators which are suitable for the layer-by-layer technique was examined to select a dye with the highest peak wavelength shift. As shown in Chapter 5, brilliant yellow was eventually selected. In this chapter three indicators were focused both individually and their combinations for deposition on the fibre optic. Among the selected indicators neutral red

exhibited a sharp shift of peak wavelength in a narrow pH range of 6 to 7, while brilliant yellow presented high sensitivity for pH range from 7 to 10. Consequently brilliant yellow was selected as the pH indicator to provide a highly sensitive sensor for wider range of pH values.

In Chapter 6 the design and characterization of a novel and high resolution wavelength dependent pH optical sensor, fabricated using the layer-by-layer technique, was undertaken. In this approach, brilliant yellow (BY) as a pH indicator and poly (allylamine hydrochloride) [PAH] as a cross-linker have been deposited on an uncladded silica fibre. A number of key parameters, such as the number of bilayers, the concentration of the BY solution and the shape of the fibre, as well as its core diameter have been varied with a view to optimizing the design and performance of the pH sensor. Two main properties, sensitivity and pK_a , have been discussed in this Chapter.

The results obtained from a series of evaluations show that the sensitivity was enhanced by reducing the concentration of the indicator solution used and by designing a U-bend configuration sensor probe with a sharply bent fibre. However, when making an overall comparison, the straight (unbent) fibre probe resulted in a more sensitive probe when compared to the use of a high radius bend. Further, utilizing a small core diameter of the fibre allows a wide pH range to be measured and with high sensitivity. Additionally, the performance was shown to be improved for measurements over a narrower range of pH, by using a fibre with a larger core diameter. Considering the effect of the number of layers, work carried out has shown that probes with 5-6 bilayers presented the

best performance. The sensitivity has been shown to diminish when more than 6 layers were used and the sensing range shifts towards higher pH values. When monitored, the value of pKa (the dissociation constant) of the thin film showed the smallest change of any of the design factors considered. In summary, using a larger core diameter, employing a larger curve radius, a higher number of bilayers, a higher concentration of the indicator solution and applying PAH as an outer layer, all cause a higher pKa value and as a result the probe sensitivity moves towards alkaline region. Consequently, the U-shaped probe with a 1.15mm radius coated with 6 bilayers of (PAH/BY) while the concentration of the BY solution was 0.25 mM demonstrated the highest average wavelength shift of 5.45 nm for a sample of 0.2 pH units from pH 7 to pH 9 with pKa 8.0.

To date, for most of the pH sensors developed, their sensitivity has been determined through intensity-based measurement, which can be prone to error. Limited research has been studied on optical sensors which work based on wavelength shift, while the highest sensitivity for their sensors was not very significant e.g. 0.32 nm/pH unit and -0.45 nm/pH unit for acid and alkali solutions, respectively [1], or 0.6 nm/pH unit and -0.85 nm/pH unit for acidic and alkaline solutions, respectively [2]. However, the present study was designed to use wavelength change as the key measurand and to optimize the wavelength-dependent pH sensor so that it offered high resolution and sensitivity i.e. 5.5 nm for a sample of 0.2 pH units or ~ 27 nm/pH unit, which is the first achievement for such a fiber optic sensor so far.

Alternatively, the pK_a value was influenced by the previous key parameters, leading the sensitive area to alkali or acidic region by slightly changing the structure of the layers, reflecting another novelty of this work.

It is important to create stable and durable sensors to meet the needs of users for operation under extreme environments i.e. very low or very high pH. The main aim of the study in Chapter 7 has been to prepare a number of such sensors and compare the performance of three different stabilization approaches used for the development of an effective wavelength-dependent pH-sensitive optical sensor. Techniques such as employing heat treatment, the deposition of two layers of a PAH/SiO₂ (poly (allylamine hydrochloride)/Silica nanoparticle) thin film and the deposition of two layers of APTMS/SiO₂ (3-Aminopropyl-trimethoxy silane/Silica nanoparticle) as topping layers have been studied to determine the optimum approach to creating a stable and reliable sensor – one yielding the same value of peak wavelength for a measurement of a known value of pH and to do so repeatably. An improvement in performance and in shelf-life, stability and re-usability of the sensor has been achieved by the addition of two bilayers of APTMS/SiO₂ in the work carried out. As storing the samples coated by (APTMS/SiO₂)₂ for a week has been shown to have a negligible effect on the peak wavelength values. In addition, applying these capping layers not only improved the sensor shelf-life but also enhanced the re-usability of the sensor such that destroying the deposited layers after 60 minutes exposure to the buffer solution results in the peak wavelength staying constant for these samples, even

after immersion on two separate occasions in the buffer solutions, for periods of 60 minutes in each case.

There are a numerous studies reported on increasing the stability of fibre optic sensors reported in the literature [3-8]; however, there has not been any evidence to show enhancement the stability of a pH fibre optic sensor fabricated by layer-by-layer approach up to now.

8.2 Future work

Even though good responses were observed for these sensors, the leaching out of the dye is an undesirable effect which occurred in the experiments. Further research in applying positively charged nanoparticles between the layers of dye might explore higher stability of the light absorbance because the stronger binding between molecules of the indicator and nanoparticles may arise.

The designated sensor probe in this research works through the pH range of 7 to 9. Immersion of the coated probe in solutions with higher pH value leads to destruction of the layers. Nonetheless, applying additional chemical interaction between molecules of polyanion and polycation comprising in multilayers i.e. covalently bonded would enhance the stability and solidity of the deposited layers. This would create a sensor probe which is suitable for higher pH measurements.

A further study could assess the effects of low temperature on sensitivity and stability of the sensor. The temperature of the polyion solutions in the stage of

preparing the sensor as well as the temperature of the pH buffer solutions in the stage of examination of the probe would be important. Since lower temperature presents higher absorbance and more stickiness to the substrate, it might affect the stability of the layers.

Due to the capability of the layer-by-layer technique to create multiple parameter sensitive films and its potential for fast and inexpensive production and due to the high demand and the need for a real time measurement for water and food safety further development of this type of sensor can be extended to detect simultaneously pH and other chemicals e.g. ammonia, chloride and heavy metals. Further research can be undertaken in designing appropriate packaging for these kinds of sensors.

Using the layer-by-layer technique as a simple, versatile and appropriate method to create a sensor works based on surface resonance plasmon (SPR) or localized SPR (LSPR) for a variety of sensing and bio-sensing applications purposes is recommended as an area for further research. Nowadays, among various bio-sensing technologies, both SPR and LSPR sensing technologies have been widely explored and reported due to their attractive features such as high sensitivity, label-free detection, fast response and real-time monitoring.

References

- [1] B. Gu, M.-J. Yin, A. P. Zhang, J.-W. Qian, and S. He, "Low-cost high-performance fiber-optic pH sensor based on thin-core fiber modal interferometer," *Optics Express*, vol. 17, pp. 22296- 22302, 2009.
- [2] M. Yin, B. Gu, Q. Zhao, J. Qian, A. Zhang, Q. An, *et al.*, "Highly sensitive and fast responsive fiber-optic modal interferometric pH sensor based on polyelectrolyte complex and polyelectrolyte self-assembled nanocoating," *Analytical and Bioanalytical Chemistry*, vol. 399, pp. 3623-3631, 2011/04/01 2011.
- [3] I. Ichinose, S. Muzuki, S. Ohno, H. Shiraishi, and T. Kunitake, "Preparation of cross-linked ultrathin films based on layer-by-layer assembly of polymers," *Polymer Journal*, vol. 31, pp. 1065-1070, 1999 1999.
- [4] H. Yamada, T. Imoto, K. Fujita, K. Okazaki, and M. Motomura, "Selective modification of aspartic acid-101 in lysozyme by carbodiimide reaction", *Biochemistry*, vol. 20, pp. 4836-4842, 1981 1981.
- [5] Q. Li, J. F. Quinn, and F. Caruso, "Nanoporous Polymer Thin Films via Polyelectrolyte Templating," *Advanced Materials*, vol. 17, pp. 2058-2062, 2005.
- [6] D. Saeki, M. Imanishi, Y. Ohmukai, T. Maruyama, and H. Matsuyama, "Stabilization of layer-by-layer assembled nanofiltration membranes by crosslinking via amide bond formation and siloxane bond formation," *Journal of Membrane Science*, vol. 447, pp. 128-133, 2013.
- [7] A. K. Sen, B. Mukherjee, A. S. Bhattacharyya, P. P. De, and A. K. Bhowmick, "Kinetics of silane grafting and moisture crosslinking of polyethylene and ethylene propylene rubber," *Journal of Applied Polymer Science*, vol. 44, pp. 1153-1164, 1992.
- [8] Y. Egawa, R. Hayashida, and J. i. Anzai, "Covalently cross-linked multilayer thin films composed of diazoresin and brilliant yellow for an optical pH sensor " *Polymer*, vol. 48, pp. 1455-1458 2007.